The Intermolecular Interactions of Branching onto Collagen Chains and Its Effects on the Formation of Nanocomposite Fibres

Zahra Bazrafshan

Submitted for the degree of Doctor of Philosophy

Heriot-Watt University

The School of Textiles and Design

December 2018

ABSTRACT

Collagen is an important biomimetic material. Several attempts to electrospin this biopolymer have proved difficult due to significant denaturation and degradation occurring while being dissolved in a solvent and spun.

Acid soluble collagen (ASC) was successfully pre-treated by grafting Methyl Methacrylate-co-Ethyl Acrylate onto its chains leading to ASC-g-poly(methyl methacrylate-co-ethyl acrylate) (CME). This was not only to add stability to its structure but also allowed electrospinning of the material which would otherwise have a deteriorating effect on its degradation rate and would have required post treatment. Experimental relations depending on monomer feed ratios and physiochemical properties of side chains that affect fibre formation, diameter, and distribution were investigated. Increasing the number of branching onto ASC chains can significantly reduce the deteriorative impact of electrospinning conditions along with improving its stability in high humidity conditions. The short chain branching onto ASC chains can effectively influence the fibre thermal stability while long chain branching provides a higher density of chain entanglements that improves fibre uniformity.

The study has shown how to process a composite fibre which can consist of CME with a structurally and electrically incompatible polymer, by using coaxial electrospinning. Nylon 66 has been taken as an example of this methodology. By tailoring the intensity of the electric field, different fibre content was achieved from the core and shell components, leading to varied physical properties; thermal, mechanical and degradability. The effect of chain orientation and intermolecular interactions between two structurally different polymer chains were investigated; custom-built electrostatics and supplementary bonding e.g. hydrogen bonds were identified the major factors for the design of reinforced CME/nylon 66 core-shell fibres.

Finally, a functionalisation methodology has been successfully established in which SMART nanofillers, such as graphene oxide (GO) is attached to CME. By increasing the GO content, significantly increases were achieved in the performance of polymerisation onto ASC. This nanofiller can improve the physiochemical properties of ASC chains, the same as the grafted side chains. It was found that humidity and temperature play key roles in the degradation rate of GO-CME composite; above 50 ^{o}C, GO is not as stable as branches on the surface of collagen chains.

The impact of this research is in the ability of collagen to be used in a variety of applications by making it more stable via grafting from new end groups. In consequence, new methodologies in electrospinning of nanofibres; composite fibres and smart nanofillers become possible, imparting new properties and new possibilities of this biopolymer for numerous end uses.

DEDICATION

To my life-coach: because I owe it all to you. Many Thanks!
To my parents, who are ready to do everything to see me happy!
To my beloved Ali, who was patient on my absence at home!
To Ghazale & Bahare, who was growing up fast while I was passing through the steps of succeed!
To my sister and my niece, Somaye & Helia in a lovely smile of happiness!

Acknowledgment

First and foremost, I would like to express my profound gratitude to Prof. Dr. George K. Stylios for his close support and constructive feedbacks during my research. By admitting me to his research group, he made it possible for me to get into a new scientific world. From the first day on I was inspired by his immense knowledge and his motivation to conduct the research with a real impact. His valuable guidance and advices patiently helped me to learn how to face the challenges by thinking out of the box while never losing sight of the overall picture of visions. Stylios, thank you for the confidence you have placed on me as an umbrella. I am greatly indebted to him. It has been a great honour for me to be his PhD student.

Moreover, I appreciate the constant approachability and the open manner of Dr Danmei Sun for investing her precious time to co-examine this thesis and also for her interest in my work. She is a brilliant scientist, accessible to any question at any time.

My sincere gratitude also go to my parents, husband, siblings, and, who have provided me with decent and emotional support in my life. I am also grateful to my other family members and friends who have supported me in this way, with a special mention of gratitude to Rosemary Lee who was available any time to make my little world better with her wisely strong words and humour. There are times when a student can't get the work done on time due to some reason but needs to talk, then you were so welcoming with your lovely smile to me.

I especially would like to thank Dr Roger Spark. I greatly benefitted from his versatility, helpfulness while working in the organic chemistry laboratory. Thank you, Roger, for the never-ending discussion about science, prosperous working area in the chemistry laboratory and everything else.

I am also very grateful for all of the help and assistance I have received from Dr Georgina Rosair, Dr Brain Hutton, Dr David Ellis and Dr Sarah Keith; with a special mention of appreciation to Louise Bingham, Ruth Paterson, Jim McVee, Jane Robertson, Fay Locki, Avril Birtwistle, and Gayle Poddubecki for their punctuality and approachability.

And, to all research staff and students in general. It was fantastic to have the opportunity to work majority of my research beside them from undergrads to PhD students.

ACADEMIC REGISTRY

Research Thesis Submission

Name*:*	ZAHRA BAZRAFSHAN		
School:	SCHOOL OF TEXTILES AND DESIGN		
Version: *(i.e. First, Resubmission, Final)*	FINAL	Degree Sought:	PhD

Declaration

In accordance with the appropriate regulations I hereby submit my thesis and I declare that:

1) the thesis embodies the results of my own work and has been composed by myself
2) where appropriate, I have made acknowledgement of the work of others and have made reference to work carried out in collaboration with other persons
3) the thesis is the correct version of the thesis for submission and is the same version as any electronic versions submitted*.
4) my thesis for the award referred to, deposited in the Heriot-Watt University Library, should be made available for loan or photocopying and be available via the Institutional Repository, subject to such conditions as the Librarian may require
5) I understand that as a student of the University I am required to abide by the Regulations of the University and to conform to its discipline.
6) I confirm that the thesis has been verified against plagiarism via an approved plagiarism detection application e.g. Turnitin.

* *Please note that it is the responsibility of the candidate to ensure that the correct version of the thesis is submitted.*

Signature of Candidate*:*		Date:	

Submission

Submitted By *(name in capitals):*	ZAHRA BAZRAFSHAN
Signature of Individual Submitting:	
Date Submitted:	

For Completion in the Student Service Centre (SSC)

Received in the SSC by *(name in capitals):*			
Method of Submission *(Handed in to SSC; posted through internal/external mail):*			
E-thesis Submitted (mandatory for final theses)			
Signature:		Date:	

Please note this form should be bound into the submitted thesis.

TABLE OF CONTENTS

LISTS OF TABLES AND FIGURES

LISTS OF TABLES

LIST OF PUBLICATIONS

1. **One-pot approach synthesising and characterization of random copolymerisation of methyl methacrylate-co-ethyl acrylate with broad range of glass transition temperature onto collagen.**
   Bazrafshan, Zahra; Stylios, George K.
   In: Polymer Engineering and Science, 28 July 2017.
   Research output: Contribution to journal › Article
2. **Custom-built electrostatics and supplementary bonding in the design of reinforced Collagen-g-P(methyl methacrylate-co-Ethyl Acrylate)/ Nylon 66 core-shell fibres.**
   Bazrafshan, Zahra; Stylios, George K.
   In: Journal of the Mechanical Behaviour of Biomedical Materials, 11 July 2018.
   Research output: Contribution to journal › Article
3. **A novel approach to enhance the spinnability of collagen fibres by graft polymerisation.**
   Bazrafshan, Zahra; Stylios, George K.
   In: Journal of materials science and engineering C, 8 September 2018
   Research output: Contribution to journal › Article
4. **High Performance of Covalently Grafting onto Collagen in The Presence of Graphene Oxide**
   Bazrafshan, Zahra; Stylios, George K.
   In: Nanomaterials, 9 September 2018
   Research output: Contribution to journal › Article
5. **One-Step Fabrication of Three-Dimensional Fibrous Collagen-Based Macrostructure with High Water Uptake Capability by Coaxial Electrospinning**
   Bazrafshan, Zahra; Stylios, George K.
   In: Nanomaterials, 8 October 2018
   Research output: Contribution to journal › Article
6. **Recent development in spinnability of collagen as a biomimetic material**
   Bazrafshan, Zahra; Stylios, George K.
   In: International Journal of Biological Macromolecules
   Research output: Contribution to journal › Review Article

Chapter 1 Introduction

Over the past few decades, there has been significant use of polymers for various applications. This is because of the advantages they offer such as high productivity and ease of functionalisation. Among them, natural-based polymers have been receiving much attention due to their availability and biodegradability, which made them suitable for specific end uses. Polymers irrespective of their type are modified to suit end-user requirements by tailoring their properties.

This chapter deals with the basics of polymers and how they may be processed via spinning methods. Before discussing the methods of preparation of the biopolymers and their performance, we describe the types of polymers, their microstructure, and their chemical composition. Particular reference is given to the uniqueness of nanofibres from biopolymers processed by novel electrospinning technology.

1.1 Types of polymers and polymerisations

Polymers as macromolecules are formed from numerous simple organic repeating structural units known as monomers, and the polymer formation process in which the monomers covalently bond together is called polymerisation. A polymer molecule can consist of a massive number of linked monomers that may have a linear, branched, or network structure [15, 16].

The molecular structure of a single polymer chain can be linear, which is schematically signified by a simple line (straight, zigzag, or wavy) of a finite length, Figure 1-1a. The molecule of a branched polymer chain is represented by short/ long branches on a line of finite length, Figure 1-1b. Whilst a cross-linked polymer is characterised by a network construction of polymer chains [17, 18], Figure 1-1 (c and d).

On the other hand, polymers can be obtained by using addition and condensation polymerisation. The formation of a polymer by addition polymerisation is a chain reaction induced by the conversion of alkynes to long-chain alkanes. Under specific conditions, when a chain conversion is initiated, it can continue until it is stopped. The major steps of this reaction are (i) initiation, (ii) propagation, (iii) termination. The polymers formed are called addition polymers e.g., polyethene and polypropylene. By contrast, some polymers are formed by condensation polymerisation. In condensation polymerisation, when a bond is formed between two monomers, a small molecule such as water or methanol is lost as a by-product. A well-known example is Polyamide 6 as a condensation polymer [16, 19, 20].

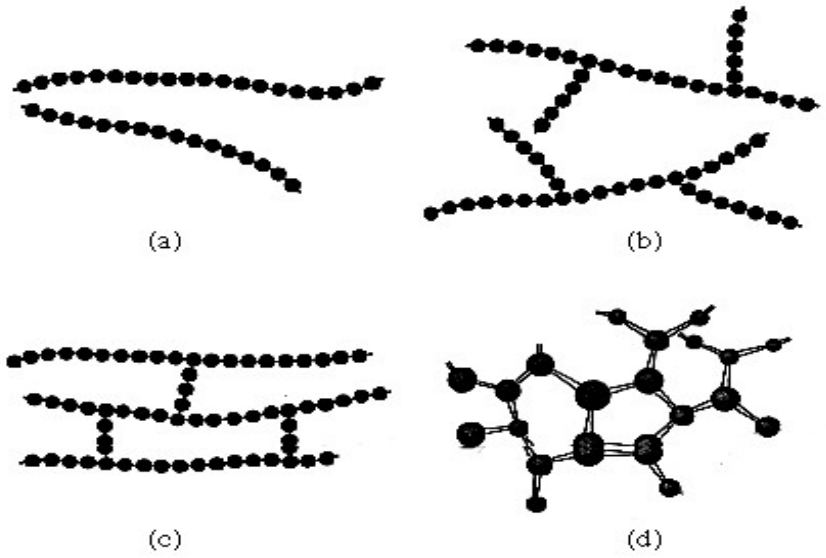

Figure 1-1 Molecular structure for different types of polymers [17, 21].

The other classification is attributed to the polymerisation mechanism, dividing polymerisations into step and chain polymerisation [16]. In other words, the condensation–addition classification deals with the arrangement or structure of the polymers, while the step–chain classification is concerned with the mechanism of the polymerisation processes. However, these classifications can be used synonymously, since most condensation polymers are constructed by step polymerisation methods and almost all addition polymers are constructed by chain polymerisation methods [16, 22]. There are some other classifications based on origin, thermal response and mode of formation, but there are outside the scope of this discussion.

Copolymers

During the polymerisation, copolymers are composed of more than one type of monomers, as structural repeating units; the copolymerisation can result in new and desirable properties [23]. Depending on the reactivity of monomers used, a composition variation occurs that caused by the varied sequences of monomer units, as illustrated in Figure 1-2.

Therefore, copolymers can be characterised by random, alternating placement of monomer (A) and monomer (B) as well as AB-block copolymers that consist of a block of A followed by a block of B and ABA-triblock copolymers representing A blocks at both ends that limit a B block in the middle. In addition, graft copolymers can be formed by polymerising B in the presence of a fully polymerised chain of A [16].

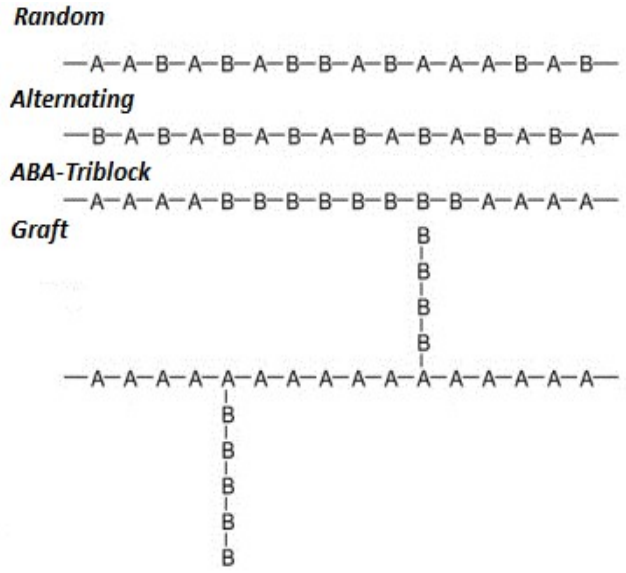

Figure 1-2 Structures of copolymers containing A and B repeating units [1-3]

Graft copolymers are defined as a branched polymer in which the components of the side chains are different from the main chain. The graft copolymers has been employed for decades. Grafting methods for copolymerisation result in materials that are further chemically, thermally and structurally stable than their homopolymer counterparts. These methods are not possible without A as a host polymer, since these reactions are due to chemical modification of A chains. The reaction mechanisms that employed to synthesise these copolymers, consist of anionic/ cationic polymerisation, free-radical polymerisation, , atom-transfer radical-polymerisation (ATRP), living polymerisation techniques, etc. The development of graft copolymers can be originated from the coupling of the functional group of backbone (A) with the end-group of B that are both reactive. It is also possible to introduce active sites (initiators) to initiate functionality to A chains as a host polymer and monomer/macromonomers of B to be grown as branches. The initiating sites results in initiating both sides of A and B to be covalently grafted. Although the number of side grafted molecules can be controlled to some extent by the number of active sites, there can be a dissimilarity in the lengths of side chains due to effect of steric hindrance and kinetics of reactants. The graft copolymerisation methods allow branches to be grafted heterogeneously or homogeneously based on the reactivity of end groups/ initiated molecules that are available in the reaction. The difference in distribution of grafts can significantly affect the physical properties of the grafted copolymers [5, 24, 25].

1.2 Origin of polymers

Synthetic polymers, namely man-made polymers, have received significant attention over the past few decades due to their durability, process ability, high tensile strength, and low cost [17, 26]. Hence, it is not surprising that synthetic polymers have found their way into a wide range of applications since almost all aspects of everyday life are affected by synthetics [26]. However, heavy consumption and high disposal of synthetic polymers have also resulted in environmental issues (health and aesthetic problems), especially synthetic polymers made from crude petroleum, as they possess a high resistance to bio-degradation and there is diminishing availability of fossil resources. Furthermore, difficulties in the recycling of synthetic polymers that have been reported such as impurities (additives/fillers added up to polymers) and insufficient quality of recycled material, is the other main concern when using synthetic polymers.

On the other hand, polymers from renewable resources have been introduced as the other polymer categorisation being used in specific end uses. The advantage of consuming renewable resources such as biomass is clear, due to their high availability and fast naturally replacement [26-29]. Therefore, we can consider natural polymers, including biopolymers such as polysaccharides, natural silk, natural gums, natural rubber, proteins, nucleuo-proteins, and other natural fibres, including cotton (cellulosic), cellulosic and lingo-cellulosic, ramie, jute, coir, flax, sisal, and hemp. In other words, the origin of polymers (fossil fuels vs. renewable resources) and degradability (durable vs. biodegradable) are differentiated via this classification where the end of polymer life is particularly important to distinguish biodegradable polymers and durable renewable or biomass-derived polymers.

There is one more group, namely semi-synthetic (modified natural) polymers that are often synthetically modified [26, 27]; this is currently one of the most rapidly growing fields in material science. The aim is typically to alter or improve their characteristics. This is a highly interdisciplinary field that includes polymer synthesis, modification, and processing. In this regard, chitosan-based materials derived from chitosan as a polysaccharide having reactive functional groups and high adsorption capacity can be considered as an example [30]. These characteristics highlight the high suitability and wide variety of applications for which chitosan can be used.

Biopolymer: Biobased/ biodegradable

The terms relating to biopolymers which are widely used to describe two concepts are recognised: (i) polymers from biomass (a renewable resource) such as agro-polymers

(e.g., proteins or cellulose), and (ii) polymers with biodegradability characteristics [26, 27, 31].

Biodegradable polymers are classified by their synthetic process (Figure 1-3): polymers from (i) agro-resources (renewable resources), (ii) synthetic polymers from monomers found from agro-resources such as polylactic acid (PLA), and (iii) biodegradable polymers formed from fuel resources and polymers of microbial products such as poly hydroxyl alkanoates (PHAs) [10, 31-33]

Among them, proteins as agro-polymers are from renewable resources that are produced in the body of animals, bacteria and plants. Although a relatively numerous type of proteins have been identified, only a few have been used for industrial end uses due to their low product performance in pure forms [10, 31, 32].

Proteins are generally comprised of polymers from a series of amino acids (Figure 1-4). The amino acid arrangements in protein chains then result in a variety of chemical structures and physiochemical properties. The inter- and intra-molecular interaction of the amino acids determine the chemical reactivity and the final 3D structure of amino acids. Biochemists mention four different features of the unique structure of a protein [78]: (i) primary structure comprising amino acid sequences, (ii) frequently repeating primary structure stabilised by hydrogen bonds establishing a secondary structure

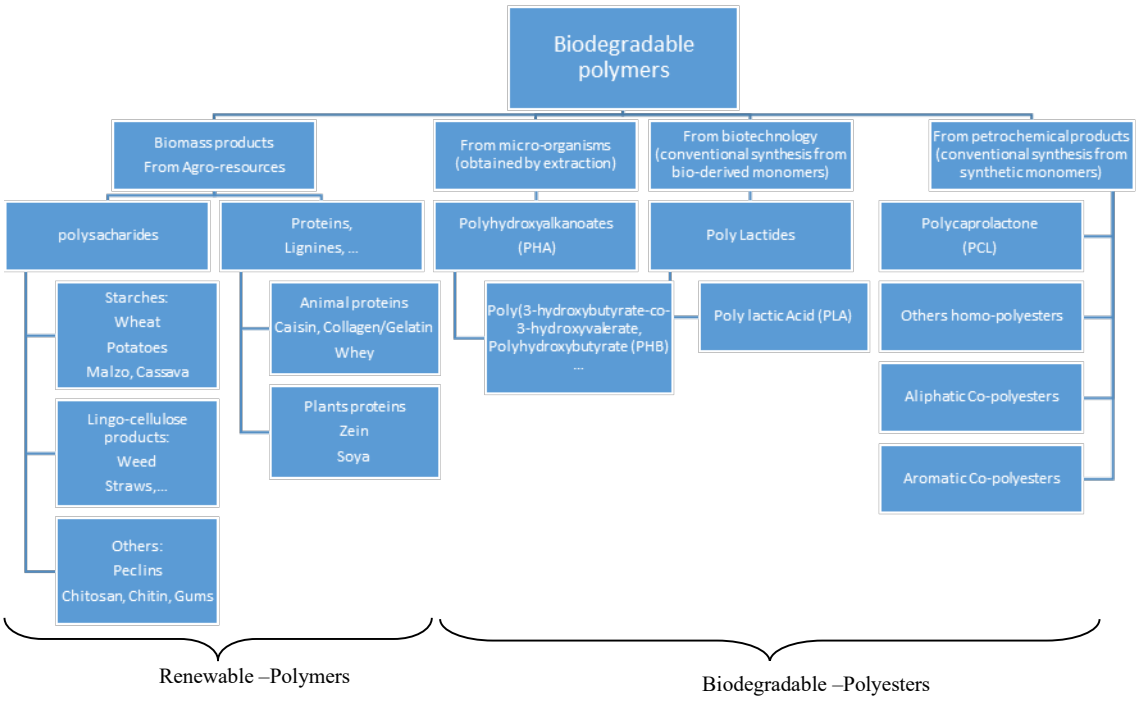

Figure 1-3 Classification of the main biodegradable polymers [10].

(Figure 1-4) e.g., the alpha helix and the beta sheet, (iii) tertiary structure that is the final form of a protein, consisting of the spatial arrangement of the secondary structures, and (iv) quaternary structure shaped by a number of proteins functioning as a complex [10].

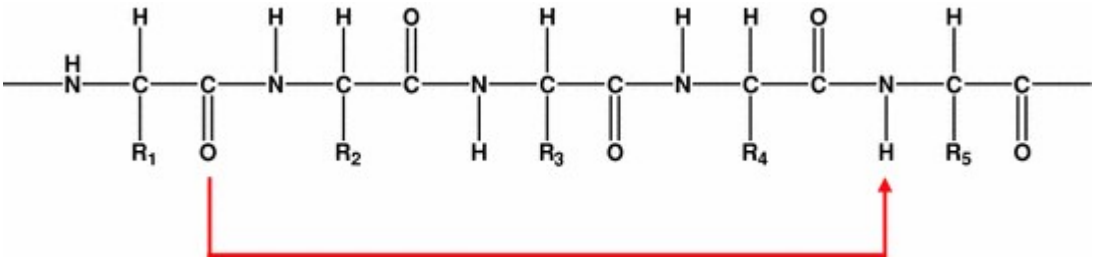

Figure 1-4 A typical amino acid sequence representing primary chemical structure; hydrogen bonding interaction between the amino-acids to form the secondary structure (arrow) [10].

The final structure of proteins is typically characterised, according to their solubility and their special feature, as fibrous, globular, or membrane [34]. Fibrous proteins consist of regular linear structures whereas globular proteins tend to be irregular and roughly spherical. The protein chain is folded to form a colloid, so that their hydrophobic side is in the interior of the aggregated colloid whereas their outer hydrophilic segment are mostly softened in aqueous media. By contrast, in membrane proteins, hydrophobic side of amino acid chains is oriented outwards to interact with the cells from their non-polar phase [34, 35].

Proteins are mostly processed by the same approaches as polysaccharide-based materials such as formulation (blending) with plasticizers and cross-linkers. The most commonly used plasticizers for proteins are (a combination of) multifunctional alcohols such as glycerol, sorbitol, poly ethylene glycol, propylene glycol, and di- and tri-ethanolamine [10, 36-40]. As shown in Figure 1-5, cross-linkers that randomly function as molecular bridges contain at best two reactive ends to attach to tailored functional groups available on primary amines, and secondary structure to alter the physical properties of proteins [41, 42].

Collagen is the main component of connective tissues, comprising 25% to 35% of the protein contents in the whole-body of mammals [43]. Among the 29 types of collagen discovered so far, 80–90 % of them consist of types I, II, and III [21, 44]. Based on the degree of mineralization on collagen, tissue mass can be rigid such as bones, compliant like tendons, or having a gradient property from rigid to compliant like cartilages.

Collagen is mostly identified in the shape of oriented fibrils in fibrous tissues, Figure 1-6. The diameter of collagen fibrils varied between tissues such as tendon (200 nm), skin

(approx. 100 nm), cornea (20 nm) and cartilage (approx. 50 nm)[45]. This variation in fibril diameter can be in correlation with their mechanical properties [46, 47].

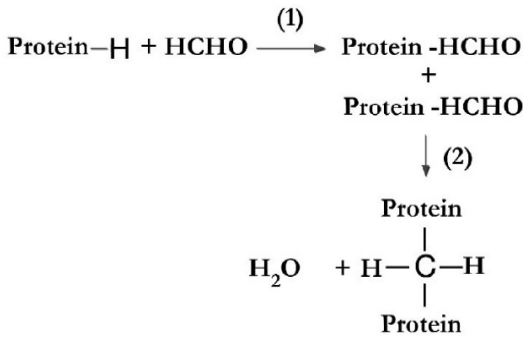

Figure 1-5 Protein Interaction to Formaldehyde as a cross-linker (1) Initial reaction (2) Late reaction to form a methylene bridge [48].

Interestingly, a bimodal distribution of fibril diameter has been discovered in some tissues, the spaces between the large fibres are filled by fibres with small length. This arrangement allows a high collagen content in tissue mass with highly maintained flexibility in tissue functionality. With maturation in collagen tissue, the diameters of fibrils mostly increase and are possibly either uni-modularly or bi-modally distributed, whilst fibril diameters decrease with ageing and have a tendency to bimodality in various tissues [47].

The overall structure of collagen is made up of a triple helix that is typically composed of two identical secondary chains (α1) and one additional chain (α2) that varies slightly in its chemical composition [34]. According to the source of collagen, the amino acid composition differs. In the secondary structure of collagen, the most regularly repeating amino acids are Glycine, Proline and Hydroxy Proline, Figure 1-7. The most common sequence in the amino acid primary structure of collagen is Glycine-X-Hydroxy Proline and Glycine-Proline-X, where X is any amino acid other than Glycine, Proline or Hydroxy Proline [47].

The microstructure of Collagen is not soluble in organic solvents. The physical properties of collagen are considered depending on the age and the type of the collagen source [34, 49]. Collagen, like other bio-based polymers, cannot be found in high purity. Collagen is mostly purified by the partial hydrolysis from skin and bones releasing from some chemical bonds. This transition causes a significant disarrangement in the collagen macrostructure resulting in high degree of hydration onto destabilised chains and solubilisation in water subsequently. In other words, this chemical treatment breaks the covalent and non-covalent bonds to denature the triple helix, leading to helix-

to-coil conversion. The degree of this irreversible denaturation depends on the severity of the process and considered as a function of pH, temperature, and time [35, 50, 51]. The functionality of soluble collagen is determined by the molecular weight distribution, structure, and composition of its hydrolysed chains [31, 44].

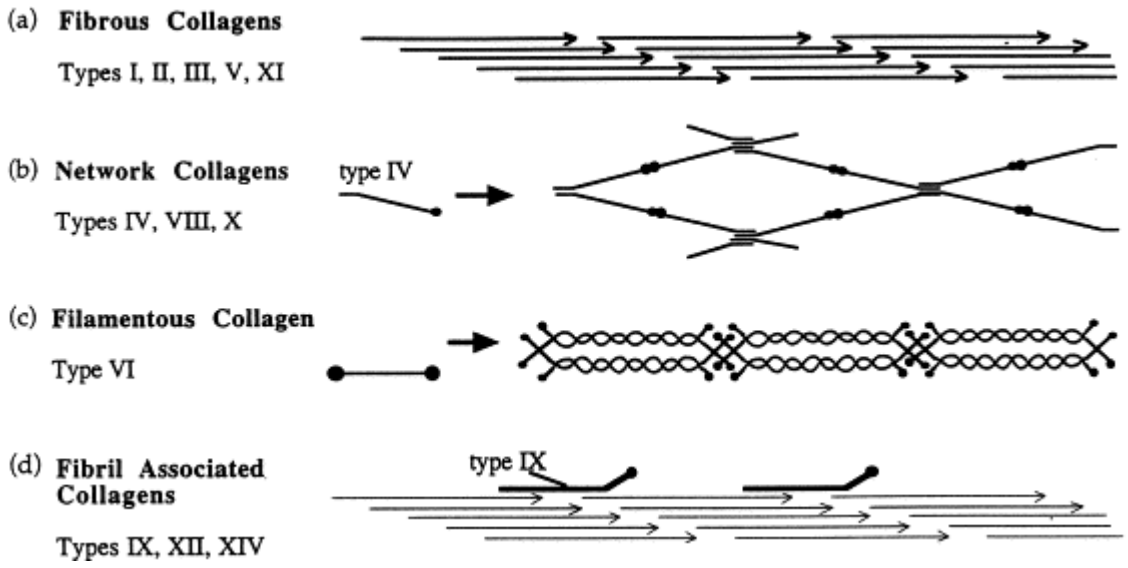

Figure 1-6 Illustrative demonstration of the aggregated simulations of different types of collagen as superfamily of proteins [45].

However, this chemical treatment can result in the followings: (i) three randomly coiled independent α-chains, (ii) an independent α-chain along with a β-chain (two covalently bonded α-chains), and (iii) a γ-chain (three covalently bonded α-chains linked) [52].
Obviously, α, β and γ forms of collagen represent a wide variety of molecular weights. The molecular weight of α-form typically differs from 80,000 to 125,000 while in the β-from and γ-form, the molecular weight variations are roughly from 160,000 to 250,000 and 240,000 to 375,000, respectively [52].
The presence of functional groups such as –NH2, –OH, and –COOH in the soluble collagen causes this bio-based polymer to be redeveloped along with specific molecules and/or nanoparticles for various applications [53]. The collagen-based materials are then mostly used for medical and cosmetic purposes, for supporting, healing and repairing of body tissues [10, 43, 44].

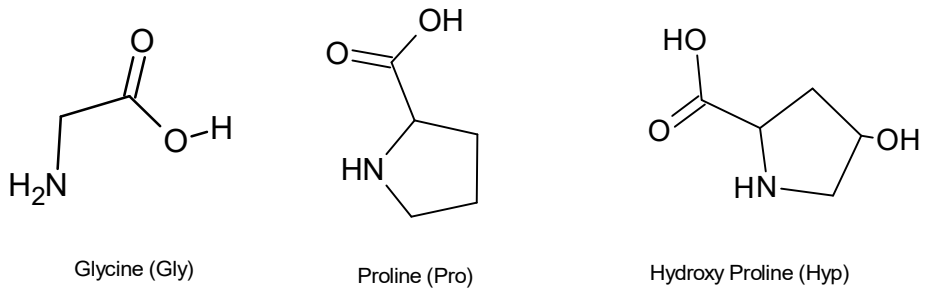

Figure 1-7 Chemical structure of Glycine, Proline and Hydroxy Proline[52].

1.3 Application and physical properties of polymers

Obviously, the diversity of polymers from natural to semi-synthetic and synthetic exhibit a wide variety of physiochemical properties [17, 26]. There are parameters that determine the reproducibility of polymer properties, e.g. molecular weight, specific molar cohesion, the linearity of chain structure, polarity, crystallinity, molecular symmetry, thermo-mechanical history. As a simple example, a polymer with a greater molecular weight exhibits a higher density of chain entanglements, hence typically representing a higher tensile strength (TS), viscosity (η) and melting temperature (Tm) [54].

In addition, a low degree of branching makes a polymer less resistant to solvents, and heat due to increased molecular mobility. By contrast, high branching densities and ultimate cross-linking reduce the chain flexibility of the same polymer providing higher degrees of chain entanglement. Thereby, limiting or removing molecular mobility typically improve thermal and dimensional stability, and cause less/ non-solubility, e.g. amino resins, cured phenolics, vulcanized rubbers and epoxy resin systems are examples of network and cross-linked polymers [23].

Furthermore, it is believed that intermolecular bonding, such as hydrogen bonding between the functional groups of polymer chains, significantly increase the cohesion property that results in higher stiffness, rigidity, melting temperature, crystallinity, and tensile strength of a polymer [55]. More specifically, a polar polymer chain applies high attractive forces on neighbouring molecules in contrast with non–polar polymer systems. For instance, the methylene linkages are shared between polar Poly Amide 6 chains —(NH–$(CH_2)_5$–CO)$_n$— and non-polar polyethylene chains —(CH2–CH2–)$_n$. The strongly polar CO–NH intermolecular bonding occurs at both ends of each $(CH_2)_5$ chain unit. In this case, the cohesive attraction between the chains of Polyamide is significantly higher when compared with Polyethylene chains with the same chain length. Hence, polyamide 6 can form massive intermolecular hydrogen bonds in the phase transition while processing e.g. through the melt spinning fibre formation. These

hydrogen bonds occur between N–H and C=O functional groups of neighbouring chains leading to significant improvement in tensile strength due to the enhancement in the crystallinity of the drawn polyamide fibres [56].

Even though polyethylene represents a low molar cohesion, it is well-defined as a suitable plastic due to its high mechanical strength. In contrast with polyamide 6, the high tensile strength of this polymer is typically due to the symmetrical chemical structure of the monomers repeated in polymer chains of —(CH2–CH2–)$_n$, enabling its chain molecules to be shaped into a matrix and induce crystallinity and tensile strength [16, 17]. The effect of H–bonding and molecular symmetry can further be confirmed by the chemically modified cellulose, as an obvious example in defining polymer properties, Figure 1-8 [46].

Basically, cellulose fibres have good mechanical strength and solvent resistant due to having numerous intermolecular H-bonding between the –OH groups. To regenerate cellulose as raw material, it is commonly modified by esterification or etherification upon hydroxyl groups in selective solvents [10, 31, 43]. Because of such chemical modifications (substituted ether or ester groups such as –OCH_3 in methylcellulose, or –ONO_2 in nitrocellulose to hydroxyl groups), the high architectural symmetry of the cellulose chain lost. However, extensively modified products display enhanced strength features compared with incomplete derivatives, since it is assumed that in the case of complete modification the molecular symmetry is reobtained [10, 22, 36, 43]. Hence, the properties of polymers can be considered by their applications as fibres, films, plastics and rubbers [57].

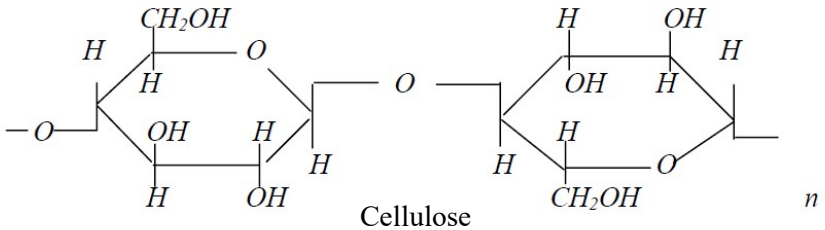

Cellulose

Figure 1-8 Molecular structure of Cellulose [10, 31, 43].

1.4 Fibres and fibre formation methods

Typically, fibres are formed from natural and synthetic materials which their lengths are considerably longer than their width [58]. Fibres are used mostly to produce other assemblies considered by their functionalities depending on tensile strength and modulus. A polymer is generally characterised by linear structure, high molecular

symmetry, high cohesive energy density established by polar functional groups, and high crystallinity in the applied regions of temperature [16, 23, 54].

It is also believed that the reversible tension deformation of aromatic rings in backbone chains can be supportive as identified in polyethylene terephthalate fibres. Even though, these findings cannot be generalised to all polymeric systems, extensive intermolecular interaction such as hydrogen bonding mostly play a key role in fibre formation technologies that can be seen in regenerated cellulose fibres from cellulose acetate and protein-based fibres such as animal fibres, acrylic based fibres from polyacrylonitrile and polyvinyl alcohol and polyamide based fibres [54].

Furthermore, the tensile strength of the fibres with anisotropic properties is typically considered by the degree of molecular orientation as a function of aligning along the fibre axis in time, which results in fibre diameter reduction [16, 54]. More specifically, when (semi)synthetic fibres are spun, they are drawn to orient along the fibre direction. Hence, the stiffness of carbon-carbon bonds in the backbone chain of linear polymers is reinforced along with fibre direction, as shown in Figure 1-9. This has been achieved in aramid fibres and other aliphatic fibres.

In recent years, fibres have undergone significant growth in developing synthetic and modified polymer fibres, e.g. para-aramid fibres (Armas, Twaron, Kevlar), UHMWPE fibres (Dyneema, Spectra), heat-resistant polyimide fibres, composite fibres with core-shell structure, and fibres grafting from a variety of nano- and micro-particles forming different carbo-polymers compounds, such as silver and carbon nanotubes [54].Therefore, aside from the textile industry, the high molecular orientation found in fibres can be utilised as reinforcing agents within the polymeric matrix of composites [59, 60].

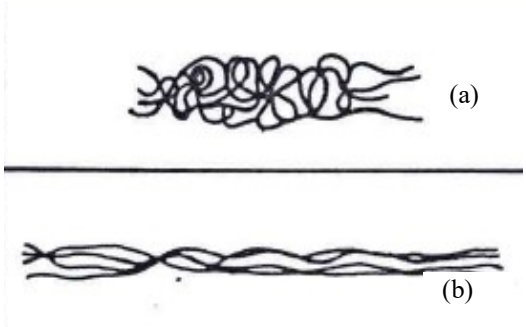

Figure 1-9 Molecular orientation of polymeric chain on spinning (a) non-stretched (b) stretched.

Among the previously mentioned factors, molecular weight and long molecular chain length of a polymer play a key role in fibre formation [61]. The minimum required molecular weight for fibre formation differs with the chemical nature of the polymer. In

general, the processability of a fibre polymer can be determined by the interchain cohesive forces and the orientation degree of the polymer with specific molecular weight [36, 61]. Typically, linear polymers from compatible monomers without bulky side groups have this ability to form fibres whereas highly branched polymer chains significantly reduce fibre orientation. Moreover, the availability of reactive side chains and the backbone chain result in a cross-linked three-dimensional polymer network (phase segregation). These problematic polymers are not spun into functional fibres through conventional fibre spinning methods [16, 61].

In conventional fibre spinning methods, semi-synthetic and synthetic fibres are manufactured by "extrusion", i.e. driving a viscous liquid through the channels of an apparatus called "spinneret" to fabricate continuous fibres of polymer which are solid in their initial state. Therefore, the fibre-forming polymers encounter phase transition into a fluid state to pass through the spinneret, which is typically reached at the melting temperature in thermoplastic polymers. Also, they can be dissolved in a suitable solvent which is more appropriate for semi-synthetic polymers such as cellulose-based fibres.

However, there are polymers that cannot be melted or dissolved easily. In this case, they need to be chemically treated to form thermoplastic or soluble derivatives. For instance, some recent researches have been attempted to form some special fibres from appropriate derivatives of polysaccharide-based polymers [61, 62]. These methods comprise: (i) derivatisation with a single-substituent, (ii) multi- substituent derivatisations, (iii) blending of derivatives with synthetic polymers, and (iv) graft polymerisation. For Cellulose derivatives as a well-known category of polysaccharides, these methods have been used to control their molecular structures and orientations in order to increase their functionality over the past decade. These attractive modifications are basically for improving the mechanical properties, controlled biodegradability, cytocompatibility, and optical properties [63].

However, due to imparting more molecular chain orientation and potential strength into the fibres, the spun filaments are typically drawn while they are hardening, or even after solidification as a post-treatment. The effect of this post-treatment on chain orientation along the fibre axis is well defined for creating a significantly high tensile strength in fibrous assemblies [16, 56, 61, 62].

The common spinning methods are shown schematically in Figure 1-10. Melt spinning is most appropriate for polymers that can be melted without decomposition. Dry and wet spinning methods are applied for polymers that can be dissolved in a solvent developing a polymeric solution. Melt spinning, dry spinning and wet spinning (Figure

1-10) are considered as conventional methods for fibre formation with high performance in spinning speed. However, electrospinning is the other most common spinning method for fabricating fibres with fascinating properties [61, 62].

1.5 Electrospinning

Electrospinning is a versatile and flexible method for fibre formation which derives from electrostatic spinning. This method employs electrical forces to fabricate fibre in diameter ranges from micrometres down to 100 nm using a wide variety of natural to synthetic polymers [61, 62, 64]. In this method, fibres are formed with a high surface-to-volume ratio in contrast with common fibres. Although the term of electrospinning is being using since around 1994, it was first introduced more than 70 years ago when a series of patents were published by Antonin Formhals between 1934 and 1944 describing an experimental methodology to produce polymer filaments through an electrostatic force [65]. For textile fibre electrospinning, Formhals' first patent, US Patent No.: 2116942; 1934; was attributed to the fibre formation of cellulose acetate, which was dissolved in acetone and monomethyl ether of ethylene glycol with applying a voltage of 57 kV. So far, several patents for electrospinning polymers as melt and solution have been issued which confirm the highly potential importance of this technique for the development of materials [66, 67].

It is interesting to note that the electrospinning has achieved tremendous attention in the laboratory and industry due to its potential in a wide variety of novel fibre formation that may be otherwise difficult by means of conventional spinning methods. This method has a high capability for regulating nanofibre composition to achieve the desired properties from their functionality, along with various fibre morphologies in size and shape [68].Even though, this method is well-known for manufacturing non-woven fibrous fabrics in the textile industry, the main development of electrospun fibres has been in tissue scaffolding where the high surface area and porosity characterise the functionality of electrospun mat [69]. A various attempts have been implemented to fabricate electrospun fibres from a wide range of natural-based and synthetic polymers such as polylactic acid (PLA), polyurethanes, silk fibroin, collagen, cellulose, chitosan/collagen [67].

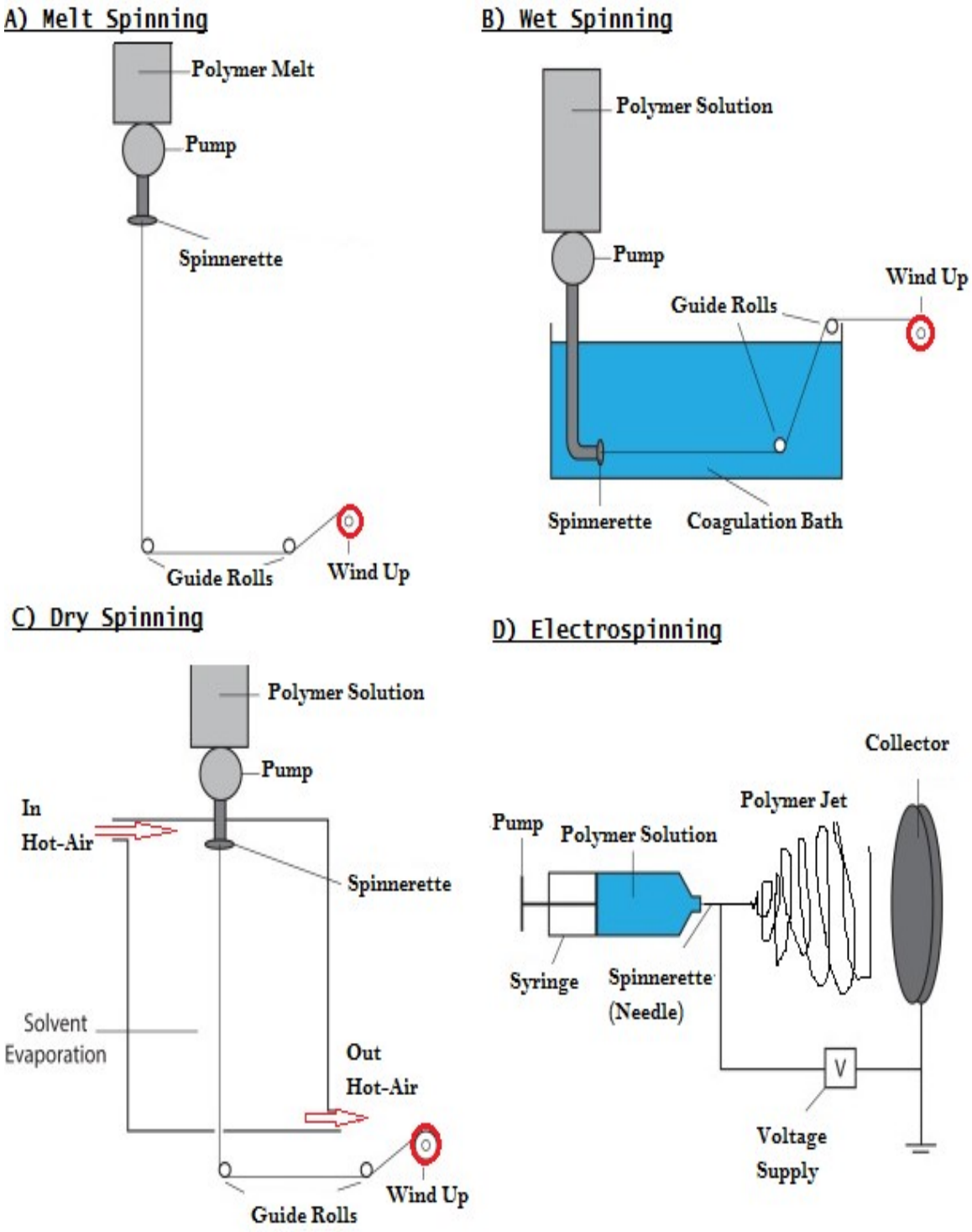

Figure 1-10 Schematic of common spinning methods [70]

And also, post-treatment procedures have extended the effectiveness of nanofibres which can be accomplished through conglutination, vapour coating, surface chemical treatment, and thermal processing in specific circumstances [71].

Despite the significant advantages of electrospinning, the fibre formation productivity (low production speed) is a challenge that can limit end uses demanding large quantities of fibres. More specifically, the nanofibre scale-up applying single polymer jet is not very applicable in this processing method. To address this issue, several research groups have attempted to introduce improved methodologies, such as bilayer electrospinning (the upper layer supplying a polymer solution whereas the lower layer being a ferromagnetic suspension), bubble electrospinning (bottom-up gas-jet electrospinning), and multiple nozzles (spinnerets) arranged in a line, circle or matrix [61, 62, 66, 67]. In this part of the work, the principals of the electrospinning process and their influence on the fibre morphology are considered as discussed below.

1.5.1 Electrospinning process

A representative electrospinning set-up is shown schematically in Figure 1-10D. Generally, an electrospinning apparatus comprises a set of three main components including a high voltage power supply, a spinneret (e.g. pipette tip, single/multi-needle), and a grounded collector (typically a metal plate or screen and a rotating drum) [64]. Polymer melt, or solution, is connected to a high voltage power supply to increase the fluid electrostatic potential of a certain polarity. It is essential for polymer chains that have a high degree of molecular entanglement based on inter and intramolecular interactions.

The surface charge of ready-to-jet polymer droplet that formed at the tip of the spinneret is dependent on the intensity of the electric field; by increasing the electrostatic force, the polymer jet is initiated to be ejected. On the other hand, the surface charge reacts reversely to the surface tension of the droplet, resulting in a "Taylor cone" by increasing the intensity of the electric field. This phenomenon is mostly caused by the strong electrical repulsive force that dominates the surface tension of the charged polymer fluid [67].

In this process, the polymer melt/solution is gradually fed into the capillary spinneret held there by its surface tension force. When it encounters the electric field, an electric charge (mostly positive) is induced on the fluid surface. Once the intensity of the electric field reaches a critical threshold, the repulsive electrical force dominates the surface tension force. Eventually, a polymer jet is initiated to eject from the tip of the spinneret towards the minimum of the dipole energy (the grounded collector).

Then a rapid and unstable electrically driven bending/whipping of the solidifying polymer jet is formed in the area between the tip and the collector (bending instability)

results in a thin fibre deposited on the collector. Thus, the overall electrospinning process is characterized as an easy-to-apply system for fibre formation [64, 66]. By controlling the process, fibres in nano to micrometre scale diameters are being produced, which can contain a number of cross-sectional features such as branches, beads, or buckling coils and zigzags [71].

1.5.2 Polymers in electrospinning

A variety of polymers have been processed by electrospinning to produce fine fibres used in wide-ranging applications. These applications have been reported of using various natural, semi-synthetic and synthetic polymers. Table 1-1 demonstrates the diversity of polymers recently processed by electrospinning with their characterization methods and example applications.

According to Table 1-1, the following aspects can be concluded: (i) multi-functionally of the polymers can be simply electrospun in a polymeric system consisting of more than one polymer, (ii) ability in forming unique topography and morphology as studied by SEM, (iii) depending on the end use, this nanotechnology can be used for any fibrous assembly requiring (i) and (ii).

Table 1-1 Polymers applied in electrospinning, and their applications and characterization methods

Polymers	Applications	Characterizations	References
Poly(vinyl alcohol) & poly(acrylic acid) blends grafting from poly(amidoamine)	Water treatment membranes	SEM[a], TEM[b], *in vitro* antimicrobial activity analysis	Amariei, G. et al, 2017[72]
Poly(vinylidene fluoride) & poly(ethersulfone) blends	Oil/water separation	SEM, FTIR[c], TG-DTG[d], EDS[e]	Cao J. et al, 2017[73]
Zein	Food packaging	XRD[f], TGA[d], H^{-1} NMR[g]	Aytac Z. et al, 2017[74]
Poly(acrylonitrile-co-butadiene)	Filteration	SEM, Tensile Test	Zhang X. et al, 2017[75]
Lecithin & Poly(caprolactone) blends	Tissue scaffold	SEM, Water contact angle, Tensile testing, *In vitro* differentiation	Coverdale B. et al, 2017[76]
Cellulose acetate & poly(lactic acid) blends	Neural tissue scaffold	SEM, Water contact angle, *In vitro* degradation	Naseri-Nosar M. et al,2017[77]
Gelatin & oxidized phenolic compounds blends	Tissue scaffold	SEM, FTIR, XRD, DSC[h]	Tavassoli-Kafrani E. et al, 2017[78]
Sodium carboxy methyl cellulose-g-methyl acrylate & poly(ethylene oxide) blends	Drug delivery	ESEM[i], Water contact angle, FTIR, Antimicrobial activity, *in vitro* human fibroblast cell culture	Esmaeili A. ; Haseli M. 2017[79]

Polymers	Applications	Characterizations	References
Poly(caprolactone) & poly(lactic acid) blends	Dye removal	SEM	Sarioglu O. F. et al, 2017[80]
P(vinylidenefluoride-co-trifluoroethylene)	piezoelectric smart fabrics	SEM, DSC, Tensile testing	He, F. A. et al, 2017[81]
Keratin/4-Vinyl Benzene Boronic & Poly(vinyl alcohol) blends	Tissue scaffold	SEM, FTIR, *in vitro* cell culture	Deniz D. Y. et al, 2017[82]
Chitosan & Poly (ethylene oxide) blends	Compost leachate	SEM, Electrical Conductivity	Simonič M. et al, 2017[83]
Polyurethane & Tetra-butyl ammonium chloride blends	Waterproof breathable textiles	FESEM, Tensile testing, air permeability, water contact angles, moisture transport, washing resistance performance	Ju J. et al, 2017[84]
Poly(vinyl butyral)	anticorrosive dyeing enhancer	colorimetry, SEM	Yan X. et al, 2016[85]
Polyurethane & Nylon 66 blends	Waterproof Clothing	Tensile testing, SEM, air& water vapour permeability, Water contact angle	Amini G. et al, 2016[86]
Cross-linked gelatin & Poly(ethylene terephthalate) blends	Tissue scaffold	SEM, TEM, Mechanical testing	Pezzoli D. et al, 2017[87]
Poly(3-hydroxybutyrate), poly(e-caprolactone), silk, poly(lactic acid), polyamide, & Collagen	Tissue scaffold	SEM, cell compatibility *in vitro*	Castellano D. et al, 2014[88]
Poly(methyl methacrylate) & poly(ethylene glycol)blends	Wound dressing	SEM, water absorption capacity, surface hydrophilicity, *in vitro* drug release profile, and *in vivo* ant fibrotic effects	Poor Masjedi M. et al, 2016[89]

[a]Scanning electron microscopy.
[b]Transmission electron microscopy.
[c]Fourier transform infra-red.
[d]Thermogravimetric analysis.
[e]Energy-dispersive X-ray spectroscopy.
[f]X-ray diffractometry.
[g](Hydrogen) Proton nuclear magnetic resonance.
[h]Differential scanning calorimeter.
[i]Environmental scanning electron microscope.

1.5.3 Natural and synthetic polymers

Table 1-1 is an example of the variety of approaches that have recently received attention. Various polymers can be electrospun and their nanofibres can be used in various applications from bio-medicals to clothing. As extensively reported, bio-medical applications require materials with high biocompatibility and low

immunogenicity which can be simply fulfilled by biodegradable polymers such as natural polymers compared to synthetic polymers [90-92]. Typical natural polymers that have been extensively electrospun consist of collagen/gelatin, chitosan, cellulose acetate, chitin, casein, fibrinogen, and silk protein.

In general, electrospun fibres of natural polymers offer higher clinical functionalities. Among natural polymers, proteins display a high capacity of cell attachments as part of their intrinsic behaviour due to their reactive amino acid sequences, such as arginine, glycine, and aspartic acid [93]. However, chain degradation of natural polymers has been recently reported during electrospinning. For instance, collagen is a leading biopolymer that is used extensively in tissue engineering applications due to its excellent biological properties. Nevertheless, Zeugolis et al. denoted that electrospinning can significantly deteriorate the functionality of collagen [94].

Over 500 research papers published from 2015 to 2017, very few focused on electrospun fibres from pure natural polymers and about 10 to 15 percent used blended systems of natural polymers and semi-synthetic and synthetics (based on web of science core collection database). The main reason for this may be due to the lack of the required stability of natural polymer characteristics. The main reason may be the delicate structure of pure natural polymers that are likely to be easily degraded when encountering harsh processing conditions during electrospinning, such as highly polar solvents and elevated electrical instabilities. On the other hand, (semi)synthetic polymers can provide various advantages when compared with pure natural polymers since they can have a variety of stable properties such as required degradation rate (defined life time) and combined mechanical properties such as strength and elasticity [95].

To better understand collagen as one of the most important natural polymers, the next section deals further with its advantageous and challenges.

Collagen as a biopolymer in electrospinning

Collagen can be isolated and purified in large quantities. The physical, chemical, structural, and immunological properties of this biopolymer have been well defined. considering its physiochemical properties, collagen is biodegradable, biocompatible, non-cytotoxic, and can be processed into a wide range of features including cross-linked sheets, films, beads, fibres, sponges, and meshes [96].

Collagen has already found significant usage in biomedical materials, such as tissue scaffolds, burn and wound dressings, vascular grafts and drug delivery systems [97].

The diversity in collagen usages is due to mimicking the native tissue structures and also the similarities of this biopolymer in all living species [98]. More specifically, since the native structure of collagen is mostly found as fibrous network/filament/fibril, as shown schematically in Figure 1-6, the development of electrospun collagen can represent unique characteristics. For instance, How et al. (1992) attempted to perform electrospinning of collagen applying type I collagen of calf skin, Hexafluoro-2-propanol (HFP) as solvent and characterized with SEM and TEM. The electrospun collagen fibres were then suitable to be used for wound dressings and vascular grafts in vitro to closely mimic the native collagen network [99].

A comparative research on cross-linked and non-cross-linked electrospun collagen using glutaraldehyde as the cross-linking agent claimed that cross-linking as post-treatment can reinforce the mechanical properties of the electrospun fibres, however new challenges were encountered, such as increasing the diameter of collagen nanofibres and a dimensional increase of the scaffolds [100].

Furthermore, Matthews et al. attempted to control the deposition of the electrospun fibres on a grounded collector to simulate the 3D geometric placement of collagen fibrils in native tissues from aligned to random deposition, Figure 1-11. Due to the excellent inherent properties of collagen nanofibres, they believed that the electrospun nanofibres represent an ideal tissue engineering scaffold. They claimed that the collagen required to be selectively deposited to mimic the native tissue. Even though they observed a significant non-uniformity on the size of electrospun fibres, they suggested that the final shape adjustment of the accumulated electrospun fibres can be simply

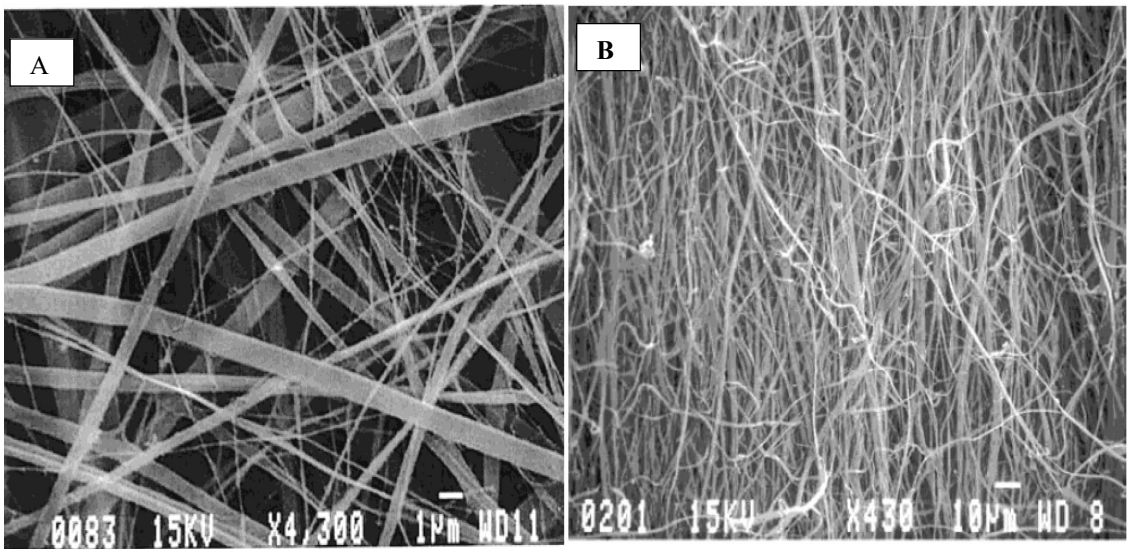

Figure 1-11 A) SEM image of random orientation of electrospun type I collagen from human placenta, fibre diameter ranges from 100 to 730 nm. B) SEM image of electrospun collagen type I calf skin collected onto a rotating drum at 4500 rpm.

accomplished by electrospinning. Also, they concluded that both the type and source of collagen have a direct impact on fibre morphology as concluded by the electrospinning process of isotype collagen (type III vs. type I) from the source (type I placental vs. type I calfskin) [101].

However, certain properties of pure collagen have been adversely influenced by poor dimensional stability, mechanical strength and low elasticity [102]. The need for enhancing mechanical properties, electrospinning of collagen has been practiced by blending with other compatible polymers in tissue engineering applications [103-105]. Even though blending systems can be simply electrospun, the electrospinning of collagen-based copolymers has received a little attention. The principal of copolymer electrospinning is dealt with in the following section.

1.5.4 Copolymer electrospinning

It is well established that copolymer electrospinning exhibits enhancement in desired properties in polymeric materials including tailored mechanical strength and thermal stability. As discusses in section 1.1.1, the copolymerisation method can produce new materials with desirable properties. For instance, the thermal properties of poly (methyl methacrylate) is enhanced through copolymerisation of Methyl Methacrylate and Methacrylic acid resulting in poly(MMA-co-MMA). This is due to the fact that the glass transition temperature (T_g) of poly (methacrylic acid) is higher than poly (methyl methacrylate) and it also shows a greater degradation temperature (T_d) due to formation of anhydride upon heating [106].

When this method is properly employed, the performance of electrospun materials from copolymers is considerably enhanced in contrast with that for homopolymers [67]. Furthermore, the feasibility of spinning from copolymers is one of the significant advantages over electrospinning which cannot be achieved simply through conventional spinning methods [95]. Copolymer electrospinning is applied for structural engineering applications through methods of copolymerisation when they are incorporated with organic/ inorganic fillers. In recent years, this aspect of copolymer electrospinning has received much attention that has the potential to extend the use of the electrospun fibres in more innovative applications. For instance, Zhang, et al. investigated the performance of electrospun poly (acrylonitrile-co-butadiene) elastic fibre mats in terms of pore diameter and permeability of NaCl nanoparticles from an aerosol flow. They focused on the optimisation of the elasticity of this copolymer to increase the performance of

filtration in terms of decreased pore diameter and permeability in both stretched and non-stretched conditions [75].

Alternatively, Cheng et al. [73] developed a novel copolymer investigation on a graft polymerisation method resulting in poly (vinylidene fluoride)-g-poly (acrylic acid). The resultant copolymer was then electrospun into a unique tree-like morphology. They suggested that poly (vinylidene fluoride)-g-poly (acrylic acid) can exhibit pH-responsivity from its poly(acrylic acid) segment while the poly (vinylidene fluoride) segment can submit an ultrahigh specific surface area of the membrane (branched fibres from trunk).

In biopolymers, when hydrophobic bio-polyesters are incorporated with a proper hydrophilic polymer segment, they can represent a significant increase in cell attraction [67]. Apart from tissue engineering applications, other physical properties are tailored such as structure, morphology, pore size and distribution, mechanical properties, and biodegradability by using copolymers in electrospinning. Among them, reinforced mechanical properties may be the most studied aspect of copolymer electrospinning in biopolymers [67, 107, 108].

For instance, Kai et al. [109] illustrated that the electrospinning of lignin copolymerisation can be considered as an effective approach for enhancement of the functionality of lignin. Hence, they synthesised a series of lignin-based copolymers (lignin-poly (ε-caprolactone-co-lactide)) via solvent-free ring-opening polymerisation; copolymers were then processed into nanofibres. This approach was not only to enhance the processability of the lignin through copolymerisation, but also the nanofibres of copolymers benefit from higher mechanical properties of the bio-polyester segment.

1.5.5 Effects of electrospinning parameters on fibre morphology

A typical electrospinning process is conducted by various parameters that are generally categorised into solution, process, and ambient parameters. Solution parameters comprise conductivity, surface tension, viscosity, and molecular weight. Process parameters consist of applied electric voltage, tip to collector distance and flow or feeding rate, and ambient parameters of relative humidity and temperature. Each of these parameters can considerably influence the fibre morphology achieved through electrospinning. Effective adjustment of these parameters is done to result in nanofibres with desired morphology and diameters. In Table 1-2, electrospinning parameters and their corresponding effect on fibre morphology are illustrated.

1.5.5.1 Processing parameters

(a) Applied voltage

The applied voltage is the most important component in the electrospinning process that differentiates it from conventional spinning methods. When reaching the threshold voltage, the electrospun fibres start to be formed. In fact, the applied voltage provide the essential charges to the polymer solution to jet towards the low dipole energy.

Table 1-2 Electrospinning parameters and their effect on electrospun fibre morphology.

Parameters	Effect on fibre morphology	References
Process parameters		
Voltage (Electrostatic)	Reduction in fibre size and distribution with increase in voltage.	Shin et al.[110]; Demir et al.[111];
Distance between tip and collector	Uniformity of fibres in optimised TCD; bead formation in too small and too large TCD	Ki et al. [112] ; Geng et al. [113]; Buchko et al. [114]; Zhao et al. [115]; Zhang et al. [116]
Polymer feeding rate	Decrease in fibre diameter with flow rate reduction, bead formation with too high flow rate.	Sill and Recum [117]; Zhang et al., [118]; Zhang et al.[119];
Solution parameters		
Conductivity	Reduction in fibre diameter with increase in conductivity.	Nayak et al.[120], Sun et al., [121] Okutan et al. [122]
Surface tension	High surface tension leads to instability of jets; no certain relation with fibre morphology.	Shin et al., [110]; Zhang et al. [118]
Viscosity	Highly increased fibre diameter, low-beads/ bead free fibre formation with increase in viscosity	Nayak et al.[120], Zhang et al., [118], Zhoa et al.[123] Zong et al. [18, 124] Son et al. [124]
Polymer concentration	Increased fibre diameter from increased concentrations	Heider et al.[125], Zong et al.[18], Kim et al., 2005 [126]
Molecular weight of polymer	Decrease in the volume of beads and droplets with increase in molecular weight.	Gupta et al., 2005; [127] Law et al., 2017 [91], Gong and Wu, 2012 [128]
Ambient parameters		
Humidity	Circular pores on the fibres result from high humidity	Bak et al [129], Li and long [130], Li and Xia [131]
Temperature	Increase in temperature results in decrease in fibre diameter.	Reneker and Chun [132]

There is no disagreement about the effect of applied voltage on the electrospinning process when the intensity of the electric field leads to fibre formation. Even though, in most cases, it is believed that an increase in the intensity of the electric field causes a significant decrease in the diameter of electrospun nanofibres as well as a rapid evaporation of solvent, Renekar and Chun [132] claimed that the intensity of the electric field has no significant effect on the fibre diameter in electrospun poly (ethylene oxide). They also concluded that higher applied voltages can lead to more ejected polymeric chains and this may induce a higher fibre diameter.

This viewpoint has been further investigated by some other researchers referring to the effect of higher voltages on producing even more bead formation [114, 118, 133]. Thus, it is obvious that applied voltage clearly affects fibre diameter, but the impact of this concept can simultaneously be in interaction with other parameters affecting the morphology such as solution properties and the distance from tip to collector.

(b) Tip to collector distance

The tip to collector distance is considered as an important parameter to control the fibre morphology; it gives the polymer jet the opportunity to stretch while the solvent evaporates away or while the fibre hardens in the case of a polymer melt. This distance should be optimised to provide the fibres enough time to be solidified before accumulating on the collector. Otherwise, beads can be perceived with collections that can be either too close or too far [112, 113].

However, there are some conflicting viewpoints that the influence of the tip to collector distance on fibre morphology is not as important as other parameters and this has been observed in electrospun poly(vinyl alcohol) fibres [118], electrospun fibres of gelatin [112] and electrospun fibres of chitosan [113]. Nevertheless, Buchko et al. suggested that smoother two dimensional electrospun fibres can be fabricated with smaller tip to collector distances, whilst for increased tip to collector distances the accumulating fibres tend to be curve shapes [114]. In brief, there should be an optimal tip to collector distance to help solvent evaporation from the electrospun fibres.

(c) Flow rate/ Feed rate

The feed rate of the polymer solution/ melt from the syringe is a key parameter since it provides a required polymer concentration to the spinneret. It can affect the polymer jet frequency and phase transition rate (liquid to solid). Typically, It is reported that the pore size and fibre diameter increase with increased polymer feed rate [134] and also it is reported that high feed rates lead to beaded fibres due to the lack of sufficient solidifying time prior to accumulation [67, 135].

However, there is high agreement that lower feed rates are more favourable since the solvent has enough time to evaporate away or in the case of the molten polymer jet, more hardening occurs [67], even though this can simply increase the process time.

(d) Type of collector

The type of collector is another important factor in the electrospinning process. The collector is typically a conductive substrate to attract the electrostatically charged fibres; aluminium foil is generally used as a collector. The difficulty of transferring of the delicate fibres; and the necessity of patterned fibres for some applications, other types of collector such as conductive fabrics, conductive papers, pins, wire mesh, rotating cones, rotating rods, rotating drum, rotating wheels, parallel bars, and also coagulation bath such as water, methanol, and ethanol have been explored [71, 119, 136-143].

The idea may be that less surface area of conductive collector can have distractive effects on fibre collection such as bead formation or uneven fibre distribution. In a comparative study, Eda and Shivkumar used an aluminium foil and a wire screen of the same dimensions; they received better functionality from the wire screen. Also, they have shown that less surface area can facilitate fibre transfer to other substrates [144].

Generally, the functionality of nanofibres can be determined by the design of a collector which causes geometric fibre shaping and patterning. For example, Wang et al. evaluated three different predesigned collectors of static copper wires, rotating mandrel and rotating drum. From the morphology and the alignment of fibres, they revealed that poly (ε-caprolactone) nanofibres can be achieved with ordered pattern and architecture. Also, form their observations, they realised that the lesser fibre diameter is achieved from the rotational speed while the random fibre orientation is obtained at 0 rpm; this can be because of mechanically stretched fibres using rotating drum that produces more fibre alignment with increasing the rotation speed [140].

Furthermore, Bazbouz and Stylios testified [145, 146] a technique that can produce a bundle of aligned electrospun fibres of Nylon 6 suspended between two grounded disks. Similarly, Depra et al. introduced high fibre alignment from poly (ε-caprolactone) using split electrodes. Typically, those collectors include two conductive surfaces or blades separated by a distance where aligned nanofibres are deposited. Hence, the fibre alignment is a factor that is determined by the collector and its rotational speed which is used by many research groups in different fields, using rotating drums or rotating spindles [137].

Even though artistic patterns are being mentioned in some approaches, enhancing the mechanical properties of nanofibres is the most studied aspect when anisotropic

properties of nanofibre mats are tailored. This result has been mostly achieved through fibre alignment using rotating collectors [66, 147-150].

1.5.5.2 Solution parameters

(e) Electrical Conductivity; surface chargeability density

Polymers show electrical conductivity with some exemptions of dielectrics. Polymers generally provide a higher mobility within the solution electron phase [120, 151]. In electrospinning, the conductivity of a polymer solution/melt is mostly determined by the polymer type, the solvent (if required) and also the presence of fillers such as ionised salts. It is commonly reported that electrospun fibres with a lower fibre diameter can be achieved from the high electrical conductivity of solutions/melts in contrast with fluids in low electrical conductivity that may induce a poor polymer jet orientation [151, 152].

Obviously, the types of polymers significantly affect the electrical conductivity of a polymer solution/melt. Since polyelectrolytes release counter-ions in solution affecting the ionic strength of the solution, polycations and polyanions are electrically conductive in solution. It is well known that natural polymers such as proteins are mostly polyelectrolytic [67, 153]. For instance, Li et al. reported that reduced fibre diameter can be achieved by using proteins such as collagen and gelatin (denatured collagen) as compared to some synthetic polymers [29].

Also, the charge density of the polymer jet is strongly affected by increased ions in solution, thus subjecting the polymer jet to higher tension with increasing intensity of the electric field. For the first time, Zong et al. evaluated the effect of ions by considering the presence of ionic salts such as NaCl and KH_2PO_4 on the diameter and morphology of electrospun fibres of poly(D,L-lactic acid) and poly(L-lactic acid) [18]. However, it has been also reported that highly conductive solutions cannot be stable in strong electric fields resulting in varied bending instability of polymer jets and wide fibre diameter distribution thereafter [110, 142, 154, 155]. So, it seems that there is little agreement on the concept of higher conductivity leading to better performance on morphology. This claim has been proved by a set of similar mathematical modelling of varied polymers performed by Yarin et al. and Shin et al. They emphasised that the correlation between feed rate and rheological behaviour of polymer solution/melt can control the morphology of the electrospun fibres along with increased conductivity [110, 155].

(f) Surface tension

Obviously, the solvents play a key role in the surface tension of the polymer solution. In fact, bead free fibres can be formed by reducing the surface tension of the polymer

solution/melt. According to Haghi and Akbari , since lower surface tension of a fluid accelerates the process at a lower intensity of the electric field, then fibres, droplets and beads can be formed as a function of surface tension [133]. Nevertheless, the certainty of a lower surface tension of a fluid is not always desirable since this parameter can be compensated by other electrospinning parameters altering their upper and lower boundaries [116, 156].

(g) Viscosity and concentration

Viscosity of the polymer solution/melt is one of the most important parameters determining fibre morphology. However, it seems that this parameter is more significant in melt electrospinning, when the polymer concentration determines the viscosity of the electrospinning solution [120, 157]. In the electrospinning process, fibre formation basically requires a minimum solution concentration, which can start with a mixture of beads and fibres at low concentrations, and with an increase in concentration uniform fibres with enlarged diameters are formed. At very high viscosity/concentration, polymer solution/melt typically leads to extended relaxation times, modulus of elasticity and the entanglement viscosity, which can prevent the bending/whipping of the ejected polymer jets during electrospinning. Therefore, the increase in viscosity and concentration can significantly increase the diameter and the uniformity of the fibres [112, 155, 158, 159].

(h) Molecular weight

Obviously, polymer molecular weight plays a key role on the rheological behaviour of the polymer solution/melt, such as surface tension and viscosity, indirectly impacting the electrospun fibre morphology [133]. For instance, Gupta et al. synthesised a linear homopolymer of poly methyl methacrylate in various molecular weight from 12,470 to 205,800 $g.mol^{-1}$ to explore the effect of molecular weight. They noticed that the number of droplets and beads decreased with an increase molecular weight [127].

However, it has also been considered that high molecular weight polymers are not necessarily required in the electrospinning process if complementary intermolecular interactions such as hydrogen bonding can provide the required chain entanglement. Applying this principle, scientists have electrospun oligomer sized polymers, such as phospholipids from lecithin, into nonwoven mats [160-162].

1.5.6 Applications and prospects of electrospun nanofibres

Recently, researchers have considered the functionality of electrospun fibres in the shape of single fibres, aligned fibres, nonwoven mats and twisted yarn, as these provide

several advantages over conventional spinning methods. As mentioned above, a wide range of polymers can be electrospun into nanofibres with high surface to volume ratio and high porosity by using electrospinning. In fact, the manipulation of the solution and process parameters can be easily implemented to achieve desired fibre morphology for specific end uses. Electrospun fibres have applications in biotechnology, tissue engineering, wound healing, drug delivery systems, vascular graft implants, filtration, defence and security, protective clothing, energy storage and harvesting, optical sensors, environmental engineering and in many other areas [156, 163]. According to Bhardwaj et al. [67], we can see substantial more research in the medical and biotechnology fields and then the filtration applications when compared to other kinds of research.

For development of the electrospun fibres, various new innovations are being applied based on coaxial electrospinning, mixing and multiple electrospinning. Coaxial electrospinning is used to fabricate nanofibres from two polymeric systems by a coaxial spinneret; then the core of fibres is filled with one polymer while the shell is formed by the other polymer [164].

The coaxial electrospinning method facilitates some problematic polymers which are difficult to process individually. By *in-situ* integration of polymer materials in the radial and axial directions, this methodology provides a high possibility to achieve novel properties and multi-functionalities for nano-scale applications. However, for development of the properties of nanofibres, there is a variety of ongoing research to scale up this process. In the future, nanofibres will be used in an ever wider range of applications projecting physiochemical properties. Using copolymerisation methods and *in-situ* polymer mixtures can be implemented to obtain developed properties in electrospun fibres, for instance. And, upscaling production is an area that significant research progress needs to take place in future.

1.6 The aims and project objectives

Purified collagen, as a super hydrophilic biopolymer, represents a lack of sufficient mechanical strength and unstable degradation due to properties lost during dissociation of cross-linked chains in isolation processes. Among the drawbacks of isolated collagen molecular chains (collagen chains), reinforcing the mechanical properties of collagen turns out to be a significant challenge. This issue becomes more important when tailored applications aiming to benefit from the inherent advantages of this biopolymer become not successful.

Another basic requirement of collagen is to have a stable and predictable degradation rate. Previous research suggested that the degradation rate of purified collagen is much faster than that for the native tissues [165-169]. To control the super-hydrophilicity and the degradation rate of the purified collagen chains, reducing the hydroxyl group on the collagen chains is inevitable [170, 171].

1- Hence, to reduce the hydrophilicity, collagen can be modified by a graft polymerisation method in which a variety of monomers can be randomly branch over the surface of collagen chains. Hence, the modified collagen can benefit from a newly achieved structure while receiving some of the physiochemical properties of grown branches, such as thermal and mechanical. Graft polymerisation onto collagen chains has been of interest to several research groups since 1972 considering the polymerisation parameters with various monomers having the vinyl group in their unit structure [172-175]. This method is basically applied for the production of hydrogels; the hydrogel should then display water-swelling behaviour. In fact, when the collagen chains are covalently bonded with hydrophobic materials as side branches, they prevent the hydrophilic main chain from dissolving.

2- However, when using the final product of a polymerisation system is aimed, the processability of the product should be also evaluated. We modified the surface of isolated collagen chains via graft polymerisation as pre-treatment and then considered the processability of the collagen graft copolymer to promote its features and properties. Hence, the collagen graft copolymer was electrospun using a typical electrospinning method. We hypothesised that the electrospun fibres from a branched structure of collagen graft copolymer exhibit advantages over fibres formed from pure collagen chains for specific end uses.

   Branching on collagen chains allows (1) control of branching density for tailored degrees of water absorption, (2) control of degradation for specific end-uses, (3) control of the chain entanglement in low concentrations, (4) additional end tails and functional groups that can potentially expand corresponding applications to deliver or attract target materials which are typically used in drug delivery systems or smart filtrations.

   Hence, one of the primary research objectives is to understand the influence of branching on fibre formation from the collagen graft copolymer, and the rheological/electrospinning relationships of the branched chains, which enable us to engineer the required functionality of collagen.

3- The other main objective of this research is the mechanical reinforcement of the fibres from the graft collagen copolymer when can be processed by coaxial electrospinning. In fact, a reinforcing agent was selected from typical well-identified polymers with a linear semi-crystalline structure (Nylon 66) which can be optionally replaced with any linear bio-polyester such as poly (ε-caprolactone). The coaxial electrospinning set up is like that of typical electrospinning, with the exception of the coaxial needle that is used as a spinneret. Both outer and inner capillaries are linked to a high voltage power supply simultaneously and the nanofibres are combined during solvent evaporation, bending, and stretching. The viscosity, surface tension, conductivity and feed rate of the two fluids affect the stability and uniformity of the polymer jet. The custom built nanofibres from the core-shell composite structure can then have the advantages from both components at the same time. The hydrophilic segment swells in contact with the moisture source, whilst the core material deliver relatively high mechanical strength.

4- The last main research objective is to understand the effect of nanofillers on grafting parameters such as grafting performance and grafting efficiency [169]. Nanofillers, due to their large surface-to-volume ratio, allow them theoretically have higher interactions with the polymer matrix. The newest class of 2-dimensional carbon based nano-sheets, graphene oxide, was used to study its interaction with collagen as the host polymer in branching. To the best of our knowledge, the effect of nanofillers, such as graphene-based nanofillers in improving the performance of in-situ polymerisation has not received any attention. During graft polymerisation, graphene oxide nanosheets provide numerous functional groups to be joined by initiated collagen chains as well as macromonomers. As a mechanical reinforcing agent, the presence of graphene oxide can be the most beneficial approach for collagen graft nanocomposite. This study was not limited to composite nano-layers, we also studied more challenging systems in which the collagen graft nanocomposites were electrospun into nanofibres.

Hence, the thesis in hand represents a novel approach to fabricate (co)electrospun fibres from collagen-based materials since collagen is available in huge quantities from animal by-products. Approaches tailoring the performance and spinnability of the modified collagen are proposed based on the fact that the field of textiles sits in the intersection of the disciplines of polymer and fibre science. In this research, reinforced mechanical

properties, thermal stability and water resistance of the electrospun fibres are considered. The characterisation of the findings is evaluated considering the influence of branching and intermolecular interactions. Hence, we are determined to introduce a novel approach that adds new knowledge to fibre spinning of collagen graft copolymers/composites.

After the introductory chapters (1-3), the thesis is arranged as follows:

In chapter 4: *Synthesising and characterization of copolymerisation of methyl methacrylate-co-ethyl acrylate onto collagen*

In polymers, and particularly in natural based polymers, it is essential to modify their properties to desired specifications. The natural based polymers are very attractive to provide new materials and applications with specific properties. This is due to their diverse variations in type and availability, modification methods, final processing etc. [176-178]. Grafting polymerisation as one of the most promising modification for biopolymers, is a technique in which the surface of the main backbone is modified through covalently bonded monomer(s) that introduced onto its chain [142, 179].

In this chapter, collagen was solubilized by acid treatment. Subsequently, binary different vinyl monomers of Methyl Methacrylate (MMA) and Ethyl Acrylate (EA) in a varied feed ratios were grafted onto the acid soluble collagen (ASC) with the aim of benefit from the amphiphilic behaviour along with the firmness and the plasticizing capacity of the resultant copolymer. The branched structure of modified collagen was then characterised due to the presence of more than two end groups, which comprise a class of collagen-based copolymer between its native structure and polymer networks, typically achieved by cross-linking methods.

In chapter 5 and 6: *Investigating the electrospun fibres of Collagen-g-poly(Methyl Methacrylate-co-Ethyl Acrylate)*

Due to the varied branching density that grown on the backbone of collagen, any change in viscosity of the electrospinning solution can significantly affect the processability of the collagen graft copolymers. Therefore, the effect of different branch densities of copolymers grown on collagen graft copolymers was investigated by electrospinning as a processing method. The fibre formation/processability of dissolved collagen graft copolymers having an optimised viscosity was evaluated by using response surface methodology. The electrospun fibres of collagen graft copolymers were then investigated in terms of surface characterisations, such as morphology, thermal stability, and hydrophilicity.

In chapter 7: *Enhancing the mechanical properties of Acid Soluble Collagen-g-poly (MMA–co–EA)/Nylon 66 Formed by Coaxial Electrospinning*

Electrospun fibres can be collected in the form of a textile (overlay bundles), where the fibres are oriented parallel to the direction of the rotation of targeted collecting point. In this chapter, the collagen graft copolymer was used to take advantages of the branched structure of polymer chains providing high chain entanglements. The coaxial electrospinning method was utilised to study the effect of electrically and structurally varied materials on fibre formation and fibre morphology when the collagen graft copolymer and Nylon 66 were electrospun as the shell and the core components, respectively. This was for studying the effect of the electrostatic field on fibre contents and the associated properties.

Furthermore, the alignment and the core-shell composite structure of the electrospun fibres were tailored to reinforce the mechanical properties of the composite fibres. Full characterisation of chemical, thermal, and hydration degree and degradability of the produced fibres was implemented, where the electrospun fibres benefitted from complementary bonding between the core and the shell components. Mechanical characterisation including Stress-strain curves and the deformation mechanism were investigated.

In chapter 8: *Investigating high performance of covalently grafting onto collagen in the presence of Graphene oxide (GO)*

Undesirable polymer chains can be formed unavoidably in many polymerisation reactions, including grafting polymerisation. This can significantly affect the final product performance and efficiency when undesired by-products are formed in significant quantities. This chapter aims to facilitate the decision making for various applications in ordFer to benefit from the modified collagen through graft polymerisation methods where the high performance of grafting copolymers is achievable through the presence of nanofillers.

Hence, this study was performed with the presence of purified collagen, graphene oxide nano-sheets, and binary monomer mixture of methyl methacrylate and ethyl acrylate (MMA–co–EA). Graphene oxide was used as nanofiller, and the effect of graphene oxide loadings was investigated in the performance and efficiency of the grafting of collagen copolymer, ASC-g-poly(methyl methacrylate-co-Ethyl Acrylate). The processability of the achieved nanocomposite was then evaluated through casting and electrospinning processing methods. The physiochemical properties were studied to

better understand the effect of the presence of graphene oxide content in collagen graft nanocomposites. To modify the collagen, this research highlights the importance of introducing functional groups of graphene oxide and substitution of graphene oxide loadings as an active nanostructure filler to high monomer feed ratios for improving the physiochemical properties of collagen. This approach is important for applications requiring reinforced mechanical properties and limiting degradation rate of collagen-based nanocomposites.

Chapter 2 The effects of factors on the spinnability of collagen chains: Literature review

One of the most important and essential aspects in material development is the selection of a starting material; one is highly available and to some extent achieves added value when processed. Collagen is one of the most abundant biopolymers that can be selected within biomimetic materials [97, 180-182]. Collagen is typically found in fibrous tissues such as tendons, skin, and ligaments, which comprise about one half of total body. It is also abundant in cartilages, bones, corneas, gut and blood vessels [97]. Thus far, 29 types of collagen have been recognized and categorised. Among them, type I forms over 90% of the collagen of the body, which is commonly found in tendons, skin, bones, ligatures, vascular, and organs; even though these statistics can differ with age and injuries [183].

It is widely in agreement that collagen provides mechanical stability, strength, and elasticity to native tissue and it is the main structural material in biology. As shown in Figure 2-1, a collagen fibril is fully constructed from the biochemical details of the

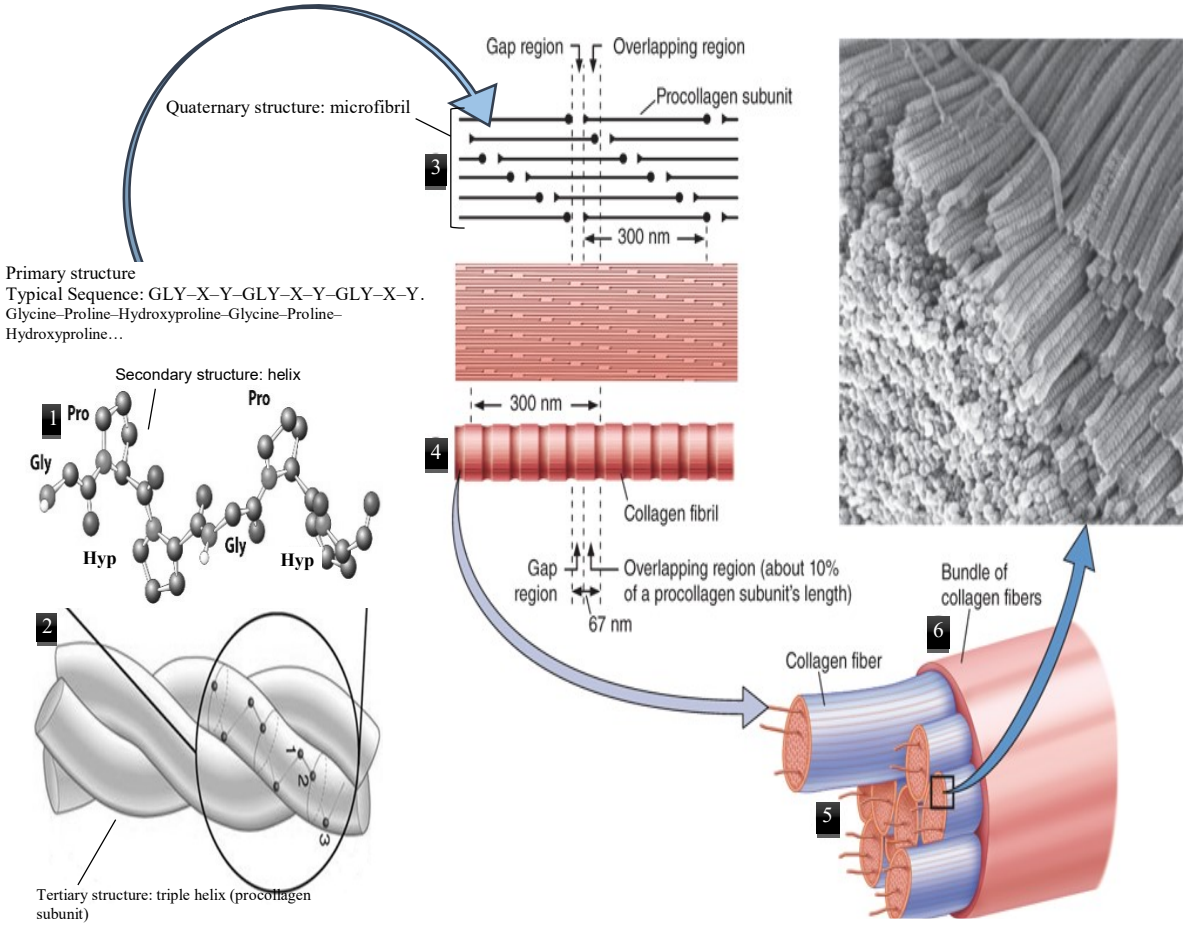

Figure 2-1 Structural hierarchy of collagen fibrils (adopted from Ref. [13, 14] .

amino acid sequence from structural polymers and nanoscale chain arrangements.

According to Gautieri [184] et al., the fully hydrated collagen fibrils exhibit Young's modulus of about 300 MPa and 1.2 GPa for deformation strain of less and more than 10%, respectively. The dehydrated collagen fibrils represent a considerably increased Young's modulus of about 1.8 to 2.25 GPa due to tighter molecular packing. However, from their experimental data and numerical analysis, they suggested that the mechanical strength of collagen fibrils are caused by the hierarchical structure of the collagen fibrils in the nanoscale, where the deformation mechanism comprises the straightening of twisted triple-helical collagen chains and then axial stretching followed by chain uncoiling [184].

This claim has been studied by some other research groups confirming the strength of collagen that is induced by the hierarchical makeup of the collagen chains [13, 185, 186]. However, it is widely accepted that uncoiled collagen chains (α- chains) in the primary and secondary structures cannot provide the required mechanical functionality for native tissues [187, 188].

In fact, uncoiled collagen chains are the product of the purification and isolation process that is being used as the pure collagen, Figure 2-2. More specifically, collagen can be readily isolated and purified in large quantities. As shown schematically in Figure 2-3, pure collagen is typically prepared by alkaline or acid hydrolysis of animal skin and bones. The collagen chains are biocompatible, non-cytotoxic, biodegradable, and can be processed into a variety of shapes including fibres [96].

Despite the fact that pure collagen loses its properties induced from the hierarchical structure in native tissue, the unique physiochemical properties from α- chains are still present in the degraded collagen. For instance, due to the similarities between the collagen chains and the natural wool, it can enhance the dyeability of other biopolymer such as cellulose when they are spun as a composite viscose rayon filament [189]. Also, collagen chains can be used for water treatment due to the high reactivity of this protein with the colorants/ pollutants normally used in textile industries [190] These two examples emphasise the excellent properties of this biopolymer that can be used in applications where the properties of collagen end groups are tailored.

To mimic the structure of collagen fibrils in native tissues, collagen-based fibrous assemblies received extensive attention. Even though the amount of collagen and its derivations being used in textile applications is far away from expectations, this versatile biopolymer has already found considerable usage in biomedical fibrous membranes and in clinical treatments over the past decade, such as in drug delivery

systems, wound and burn dressings, heart valves, nerve regeneration, ocular surfaces and vascular grafts [97]. Hence, in this review, we are to deal with recent successful collagen-based fibre spinning. The effect of modification methods, process conditions, and the source of the collagen will be considered in relation with the spinnability of this biopolymer.

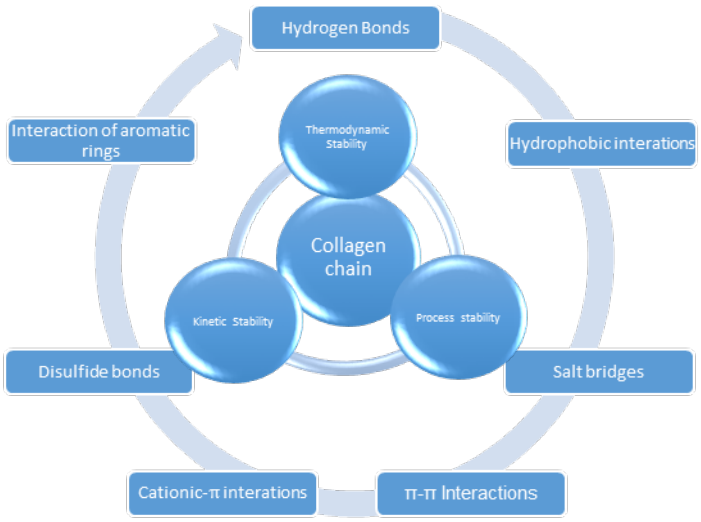

Figure 2-2 Summary of intramolecular bonds available in hierarchical arrangements affecting the process, kinetic and thermodynamic stability of the collagen chains as a protein [191, 192].

2.1 Modification methods

As the collagen chains represent poor mechanical strength, low dimensional stability, reduced elasticity, and also high degree of hydration and eventually rapid degradation, they are subjected to modification methods [99]. Apart from the severity of these drawbacks affected by the extraction and processing methods, this biopolymer has not been recently processed individually free from modifications as either pre– or post–treatments. To stabilize collagen chains into an engineered biopolymer, the modifications is applied due to compromising a variety of biological and physicochemical properties of the collagen chains [98, 190]. So far, the spinability of this polymer has been explored by using four possible approaches as modification methods: cross-linking, blending, grafting and conjugating.

2.1.1 Crosslinking modification approach

Many studies have been dedicated to the crosslinking modifications, which mostly aim towards reducing the super hydrophilicity of collagen fibres, Figure 2-4. In these methods, fibres comprise more collagen chain contents. However, non-uniformity in

cross-linking is more likely to occur since this method is mostly applied as post-treatment onto the already formed fibres. Also, the fact that the unavoidable addition of unreacted toxic agents may exist in the final product, becomes challenging and compromises specific end-uses [191]. For instance, Aldehydes such as glutaraldehyde (GTA) and formaldehyde (FA) are bi-functional reagents, which are typically used to chemically modify polypeptides and polymers for various applications due to its high reactivity, availability and low cost [192-195].

They covalently bond to amino acids but can also bind to other similar chains, increasing the non-uniformity in cross-linking. The direct usage of high concentrations of aldehydes may prove challenging for fibres to be used in hygiene and medical products. Also, due to low level of cross-linking of the aldehydes in low concentrations, the performance of the fibres from poly-peptides are likely to be reduced by low uniformity of cross-linked amino acid chains [192]. To eliminate the effect of toxic cross-linking agents in collagen-based fibres, cross-linking with sugars (e.g. Genipin) for pharmaceutical applications has been also used, which can also boost the water resistance and mechanical strength [196, 197]. This non-permanent reaction is regarded as the Maillard reaction, which is a reversible chemical reaction between sugars and amino acids; this reaction only makes physical changes in the polypeptides [198].

The zero-length cross-linker 1-ethyl-3-(3-dimethylaminopropyl) carbodiimide (EDC) in combination with *N*-hydroxysuccinimide (NHS) are also the other common crosslinking agents that make the collagen cross-linking possible through catalyzing covalent bonds between amino groups and carboxylic acid [199, 200]. Again, other components containing carboxyl groups, such as glycosaminoglycans, can also be cross-linked.

In addition, Transglutaminase (TGase) is a highly specific enzyme catalyzing collagen cross-linking between intra- and inter-chain glutamine and lysine peptide residues in collagen structures with the release of ammonia, but this method only targets specific amino acids [201]. To examine the functionality of the cross-linked collagen-based fibres, Huang et al. [196] used four different cross-linkers; GTA, Genipin, EDC, and NHS. They observed varied physical properties and biological behavior on fibres from different cross-linkers: e.g., the fibre morphology of fibres vanished with GTA; Genipin preserved the fibres architecture only for a short time period and crosslinking with an EDC-NHS combination showed better results in preserving the fibre morphology after process optimization.

There are also some other post-treatment (e.g. UV radiation, gamma radiation, dehydro-thermal treatment) identified as physical treatment for collagen cross-linking [202].

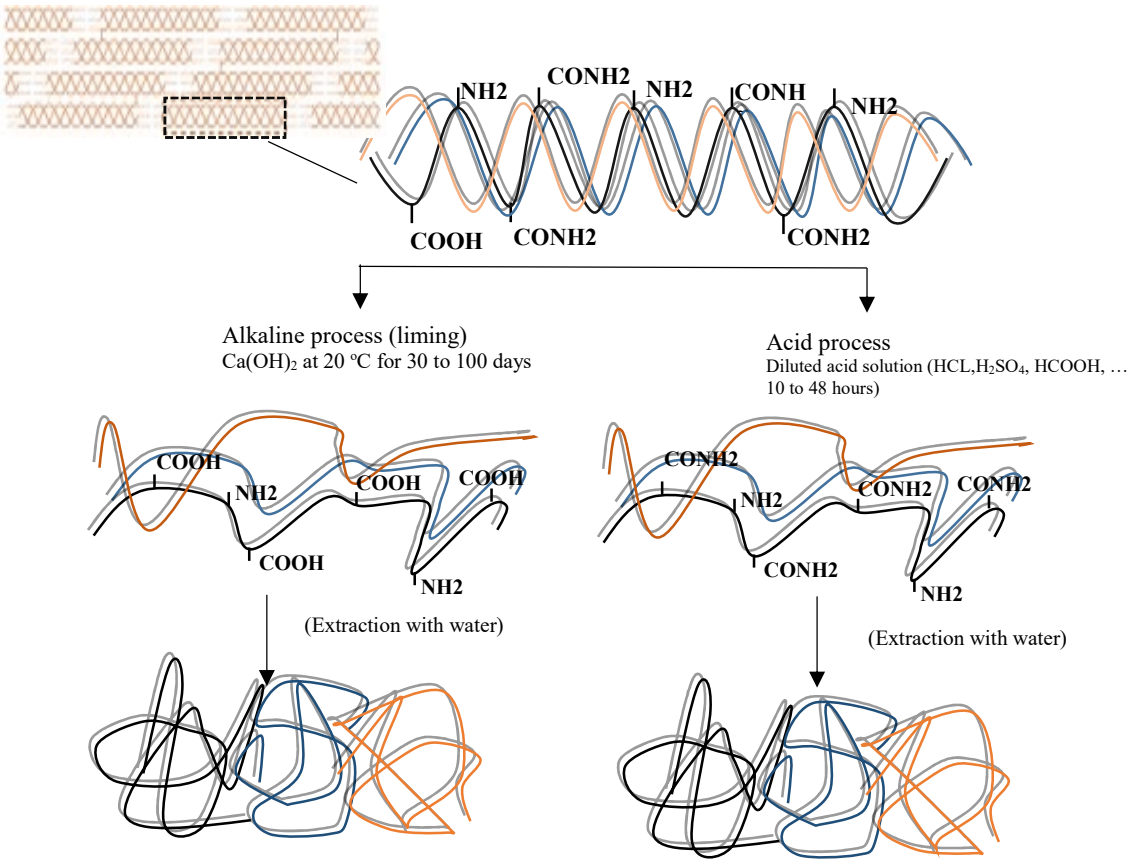

Figure 2-3 Common methods used for extraction of collagen chains consisting of Alkaline and Acid treatment [6].

According to Tonndorf et al. [191], it was evaluated whether riboflavin-induced photo-crosslinking could be used as a non-toxic alternative to glutaraldehyde (GTA)-crosslinking for the preparation of wet spun collagen filaments. They successfully concluded that the combination of riboflavin and UV light leads to cross-linked collagen filaments as GTA does. Furthermore, riboflavin cross-linked filaments exhibited a higher cytocompatibility for human mesenchymal stem cells compared to GTA-crosslinked filaments.

Interestingly, to enhance the mechanical strength of the collagen fibres, there are some efforts applying epoxy compounds used as cross-linkers to be processed along the collagen chains as a polymer matrix or coat the superficial surface of the processed collagen chains [203]. Cross-linking with epoxy compounds such as ethylene glycol diglycidyl ether, diglycerol triglycidyl ether and allyl glycidyl ether, has been claimed to maintain good biocompatibility while enhancing mechanical properties and water resistance [203, 204]. However, the reaction of collagen chains with epoxy compound, and their temperature and pH dependence, by the reduction of the primary amine groups (NH_2) as a function of time is the matter of fact that can increase the processing time [205, 206]. This claim was examined by Stoessel et al. [207] when they applied a

complex blending system including a set of polymers and cross-linking agent (ethylene glycol diglycidyl ether, EGDE) to achieve cross-linked fibres while wet spinning, as shown in Figure 2-5. However, they recommended that to achieve more stable fibres in unstable humidity, double-cross linking is required as post-treatment; Heat-treatment improves the water-resistance of the prepared fibre cross linked by epoxy compounds followed by post treatment of FA and Fukai et al. [193] also suggested that heat treatment, gamma-Irradiation and treatment with GTA improve the stability of the collagen fibres.

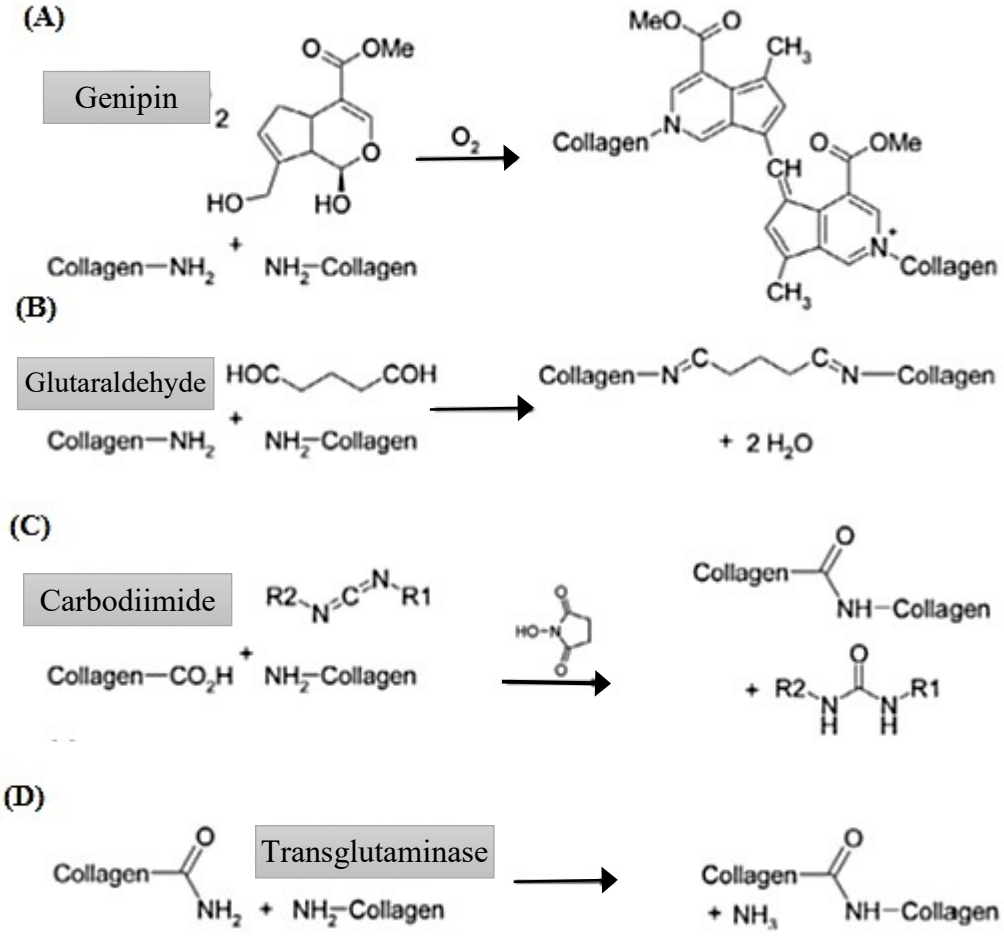

Figure 2-4 Collagen cross-linking reactions [206].

Although this approach has received a great attention from conventional fibre spinning methods such as wet spinning and gel spinning [192, 193, 207], to the best of our knowledge, considerably fewer studies have been dealt with this cross-linking approach processing via typical electrospinning method; this can be due to the viscosity change happening during the processing in high concentrations of epoxy compounds.

In general, any physical/chemical post treatment may produce a low degree of cross-linking, as the reaction is likely to only happen on the surface of the fibres, whilst a chemical treatment may lead to toxic compounds as undesired by-products, and hence less appropriate for medical applications. Therefore, any crosslinking method has its own limitations, from their toxicity and non-stability to non-uniformity in their performance. Also, from our understanding, apart from the functionality and performance of each cross linking agent, the cross-linking process when is applied individually as post-treatment and the sole modification method on spun fibres, it is difficult to be controlled as a function of exposure time, temperature, and concentration simultaneously, and may affect the morphology and hydrophilicity of spun fibres.

2.1.2 Blending modification approach

Researchers have also focused on blending systems of electrically and structurally compatible polymers to enhance the physiochemical properties of collagen fibres. For instance, Sionkowska et al. [208] characterised the intermolecular interactions of collagen and chitosan blends as Polycations. They found that the hydrogen bond forces between the collagen and chitosan resulted in the collagen-chitosan blends to be miscible and spinnable simultaneously. This example has been studied by several research groups using different processing method; for the first time Hirano et al.[190] investigated the wet spun collagen-chitosan and Chen et al. [209] also examined the spinnability of collagen-chitosan blends through electrospinning to enhance the mechanical properties of collagen chains. From their results, the optimum biological and mechanical properties were reached in lower collagen contents when the ratio of collagen-chitosan was 1:4. From the above-mentioned examples, a blending system can be useful for mechanical reinforcement.

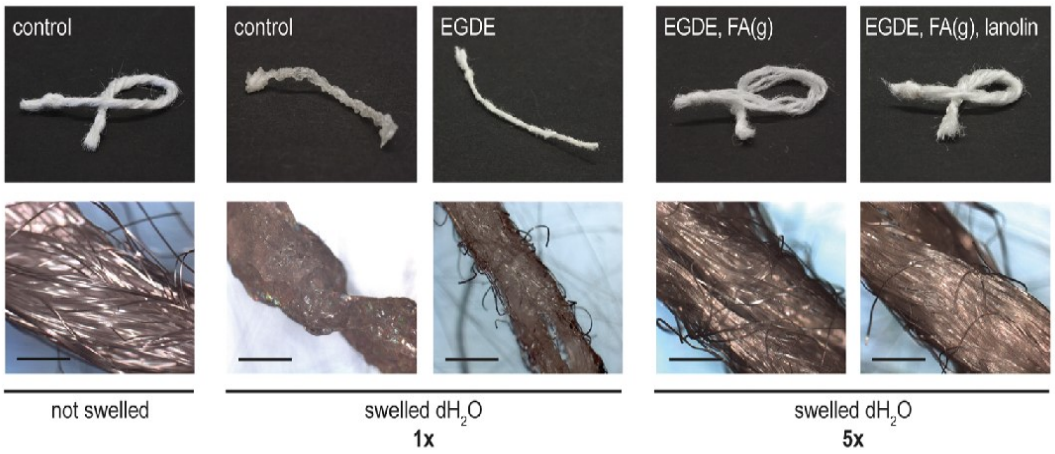

Figure 2-5 Images of collagen-based yarns from a complex blending system representing the requirement of double crosslinking by aldehydes as post treatment [207].

However, reduction in collagen content is unavoidable due to the presence of other polymers [210], furthermore according to recently published papers, the resultant fibres are still required to be cross-linked [211, 212] Even though, this modification method is not as simple as it seems; phase segregations and viscosity changes are simple examples of incompatible (co)polymeric fluids. Phase segregation is a common challenge that needs to be considered in material selection, when polyelectrolytes can form a network of electrostatic attractions and repulsions [92, 213]. The formation of electrostatically charged network is highly dependent on the characteristics of both electrolytes, such as charge density, chain length (molecular weight), ionic strength, and concentration of polymer solution. Many investigators have reported that increasing concentrations of polyelectrolytes in solutions leads to formation of larger network [214]. This critical issue is due to different properties such as electrical and structural that have significantly limited the use of collagen-based materials to be processed along with a variety of structurally and dynamically rich polyanions [92, 215].

2.1.3 Grafting modification approach

The other identified modification method for biopolymers and more specifically collagen chains, is grafting polymerisation. In the past, the effects of various parameters in grafting modification onto biopolymers have been investigated to form corresponding radical on the chains [48, 216]. Those investigations were conducted radicals by applying varied kind of vinyl monomers such as butyl acrylate , ethyl acrylate, methyl acrylate, acrylonitrile, methyl methacrylate, and methyl methacrylate-co-ethyl acrylate with a varied amount of initiators [21, 101, 217]. The main objective of most investigations in this field have been also focused on reducing the hydrophilic behavior and possessing the collagen, however due to structurally changed collagen chains into a branch structure, the collagen graft copolymer may receive new properties from the new molecular structure of branching and the branches themselves varied from their origin. Increased viscosity and density is one of the most important factor that needs to be considered for fibre spinning to prevent non-uniform fibre formation [20, 47]. For example, CN0214594 Chinese Patent entitled "collagen composite fibre and its production method" revealed a method of producing biocompatible collagen/polyvinyl alcohol (PVA) fibres from purified collagen modified by grafting with olefin monomers and mixed with PVA to form a spinning solution, and processed through a complex procedure using wet spinning, stretching and further post-treatment (acetalization). This

example signifies the grafting methods combined with blending systems to form spinning liquid with certain density and viscosity.

Little attention has been given to development of collagen-based fibres which have been structurally modified by graft polymerisation, existing research to align collagen chains and produce collagen fibres is scarce. Again, this is likely to be due to the fact that the grafting of vinyl monomers leads to modification of structural, rheological and morphological properties. In our previous work, grafting polymerisation of methyl methacrylate-*co*-ethyl acrylate was applied to modify the surface of collagen chains. We realised that the branched copolymer on the surface of collagen significantly influenced the initial viscosity. Since chain entanglement is crucial for fibre formation during electrospinning, the dependency of entanglement concentration on branch densities possessing the same viscosity was investigated; in which the mean fibre diameters of all considered samples remained broadly constant. We found that increasing the number of branching onto collagen chains significantly increased the stability of the collagen-based fibres under high humidity conditions and the long chain branches can provide a higher chain entanglement density leading to the more fibre uniformity [20].

However, there are some interesting studies considering the collagen properties that are covalently bonded on a pre-processed substrate. A pre-processed substrate can be in the form of fibres, fabrics, films of polymers, and composites. Jou et al. [218] reported Fibres of poly(ethylene terephthalate) (PET) were grafted with acrylic acid. The resulting fibres were further grafted with chitosan and collagen by means of esterification. Their results indicated that growing branches of chitin-collagen on PET fibres improved the multi-functionality of the composite fibres; whereas Yuan et al. [219] implemented almost the same procedure focusing on surface modification of PCL substrates using collagen covalently immobilized by poly (meth acrylic acid) via surface-initiated atom transfer radical polymerisation.

2.1.4 Conjugation modification approach

The field of covalently conjugation and its potentials have already been proved by many research groups for the delivery of proteins and drugs. This approach has been also found to be able to conjugate peptides with specific polymers or other proteins that is normally mediated by NHS and EDC in an optimized reaction time and pH [220]. However, to process collagen chains into fibres, little research has been conducted on the conjugation of synthetic polymers (i.e., PCL, Poly(lactic acid) (PLA), and poly

lactic-*co*-glycolic acid (PLGA), poly amides) onto natural polymers as pretreatment. As an example, a successful attempt to prepare a biosynthetic collagen based copolymer has been described by Gentile et al. [221] They electrospun the conjugated PCL/Collagen where the conjugation of the materials was evidenced by the presence of C–N and N–C=O bonds, the reduced fibre diameter was observed in compare with normal PCL/Collagen blends. This approach was to improve the miscibility of these two useful biopolymers in tissue engineering benefitting from good mechanical and biological properties; synthetic polymers possess attractive mechanical and physicochemical properties and natural molecular composition improves cellular adhesion and growth. From their observation on potential collagen release in water, post treatment of cross-linking may be required for some applications applying this modification method.

On the other hand, recently other interesting studies have been also reported focusing on increasing the stability of collagen chains by conjugating with active nanofillers such as Graphene oxide (GO). The covalent conjugation of GO to collagen nanocomposite have been evidenced by significantly reduced oxygen and carbon dioxide permeation on GO plane and edges [47, 222] and the increased the fibre stiffness without cytotoxicity has been reported in low concentrations of GO [222, 223].

According to Panzavolta et al. [222], the size of the nanofillers when processed with the collagen fibres can be problematic causing non uniformity and increased size for spun fibres; the size of GO sheets is comparable to the size of e.g. the nanofibres (~ 200 nm), even though this notable GO decoration on fibre surface can be beneficial for applications that require highly active functional groups of GO on the surface of the fibres, Figure 2-5. Furthermore, the high chemical affinity of these two materials hinders the denaturation of collagen chains and origins a nearly ideal mixing in the GO–collagen composite. This claim were also proved in our previous study[47] benefitting from covalent and non-covalent conjugation of the GO–collagen nano composite fibres, however we observed that the stability of GO–collagen composite fibres are dependent on the temperature; by increasing the temperature above 50^{o}C, the collagen release may occur in water more rapidly.

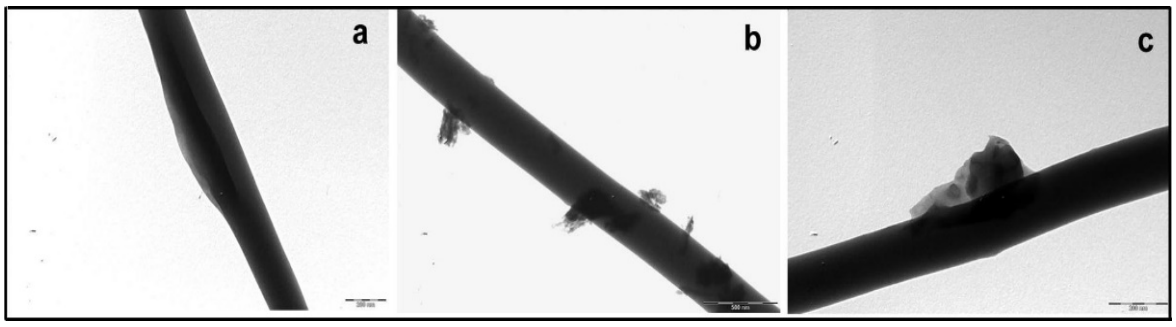

Figure 2-6 TEM images of electrospun mat showing GO sheets decorated (b) on the surface or (a and c) partially embedded into collagen-based fibres. Scale bar: 200 nm (a and c); 500 nm (b)[222].

2.2 Fibre spinning methods

In general, a spinning method is chosen by considering the properties of the material(s) to be spun. To process collagen chains, they must be converted into a fluid phase. Due to the low denaturation temperature of collagen, it is problematic to utilise melt spinning methods. Hence, collagen is typically processed via solution-based spinning methods.

Two key strategies may be considered:

(i) Conventional fibre-spinning through methods comprising dry-spinning [229, 230], gel-spinning [203, 231], and wet-spinning [202, 232-234], which are typically processed by post-drawing to achieve tailored fibres;

(ii) Direct fibre formation into micro- or nano-sized fibres by using electrospinning.

To the best of our knowledge, protein-based fibres have been prepared mostly by wet-spinning among conventional spinning methods, [62, 212, 235] as schematically shown in Figure 2-6. However, both above approaches have been efficiently applied to collagen, forming a mass of wet spun fibres with aligned orientation [202, 236] (Figure 2-6) to electrospun nanofibres with large surface area-to-volume [100, 101, 182, 204].

As an example of wet-spinning, Stoessel et al. [202] characterised wet-spun continuous gelatin filament fabrication with customized pre-treatment with a ternary raw materials of isopropanol, water and plasticizer, whereby superior tensile modulus (up to about 4 GPa) was achieved depending on the spinning set-up and the content of cross-linker/ plasticizer (triethylene glycol and ethylene glycol) using up to 200 wt. % of gelatin initial weight. The resulted fibres displayed wet stability depending on the solution content and post treatments with cross-linkers and heating.

This complex procedure has been suggested for the design of textile structural design appropriate for clinical consumables. Even though the conventional spinning methods e.g., dry spinning or wet spinning, result in the formation of well-defined fibrous blocks [62, 202, 233, 234, 237], relatively high fibre diameters (20- 400 µm, Figure 2-7) as an obvious feature of spun fibres and also high uses of volatile organic solvents for solution preparation and coagulating bath, complex spinning process and timely post-treatments should be considered for practical use in larger scale [230].

By contrast, the interest in fibre formation using the electrospinning methods has received a great deal of attention due to its high flexibility in controlling fibre morphology, orientation, dimensions, and porosity as discussed in sections 1.4.3 and 1.4.5. This method relates to features of electro-spraying and solution-dry spinning which do not necessarily involve coagulation chemistry or high temperatures to fabricate collagen fibres from solution. This inexpensive method can form fibres from large to complex (bio)polymers [135]. More specifically, electrospinning has been applied to form collagen fibrous webs to mimic the native tissue architecture.

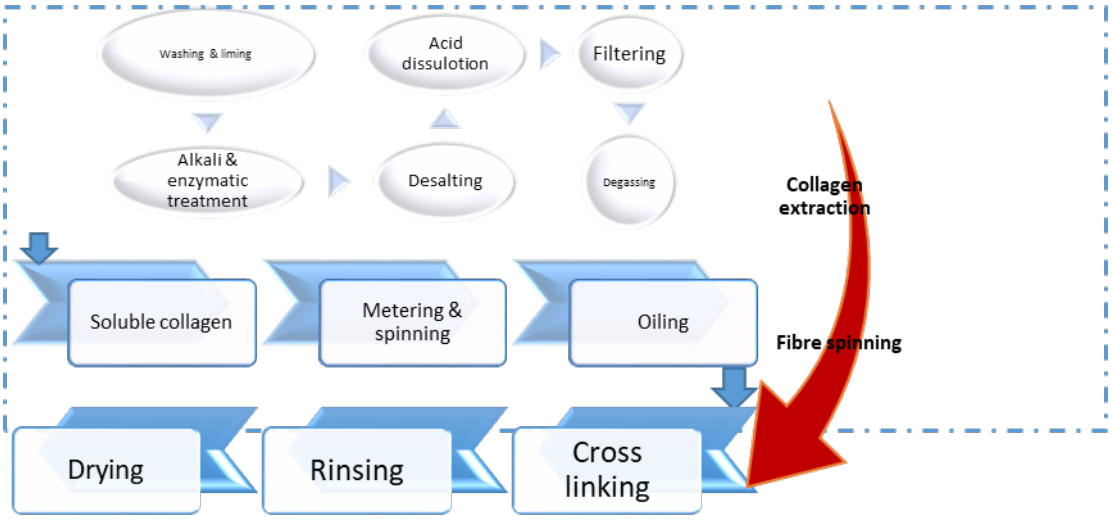

Figure 2-7 Block diagram of extraction of collagen chains followed by a wet-spinning and a cross-linking method [212].

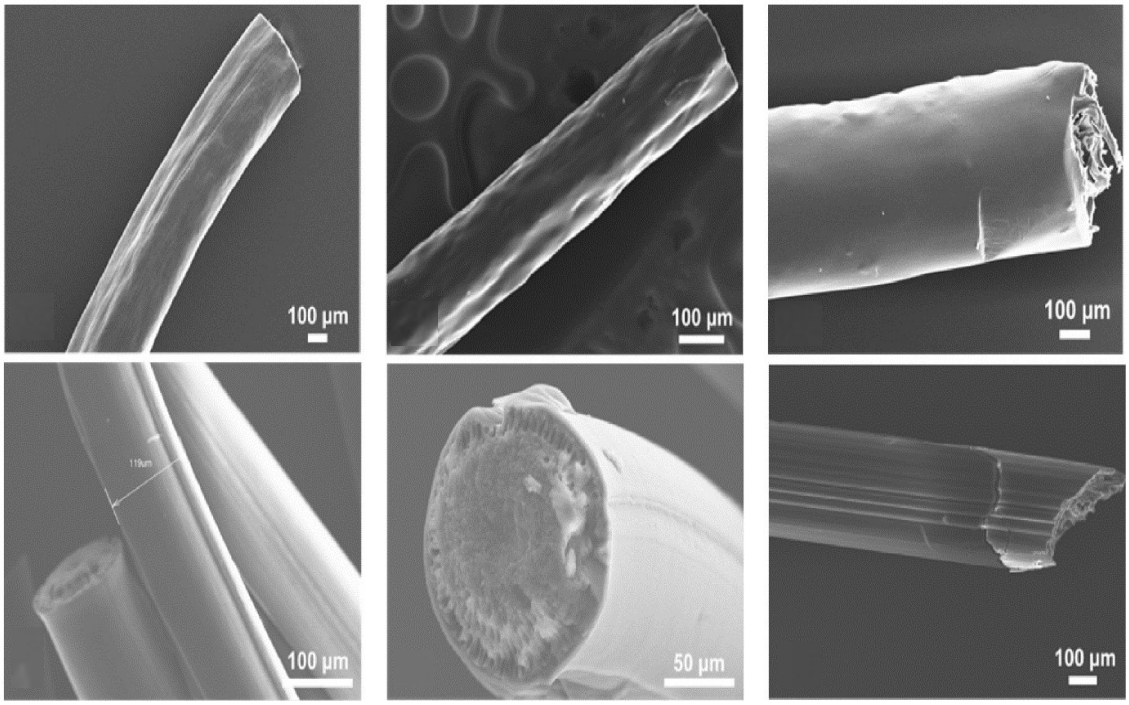

Figure 2-8 SEM images of wet-spun fibres from collagen-based materials obtained with various solvent and coagulating medium conditions when different fibre diameter achieved approximately from 110–450 µm [233].

Like conventional fibre spinning methods, collagen fibres from electrospinning are generally cross-linked as post-treatment or blended with other (bio)polymers to reach tailored physical properties [91]. Despite being appropriate to random deposition of collagen fibre [129] or along a defined axis [107], the electrospinning of collagen fibres represent limited possibilities with regard to structure customization, three-dimensional geometry and morphology protection in functional environments [238].

In general, electrospinning has the possibility to form customized fibres such as coaxial fibres when using a coaxial spinneret through in situ blending (Figure 2-8). A coaxial spinneret allows two different polymer solutions to be processed simultaneously in order to form a single coaxial fibre where the core content are encapsulated by the shell [116, 239, 240]. This method provides better spinnability of problematic polymers e.g. with low molecular weights, custom-made molecular conformation, and compositions with limited solubility [38, 79, 164, 240].

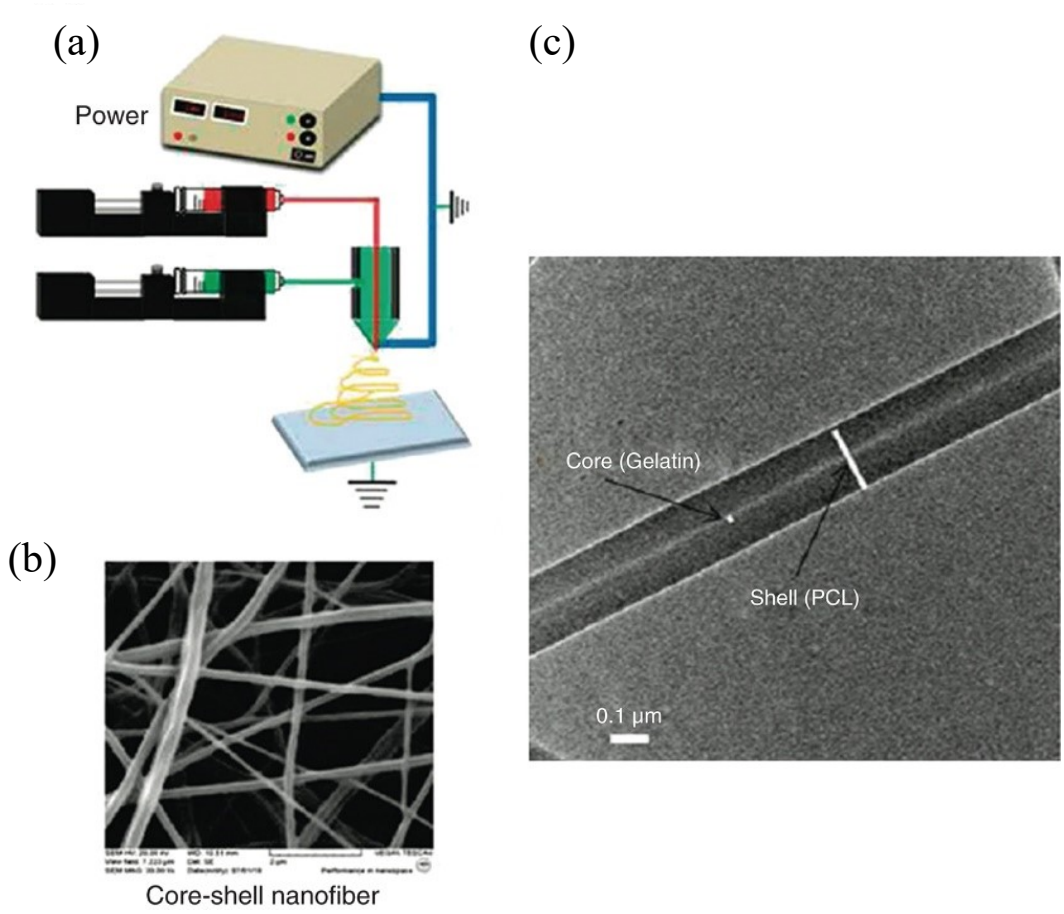

Figure 2-9 a) Schematic diagram of coaxial electrospinning, b,c) two different materials can be incorporated in the core and shell single fibre of different polymers [241].

Zhang et al. [116] investigated the uniformity of collagen coating on poly (ε–caprolactone) (PCL) prepared by coaxial electrospinning, in contrast with rough collagen deposition by soaking; whereas Huang et al. [242] reported approximately the same procedure while focusing on the fibre formation and mechanical characterizations. Thus, they added a new approach to coaxial electrospinning of collagen that can be regarded as an advantage over conventional spinning methods, not only in developing functionalized fibres but also in elevating their mechanical properties.

In coaxial electrospinning, the jet stability and fibre characteristics are not only influenced by the solution, process and environmental parameters, but also the solution-solution compatibility can affect the eventual fibre morphology. For instance, the inner and outer solvents can be a factor determining the immiscibility of the core and the shell components during fibre spinning [238]. Thus far, a number of researches have ascribed the core-shell fibre formation using a miscible solvent or the same solvent, for the core and shell components [92, 116, 239, 243], even though the effect of miscible solvents has not been clearly explained.

Viscosity and surface tension are critical factors for solutions to achieve a single fibre from both the core and shell components. This is due to the fact that the degree of polymer chain entanglements determines the viscosity of the solutions and intermolecular interactions cause the surface of the fluid to minimize the surface area. More specifically, high molecular weight polymers or increased polymer concentration lead to the formation of clogs/beads formation in the polymer jet, not allowing core-shell fibres to be stretched [244]. For instance, Zhang et al. [245] considered the effect of concentration on fibre morphology. They realized that, by increasing the core and the shell concentrations, the resulting fibres are of higher diameter. According to Lu et al. [238] to achieve tailored core-shell electrospun fibres, the spinnability of the shell components is the most important factor. Also, for each spinnable polymer solution, the solution conductivity must be in a range that often referred to as a "Leaky Dielectric" [246]. The behaviour of a fluid placing in an external electrical field has been discussed in detail in the references by Hohman et al. [247, 248], as well as Schnitzer et al. [249] and earlier work by Saville [246]. Hence, to prepare uniform coaxial fibres, the optimal solution-solution parameters require to be determined.

To produce higher volume of fibre spinning from collagen-based materials either as mixed-fibres or multi-layered fibres, multiple spinnerets are utilised sequentially or concurrently. This allows a set of polymeric solutions to produce higher volume of nanofibre nonwoven mat with desired mechanical, chemical and biological properties. For instance, Kidoaki et al. [250] designed ordered mesoscopic assemblies of scaffolds and matrices of nano to micron-sized fibres for tissue-engineering devices comprising multi-layering and mixing electrospinning. They used four components of type I collagen, styrenated gelatin (ST-gel), polyurethane (PU), and poly (ethylene oxide) (PEO). A tri-layered mesh was electrospun sequentially by (type I collagen, ST-gel, and PU). The mixed fibre mesh of PU and PEO was also formed by simultaneous electrospinning. This multi-layering method was useful to control the eventual composition and mechanical properties of the fibrous matrices. This method is particularly suitable for composites with a multilayer structure, such as protecting clothes, filtration materials, and tissue engineering.

2.3 Collagen sources

As previously mentioned, collagen as a suitable for fibre-spinning can be extracted and isolated from various sources. The most studied collagen is type I from bovine /calf skin [91, 233]. Some other sources of collagen have been also studied. For instance, Choi et

al. [251] examined a fish collagen-based composite fibre to support cell biological activities and also a similar electrospinning investigation into collagen from a cold water fish has been reported by Hofman et al. [90]. They electrospun fish collagen from multiple molecular conformations (native triple helical chains, denatured whole chains, and denatured gelatin) and suggested that the varied source of collagen presenting different molecular weights. And, molecular weight is an important factor determining the morphology and quality of the electrospun fibres where low molecular weight gelatin failed to form fibres. They also found that very high collagen concentrations (above 20%) are essential to fabricate the electrospun fibres.

In a similar approach, the source of collagen has received attention as a factor that can affect the properties of fibres, according to Tronci et al. [233]. They evaluated wet-spun fibre formation using collagen with varied molecular weight; hydrolysed fish collagen and gelatin from bovine skin having low and high molecular weights, respectively. They found that the morphology and diameter of the wet-spun fibres are drastically affected by the molecular weight and other factors such as wet-spinning solvent and coagulating agent. As mentioned in chapter 1, section 1.5, Matthews et al. [101] also explained the electrospinning of collagen type I from two different sources; human placenta and calfskin. Collagen type I from human placenta resulted in less uniformity in fibres with larger diameters. Furthermore, Zeugolis et al. [252] electrospun a set of collagen solutions prepared from five different samples of varied batches of type I bovine dermal atelocollagen. They observed that even in spinnable solutions, the fibre morphologies varied from one to another. They speculated that this variation is due to differences in amino acid content related to the age and even the race of the source.

Overall, the collagen source and type can primarily affect the molecular weight and can be also counted as a secondary factor determining the fibre properties. This can be due to varied molecular weight not only from the collagen source but also within the same source; simply affected by age, race, and injuries. This factor has significantly reduced the use of this biopolymer as there is no guarantee for reproducibility of the pure collagen fibres for specific applications. And this can be the main reason for using gelatine as a collagen derivate product with identified molecular weight.

2.4 Solvents

Solvent selection is critical for collagen spinning. Typically, organic solvents, such as 1,1,1,3,3,3-hexafluoro-2-propanol (HFP), 2,2,2-trifluoroethanol (TFE), or acids (trifluoro acetic acid (TFA), acetic acid, hydrochloric acid) have been extensively used to

dissolve collagen to prepare spinning solutions. Among them, HFP, TFE, and TFA with low boiling points have been used as common solvents in electrospinning. HFP and TFE lead to the loss of the triple helical conformation of collagen due to the damage of the delicate structure of collagen [204], even though the high concentration of collagen can partially reciprocate the drawbacks of these strong solvents. This has adversely affected the fibre formation of pure collagen through wet spinning and electrospinning. Tronci et al. [233] and Hofman et al. [90] reached to this conclusion to apply concentrations of above 20% to obtain spinnable solvents.

The solvent selection is more critical when electrospinning is used as the processing method. More specifically, Zeugolis et al. [94] claimed that electrospinning of collagen from HFP leads to the formation of readily water-soluble gelatin fibres, due to seriously denaturing the uncoiled structure of the collagen chains. Thereafter, their findings were also examined by other research groups [204, 253, 254]. According to Liu et al. [253], the collagen fibres from acetic acid showed more collagen preservation structurally in contrast to the collagen fibres from HFP.

In a separate study, it was suggested that, in collagen spinning, applying weak acids such as acetic acid can preserve a larger segment of the structure of collagen chains. This result was explained further by Qi et al. [254]; they claimed that the concentration of H^+ in the solvent plays a key role in the dissolving rate of collagen when pH = -log (H^+). It is well-defined that collagen chains are amphoteric polyelectrolyte identified by carboxyl groups (–COOH) and amino groups ($–NH_2$). Since the hydrogen ions of acidic solvents are simply ionized in collagen solutions, hydrogen ions (protons) are partly adsorbed onto the surface of collagen chains and the rest can be freely moving within the solvent.

$$R–NH_2 + H^+ \rightarrow R–NH_3^+$$

where R– is the rest of the collagen chain, and $–NH_2$ is the adsorption site for hydrogen ions available on the surface of the collagen chains [254]. When more free hydrogen ions are produced by a stronger solvent, a higher amount of hydrogen ions is attracted onto the surface, which increases the electrostatic repulsion force between the collagen chains. In the same study, Qi et al. also realised that collagen chains can be significantly degraded with highly increased H^+ concentration in a spinning solution.

In brief, they suggested that when pH of a collagen spinning solution is lowered to ≤ 3.0, the high availability of H^+ may cause collagen chains to permanently unwind into

random-sized poly-peptide chains, resulting in partial failure of the biological activity of collagen chains. On the other hand, the possibility of replacing fluoro-alcohols and HFP with a mild solvent, has been examined in various studies for collagen electrospinning. For instance, to preserve the characteristics of collagen chains, Elamparithi et al. [255] used a mixed solvent of acetic acid and DMSO in a ratio of 93:7 and Meyer et al. [232] used a mixture of water, HCl, and DMSO constantly keeping the pH at about 4.0 during the wet spinning of collagen fibres. And finally, Qi et al. [254] determined that a 57 % of native collagen chains can be preserved by using a benign sodium acetate/acetic acid buffer solution at pH 3.0. Hence, it seems that unmodified isolated collagen chains are unavoidably affected; resulting in significantly damage to the structure of the collagen chains during spinning.

2.5 Additives/reinforcements

As previously mentioned, purified collagen may lose its physiochemical properties from the hierarchical structure passing through two stages: (1) in isolation and extraction and (ii) in processing. Therefore, collagen fibres basically represent poor mechanical properties, and thermal and water instability. Accordingly, polymer/nanofiller additives have been found to be important in improving the physiochemical properties of collagen fibres.

The presence of additives in the collagen-based polymer matrix serves to reinforce the mechanical behaviour of the composite nanofibres. A variety of additives have been proposed for this purpose including compatible synthetic polymers, clays, synthetic silicate nanoparticles, hydroxyapatite and carbon nanofillers [256, 257]. Poly (ε-caprolactone), poly(3-hydroxybutyrate-co-3-hydroxy valerate) and Poly(glycolic acid) are examples of synthetic polymers that have been incorporated with collagen fibres as a reinforcing agent for tissue engineering [116, 227, 258].

In general, composite fibres can be prepared mostly through three processes including blending, coaxial spinning, and fibre mixing and multi-layering. Apart from the spinning methods and their corresponding challenges, the compatibility of the solution components is a critical aspect in blending systems to fabricate the composite fibres. Phase segregation is a common challenge that needs to be considered in additive selection, when polyelectrolytes can form a network of electrostatic attractions and repulsions. As an example, collagen has been blended with elastin and chitosan to prepare composite fibres [259, 260].

Coaxial spinning is another method in common between conventional spinning methods and electrospinning methods. However, coaxial electrospinning is more straightforward to produce composite electrospun fibres in which collagen can be electrospun as either the core or the shell layer [116, 239]. Due to its hydrophilic behaviour, collagen can be processed as the shell with a synthetic polymer in the core as reinforcement agent.

Again, the immiscibility of the solvents has been considered as a potential challenge in producing the coaxial collagen nanofibres [116, 238, 243]. Hence, collagen and the synthetic polymer require to be dissolved in a miscible solvent. To achieve a tailored fibre diameter, the core and the shell components are then extruded through the inner and outer capillaries of a coaxial needle at an appropriate feed rate and process set-up.

To produce multi-layered collagen-based composite fibre mesh, different polymeric solutions were spun sequentially which is only possible via multi-layering electrospinning. Hence, each layer of the multi-layered fibre mesh has its own structural and physical features. Apart from multi-layer electrospinning, *in-situ* mixing electrospinning comprises simultaneous electrospinning of at least two different polymeric solutions from separately fitted spinnerets to produce composite collagen fibre mesh. Again, this strategy is like the multi-layering method, only it can be performed through electrospinning.

To produce composite collagen fibres, carbon nanofillers are a relatively new class of fillers that have been recently subjected to a wide variety of applications due to their high specific surface [257, 261-264]. In the last few years, one-dimensional carbon nanotubes or nanowires (CNTs), and two-dimensional nano-sheets (graphene and its derivatives) have been explored extensively [265].

Nanofillers can be introduced to a collagen component during solvent processing. The solvent processing refers to a suspension in which a nanofiller is dispersed, then simply added to a solvent where collagen is dissolved as a host polymer [257, 266]. This method is classified as a modification based on non-covalent interactions [267-269]. In the last few years, several research groups have attempted to apply this methodology to enhance the mechanical properties of spun fibres including collagen and other biopolymers [266, 269-272].

In general, nanofiller/polymer fibres can be prepared via different spinning methods consisting of melt-spinning, wet-spinning, and electrospinning. However, this physical mixing/blending is a principle method for formulating nanofiller/collagen composites to be processed through an electrospinning method [257, 261, 267, 271, 273-276]. This method can further provide the possibility for electrospun collagen fibres to be

physically cross-linked and mechanically reinforced by the presence of nanofillers in collagen composite fibres [266, 272, 275].

However, the non-uniform dispersion of the nanofibres within the electrospinning solution is a significant challenge that may considerably affect the processability via electrospinning, as well as the morphology and mechanical properties of composite nanofibres [262, 266, 271, 272, 276, 277].

Furthermore, *in-situ* polymerisation is another approach that can be used to prepare more uniformity in the dispersion of nanofillers within the medium, benefitting from stronger interactions of covalent and non-covalent bonds between the nanofiller and host polymers [264, 278]. This method can be employed for some nanofillers with active sides such as graphene oxide [257, 267].

To the best of our knowledge, this approach has not been applied to collagen so far. In situ polymerisation represents mixing some nanofillers such as graphene oxide to the collagen in a goo solvent with the presence of initiator, followed by addition of complementary monomers. This can be another new method to prepare homogeneous nanofiller/ collagen composites that is also to be discussed in this work.

2.6 Advantages and disadvantages of reformed collagen fibres

Apart from the processing methods, collagen fibres can be produced in the micro size range from 89 to 400 μm [232, 233] and also in the range from 50 to 1200 nm by electrospinning [100, 204, 279]. For instance, Meyer et al. [232] used cylindrical and conical nozzles with diameters between 250 and 500 μm to yield fibres in the range of 89-170 μm by wet spinning whereas, Shih et al. [279] achieved three ranges of fibre diameters (50-200, 200 500, and 500-1,000 nm) from concentrations of 4, 8 and 12% w/v, respectively. These findings prove that collagen has the capacity to be spun in various fibre diameters from nano- to micron scale.

In comparison to other processing techniques, electrospinning dramatically increases the surface area-to-volume ratio, tunable diameter, and porosity. While conventional spinning methods have delivered highly aligned fibres in high quantity, electrospun collagen nanofibres can be formed in multiple geometries such as randomly or along a defined axis. The significant challenge of the collagen fibres via conventional methods may be large amounts of organic solvents employed during the spinning process or post-treatment. Furthermore, time-consuming production and complexity of the process set-up can make it unsuitable for practical use in large scale. However, the fibres

produced via conventional spinning methods generally have exhibited good water resistance and enhanced mechanical strength [202, 214, 236, 280].

By contrast, the main disadvantage of electrospun collagen nanofibres can be the significant collagen denaturation during the processing from solvents, and harsh process conditions. Furthermore, while the mechanical properties of wet- /dry- spun fibres are mostly from the post-treatment of the fibres e.g. drawing/stretching, the fibre taking-off/ detaching from the collectors in electrospinning is still in its early stages of research. Other limitations with electrospun collagen nanofibres are rapid degradation and weak mechanical strength. However, these problems can be overcome using similar methods implemented in conventional spinning methods over several decades of research.

Collagen fibre modification using reinforcement agents is one of the key strategies that has been used in numerous studies, even though grafting polymerisation methods have not received much attention as a viable modification method for collagen fibre spinning. This may be due to the changed rheological properties or reduced efficiency of this modification method when by-product formation is considerable in volume. We will show how electrospinning as a highly adjustable processing method can facilitate the fibre spinning from collagen graft copolymers and, how in situ polymerisation in the presence of nanofillers can provide a solution to increase the performance and efficiency of the graft polymerisation on collagen chains.

Chapter 3 Research Methodologies

In this chapter, the techniques that used to modify the collagen is described and the importance of characterization methods is investigated to provide correlations between the test results to be discussed in following chapters.

3.1 Synthesis of collagen graft copolymers

The collagen graft copolymer was synthesised via a graft polymerisation method in which an *in-situ* polymerisation of (co)monomers was carried out in the presence of acid soluble collagen chains. This methodology was used to modify the surface of acid soluble collagen [5, 281], in which the side chains are covalently bonded to the main backbone to form a graft copolymer with a branched structure.

In this approach, we were determined to study inter- and intra- molecular interactions of the acid soluble collagen was grafted from comonomers to be processed via an electrospinning method. This was due to a reduction in the hydrophilicity of collagen chains, which can be unstable in high humidity conditions otherwise, by introducing the hydrophobic part of a vinyl group to the backbone of collagen. This will be discussed further in the next chapters.

Graft formation with high impurities can sometimes be counted as a drawback of this methodology, which involves graft copolymer, ungrafted collagen, and homopolymer. To address this drawback, we showed in chapter 8 that the synthesis of nanostructured organic hybrid materials using covalent grafting of the monomers onto acid soluble collagen in the presence of graphene oxide is a robust method to modify collagen chains in a new composition with enhanced performance and efficiency.

Hence, this approach, using free radical grafting followed by the nanocomposite synthesis, is the novel part of this project; to apply collagen to the innovative nanostructure of composites. This methodology provides the opportunity to preserve a high portion of acid soluble collagen while processing. After grafting polymerisation, the collagen graft copolymer was purified by eliminating the homopolymerised polymer from the grafting mixture by selective extraction with appropriate solvents (boiled water and acetone). This was followed with characterization by gravimetric analysis of grafting performance (GP %) and grafting efficiency (GE %).

Grafting performance and grafting efficiency

The grafting performance (GP) specifies any increase in the weight of initial collagen exposed to grafting with a grafted (co)monomer and was calculated using the following equation [223, 225, 282]:

$$\text{Grafting performance (GP)}=(\text{Weight of graft copolymer})/(\text{Initial weight of collagen}) \quad (1)$$

$$GP(\%)=((W_1-W_0)/W_0)*100$$

where W1 and W0 are the weights of the collagen graft copolymer and the initial weight of collagen measured by a calibrated analytical balance (readability of $1* 10^{-3}$g) , respectively. GP (%) is assigned as apparent graft yield (%) that refers to weight gain fraction of grafted polymer to initial weight of collagen.

The grafting efficiency (GE) specifies the fraction of (co)monomers grafted onto collagen in contrast with the sum of (co)monomer converted to graft copolymer plus the homopolymerised polymer produced as by-product, and it was considered by the equation as [223, 282, 283]:

$$\text{Grafting efficiency (GE)}= (\text{Weight of graft copolymer})/(\text{Weight of graft copolymer+ Weight of homopolymer}) \quad (2)$$

$$GE(\%)=((W_1-W_0)/(W_1-(W_0+W_2)))*100$$

where W1, W0, and W2 are the weight of the collagen graft copolymer, the initial collagen and the homopolymerised (co)monomers, respectively, where the weight of acetone-washed copolymers was measured as W2.

3.2 Electrospinning of collagen graft copolymers

Collagen graft copolymers were then electrospun to investigate its spinnability. In this spinning method, the syringe containing polymer solution is connected to a syringe pump, which is programmable to a constant feed rate. Figure 3.1 shows a scheme of a typical electrospinning setup with a rotating drum collector that was used in this project. As discussed in chapter 1 section 1.5, the fibre formation mechanism via the electrospinning method relies on the intensity of the electric field, which is used to draw the polymer jet ejected from a spinneret. High applied voltage to a spinneret causes a repulsive force where the induced charges are distributed over the surface of the polymer droplet formed at the tip of the spinneret.

In this work, the process ability of collagen graft copolymer and collagen graft nanocomposite are studied by using a typical electrospinning method and the effect of incompatible reinforcing polymers on the physical properties of collagen graft copolymer is considered via using coaxial electrospinning as a processing method.

a)

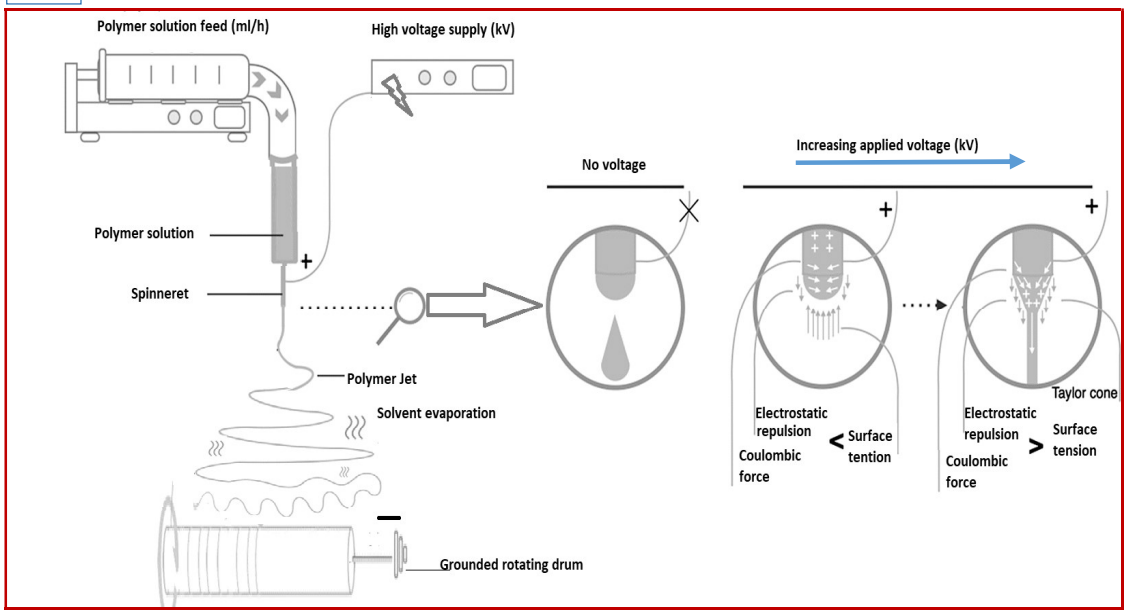

b)

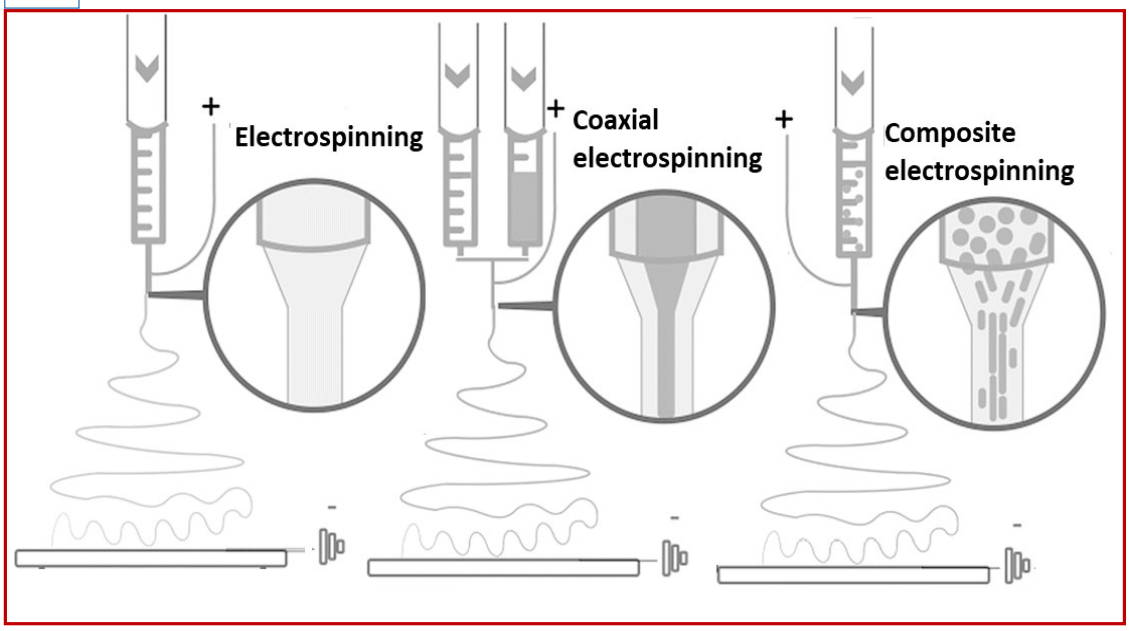

Figure 3-1 a) A typical electrospinning setup [284], b) Processing methods used for the collagen graft copolymers in current work.

Hence, as shown in Figure 3-1b, the process ability of the collagen graft copolymers is considered through:

a) Typical electrospinning as the related setup has been revealed in Figure 3-2a, consisting of a syringe pump, a high voltage supply, a rotating drum and a single spinneret;

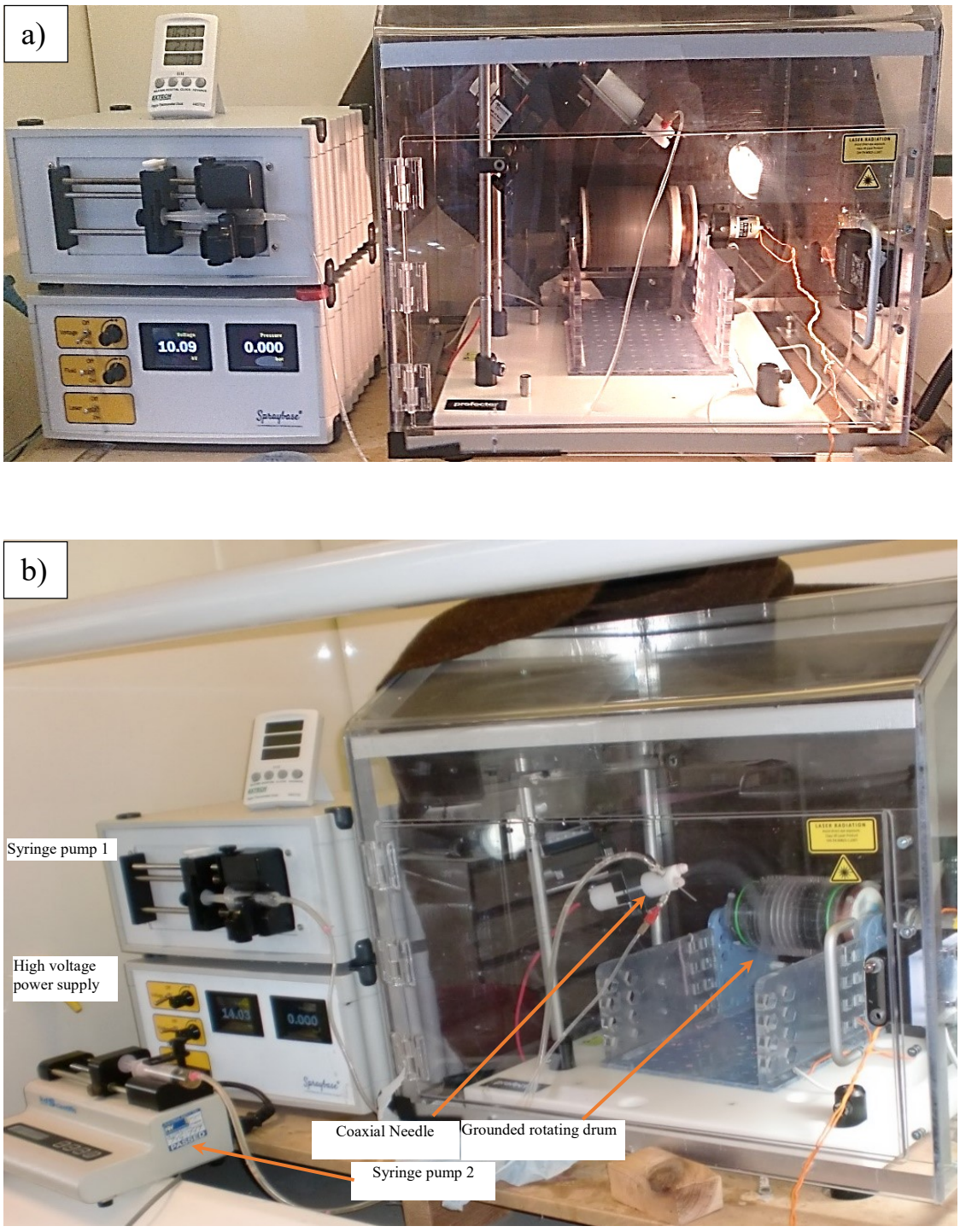

Figure 3-2 a) Image of SprayBase electrospinning apparatus used for electrospinning with a single needle and b) image of the coaxial electrospinning setup employed in current work.

b) Coaxial electrospinning using two syringe pumps for feeding the core and the shell components into a coaxial spinneret;

c) Composite electrospinning with the same processing set up as the typical electrospinning in which a composite solution consisting of copolymers and nanofillers are fed into a single spinneret.

As mentioned in the first chapter, the principal of the typical electrospinning is almost the same in all polymer solutions. In fact, the product of this process is fabricated depending on the correlation between the solution parameters and the process conditions.

However, in coaxial electrospinning, as shown in Figure 3-2b, there is a further set of parameters. Namely, solution-solution compatibility from varied viscoelastic behaviour to varied dielectric properties when they encounter a strong external electric field to form a single fibre or bimodal fibres. We will use this methodology to reinforce a composite fibre when its mechanical properties are part of our considerations.

3.3 Characterization of Graft Copolymers

After graft polymerisation, a branched collagen copolymer is obtained as a desired product. The physical and chemical properties of processed collagen graft copolymers depending on the density of branches on the surface of collagen chains were considered and analysed by the following characterizations.

3.3.1 Water Absorption Capacity (hydration degree)

When monomers or their binary mixture are grafted onto the super hydrophilic collagen chains, the collagen graft copolymer gains amphiphilic characteristic, and the copolymer absorbs a reduced amount of water depending on the density of the grown branches that introduced to the main backbone of collagen. The water absorption capacity (hydration degree) of collagen graft copolymer is calculated by the following equation [223, 258, 282]:

$$\text{Water absorption capacity (\%)} = ((W_t - W_i)/W_i)*100 \quad (3)$$

where W_i and W_t are the weight of dry copolymer and swollen copolymer at a specific time (t).

3.3.2 Biodegradability

Depending on the monomer grafted onto the collagen chains, the copolymer undergoes a reduced degradability. The degree of degradation was estimated from the mass loss.

The samples were pre-weighed precisely (about 100 mg each, n=5) and added to 50 ml of PBS (pH 7.4), containing 0.02% of sodium azide as a bacteriostatic agent [285]. At pre-determined time intervals, a group of each sample was regained, rinsed with distilled water to remove residual buffer salts, and dried in a vacuum oven at room temperature to constant weight. The mass loss was measured gravimetrically by comparing the dry weight remaining at a specific time, with the initial weight.

$$\text{Residual mass } (\%)=((m_0-m_t)/m_0)*100 \quad (4)$$

where m_0 and m_t are the weight of initial collagen graft copolymer and collagen graft copolymer at a specific time of (t), respectively.

3.3.3 Confirmation of the Grafting onto collagen

The grafting onto collagen, after passing through the processing methods, was evidenced by degree of hydration measurements as described above, and tensile/tension test, NMR, FTIR, UV-Vis, X-ray crystallography, and elemental, thermal, and morphological analysis as following:

Mechanical Properties

Tensile testing as a fundamental test was performed using an Instron 3345 under controlled loading and tension. As shown in Figure 3-3, a tensile test involves mounting the specimen (n=5, Figure 3-4) in the tester before subjecting each to tension. The tensile data collected, based on the extent of elongation and in area of each specimen as a function of load, tension and time, in which the tensile load is recorded as a function of increasing gauge length.

Figure 3-4 shows the twisted fibre yarn tested by the Instron tensile testing apparatus following the yarn tensile testing standard (BS–EN–ISO 2062:2009), where the fibre yarn samples that prepared with the same linear density using ASTM D5344– 99(2017). Mechanical properties such as tensile strength, Young's modulus are then calculated automatically, and stress-strain curve is plotted for each group of specimens. The advantage of stress-strain curves, in contrast with load-extension curves, is that the stress vs. strain is effectively independent of specimen dimensions.

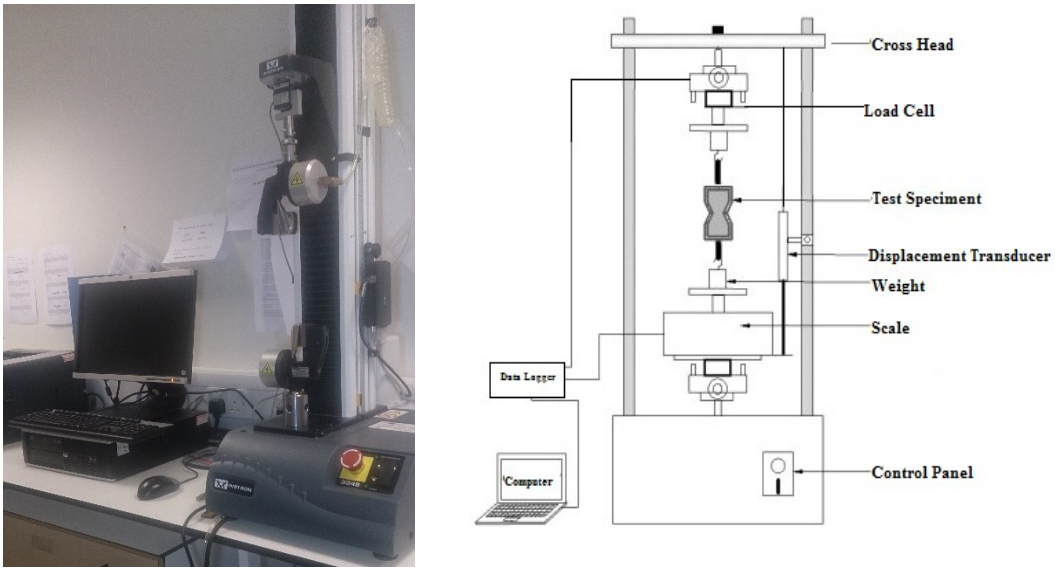

Figure 3-3 Instron Testing machine 3345K7484 based on dual-acting crosshead (up and down), Schematic diagram of Tensile Testing Machine.

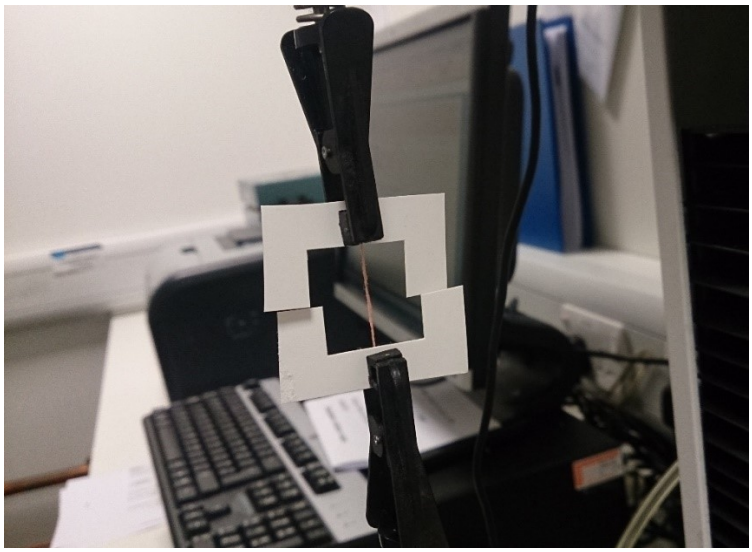

Figure 3-4 An example of test specimen mounting performed in the current work.

NMR Spectroscopy

Nuclear Magnetic Resonance (NMR) is an analytical method that is used in research and quality control for determining the structure and also the purity of materials. NMR can quantitatively analyse mixtures containing known compounds. Even though there are methods including C-NMR and N-NMR, hydrogen (^{1}H NMR) is the most common atom used in NMR spectroscopy.

In this work, ^{1}H NMR or proton magnetic resonance of the synthesised collagen graft copolymers will be discussed in which each group of equivalent protons gives rise to a signal. Equivalent protons are protons that have identical signals to branch points and

also end groups in the same environment. Hence, ^{1}H NMR was used to determine the key points of the structure of branches grown on the backbone of collagen using the four components shown on the spectra including chemical shift, number of signals, splitting patterns , and integration using a Bruker AVI 400 MHz as shown schematically in Figure 3-5.

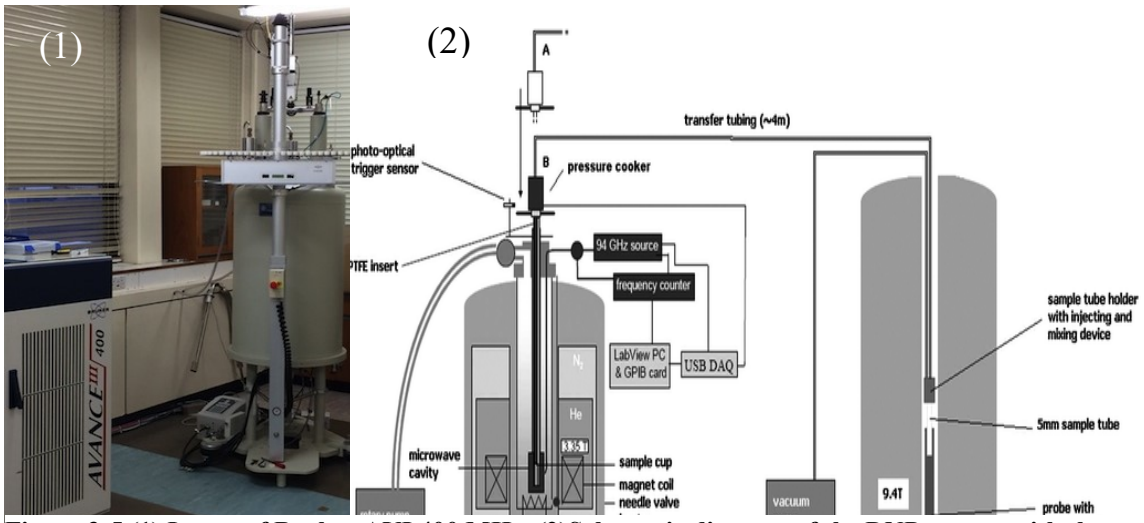

Figure 3-5 (1) Image of Bruker AVI 400 MHz, (2)Schematic diagram of the DNP system with the transfer line to the 400 MHz spectrometer [7].

Fourier transform infrared spectroscopy (FTIR)

FTIR is a physical science based on molecular vibrations to record an IR spectrum via transmittance/absorption of components of a material. The Fourier Transform term is induced from a mathematical algorithm to convert raw data into an inclusive spectrum. The main components of this methodology are IR sources, Detectors and Beam splitter. This method is the most straightforward way to measure the extent of a light beam that is absorbed by a sample at varying wavelength (λ).

The beam from a polychromatic IR source is altered to different frequencies by a certain configuration of a set of fixed and moving mirrors, providing a second data point. This cyclic procedure is repeated to measure light absorption at the mirror positions. Subsequently, a computer collects the raw data (light absorption at each mirror position) and calculates the absorption degree at each wavelength (λ), as shown in Figure 3-6 [11, 286]. FTIR spectra provide details about the molecular structure of a substance. The molecular analysis represents the primary chemical structure, intramolecular molecular conformation, hydrogen bonding, orientation and crystallinity [11].

In this work, FTIR spectra were presented in transmittance/absorbance scale for each quantitative analytical discussion using a Thermo-Nicolet Avatar 370 DTGS at room temperature, and samples for FTIR Spectroscopy were prepared as sample/KBr Disks. The chemical group of collagen graft copolymer and new peaks in the FTIR spectrum of grafted copolymer were studied in particular, which were not observed at the same wave number in the spectrum of each component individually.

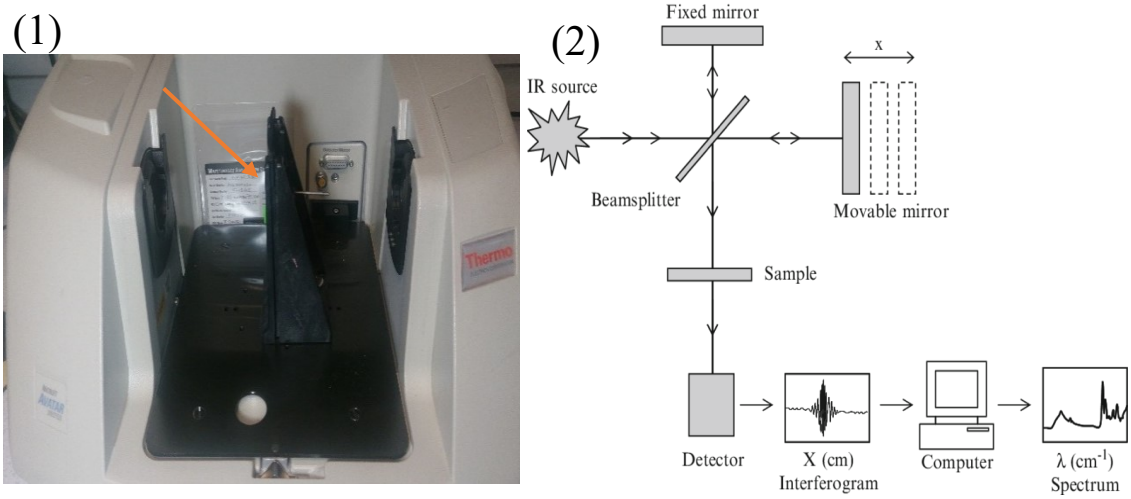

Figure 3-6 (1) Sample holder of a Thermo-Nicolet Avatar 370 DTGS, (2) A schematic image of Michelson's interferometer; A simple interferometer with a beam splitter connected to a computer [11, 12].

UV-Vis spectroscopy

Ultraviolet and visible (UV-Vis) absorption spectroscopy (Figure 3-7) is the measurement of the attenuation of a beam of light after it passes through a sample, or after reflection from a sample surface. Absorption measurements can be at a single wavelength or over an extended spectral range.

This analysis is performed to study the chemical compounds of a sample by measuring the intensity of light, and the intensity is proportional to the wavelength. Compounds can be determined by absorbed UV or visible light that varies from compound to compound. To collect data for UV-Vis graph, we used a Perkin-Elmer Lambda 35, as shown in Figure 3-7.

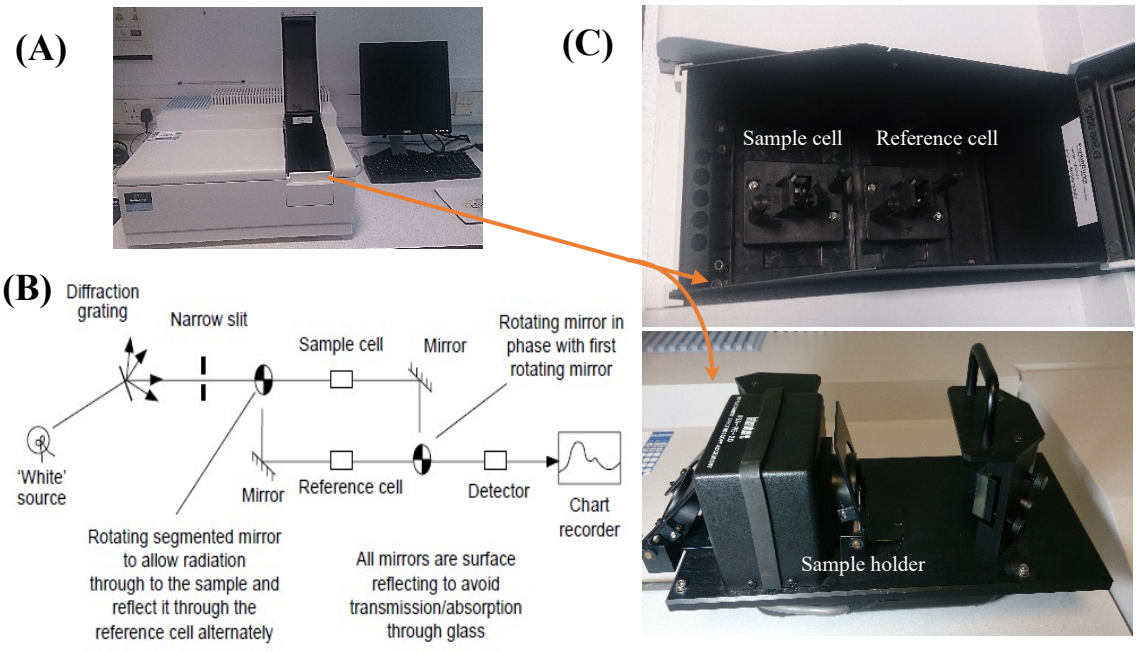

Figure 3-7 A) UV–VIS Spectrophotometer (Perkin-Elmer Lambda 35), B) Schematic diagram of a UV–VIS Spectrometry [7, 13], C) Sample holders where the sample can be in a solid phase or a dissolved/disperse in a liquid phase.

X-ray Crystallography

This is a scientific method to determine how particles/nanofibres are arranged inside crystals. In an X-ray crystallography instrument (X-ray Diffraction spectroscopy, XRD), the sample is compacted into a sample holder, so that it is flat and level with the top of the sample holder to minimise errors in peak positions. As shown in Figure 3-8, we used this analytical machine for both the nanofibre samples as well as the powder samples. As shown in Figure 3-8, the instrument was a Bruker D8 Advance powder diffractometer, operating with Ge-monochromated Cu Ka1 radiation (wavelength = 1.5406 Å) and a Lynx-Eye linear detector in reflectance mode.

Data were collected using the Bruker XRD Commander program over the angular range 5-85 degrees in two-theta over one hour per sample, with steps of 0.009 degrees and step times of 61.6 seconds. Patterns are from zero background using the Bruker EVA software. The generator set-up was at 40 kV 40 mA during the sample rotation at a constant rate of 30 rpm.

(1)

(2)

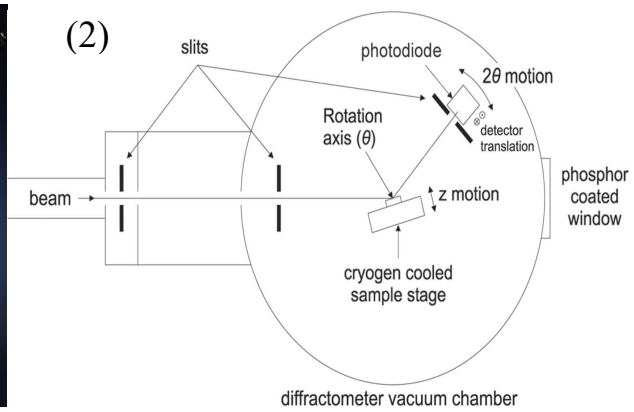

Figure 3-8 (1) Image of Crystal X-ray Diffraction (XRD), Bruker D8 Advance; (2) Schematic image of Bruker D8 Advance XRD.

Elemental Analysis

Elemental analysis is a conventional testing method to identify and quantify the elements in any unknown or known materials to determine the material composition, as shown in Figure 3-9. The samples in either powder or nanofibre are weighed to one millionth of a gram inside a small tin capsule. This capsule is introduced to the analyser's furnace which is at a temperature of 950 ºC. At this temperature the tin capsule combusts in a high oxygen environment to form tin oxide. The analyser's furnace then increases the temperature to above 1800 ºC; at this temperature, the sample is 'vaporised' and undergoes complete decomposition, to form CO_2, N_2, N_xO_y and H_2O. Then, the gases flow through a reduction tube which removes any unused oxygen and converts oxides of nitrogen to N_2. These gases are then homogenised at a precise temperature, pressure and volume in the mixing area.

A small portion of this mixture, from the sample volume, then flows through a series of thermal conductivity cells (the detector), where the 'quantity' of each gas, CO_2, H_2O, N_2 and He carrier gas, is analysed. Finally, from the initial weight of sample, C, H and N percentages are calculated.

In this work, an Exeter CE-440 Elemental Analyser was used to determine the C, H and N percentages from the collagen graft copolymers and their C: N ratio was also calculated.

(1) (2)

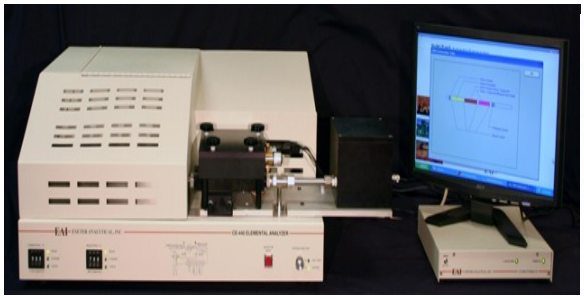

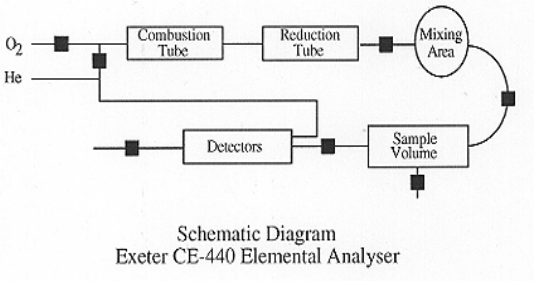

Figure 3-9 (1) Exeter CE-440 Elemental Analyser and (2) Schematic diagram of Exeter CE-440 Elemental Analyser

Differential scanning calorimetry (DSC)

DSC is a thermal analysis technique to study the heat capacity of materials as a function of temperature. As shown in Figure 3-10, a substrate with a defined mass is heated or cooled and the fluctuations in its heat capacity are compared to a known reference with a specific heat capacity over a range of temperatures and the data are recorded as any alteration in the heat flow. A computer is connected to act as a remote control which holds a program for DSC analysis to increase linearly the temperature based on a defined rate.

When the substrate encounters a physical transformation, different heat flows between the substrate and the reference are recorded. This varied heat flow related to exothermic or endothermic events. This allows for the detection of main transitions such as glass transitions and phase transitions. The result of a DSC analysis is a curve of heat flow vs. temperature or time. This curve is utilised to calculate enthalpies of phase transitions (ΔH) by integrating the peak corresponding to a specified transition: based on the calorimetric constant of the substrate and the area under the curve [287, 288].

DSC is widely utilized for investigation into polymeric materials to characterise and to compare their thermal transitions, even though this method does not identify the compositions of materials [289, 290]. Additionally, DSC is an appropriate method for assessing thermal stability in proteins such as collagen [289], where the thermal stability of the protein chains is analysed as protein stability that differs according to their inter/intramolecular interactions such as dipole-dipole attractions, Van der Waals forces and hydrophobic segments [286]. To study the effect of these interactions on thermal behaviour of samples, DSC analysis was performed to characterise the thermodynamics and denaturation of collagen graft copolymer using a Mettler DSC 12E in which the denatured state of the collagen chains was demonstrated

from the irreversible broken bonds following several unfolding processes. In general, a modified biopolymer is more thermally stable, since it possesses a higher melting temperature (T_m) and/or a higher denaturation temperature in contrast with others in the same category [191, 291].

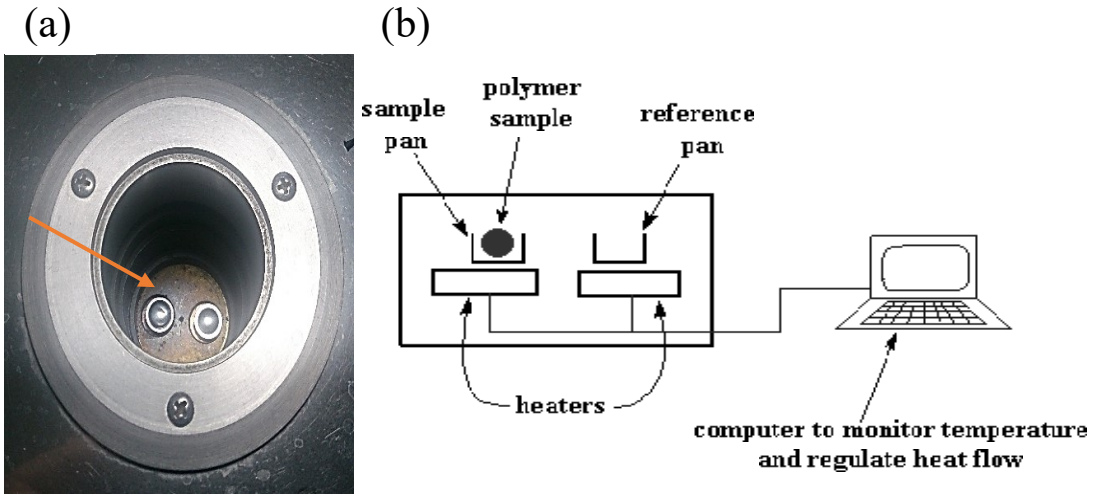

Figure 3-10 (a) Position of the substance sample and the reference sample on heaters (Mettler DSC 12E) and (b) A schematic image of the DSC instrument that is controlled by a computer.

In other words, this analysis is used to determine the effect of grafting on the thermal properties of the processed collagen graft copolymer individually and also along with reinforcing polymers and nanofillers. More specifically, any shift towards a higher temperature in thermal behaviour is evident for increased thermal stability of the components. Even though, DSC is typically to record exothermic and/or endothermic events and glass transition temperatures (T_g), this technique is also used to study oxidation and decomposition events in collagen-based nanocomposite.

Thermogravimetric analysis (TGA)

TGA is a thermal analysis in which the mass of a sample is continuously recorded as a function of temperature and time. TGA is typically performed as a complementary technique to identify an unknown polymeric composite based on its residual mass over time. Measures are mainly used to evaluate the composition of materials and to estimate their thermal stability [257]. This analysis can characterize materials that exhibit weight loss or weight gain due to physiochemical transformations such as decomposition in which chemical bonds are broken down, and evaporation which is loss of volatiles with

increasing temperature that are distinguished by weight loss through TGA analysis in contrast with events such as oxidation and absorption that come with weight gain.

As shown in Figure 3-11, a representative TGA consists of a precise balance with a sample pan placed inside a furnace with a programmed temperature regulator. The temperature is typically increased at a constant rate to encounter a thermal reaction. The raw data are displayed by a plot of the mass or the percentage of initial mass (y-axis) vs. temperature or time (x-axis), which is defined as the TGA curve.

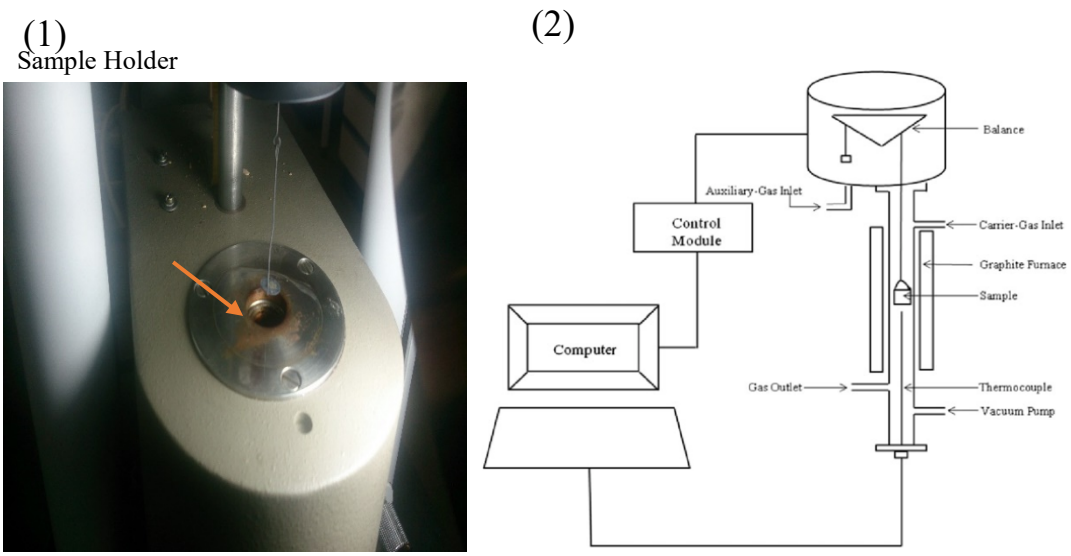

Figure 3-11 (1) Sample Holder image of a Mettler TC 10A/TC 15 Instrument and (2) A schematic of TGA set up used for the analysis.

In this work, TGA was carried out by using a thermogravimetric analyser, Mettler TC 10A/TC 15 to study the decomposition pattern and thermal stability of collagen graft copolymers. This was to better understand thermally degradation and decomposition process of collagen graft copolymers from the TGA data of weight loss, and to what extent they can be controlled through the thermal environment.

Scanning electron microscopy (SEM)

SEM is a versatile apparatus for morphology analysis of the nano and/or microstructure chemical compositions [292]. This analysis provides information about surface features (topography of an object) and morphology (shape and size of the observable components of an object) [293]. In SEM, an electron beam (electron probe) with an accelerating voltage (typically up to 30 kV) is emitted towards a sample and scanned along parallel lines. Several indications are produced as signals from the influence of the electron interactions, which are collected to generate an image from the surface of a sample. The electron source typically used in SEMs can be a tungsten filament, a field-

emission tip, or Schottky emitter. Above the sample, there is a set of magnetic lenses to condense the electron beam down the column (Figure 3-12), while the electron beam is scanned horizontally across the specimen in two directions (x and y). The simultaneous scanning from x-axis and y-axis (raster scanning) results in the scan over a two dimensional area of the sample [293]. Therefore, The SEM image is determined by the detection of signals generated from the electron probe and sample interactions.

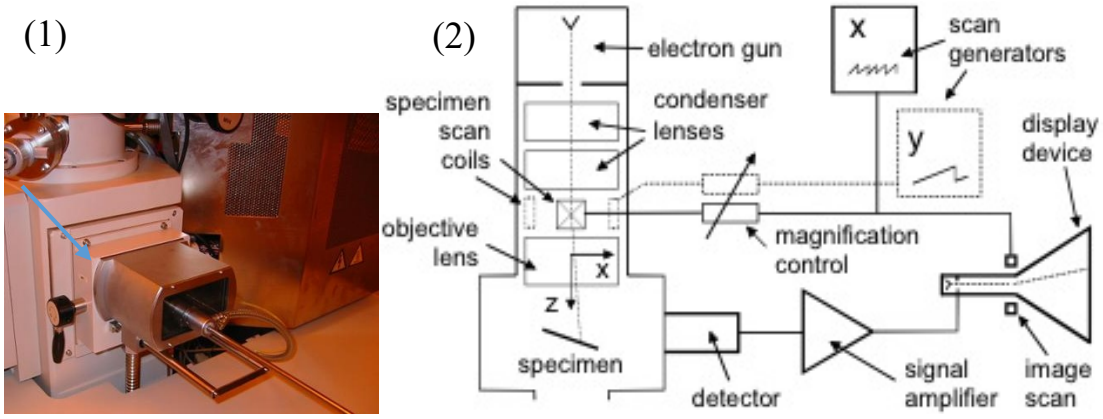

Figure 3-12 (1) Sample exchange chamber of a Hitachi 3400 Series, (2) Schematic diagram of a SEM [293].

In this work, SEM was performed to study the morphology of the processed collagen graft copolymer by using a Hitachi S-4300 at an operating voltage of 3 kV. The samples were coated with a gold thin film before SEM imaging to ensure higher conductivity, using a Polaron SC7620 Sputter Coater. For introduction of the sample to the column, as shown in Figure 3-12(1), the exchange chamber is disconnected from the SEM by isolating the electron column. The sample is screwed on to a sample holder and then on to a sample exchanging rode. The chamber is connected to the electron beam column by creating a vacuum to equalise the pressure. The sample holder is inserted into the sample stage inside the electron beam column. The SEM images are then captured after adjusting the magnification and working area.

Transmission electron microscopy

The transmission electron microscope (TEM) is a very powerful analytical tool for material science. A very thin sample that can be nanofibres or particles is exposed to a high energy beam of electrons. Hence, the interactions between the electrons and the atoms refers to features such as crystal structures and grain boundaries.

TEM, like SEM, operates on the same principals as the light microscope, but instead of light they use electrons, as shown in Figure 3-13. Because the wavelength of electrons is much narrower than that of light, TEM represents much in-depth details of internal structure.

In this work, FEI Tecnai F20 S/TEM was utilised. The aim of using this instrument was to determine the internal arrangement of composite fibre content by using electron microscopy and image processing providing access to high-resolution Cryo-EM and single fibre images.

(1) 

(2) 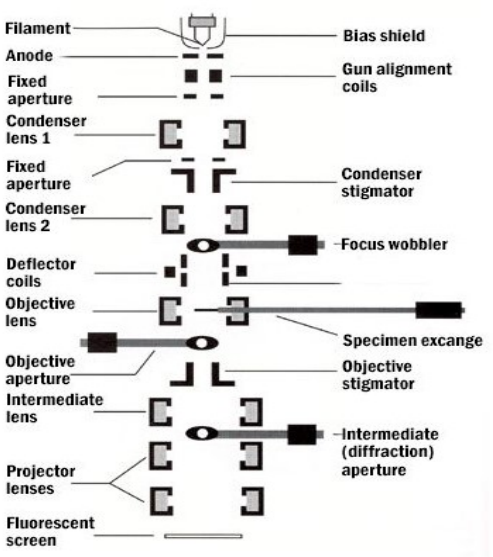

Figure 3-13 (1) Image of FEI Tecnai F20 S/TEM, (2) Schematic diagram of the TEM.

Contact angle and surface tension

Contact angle and surface tension are both surface analysis methods in which a surface interacts with other materials. Surface tension represents the cohesive/adhesive force of molecules at the surface of a material to launch the least possible surface area. Contact angle typically states the interface that exists between a liquid and a solid surface through the intersection angle between the outline of the solid and the surface of the liquid. A high contact angle (CA >90^{o}) indicates that the surface has low wettability in contrast with a low contact angle (CA ≤90^{o}) describing a surface with high wettability.

As shown in Figure 3-14, contact angle analysis is used to evaluate a solid surface interaction, while the surface tension analysis typically refers to the interfacial interactions of a liquid. The correlation between contact angle and surface tension is explained by the surface energy concept that refers to the strength of interfacial tensions

at the surface of a material, and this indicates the extent of attraction or repulsion of a surface that is implemented on contact interfaces. In polymer science, these two concepts are used in different aspects [294] .

Recently, the development in user-friendly compiling software facilitates the contact angle measurements. In the case of graft collagen copolymer, surface behaviour was calculated not only based on the relevant energy ($N.m^{-1}$) but also changes of water contact angles of the solid phase. The result of any specific mechanisms (absorption, penetrating and swelling) was explained by the effect of grafting density and the

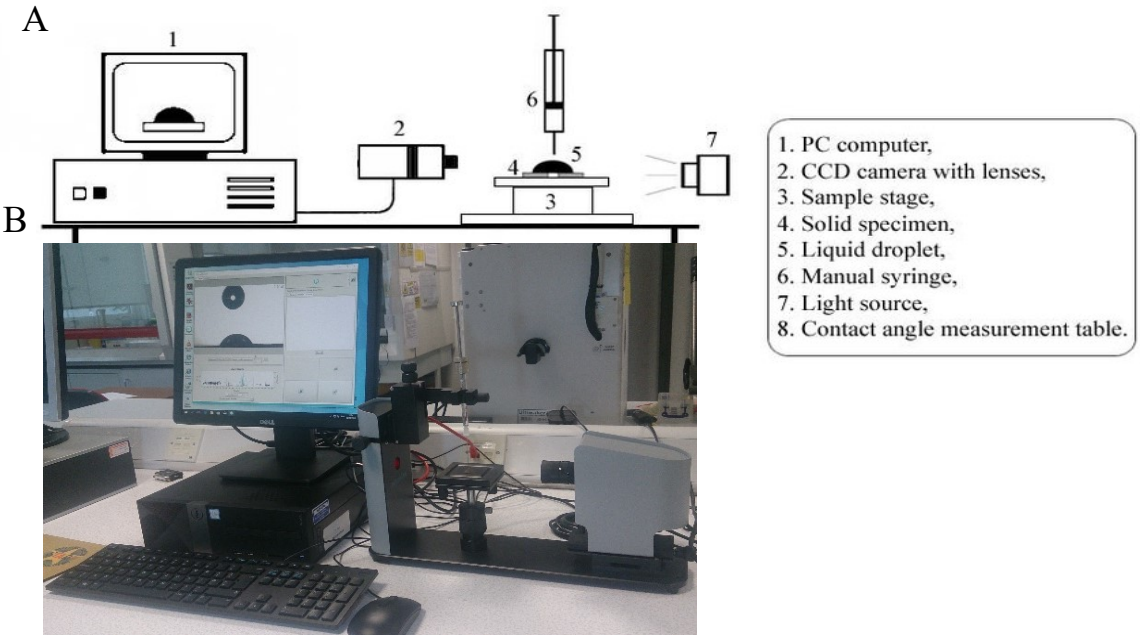

Figure 3-14 (A) Schematic diagram of contact angle measurement system [8]. B) Contact angle analyser (OneAttension v. 2.3, Boilin Scientific).

(non)polar segments of the processed copolymer in the experimental data.

This combined approach was considered to evaluate the surface wettability of the electrospun collagen graft copolymers as well as their correlation with the surface topography of the modified biopolymer by using a contact angle analyser, OneAttension v. 2.3, Boilin Scientific. The instrument was controlled by a computer to record contact angle of 10s for two rounds, the first round was carried out once the water droplet (almost 2.5µ) released to fibre mat/ film and then repeated after 10 minutes.

3.4 Statistical analysis

Statistical analysis was performed using a one-way analysis of variance (ANOVA) in Excel 2016 with significance set at $p < 0.05$. All statistical values were reported as means of standard deviation.

Chapter 4Collagen Graft Copolymers: Synthesis and Properties

In this chapter, Collagen was solubilized by acid treatment. Subsequently, binary vinyl monomers of Methyl Methacrylate (MMA) and Ethyl Acrylate (EA) in varied feed ratios were grafted onto acid soluble collagen (ASC) with the aim of benefiting from the firmness and the plasticizing capacity of the resultant collagen graft copolymers. Methyl Methacrylate (MMA) and Ethyl Acrylate (EA) possess the same volumetric density and molar mass with a wide range of difference in the glass transition temperature of their components in polymer chain (Tg≈ -5··105 °C). The main objective of this chapter is not only to reduce the super hydrophilicity of the collagen chains, but it is to consider the effect of the grafting modification on the backbone of collagen as a preservation method against the severe spinning conditions, which is to be studied in chapter 6. The main features of this chapter have been schematically shown in Figure 4-1.

The influence of important physicochemical properties of the copolymers on the shape of the DSC patterns, the conductivity where the side chains of copolymer with dielectric properties covalently bonded on ASC, initial viscosity affected by the obvious wide molecular weight distribution of the achieved copolymer based on their composition dependencies copolymer was studied. This was to achieve a new thermally stable branched copolymer of collagen for end uses such as fibres and fibrous assemblies where sufficient chain entanglements facilitate the fibre formation procedure.

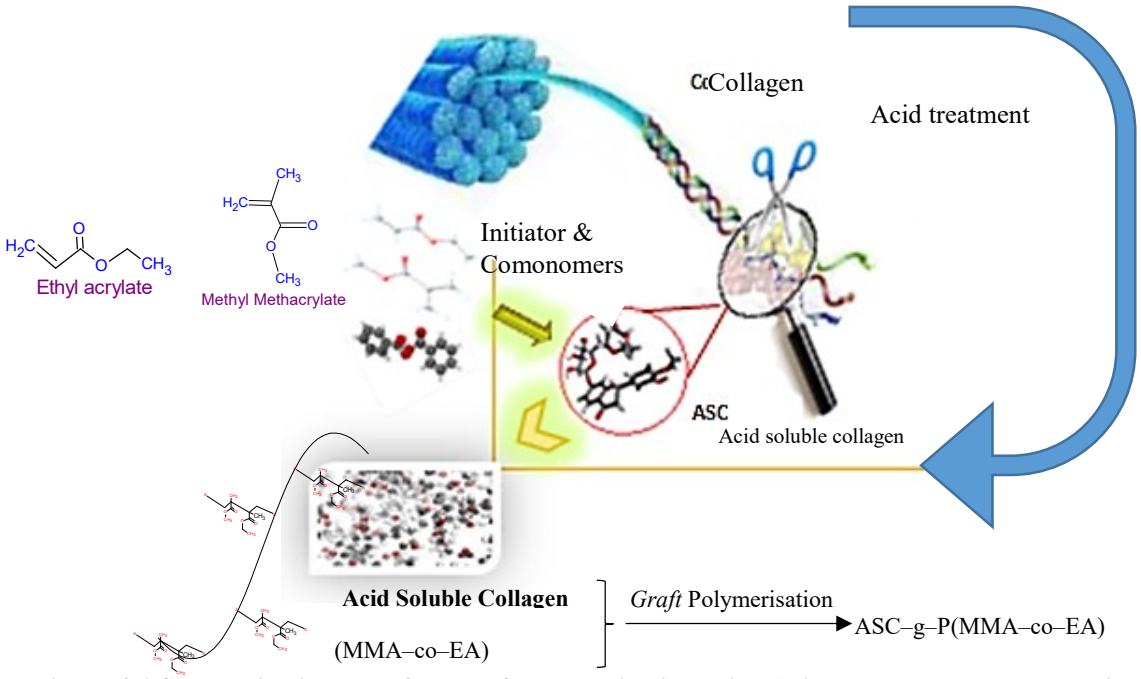

Figure 4-1 Schematic diagram of the graft polymerization using Acid soluble collagen as starting raw material to be grafted from methyl methacrylate-co-ethyl acrylate (MMA-co-EA) with the presence of Benzoyl peroxide (BPO) as a initiator .

4.1 Experimental

4.1.1 Preparation of Acid Soluble Collagen (ASC)

Acid soluble collagen (ASC, 11 g) was prepared using collagen from calf skin (Devro Plc., UK) in 0.1 M acetic acid (AA, % 99.7, Alfa Aesar) and distilled water to reach pH of 3±0.5, Figure 4-2B. The mixture was incubated for 5 h at 45 °C in a 250-ml triple necked round bottom flask and a stirrer bar was added. This step was ended up in the suddenly increased temperature of 80 °C threshold when a homogenous solution of ASC was achieved.

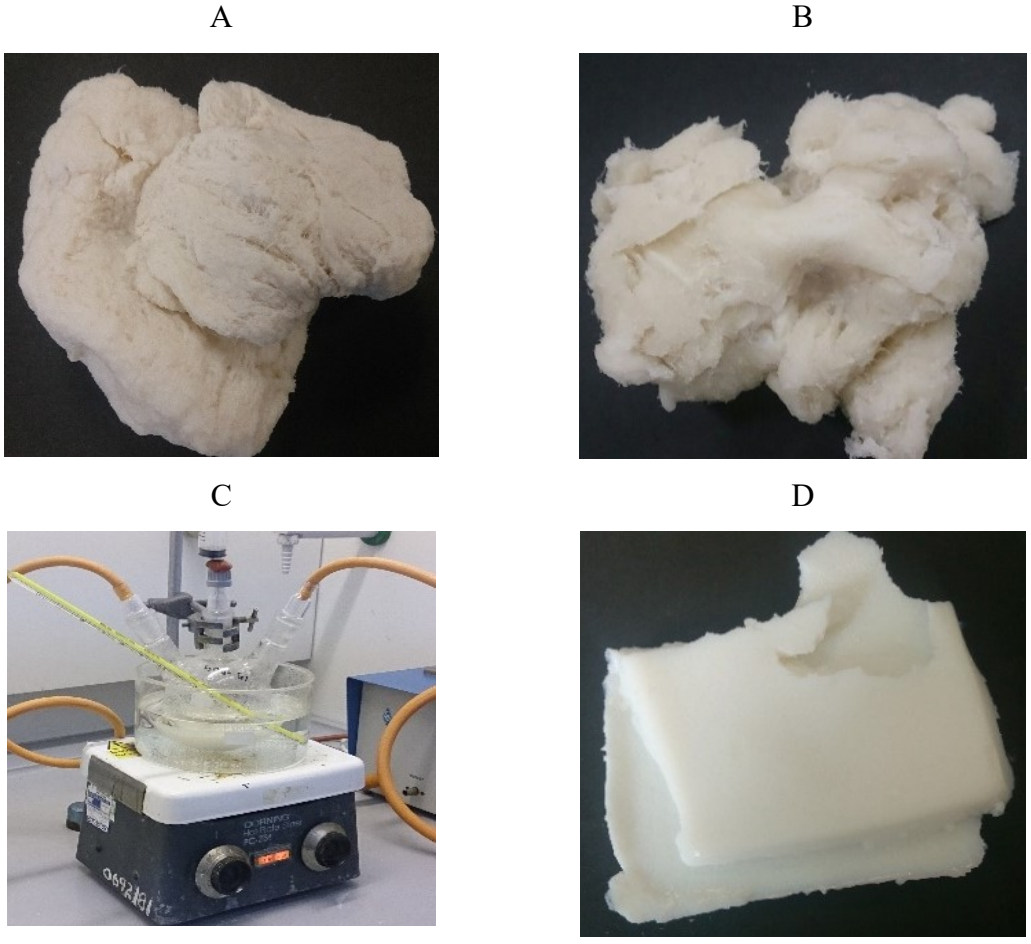

Figure 4-2 Image of a) Pre-treated collagen, b) Acid-treated collagen before subjecting to heat, c) Graft polymerisation set-up, and d) Collagen graft copolymer.

4.1.2 Graft polymerisation onto ASC

Methyl methacrylate (MMA, 99%, Alfa Aesar), Ethyl Acrylate (EA, 99%, Alfa Aesar) were used as process monomers and were passed through a column of 5% sodium hydroxide aqueous solution to remove any inhibitor that used to inhibit radical

polymerisation. Benzoyl peroxide (BPO, 97%, Alfa Aesar) was used as initiator and recrystallized in Acetone before applying.

Free radical polymerisation [221, 256] was used to synthesise the graft copolymers of distilled Methyl Methacrylate (MMA, %99, Alfa Aesar) and Ethyl Acrylate (EA, %99, Alfa Aesar) onto the solution of collagen in distilled water. In this step, the previous 250-ml three necked round–bottom flask was used as the reaction vessel, Figure 4-2C. Nitrogen gas was served through the solution while stirring. Once the desired temperature was achieved, the gentle addition of Benzoyl Peroxide (BPO) dissolved in Acetone (2 ml) as an initiator, was added to the reaction vessel within 10 min. Distilled MMA and EA monomers in the rates noted in Table 4-1 were then introduced via a syringe over 30 min.

The temperature and reaction time after adding the initiator and the monomers were fixed at 80 °C and 60 min, respectively. A stirrer speed of 2400 rpm was used constantly during the polymerisation reaction. Precipitation of the graft copolymer occurred after 15 min of reaction time, developing a milky white solution in the aqueous medium. To complete precipitation, the reaction mixture was then added to an excess of cool methanol. The solution was filtered with a glass sinter filter, Figure 4-2D, and dried in vacuum oven at 25 °C until a constant weight was obtained.

As with any conventional free radical copolymerisation reaction, poly(MMA–co–EA) can be achieved along with that of the desired copolymer (ASC–g–poly(MMA–co–EA)) owing to reactivity ratio effects or the separation of macro monomers from the main and side chains [51]. To remove by-products, as they may adversely affect further processing, the simple isolation method of selective solvent extraction based upon the difference in their solubility, was employed.

Therefore, the grafted collagen copolymer was extracted by repeated washing with hot water followed by acetone at room temperature to remove the associated ungrafted ASC and poly(MMA–co–EA). The desired copolymer of ASC-g-poly(MMA–co–EA) was dried in a vacuum oven at room temperature until constant weight was achieved. The grafting parameters were then calculated, Table 4-1.

4.2 Results and discussion

In materials, and particularly in biopolymers, it is essential to modify their properties to desired specifications. Since collagen can be modified into physiologically tolerable compounds, grafting polymerisation was used to modify the surface of purified collagen. Again, pure collagen is a natural polymer that cannot be applied freely to

specific end uses due to its inherent drawbacks such as poor mechanical properties and fast degradability as discussed in chapter 2 [101, 129, 256].

This modification was due to benefiting from its natural properties whilst at the same time adding value by introducing the monomer(s) onto its main chain. This method was employed as a pre-treatment on the delicate surface of collagen chains to create the more physically stable collagen graft copolymers for further process to be discussed in the next chapters.

4.2.1 Preparation of Acid Soluble Collagen (ASC)

The solubility profile of ASC is presented in Figure 4-3 by controlled parameters of temperature, rotation speed, time and pH. According to Muyonga [180] et al. , a significant wide molecular weight distribution is achieved through the acid isolation process of insoluble collagen that is partially inherent and partly is due to the denaturation of α-components (α1 and α2) in the isolation process [180, 293]. As mentioned in chapter 1 section 1.2, the overall structure of collagen is made up of a triple helix, which is generally composed of two identical secondary chains (α1) and one additional chain (α2) that varies slightly in its chemical composition [34].

However, this chemical treatment can result in the followings: (i) three uncoiled α-chains, (ii) an α-chain along with a β-chain (two covalently bonded α-chains) and, (iii) a γ-chain (three covalently bonded α-chains) [52]. Hence, the acid treatment on collagen results in a significant degradation of the hierarchical structure of native collagen which causes the uncoiled collagen chains to dissolve in the medium.

The pH value has an obvious influence on the solubility of the ASC, especially on the average molecular weight, due to the repulsive force between chains when the net charge residues (negative or positive) increased when the pH is within the region lower or higher than the isoelectric point [294]. It has been also reported that the solubility of collagen in weak acid can reduce the denaturation of the α-chains [180, 295].

Therefore, it is expected that the structure of the ASC segments with higher average molecular weight could be more similar to that of its parent collagen. Although the desired collagen with excellent solubility can be prepared according to its molecular weights [294], in this research, due to preserving the considerable fraction of the α-chain that has the potential to be denaturised by acid treatment, Acetic Acid was applied and the pH value was kept in the region close to the isoelectric point.

Table 4-1 Experimental plan: Water content and initiator concentration based upon the feed ratio composition for reactants used in the synthesis of collagen graft copolymers (initial amount of ASC was set at 11g).

Sample	Comonomer cont. in feed (mmol)	EA cont. (%)	MMA cont. (%)	Feed ratio ASC:(MMA–co–EA) (wt.: wt.)	Water cont. (mL)	Initiator (mmol)
S1	109.83	0.50	99.5	1:1	85	4.51
S2	219.71	5.00	95	1:2	106	9.10
S3	329.65	10.00	90	1:3	120	13.62
S4	493.47	15.00	85	1:4	145	18.16
S5	549.39	20.00	80	1:5	160	22.70

Table 4-2 Results: Change of graft parameters and contents based upon the feed ratio composition for reactants used for collagen graft copolymers.

Sample	GP (%)	GE (%)	Yield of grafted collagen (%)	$M\eta*10^{-3}$ of Branch copolymer	Weight ratio of ASC: Side grafts	Nitrogen cont. %	C:N ratio
S1	11.42	10.79	6.26	9.54	1:0.96	7.46	5.96
S2	37.14	16.47	21.85	7.89	1:1.09	4.69	8.84
S3	49.85	15.68	32.47	7.08	1:1.33	4.59	9.82
S4	57.42	13.49	34.37	8.06	1:1.68	4.35	10.05
S5	51.71	10.34	32.13	9.11	1:1.03	5.95	6.93

4.2.2 Synthesis of the ASC–g–poly(MMA–co–EA) copolymers

This part of the work presents mainly the results of our studies based on the copolymers achieved from the graft copolymerisation of MMA–co–EA onto swelled ASC in water by using BPO as an initiator that was assisted by high agitation speed. As homopolymerisation, as an undesired reaction in graft polymerisation obviously has a negative impact on the performance of the process, a controlled agitation speed can potentially prevent chaos from homopolymerisation. Hence, the agitation speed was kept at 2400 rpm to produce a uniform propagation of formed active radicals in the increasing viscosity of the medium during the polymerisation.

Moreover, water is known as a swelling agent for ASC chains that provide the chance of grafting reactions under homogeneous conditions. Thus, this solvent induces important advantages such as a better control on the degree of conversions [5, 296], a more uniform distribution of components during the polymerisation and a higher conversion yield [178].

Figure 4-3 shows the conditions of the solubilisation and the polymerisation reactions. The grafting polymerisation was considered at the starting point of 300 minutes in Figure 4-3. Table 4-1 gives a summary of the amount of raw material used in the current study. In all experiments, 11g ASC was used and the effect of varied MMA–co–EA feed ratios were examined.

The reaction mechanism for the graft copolymerisation of ASC–g–poly(MMA–co–EA) is demonstrated in Figure 4-4. Chemical grafting involves the formation of active points upon the ASC backbone. Once these (branching) grafting points are initiated and formed through thermal dissociation of BPO, copolymer chains of poly(MMA–co–EA) start to grow, resulting in branches on the main backbone of ASC.

It has been reported that due to using BPO, the following possible reactions, can occur:

a) the chain-transfer reaction between the growing chains and the backbone, forming active points upon the backbone;

b) the monomers add to active points upon the backbone to give a graft copolymer;

c) the graft copolymer chain grows on the backbone in which termination of the process is likely to occur in one of the chain-transfer or combination reactions involving the growing chain radical on the backbone [5, 19].

Hence, apart from our desired product, homopolymerised poly(MMA–co–EA), ungrafted ASC and unconsumed monomers/initiator may also be produced.

According to Table 4-2, the growing branch on the ASC incorporation correlates well with the feed ratios of MMA–co–EA in the reaction. The grafting performance and the yield of grafted collagen confirm the direct interaction of the feed ratio of co-monomers added onto ASC and the growing copolymer side chains. This can be due to the steric effect and polarity effect of the combination of ASC and co-monomers in the aqueous medium. A decrease in the grafting performance is evident at the highest feed ratio of S5 where the dominant co-monomers are more likely to be initiated and to be (co)polymerized solely in the reaction.

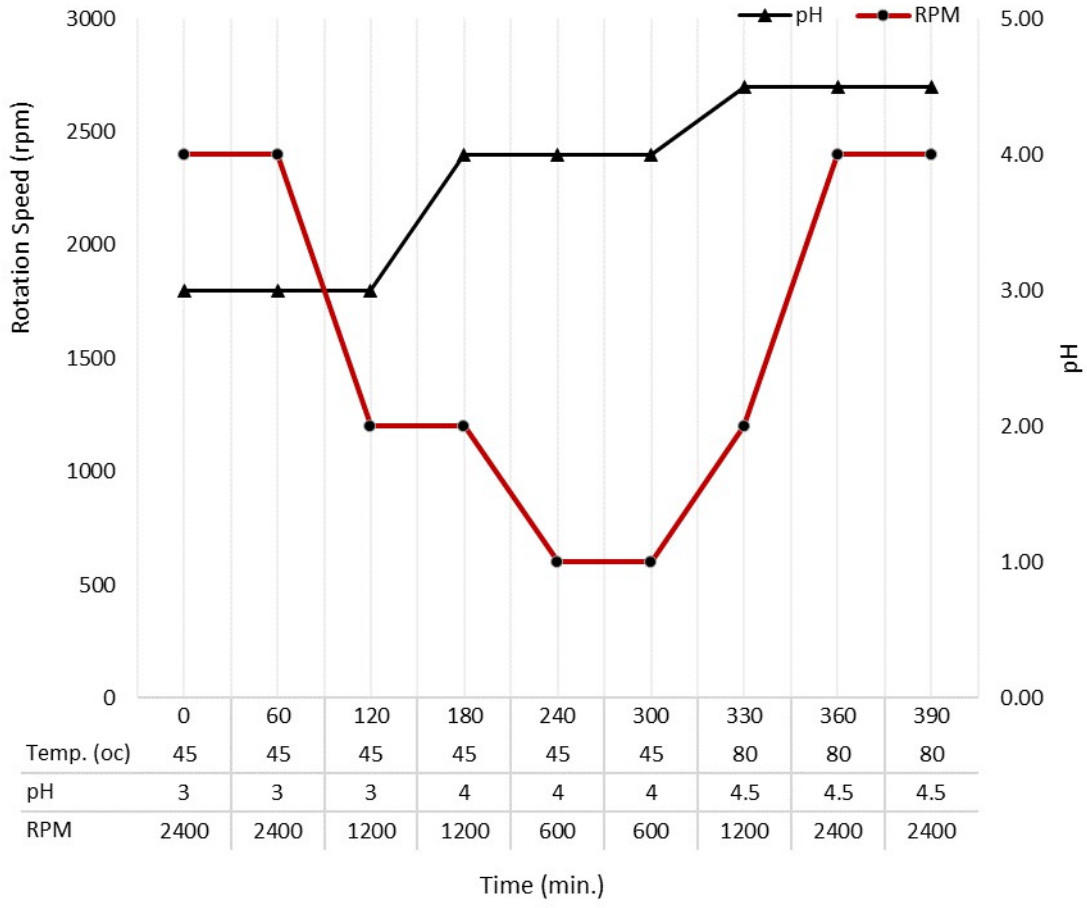

	0	60	120	180	240	300	330	360	390
Temp. (oc)	45	45	45	45	45	45	80	80	80
pH	3	3	3	4	4	4	4.5	4.5	4.5
RPM	2400	2400	1200	1200	600	600	1200	2400	2400

Figure 4-3 Change of reaction parameter values; Temperature, pH value, rotation speed and Time: ASC solubilisation time from 0 –300, Graft polymerisation process from 300-390 min.

The molecular weights of the isolated grafted branches from severe hydrolysis of ASC by HCl was then determined by visco-metric measurements in Acetone at 30 ºC [297], based on the following relationship:

$$(\eta) = 7.70\times10^{-3}M\eta^{0.70}$$

The nitrogen content (%N) of whole collagen graft polymers is the most reliable indicator that gives an insight into the extent of ASC in the collagen graft copolymers, as well as a comparison of the amount of ASC segment in the copolymers [298].

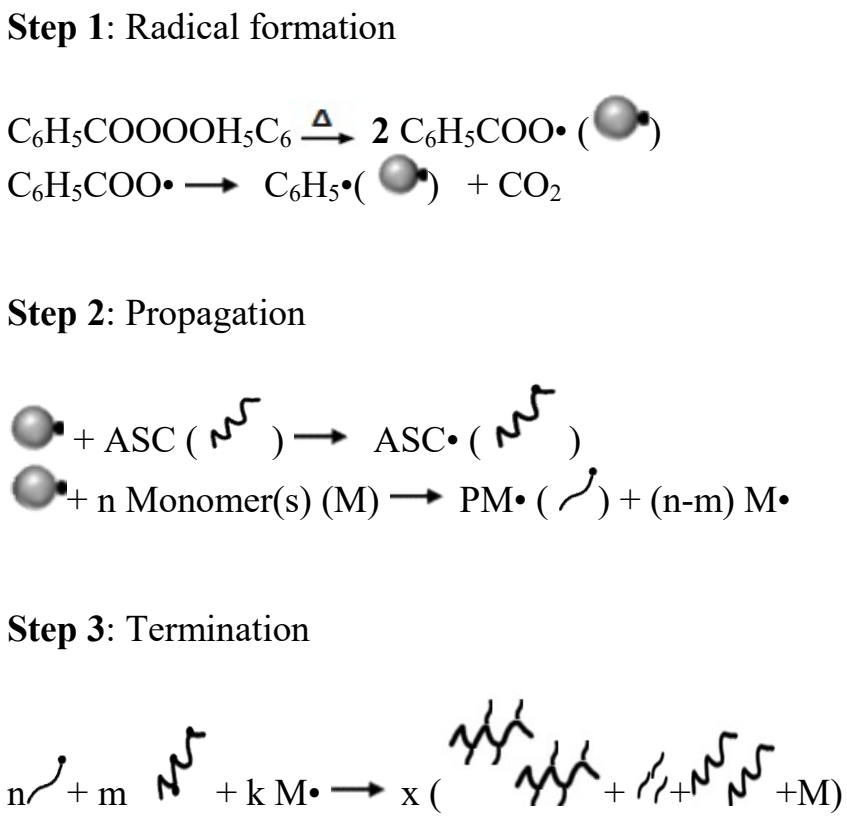

Figure 4-4 Schematic of the graft polymerization of ASC–g–P(MMA–co–EA), initiated with BPO, where n, m, k are variables indicating the number of initial, consumed and remained monomers.

Measurement of Nitrogen content is rapid, relatively cheap and requires little material and preparation. The carbon: nitrogen atomic weight ratios (C:N) of whole collagen graft copolymers were calculated to evaluate collagen preservation. About 0.3 to 0.5 mg of extracted collagen were weighed and analysed. $\%C_{\text{collagen graft copolymer}}$, $\%N_{ASC}$, and C:N ratios were measured. The results are shown in Table 4-2.

The results indicate that the ASC segment in the collagen graft copolymers is reduced in the following order (left to right): S1>S5>S2>S3>S4. From the molecular weight of branch copolymers in the samples, the grown side chains on the backbone of ASC represent the order S1>S5>S4>S2>S3, while the grafting density of the graft copolymers revealed some differences in contrast with other results where the grafting density follows the order of S4> S3>S2>S5>S1.

Overall, these results suggest that among the studied samples S1, with the highest fraction of ASC as well as the highest molecular weight of branches, is a sample that represents the lowest branching density. Also, with increasing monomer feed ratio, all grafting parameters were increased with the exception of S5 in which the monomer feeding is at its highest ratio.

Furthermore, S2, S3 and, S4 represent a decreased molecular weight of branch copolymers, higher grafting efficiencies, and lower Nitrogen content in contrast with other samples. This may be due to an increased number of grafting points on the ASC backbone.

To further provide information about the branching composition and the end groups of the collagen graft copolymers, ^{1}H NMR spectra of the samples were studied, Figure 4-5. This characterisation is beneficial due to the peak integrations for the protons associated with the branching which are determined by this method.

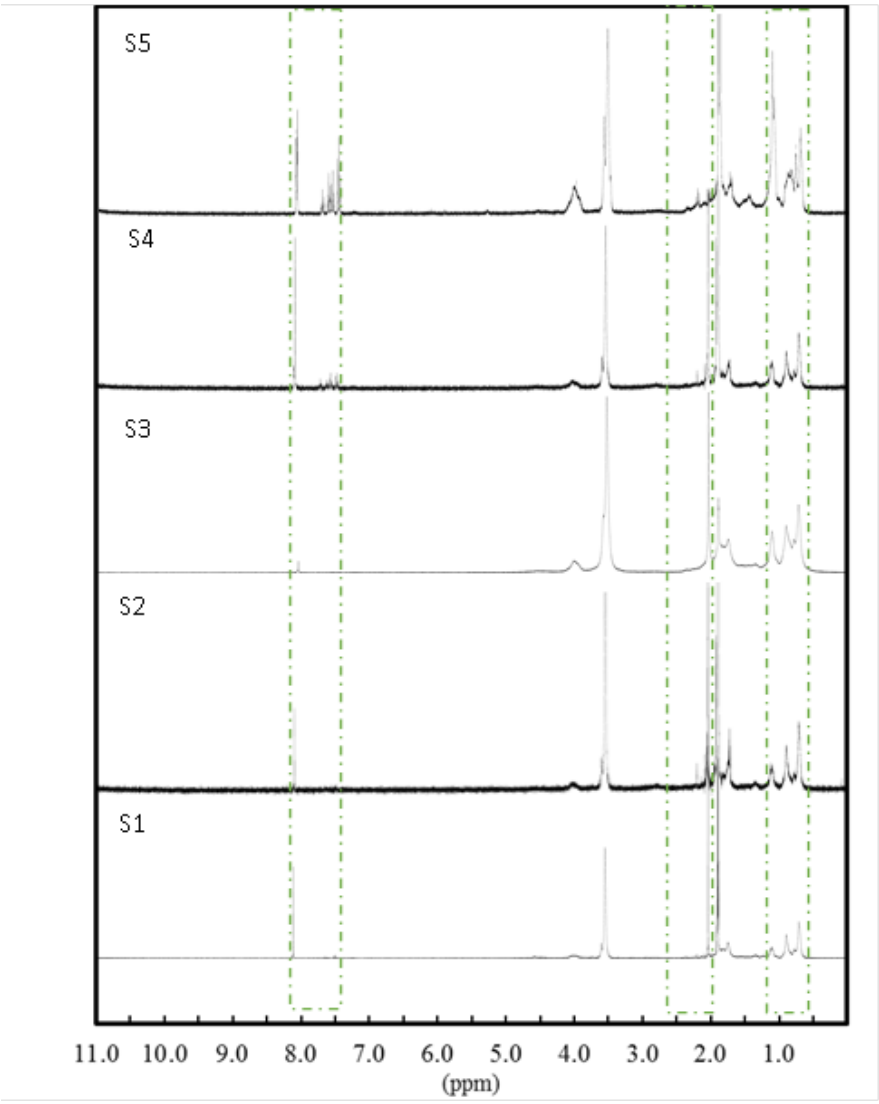

Figure 4-5 ^{1}H NMR Spectroscopy of collagen graft copolymers, S1... S5.

From Figure 4-5, the horizontal scale is shown as ppm is called the chemical shift and is measured in parts per million (ppm) [213, 299]. It is found that methylene and methine groups attached to a hydroxyl group can be differentiated by the chemical shift values range from 0.7–1.33 ppm. A resonance absorption peak for protons in α (R) where it is attached to oxygen ($RO–CH_3$) can be observed clearly with a chemical shift of 3.6–4.1 ppm. The NMR signal for the amine group becomes quite weak at the chemical shift of 1.5 ppm, and the grafting density of the reactive groups in ASC can be estimated from the composition of amino acids with reactive groups in ASC wherein react with monomers (reactant). More specifically, it can be estimated that the grafting point can be initiated where the carbon atom (C) is attached to Nitrogen (N) (RN–C–) and C is attached to C=O (R–CO–C). This can be differentiated by the chemical shift values range from 2–2.3 ppm. The NMR signal for the amide group is also significant in some samples at the chemical shift range from 7.8–8.2 ppm.

From the peak integrations for the protons associated with the branching, it can be suggested that the following order (left to right) S3>S2>S4 represents the highest branching points on the main backbone of ASC in contrast to the rest of the samples.

To identify the main characteristic features and the polymeric content of the grafted copolymer, FTIR Spectroscopy was carried out as an analytical technique used to scan test samples and observe chemical properties as described in chapter 3. To prepare the disk, the sample in KBr is prepared with an approximate weight of 1%. Figure 4-6 shows the FTIR spectra of ASC–g–poly(MMA–co–EA) as a proof of successful

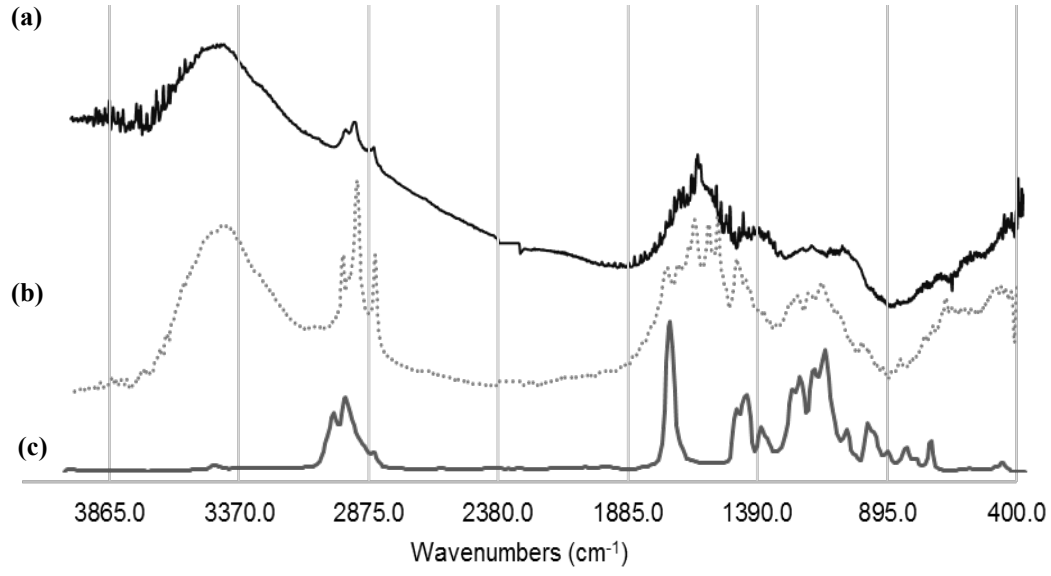

Figure 4-6 FTIR spectra of (a) ASC, (b) ASC–g–poly(MMA–co–EA); S1, (c) Poly (MMA–co–EA).

grafting and the presence of amide groups in the samples when compared with ASC and homopolymerised poly(MMA–co–EA).

Collagen has several characteristic absorption bands identified as amide A (3425 cm^{-1}), amide B (2857–2953 cm^{-1}), amide I (1621–1711 cm^{-1}) which is originated largely from the C=O stretching vibration, amide II 1466 cm^{-1} in the infrared region of the spectrum [208, 300, 301] that are absorbed by ASC–g–poly(MMA–co–EA).

Characteristic bands of poly(MMA–co–EA) were carbonyl (C=O) stretching vibration at 1720 cm^{-1}, CH stretching vibration at (2950–3050 cm^{-1}) (asymmetric) and 2865 cm^{-1} (symmetric), C–O–C stretching at 1060 cm^{-1}, and C–O–C stretching at 1260 cm^{-1} (asymmetric) [302].

Since the amide B and the amide II regions can be affected by poly(MMA–co–EA) absorptions, the amide A band and amide I were used as reference peaks to confirm the presence of collagen in the grafted copolymer. Furthermore, two new absorbance peaks can be observed in collagen graft copolymer; asymmetric vibration peak at 978 cm^{-1}, referring to α to nitrogen linkage (—N–C), and asymmetric stretching at 1158 cm^{-1} corresponding to (–CO–O–C) that can be the branching points on the main backbone of ASC.

The FTIR and ^{1}H–NMR data of the collagen graft copolymers suggest that poly(MMA–co–EA) branches were successfully grafted onto ASC through the side chain points from side groups of ASC such as hydroxyl, amino and carboxylic groups during the graft polymerisation.

4.2.3 Effect of copolymer structure on thermal behaviour of grafted copolymers

The effect of branching from two different monomers of an elastic material poly (Ethyl Acrylate), and of a brittle one, poly (methyl methacrylate), with a broad range of glass transition temperatures (Tg) on the main polymer (ASC) was investigated to obtain a flexible copolymer on to the ASC chains. The thermal analysis of collagen graft copolymers was performed by Differential Scanning Calorimeter (DSC, Mettler DSC 12E) as described in chapter 3, section 3.3.3. The DSC data were recorded within the temperature range 25 ^{o}C to 220 °C with a heating rate of 10 $°C.min^{-1}$ in nitrogen atmosphere. Sensitivity curves were obtained for thermal analysis of 8 mg of sample to evaluate changes in thermal behaviour.

As shown in Figure 4-7, the DSC curve of the collagen fibrils highlights two endothermic peaks at 85°C and 160°C for the melting point (Tm) and denaturation/decomposition process, respectively. In the collagen graft copolymers, the

melting temperature (Tm) increases to 97 °C in S1, while the Tg and T_d values are reduced to 53 °C and 147 °C, respectively. This behaviour can be affected by several parameters e.g. slight denaturing of the backbone in the polymerisation process when applying initiator which may lower the average molecular weight.

The enthalpy of denaturation (ΔH_d), on the other hand, does not change significantly with the presence of a higher fraction of synthetic polymers in the S2–S5 samples; the Tg slightly increased to 61–65 °C. These results indicate that Collagen is thermally altered by graft polymerisation in which poly(MMA–co–EA) is branched on the main backbone of collagen, as verified by the shifting of the melting peak to higher temperatures, with no considerable change on the enthalpy of denaturation and glass transition temperature of the studied samples.

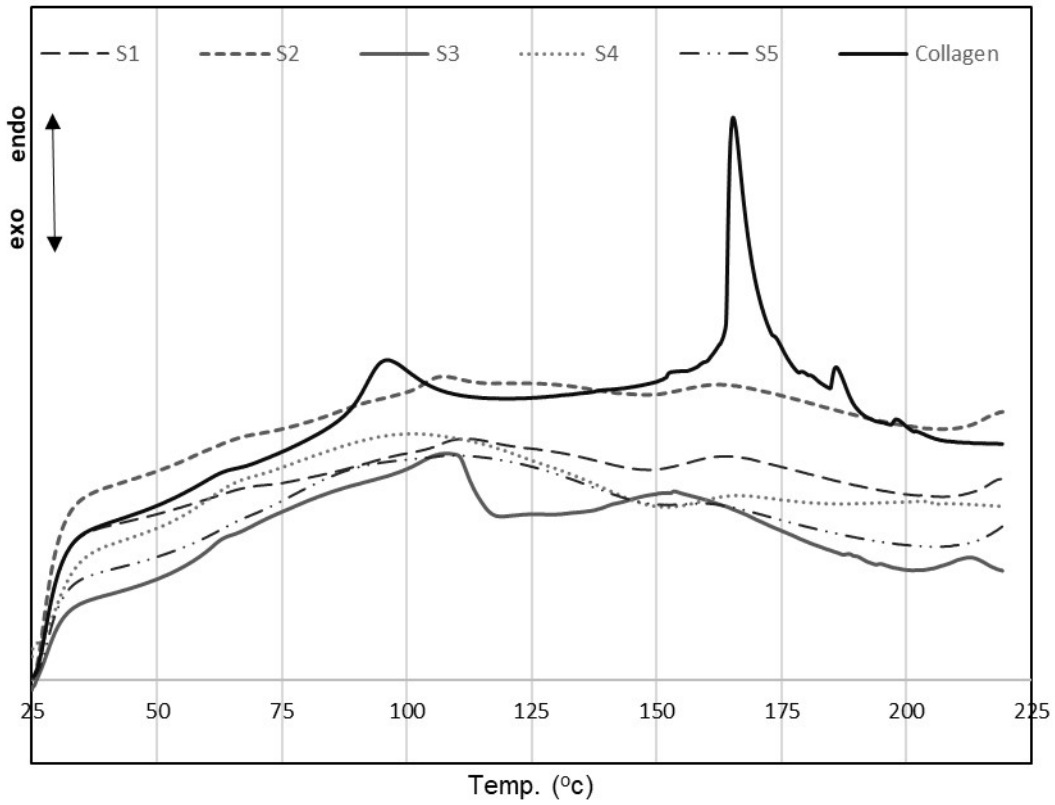

Figure 4-7 DSC Thermograms of Collagen and the resulted copolymers of different graft densities on ASC, S1...S5, using Aluminium pans, heating rate of 10 $^{o}C.min^{-1}$.

4.2.4 Effect of copolymer structure on viscosity of grafted copolymers

Inherent viscosities (η_0) were determined using a Brookfield DV–II+Pro Viscometer at a concentration of 0.1 $g.dL^{-1}$ at 20 ± 0.2 °C. Diluted solutions of ASC–g–poly(MMA–co–EA) in Formic Acid (FA, %97, Alfa Aesar) were prepared to prevent significant reduction in hydrodynamic volume of the solutions.

In earlier experiments, it was exhibited that the rheological behaviour of randomly branched polymers is widely dependent on the branch length [69, 303, 304]. In other words, for branched chains, it is accepted that there is a significant departure from the η_0–Mw relationship due to the reduced hydrodynamic volume of the branched chains at low molecular weights, and increased entanglement couplings at higher molecular weights due to increased entanglement couplings, as shown in Figure 4-8 [305].

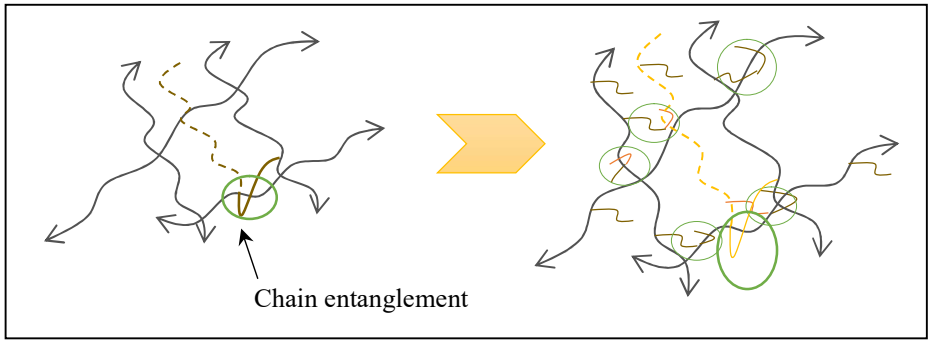

Figure 4-8 Cartoon representing the concept of increased chain entanglement by branched chains (shown by green circles).

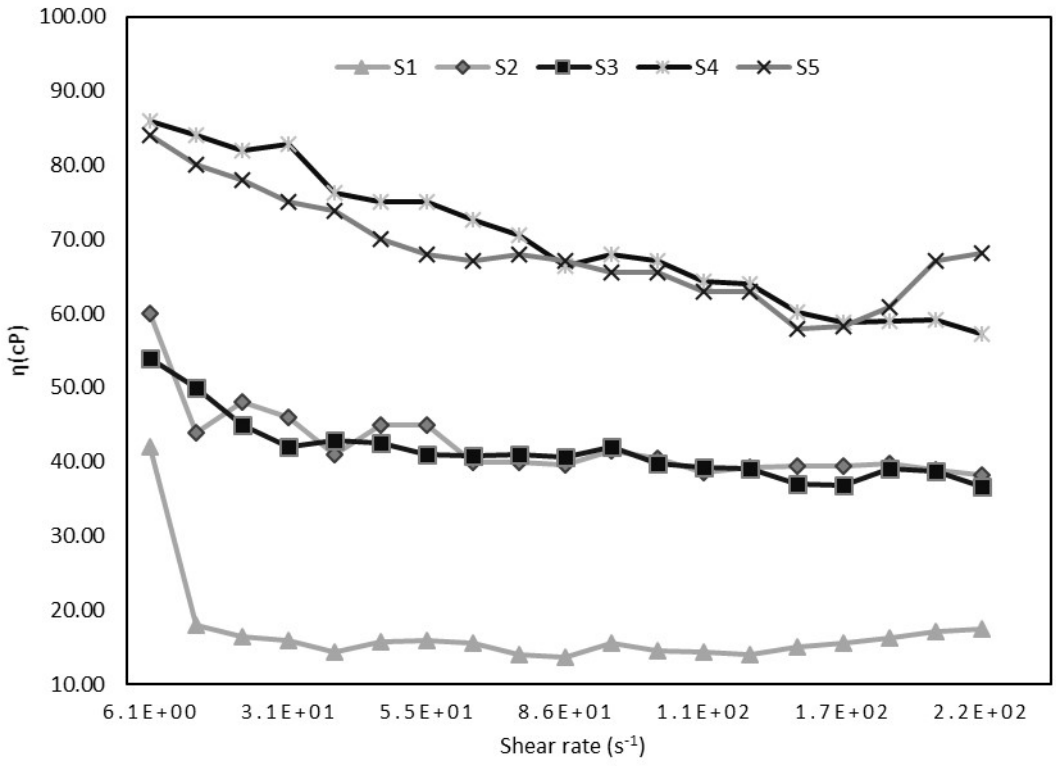

Figure 4-9 Shear rate dependence of viscosity for different branch densities on ASC. All copolymers show Newtonian behaviour over the studied range of shear rates.

Figure 4-9 shows that over the shear rate range investigated, the grafted copolymer displays Newtonian behaviour. The changed level of branching displayed significantly different viscosities (η) which is in less agreement with the molecular weight of branches, Table 4-2. On the other hand, some researchers suggest that the increased number of branches increases the viscosity compared to fewer branches at the same molecular weight [306]. Hence, in the case when the molecular weight of branches is approximately the same in S1 and S5, the reason of increased entanglement coupling can be the number of branches grown on the backbone of the ASC.

4.2.5 Effect of copolymer structure on the conductivity of grafted copolymers

The conductivity of the above-mentioned solutions of ASC–g–poly(MMA–co–EA) ($0.01 \leq C \leq 10$) was measured with the aim of comparing the conductivity of different branching levels on charge dynamics of the chains. The conductivity value was determined using a conductivity meter (HANNA HI8733), when measuring solutions of different concentrations dissolved in Formic acid (FA), Figure 4-10.

The cationic character of ASC is responsible for the higher electric conductivity compared to the poly(MMA–co–EA) with dielectric properties when they are dissolved in FA [307]. When poly(MMA–co–EA) with low dielectric constant is grafted on the backbone of amine and carboxyl group, is expected to react as a barrier against the electron mobile phase of the solution. In other words, for solutions containing ASC–g–poly(MMA–co–EA) that it is observed a sharp decrease of the conductivity value, possibly due to hydrogen bond reduction as a consequence of graft polymerisation and replacement of comonomers on the molecular chain of ASC.

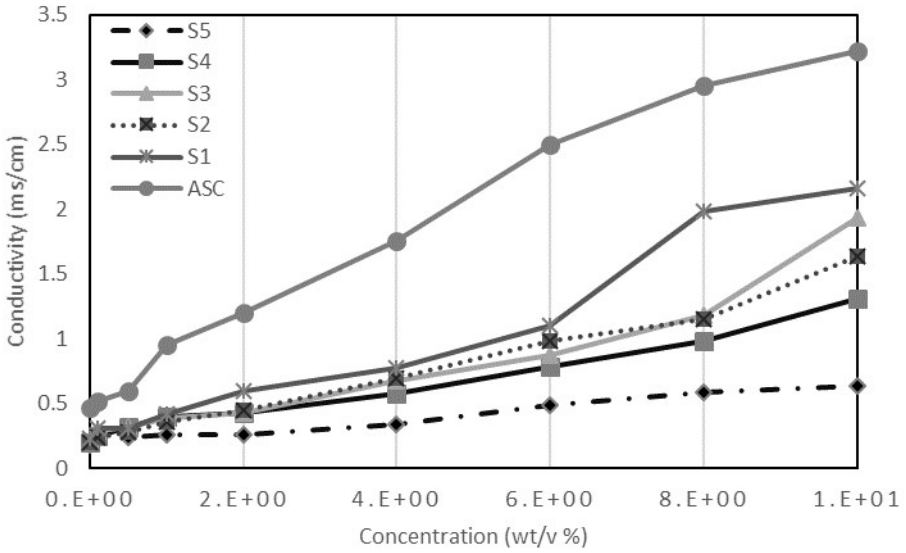

Figure 4-10 Effect of varied branching densities on conductivity value of ASC–g–poly(MMA–co–EA)

As can be seen in Figure 4-10, the conductivity values of the studied samples are significantly lower than the associated values for ASC. Interestingly, a meaningful arrangement on comonomer feeding ratios is observed, whereas S1 demonstrates the highest conductivity value. This phenomenon may be due to varied densities of branches on the main backbone of the ASC. The observations prove that the electrical behaviour of ASC as a polyelectrolyte can be significantly affected by dielectric behaviour of the branched side chains.

Chapter 5 Systematical optimisation of the electrospinning solution as a function of viscosity

The ability of the material to be processed at different scales is the aimed objective for many applications. These scales can be nano- to micro-scale when high surface–to–volume ratios of the materials are required. Nano- to micro-scale textures are mostly the first choice to increase the surface–to–volume ratio of the materials. Self-assembled features representing nano and micro textures/features have been previously reported. Also, porous membranes from different polymeric systems have been achieved by other phase separation techniques. However, during the last two decades the electrospun membranes have received much attention for different applications. Electrospun membranes are often known as electrospun nonwoven mats where the fibres are accumulated and conjugated on cross sections or along the axis in 2D depositions. In some applications the nanoscale pore size is of interest, as is the functionality of reduced-sized fibres, and in some cases the direction of the fibres is the determining factor for the functionality of the nanofibre mats. Furthermore, the 3D ordered electrospun fibres formed by a secondary factor of a designed collector or 3D self-assembles are still a new complex topic in electrospinning when they are tailored to enhance the functionality of the electrospun fibres. Hence, the functionality of the fibres determines the tailored morphology of the electrospun fibres from its architecture to a high porosity and large surface area, while defect free fibres, known as bead free fibres, are desired [120, 122, 149, 310].

Apart from the architecture of the fibres that is affected mostly by the functionality of the grounded collector, the processing parameters are widely believed to affect the morphology of the electrospun nonwoven mats, including fibre diameter and uniformity. The effect of the electrospinning parameters was discussed in Chapter 1 section 1.4. In brief, these parameters can be categorized into three main groups as shown in Table 5-1. Numerous reports studied the effects of these parameters, while each of them can affect the morphology of the electrospun fibres significantly.

Although the parameters of the electrospinning process have been well investigated, the results are inadequate to be thoroughly generalized due to their diversity and complexity. For instance, while it is believed that electrospun fibres can achieve reduced fibre diameter by increasing the applied voltage [67], it is indicated by other researches that the fibre diameter is not reduced by a higher applied voltage [9, 40, 150,

311]. They suggest that an increased intensity of the electric field is to pull a solution out from the needle, hence higher applied voltage causes more solution to be expelled, in contrast with Tan et al. [9] who suggest that the effect of the applied voltage is significantly reduced the fibre diameter when a low polymer concentration is used. It is also noted that beaded fibres are found when a too high applied voltage is used.

Table 5-1 Processing parameters in electrospinning

Solution properties	Viscosity [a] Polymer concentration [a] Molecular weight of polymer Electrical conductivity [a]
Processing parameters	Applied voltage [a] Distance between needle and collector [a] Feed rate [a] Needle diameter [a]
Ambient parameters	Temperature [a] Humidity [a] Atmospheric pressure

[a] Processing parameters considered in this work.

In brief, according to earlier works, higher voltage is reported to induce either larger diameter or smaller diameter depending on (i) mass of polymers that initiated by charge repulsion on tip of the needle to form a polymer jet, (ii) morphology of the cone (a single or multiple jet formation), and (iii) the elongation capacity of the polymer jet determined by the intensity of the electrical field and the polymer chain entanglements.

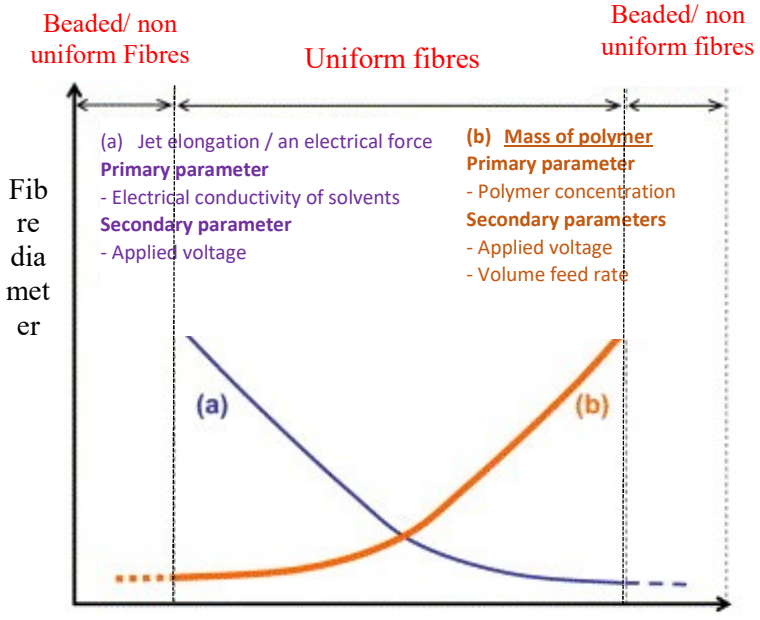

Feed rate and applied voltage can be coupled to control the mass released from the tip of

Figure 5-1 A typical processing map: (a) Polymer jet elongation (affected by applied voltage and electrical conductivity of solvents), (b) Mass of polymer jet (affected by applied voltage, polymer concentration, and flow/feed rate) [9].

the needle. According to Tan et al. [9], the electrospinning parameters can be divided into primary and secondary parameters. Hence, they systematically summarized the effect of applied voltage as the secondary parameter when can couple with either the effect of solution conductivity or feed rate to cause a morphology, as shown in Figure 5-1 [9].

However, they didn't refer to the effect of viscosity as a function of various parameters such as concentration, molecular weight and intermolecular interactions including non-covalent bonds determining the degrees of chain entanglements. This can be due to the fact that this parameter, even though it is formed by other factors, can be varied for each polymeric system that requires a more in–depth study, specifically for polymeric systems where any of the factors that affect the viscosity, may be unknown.

In this chapter, the solution properties and processing conditions of electrospinning are considered on the studied samples as listed in Table 4-1 and Table 4-2. We determine two sets of factors controlled and variable; due to the varied branching density that grown on the backbone of ASC where the viscosity change significantly affect the processability of the collagen graft copolymers. Hence, the effect of viscosity change on fibre formation / processability is optimised by using one-factor response surface methodology (One-factor RSM) as described below.

5.1 Experimental section

The earlier five samples of ASC–g–poly(MMA–co–EA) studied in chapter 4 were processed using a typical electrospinning method. To prepare the electrospinning solution, the collagen graft copolymers were dissolved in Formic Acid (FA) in varied viscosities at room temperature. For the electrospinning process, the polymer solution was placed in a 5 ml syringe with the needle gauge of 22. As mentioned in chapter 3 section 3.2, a Spraybase electrospinning apparatus was used by applying a voltage of 10 kV to the needle. Randomly oriented nanofibres were electrospun on a grounded rotating collector (surface length 25 cm, diameter 9 cm) that was located 15 cm from the tip of the needle. The prepared polymer solutions in a 5-ml syringe were then fed at a rate of 1 $ml.h^{-1}$ using a syringe pump. All electrospun fibres from varied copolymer solutions were collected and corresponding characterizations were performed after 24 h to ensure that the solvents were fully evaporated. To determine the morphology of the electrospun fibres, the nanofibres were observed using scanning electron microscope (SEM; Hitachi S-3400). The controlled factors are summarized in Table 5-2.

To study the effect of viscosity on the processability of the collagen graft copolymers, response surface methodology (RSM) was applied. This statistical model is easy to estimate and apply, even when little is known about the correlation between the process parameters. The main objective of applying RSM is to use a set of designed experiments to achieve an optimal response on viscosity as a variable factor to be used for all the studied samples. We applied one-factor methodology over 10 runs for each sample to find the relationship between the viscosity and the response of Spinnability (processability).

To the best of our knowledge, there is no specific standard to determine the exact defect free definition for the morphology of electrospun fibres. Hence, we applied the following codes for determining the quality of the electrospun fibres including zero (0), 0.75, and one (1) as shown in Figure 5-1.

Statistical approaches of RSM were employed to maximize the processability probability of ASC–g–poly(MMA–co–EA) by optimising the viscosity. This is due to the dependency of viscosity on various factors such as concentration, molecular weight, and inter molecular interaction of solution components. To optimise the viscosity which is determined by varied parameters, the upgraded one- factor modelling from its default of quadratic to cubic, thus the number of runs increased from 7 to 10 for each sample by increasing the centre points from default to 2, as shown in Table 5-3.

Hence, the model was planned for 50 runs over the variable parameter of viscosity fluctuating from 50 to 150 cP for each sample. Five responses were introduced indicating the spinnability of the electrospinning solutions at a certain viscosity.

In this experimental model, any morphology that lost its fibrous integrity/perfection is assumed as a non-spinnable indicated by a zero value in Table 5-4. The fibres which were significantly stuck to each other count as 0.75, a non-acceptable quality that is close to the desired spinnable polymer solutions; for instance, as shown in Figure 5-2, The viscosities corresponding to (A) to (D) are not spinnable (0) and the viscosities representing (D) are a case, between accounted as (0.75), (E) to (J) are assumed as spinnable viscosities (1).The fibre characterisations such as average diameter and uniformity of the spinnable samples are not evaluated in this chapter.

Table 5-2 Controlled electrospinning parameters

Sample	Solvent	Needle gauge	Voltage (kV)	Distance (cm)	Feeding rate ($ml.h^{-1}$)	Collector speed ($m.s^{-1}$)	Temperature ^{o}C	Humidity
S1	FA	22	10	15	1	1.7	25 ± 2	35–40 %
S2	FA	22	10	15	1	1.7	25 ± 2	35–40 %
S3	FA	22	10	15	1	1.7	25 ± 2	35–40 %
S4	FA	22	10	15	1	1.7	25 ± 2	35–40 %
S5	FA	22	10	15	1	1.7	25 ± 2	35–40 %

Table 5-3 Design summary

Study Type	Response Surface	**Runs**	10
Initial Design	One-Factor	**Blocks**	No Blocks
Design Model	Cubic		

Factor	Name	Units	Type	Low Actual	High Actual	Low Coded	High Coded	Mean	Std. Dev.
A	Viscosity	cP	Numeric	50.00	150.00	-1.00	1.00	100.00	35.73

Response	Name	Units	Analysis	Min.	Max.	Mean	Model
Y1	Spinnability S 1	**N/A**	Polynomial	0.000	1.000	0.550	Cubic
Y2	Spinnability S 2	**N/A**	Polynomial	0.000	1.000	0.525	Cubic
Y3	Spinnability S 3	**N/A**	Polynomial	0.000	1.000	0.475	Cubic
Y4	Spinnability S 4	**N/A**	Polynomial	0.000	1.000	0.550	Quadratic
Y5	Spinnability S 5	**N/A**	Polynomial	0.000	1.000	0.550	Quadratic

For Samples 1, 2 and 3, the cubic model is suggested by the program as shown in Table 5-2. The sequential sum of squares is revealed in Table 5-5. The extremely low p–value indicates a highly significant advantage of the designed experiments to determine a proper prediction model for optimised desirability of the variable factor. In fact, the model focused on maximising the adjusted R–squared and predicted R–squared values. From the lack of fit test, R–squared, confidence intervals (CI) and the variance inflation factors (VIF), which are automatically calculated by the software, this model is statistically significant.

Table 5-4 Design actual raw data

Run	Viscousity (cP)	Spinnability S 1	Spinnability S 2	Spinnability S 3	Spinnability S 4	Spinnability S 5
1	50.00	0	0	0	0	0
2	133.30	1	1	1	1	1
3	50.00	0	0	0	0	0
4	100.00	0.75	0.75	1	1	1
5	66.70	0	0	0	0.75	0.75
6	116.65	1	1	1	1	1
7	100.00	0.75	0.75	1	1	1
8	150.00	1	1	0	0	0
9	83.35	0	0	0.75	0.75	0.75
10	150.00	1	0	0	0	0

Table 5-5 Sequential sum of squares

Response: Spinability S #	Source	Sum of Squares	Degrees of Freedom	Mean Square	F Value	p–value Prob >F
1	Cubic vs Quadratic	0.19	1	0.19	10.23	0.0186
2	Cubic vs Quadratic	0.24	1	0.24	11.33	0.0151
3	Cubic vs Quadratic	0.33	1	0.33	20.78	0.0039
4	Quadratic vs Linear	1.87	1	1.87	60.65	0.0001
5	Quadratic vs Linear	1.87	1	1.87	60.65	0.0001

Therefore, the following final equations in terms of actual factors are suggested for each response:

$$Y1 = 3.47 - 0.14A + (1.70 * 10^{-3})A^2 + (5.85 * 10^{-6})A^3 \quad (1)$$

$$Y2 = 3.90 - 0.16A + (1.90 * 10^{-3})A^2 - (6.61 * 10^{-6})A^3 \quad (2)$$

$$Y3 = 2.76 - 0.13A + (1.91 * 10^{-3})A^2 - (7.70 * 10^{-6})A^3 \quad (3)$$

$$Y4 = -3.09 + 0.08A - (4.06 * 10^{-4})A^2 \quad (4)$$

$$Y5 = -3.09 + 0.08A - (4.06 * 10^{-4})A^2 \quad (5)$$

where A and Y1 to Y5 are Viscosity and Spinnability of S1 to S5, respectively. These formulas are very important, as they can provide simply an estimate via One-factor RSM for applied viscosities.

A

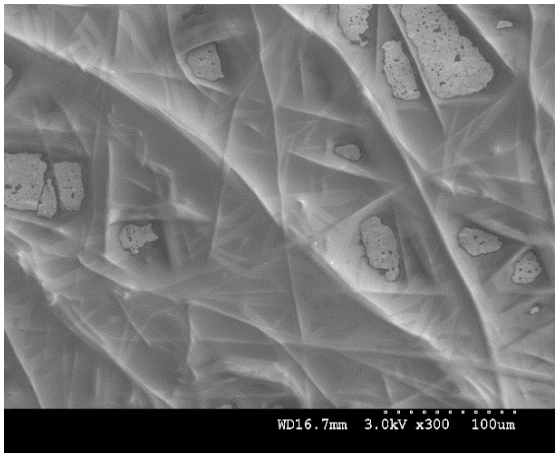

C

B

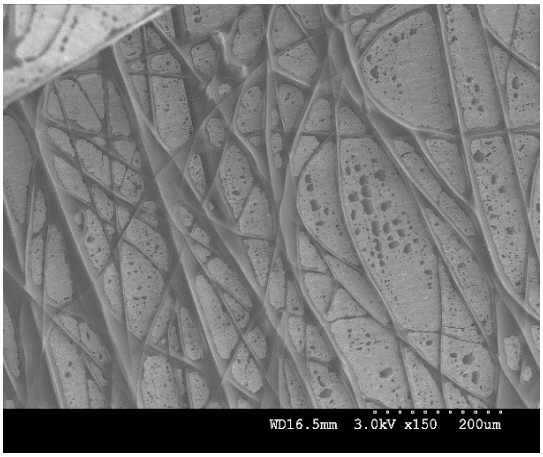

D

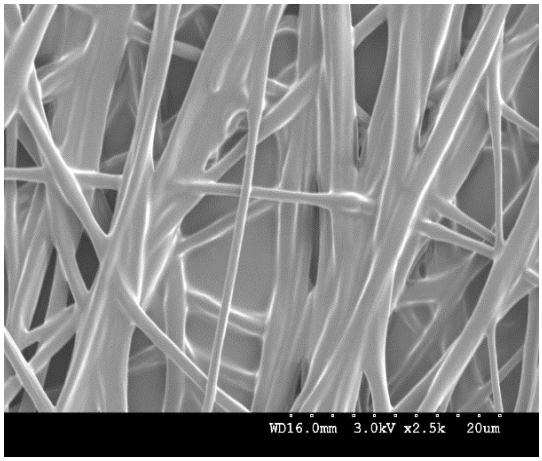

E

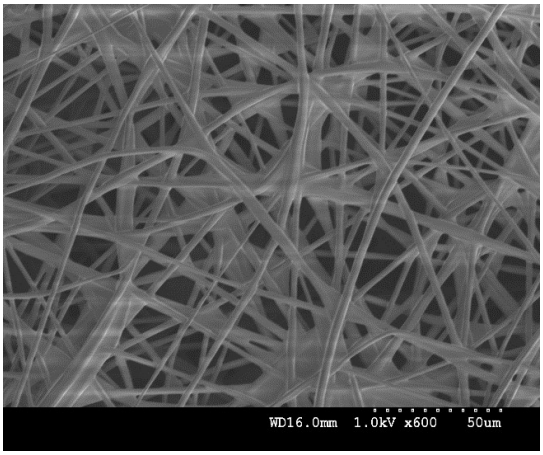

F

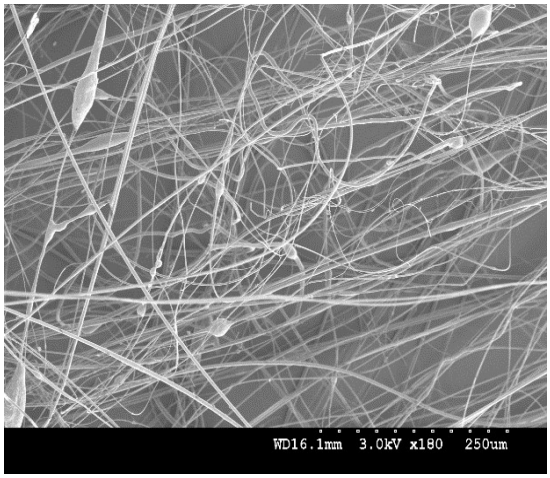

G

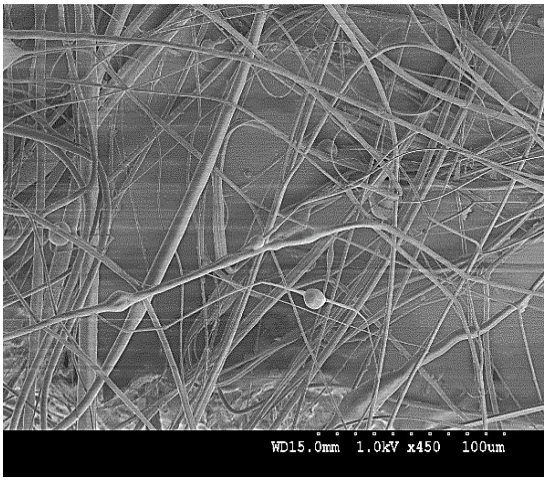

H

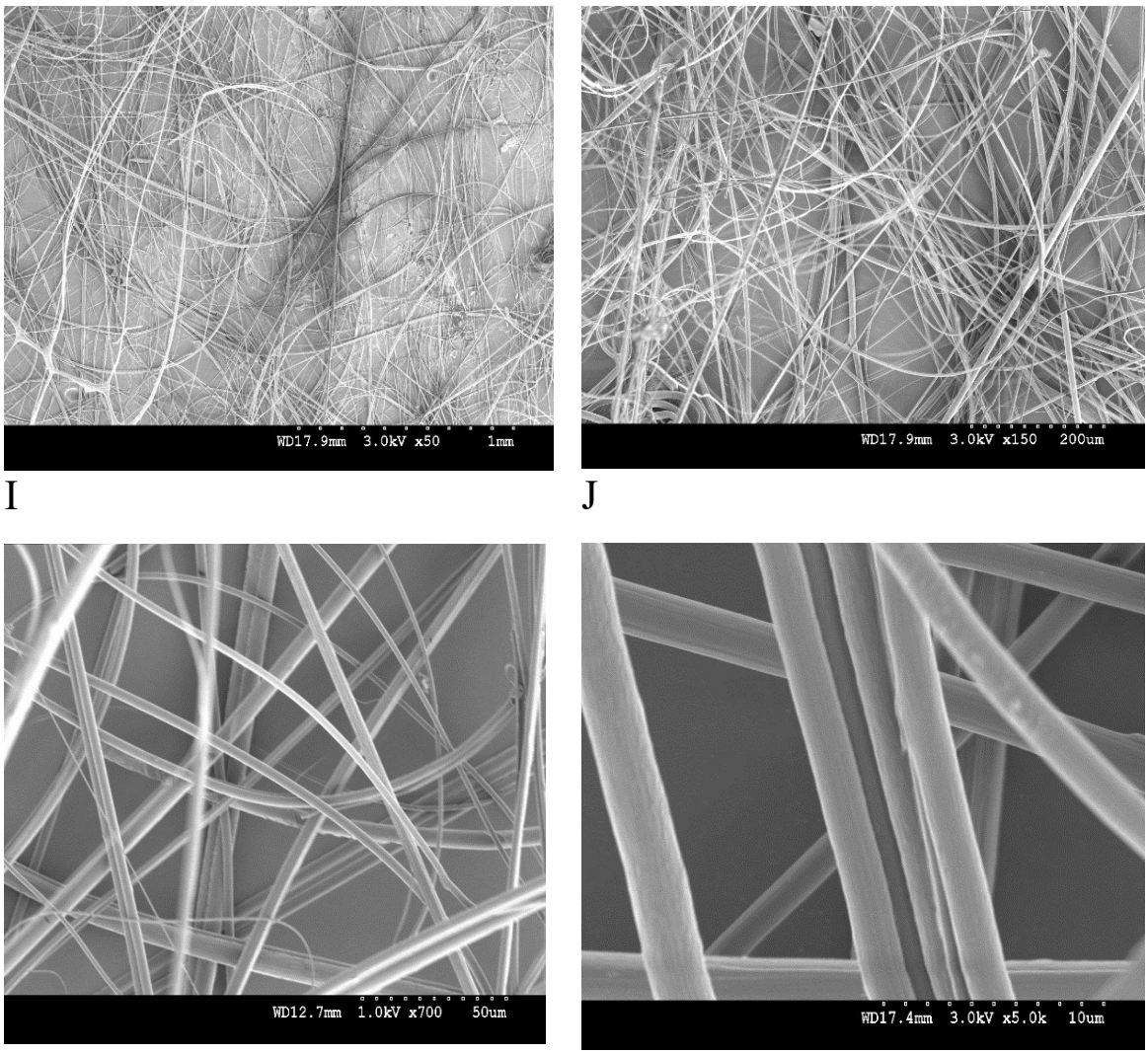

Figure 5-2 SEM image of Sample 1, with varied morphologies from varied solution viscosities. In this one-factor modelling with 10 runs, we assumed that Viscosities corresponding to (A) to (D) are not spinnable (0) and the viscosities representing (D) is a case between accounted as (0.75), (E) to (J) are were assumed as spinnable viscosities (1)

5.2 Results and discussion

Electrospinning is well known as a processing method to form custom-built fibres with a large specific surface area, in contrast with conventional spinning methods. In this chapter, we have evaluated systematically the effects of viscosity on the processability of the electrospinning solution by applying One-factor RSM. Understanding the solution viscosity of copolymers is a keystone to develop a significant model for the solutions to be studied in the next chapters.

Generally, it is believed that a spinnable solution must have a high enough concentration to provide a sufficient degree of chain entanglements. Nevertheless, the viscosity is not only proportional to the concentration; viscosity is determined by

increasing factors such as structural branching, molecular weight and molecular weight distribution, pressure, and adding of fillers and decreasing factors such as temperature, processing additives etc. and also some more complicated factors such as hydrophilic nature, and interaction of polymer molecules with the solvents [1, 312, 313]. Hence, there is no doubt that viscosity is the result of a number of factors.Again, since the viscosity is the only electrospinning parameters that is significantly affected by the structure of the copolymers and other known and unknown factors, it was optimised for our study.

From our observation, the viscosity of the spinnable solutions is strongly correlated with the formation of non-integrated fibres. During our experiments, we found that solution viscosity can be the most important factor in fibre formation due to its strong effect on branching structure of collagen graft copolymer as well as unknown intermolecular interactions that affect the viscosity during the electrospinning such as solvents as discussed in chapter 2, section 2.4.

More specifically, in proton donor solvents the highly hydrophilic segments of the acid soluble collagen prefer to be surrounded by solvent molecules rather than by the hydrophobic segments of branches. Hence, the extension of the solution viscosity of ASC–g–poly(MMA–co–EA) can additionally depend on the interaction of the copolymer-solvent, which may directly affect the viscosity of the solution.

To isolate the effect of other electrospinning settings, we considered them as controlled factors, Table 5-2, which is due to the high importance of the viscosity of solutions to be optimised. To study the lack of the fits in this model, we plotted the percentage of probability vs. residuals. It can be seen that the experimental internal statistics are well surrounded by actual experiments data that exhibit the significance of the model, as shown in Figure 5-3.

Furthermore, to better understand the correlation between the actual data and predicted data, the graphs in Figure 5-4 were plotted to study the actual versus predicted responses where the points showed some scatter around the line while some hit the high point directly. Figure 5-5 eventually shows the final stage of the response surface plot. These plots reveal how the spinnability of the samples can vary as a function of viscosity. Hence, we applied the following criteria to determine the optimised desirability point for further experiments, to be considered in the next chapter. Hence, the goals of the model were determined; a minimized viscosity and maximized responses, as shown in Table 5-6.

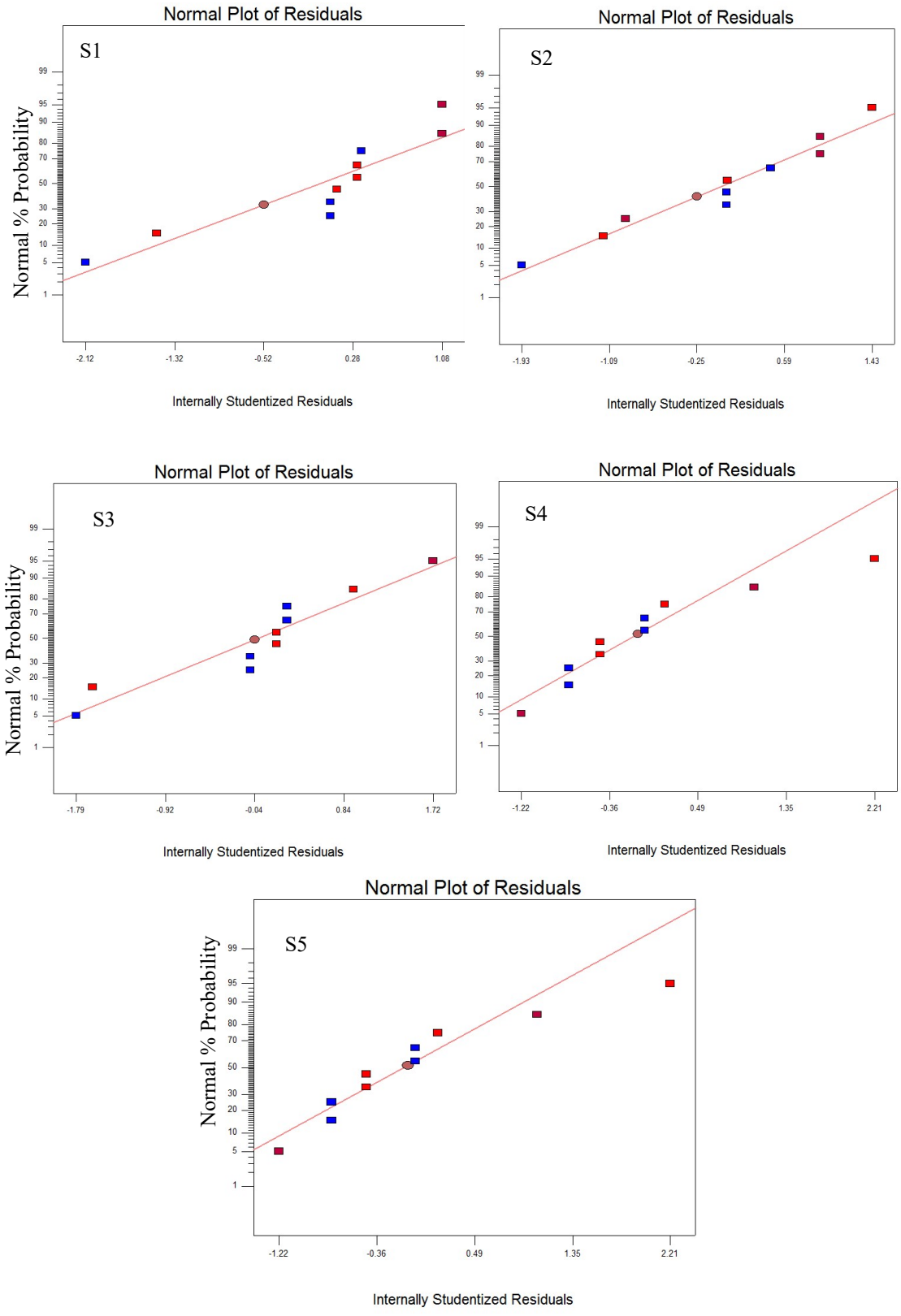

Figure 5-3 Normal plot of residuals

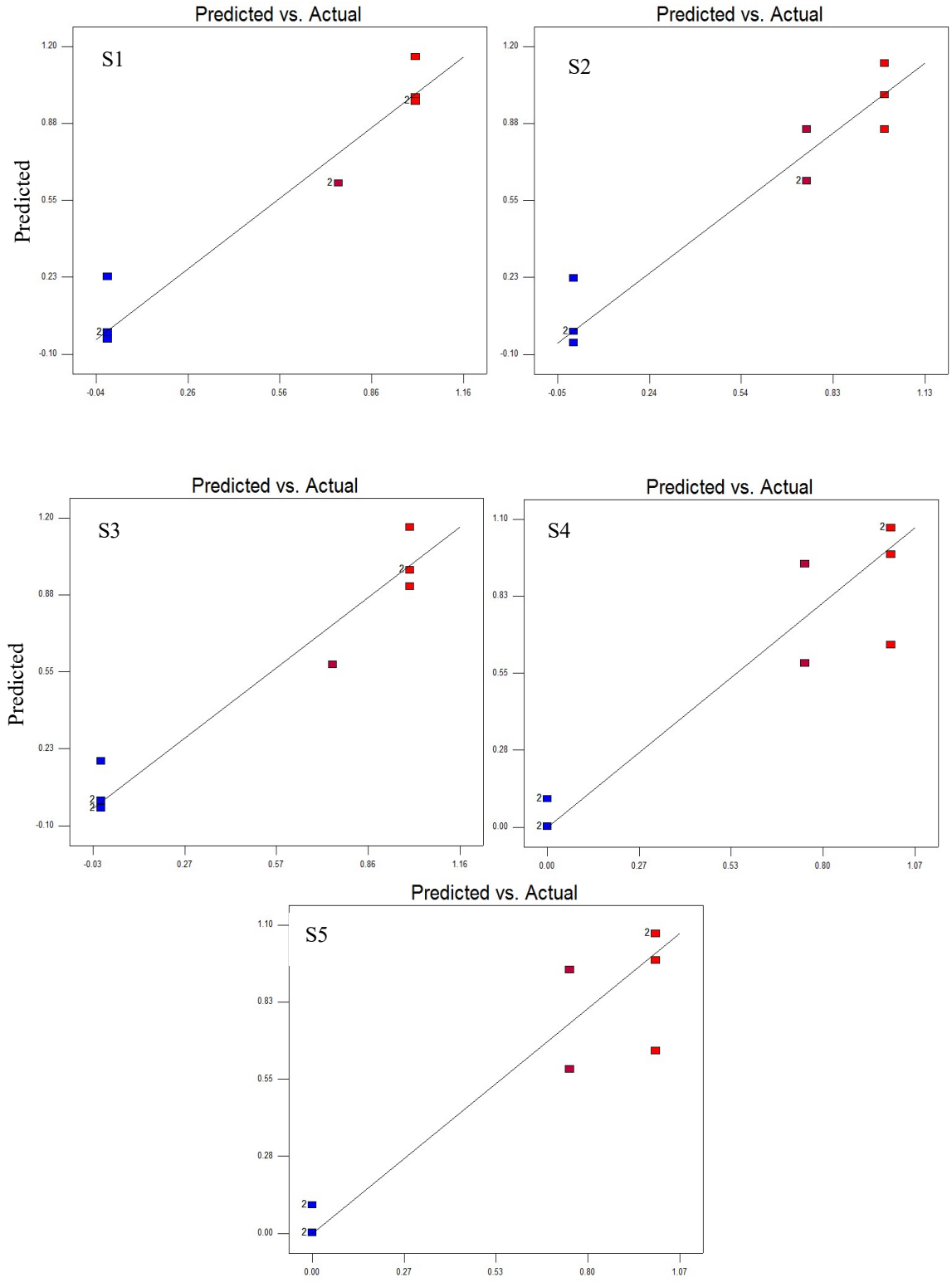

Figure 5-4 Predicted versus actual response

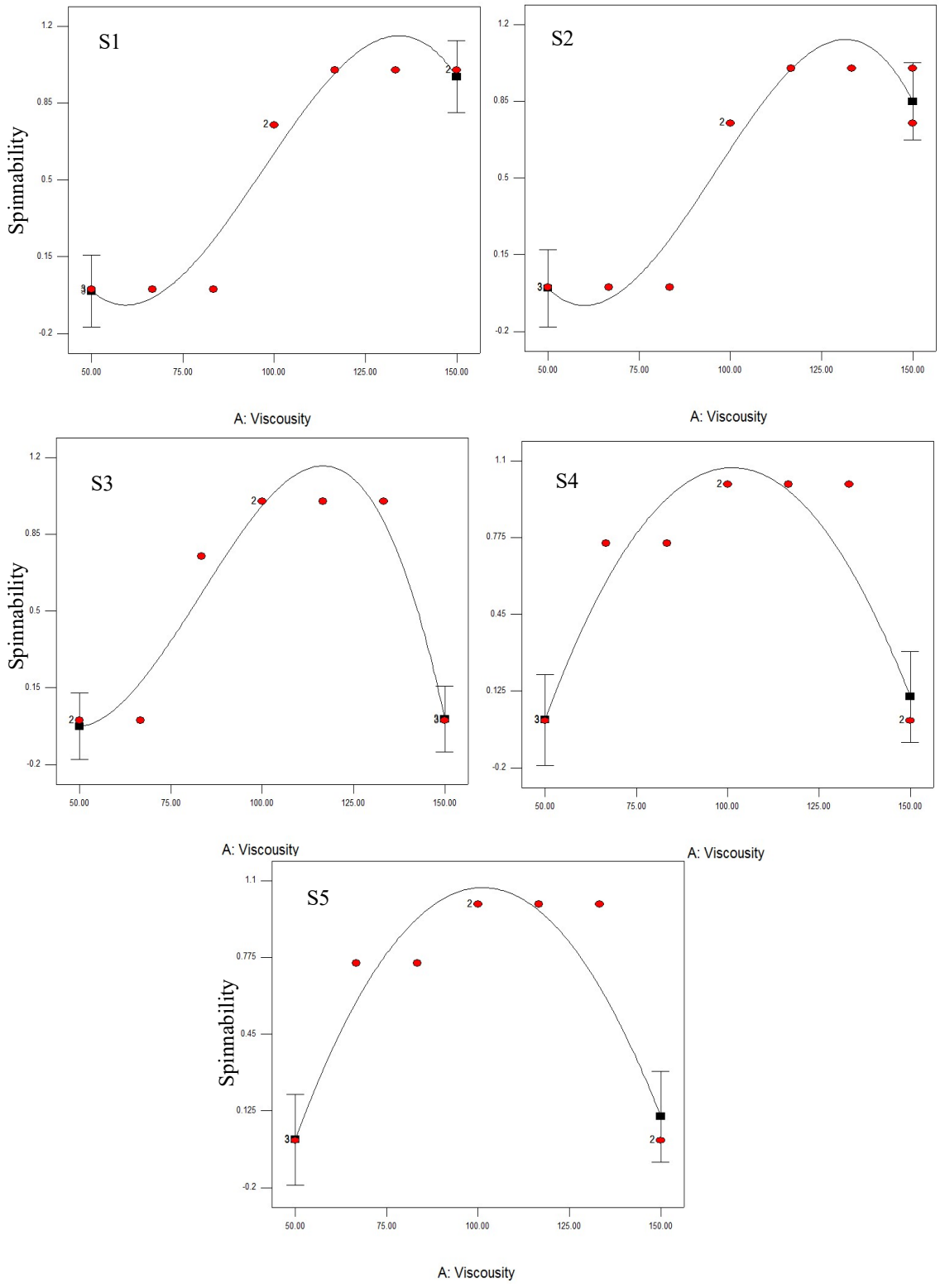

Figure 5-5 One-factor graphs for Spinnability of the samples (responses) vs. Viscosity (factor)

Table 5-6 Constrains of the optimisation criteria

Name	Goal	Importance
Viscosity	Minimize	1
Spinnability S 1	Maximize	3
Spinnability S2	Maximize	3
Spinnability S 3	Maximize	3
Spinnability S 4	Maximize	3
Spinnability S 5	Maximize	3

As shown in Figure 5-6, from the analysed statistics and the above-mentioned criteria, a solution was suggested where its desirability of prediction is 0.921.

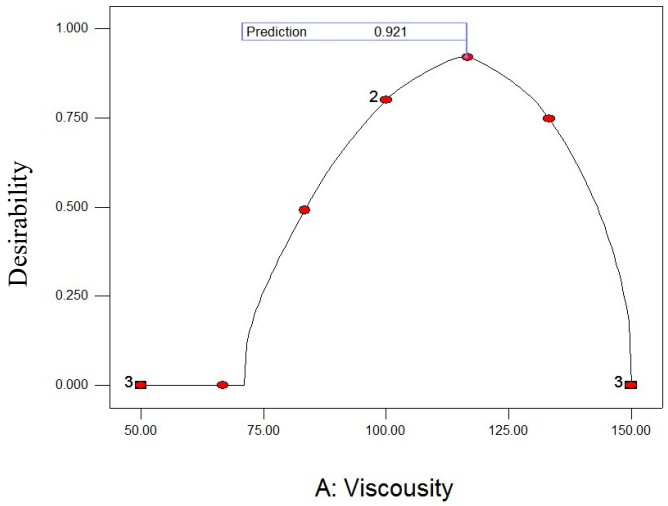

Figure 5-6 The desirability of the prediction based on the statistics and the model criteria

The desired viscosity of 117.42 is the total prediction of the model where each sample is to be highly spinnable, as revealed in Table 5-7.

Table 5-7 Prediction of each response for the most desirable viscosity

#	Viscosity	Spinnability S1	Spinnability S2	Spinnability S3	Spinnability S4	Spinnability S5	Desirability*
1	117.42	0.981711	0.991468	1.16131	0.976182	0.976182	0.921

*The selected solution

The viscosity was optimised by a set of determined goals as mentioned above to achieve the lowest viscosity of the highly spinnable solutions. This was due to two main reasons:

(i) To prevent Rayleigh instability of the polymer jet because of reduced hydrodynamic volume of the solutions which may be caused by highly chain entanglements at high concentrations.

(ii) To study the effect of the branched chains on fibre morphology that is more likely be affected by processing conditions.

Even though our calculations and predictions are based on our observations on overall morphology of the electrospun fibres, the model led to the identification of a critical optimised solution that can be used for all collagen graft copolymers. In other words, this optimised solution will allow us to examine the reproducibility of fibres using the same viscosity while the value of this viscosity is influenced by various factors.

Finally, we expect that while the same coupling terms of viscosity can be achieved as discussed above, the functionality and structural properties of the fibre samples will be varied, which will be considered in the next chapter.

Chapter 6 A novel approach of enhancing the spinnability of collagen fibres by graft polymerisation

This chapter describes the development, characterization, and investigation of the optimised spinnable viscosity suggested by One-factor RSM that was obtained in chapter 5. This is an attempt to get an insight into the structurally modified collagen fibres. Since electrospinning is believed by a several research group, as a challenging processing method for the delicate collagen chains, comprehensive surface characterizations were performed on electrospun fibres from collagen graft copolymers to investigate the effect of processing conditions on the structure and functionality of the pre-modified collagen chains. This is to suggest a methodology based on controlled branching that can be used as a tunable method of achieving certain morphologies of the fibres in contrast with the other modification methods that are performed as post treatments and their corresponding challenges.

6.1 Experimental section

The collagen graft copolymers were dissolved individually in Formic Acid (FA) stirred at room temperature until homogenous solution was achieved. To investigate the effect of poly(MMA–co–EA) content, each solution was then transferred into a 5–ml syringe connected to a needle (22–gauge) to be processed.

As shown in Figure 3-2, a Spraybase® electrospinning system was used to process all the solution samples with the following conditions: feed–rate (1 $ml.min^{-1}$), needle diameter (gauge 22), temperature (25±2 ^{o}C) and humidity (RH: 35–40 %) (using IR lamp), TCD (15 cm, distance between the tip of needle and the fibre collector), voltage (10 kV) and different solution concentrations with approximately same viscosity. The fibres were collected on a grounded rotating collector (surface length 25 cm, diameter 9 cm) at a speed of about 1.7 $m.s^{-1}$.

6.2 Results and Discussion

As was discussed in previous chapters, it is essential to modify the collagen chains to desired characteristics for specific end uses [19]. Thus far, the main objective for many research groups has been focused on reducing the highly hydrophilic behaviour of collagen chains and benefitting from controllable degradation ratio by using graft polymerisation methods [5, 219, 258, 314, 315]. These methods are typically well known to produce collagen-based hydrogels [5, 316-319].

When it comes to promoting a final product with high surface area, the electrospinning is an attractive method for the processing of polymers that can be achieved by altering the processing and polymer melt/solution factors [129, 320]. Nevertheless, this method presents its own challenges due to harsh processing parameters applied on the sensitive structure of collagen chains in order to form electrospun fibres.

For instance, Zeugolis et al. reported that physiochemical properties of the pure collagen are lost when it is electrospun into fibres [94]. They observed a reduced denaturation temperature in electrospun collagen chains that has been confirmed by some recently published studies [90, 233]. In similar work, Yang et al. revealed that 45% of the collagen mass is denatured during electrospinning [204]. Furthermore, due to a significant conformational change in collagen chains, it has been reported that the electrospun collagen fibres do not swell in aqueous media but may immediately dissolve in water [29, 182, 204, 259, 321].

The lost properties are mostly due to the fast denaturation of hydrolysing chain of the collagen in polar solvents. Even though high concentration solutions of unmodified collagen [322] and applying salt crystals[323] can slightly reduce the effect of the severe denaturation on electrostatic repulsion resulting from the build-up positive charge, the complete elimination of ions before crosslinking can be problematic for some specific morphologies.

As discussed in chapter 2, to reduce the negative effect of processing methods on collagen chains, surface modification methods on collagen fibres using crosslinking agents have been extensively recommended for post treatment [101, 122, 129, 320]. For instance, chemical crosslinking agents such as aldehydes have been typically applied to preserve the morphology of collagen fibres [129, 320]. However, due to random reaction of cross-linking agents, the end material is more likely to lose its desired morphology after post treatments [206]. Also, the rigidly fixed collagen chains are unable to represent good mechanical properties, rendering the material to suffer under non-stable humidity conditions [320].

As discussed earlier, collagen can be modified by graft polymerisation to reduce its super-hydrophilicity and to control biodegradation [45, 324, 325]. This methodology can be applied to collagen and its derivatives such as gelatine before processing [24]. In this approach, different vinyl group monomers with varied physiochemical properties can be branched over the protein chain.

To the best of our knowledge, the effect of flexible branching chains onto the structure of collagen has not been reported when the grafted polymer is electrospun on to fibres.

We hypothesize that during the electrospinning process, the branching on the main backbone can significantly preserve the collagen from extensive conformation change from electrostatic repulsion force between the collagen chains in proton donor solvents. Branch densities can present different velocities by influencing chain entanglement which is essential in fibre formation as optimised in chapter 5.

Chapter 4 gives information about the graft collagen copolymers, used as raw materials in the current study. The grafting performance and the yield of grafted collagen confirms a direct interaction between the feed ratio of co-monomers added onto ASC and the growing copolymer side chains. However, the highest grafting density is observed in S4, while S2 and S3 represent a decreased molecular weight of branch copolymers and higher grafting efficiencies in contrast with other samples. This may be due to an increased number of short length branches on the ASC backbone in these two samples.

As revealed in Table 6-1, the conductivity value of the sample solutions was determined using a conductivity meter (OAKTON, RS232 CON 110 series). As mentioned in chapter 5, the cationic characteristic of ASC is responsible for the higher electric conductivity compared to poly(MMA–co–EA) with dielectric properties when they are bonded covalently [326].

ASC–g–poly(MMA–co–EA) shows a reducing electron mobile phase when increasing the chance of more branches on ASC. The replacement of Hydrogen compounds on ASC to MMA–co–EA can lead to reduced conductivity of the solutions. Hence, the higher conductivity value of S1 can be due to having the lowest number of side branches on the backbone of ASC (Table 6-1).

With the knowledge that the surface tension of polymeric solutions tends to increase with the development of M_n, the interfacial phenomena of the prepared solutions were evaluated by applying the Nouy ring method. Hence, surface tension studies of the solutions were carried out using a tensiometer (KRŰSS). Although the corresponding values in Table 6-1 show a slight increase in some samples, all surface tension values are in the range of 31.8±1.02 $mN.m^{-1}$. This is possibly due to the wide molecular weight distribution of ASC–g–poly(MMA–co–EA) occurring in ASC extraction, as well as the side branching growth on the main backbone of ASC.

Table 6-1 Properties of the electrospinning solutions to be spun via a typical electrospinning

Sample	Concentration (% wt./v)	Viscosity (cP)	Conductivity ($ms.cm^{-1}$)	Surface tension ($mN.m^{-1}$)
S1	10.17	120±10	3.23	31
S2	6.07	120±10	1.02	30.5
S3	6.97	120±10	1.01	33
S4	4.14	120±10	1.02	31.5
S5	5.48	120±10	0.91	33

Generally, the fact that chain entanglements are essential for fibre formation has been well established [122, 327] and it has been repeatedly reported that the diameter of electrospun fibres can be increased by increasing solution viscosity [67, 107, 259, 328]. By contrast to the widely-studied electrospinning of homopolymers, the electrospinning of branched copolymers has an additional less known aspect; namely the chain entanglement density as one of the many parameters affecting the fibre formation and surface morphology which can be evaluated by viscosity. While in electrospinning the importance of chain entanglements has been widely accepted, there is no clear understanding on the required entanglements to stabilize fibre formation of non-linear polymers. This issue becomes more crucial when one segment of copolymer, ASC, is more likely to be non-stable during electrospinning [29, 182, 204, 259, 321, 329].

From the optimised viscosity discussed in chapter 5, the chain entanglement concentration was assumed to be dependent on the density of branching on ASC, along with some other unknown/known intermolecular interactions, as well as the solvent power when FA used as suitable solvent for both segments of branches and main chain in the studied samples. Hence, the effect of branching on chain entanglement density of samples was considered by fibre formation of various sample solution concentrations representing approximately the same viscosity.

Figure 6-1 exhibits the SEM micrographs of grafted copolymers S1 to S5 and also a typical example of the cross-sectional SEM micrograph of S3 (S3–a) in which the phase separation behaviour of the electrospun copolymer is observed through the porous fibres.

The surface morphology of all electrospun samples looks similar at first glance without bead deficiencies. This suggests that the polymer concentrations shown in Table 6-1 are above $2C_e$, where C_e is a function of chain entanglements and intermolecular interactions [330]. Also, the observations confirm the efficiency of the model that we applied to consider a single desirable solution for all studied samples, in chapter 5.

The mean fibre diameter and uniformity of the fibres were estimated statistically by using ImageJ software from the associated SEM micrographs. Fibre diameter scattering of each sample was also demonstrated in the associated Pareto graph in which the individual scattering values of each specific fibre diameter range is denoted in downward order by bars, and the cumulative total is indicated by the line (Figure 6-1a). The highest frequency distribution of fibre diameters for S1 was in the range of 332–1041 nm while S2 to S5 possess their frequency distribution to a greater extent of fibre diameter in the following order: (S2, 517–820 nm), (S3, 530–959 nm), (S4, 1137–1408 nm), and (S5, 1739–2141 nm).

Figure 6-1b shows the correlation between the mean fibre diameters and poly(MMA–co–EA) content of each sample incorporated into the precursor fibrous material. It must be noted that the bars on the plot are the standard deviations of the fibre diameters; the standard deviations represent the uniformity of the electrospun fibres. Hence, S4 shows the highest fibre uniformity whereas S3 represents the lowest average fibre diameter (1101 nm).

As discussed earlier, there is a clear correlation between the fibre diameters and the molecular weight of poly(MMA–co–EA) content in side chains influenced by monomer feed ratios, , in which less average fibre diameter can be formed from collagen graft copolymers possessing high density of short chains (S3 and S4).

These results are in good agreement with the viscosity graph (Figure 4-9), with a dramatic increase in solution viscosity and the performance of highly branched polymers in fibrous assemblies, which tells us the same story; that viscosity is formed by chain entanglements from intermolecular interactions.

a)

S1

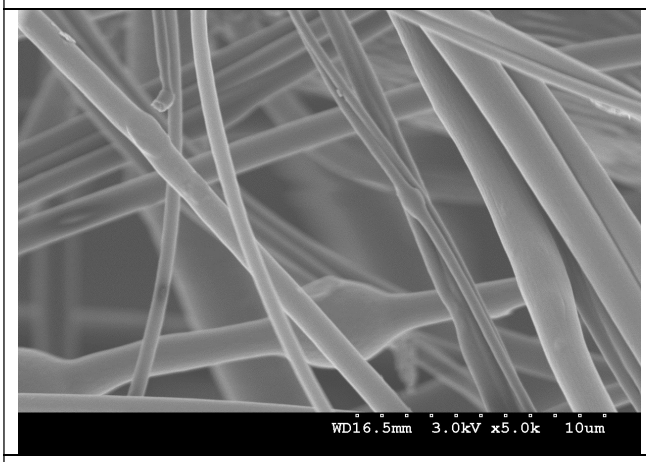
WD16.5mm 3.0kV x5.0k 10um

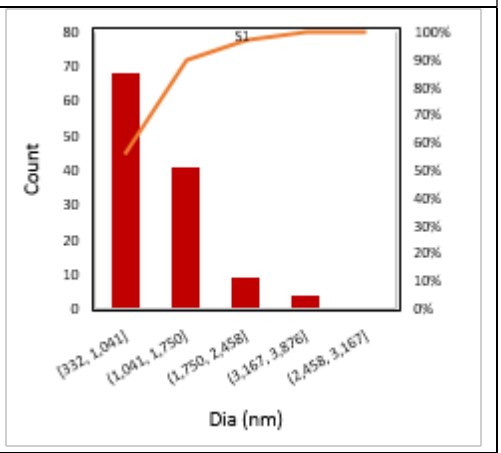
S1
Count
Dia (nm)
[332, 1,041]
(1,041, 1,750]
(1,750, 2,458]
(3,167, 3,876]
(2,458, 3,167]

S2

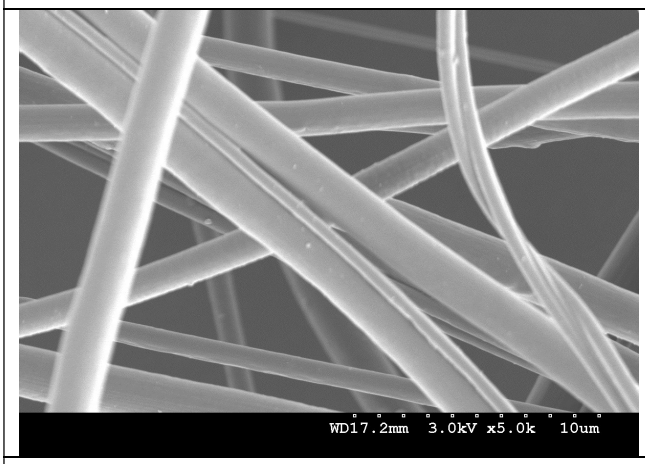
WD17.2mm 3.0kV x5.0k 10um

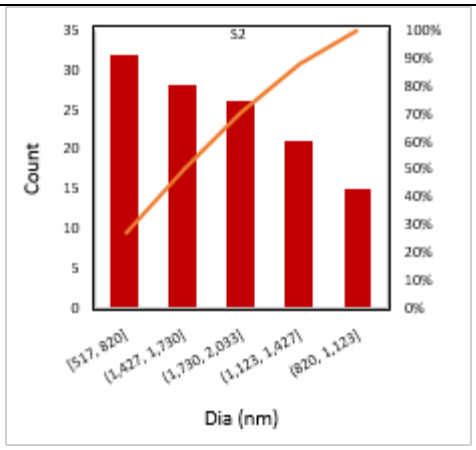
S2
Count
Dia (nm)
[517, 820]
(1,427, 1,730]
(1,730, 2,033]
(1,123, 1,427]
(820, 1,123]

S3

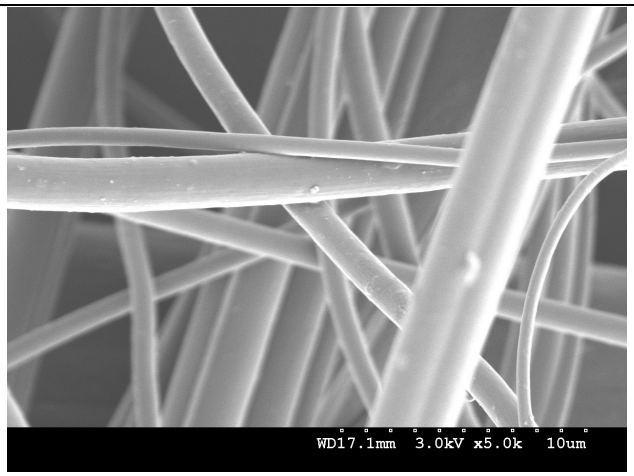
WD17.1mm 3.0kV x5.0k 10um

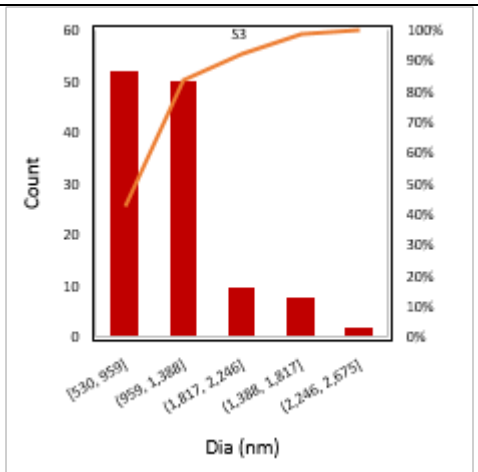
S3
Count
Dia (nm)
[530, 959]
(959, 1,388]
(1,817, 2,246]
(1,388, 1,817]
(2,246, 2,675]

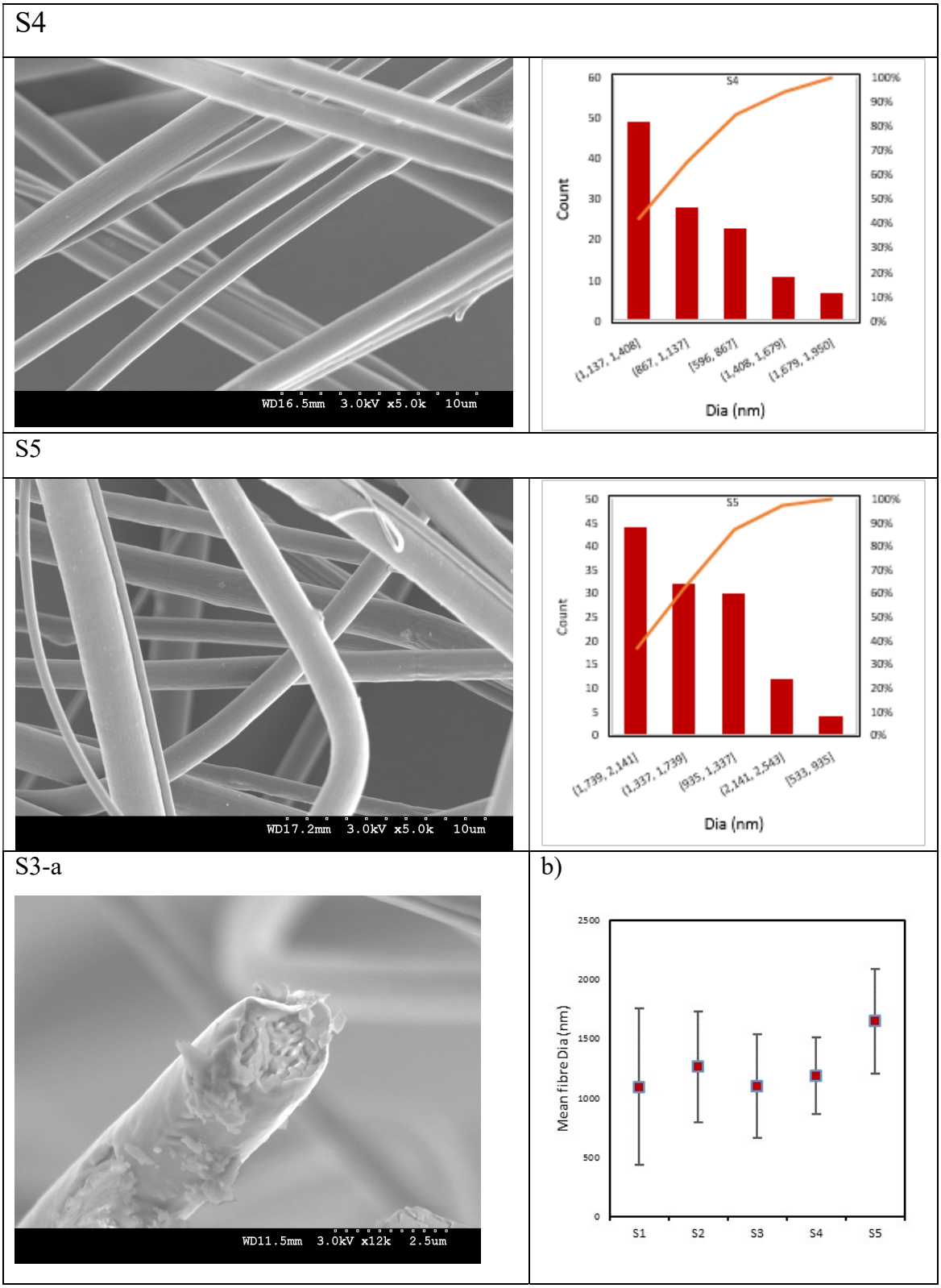

Figure 6-1 a) SEM micrographs and associated fibre diameter scattering of grafted copolymers S1 …S5 and cross-sectional SEM image of S3, formed with feed-rate (1 ml min^{-1}), needle diameter (gauge 22), temperature (25±2 ^{O}C) and humidity (RH: 35–40 %), TCD (15 cm), voltage (10 kV) and different concentrations to have the same approximate viscosity and associated pareto graph, b) The effect of poly(MMA–CO–EA) content on mean fibre diameter and uniformity (standard deviations) of the fibres

This result can be in relation with the increase in the number of end groups (polymer tails) from the increased number of grafting points and the length of branches that can be available in S3 and S4, as discussed in chapter 4. However, these results confirm that viscosity plays a leading role in fabrication of the fibres, enabling chain entanglements during stretching of the polymer jet towards the collector.

To verify our hypothesis, that the increased side chains can reduce the deteriorative effect of repulsive forces on collagen chains during the process, all electrospun samples were characterized by considering their FTIR and NMR spectra, XRD patterns, and TGA and DSC plots. This is to get an insight into the fibres of ASC–g–poly(MMA–co–EA) which were processed through the challenging process of electrospinning. Eventually, the functionality of the electrospun fibres were evaluated by additional measurements to determine their surface wettability and water absorption capacity (hydration degree).

The main characteristic features of the fibre samples were observed in their FTIR spectra, Figure 6-2. The structure of the electrospun fibres was revealed by Fourier Transform Infrared Spectroscopy (FT–IR, Thermo Nicolet Avatar 370 DTGS) at room temperature after washing the fibres with warm (40 °C) distilled water. The samples were prepared using fibres (1 wt %) in KBr.

ASC has several characteristic absorption bands identified as amide A (3425 cm^{-1}), amide B (2857–2953 cm^{-1}), amide I (1614–1711 cm^{-1}), amide II 1459 cm^{-1} in the infrared region of the spectrum [53, 297]. Characteristic bands for poly(MMA–co–EA) are carbonyl (C=O) stretching vibration at 1730 cm^{-1}, CH (–CH, $–CH_2$ and $–CH_3$) stretching vibrations at (2950–3050 cm^{-1}) (asymmetric) and ($–CH_2$) 2865 cm^{-1} (symmetric), C–O–C stretching at 1060 cm^{-1}, and C–O–C stretching at 1260 cm^{-1} (asymmetric) [331].

The amide I adsorption originates largely from the C=O stretching vibration and is specifically sensitive to the secondary structure of the polypeptides [304]. Hence, a shift towards a higher wavenumber may represent hydrogen bonding formed between chains in S1 to S5. The amide B and the amide II regions are affected by poly(MMA–co–EA) absorptions. However, the amide A and amide I bands were used as reference peaks to confirm the presence of Collagen in the fibres of the graft copolymers.

Furthermore, two new absorbance peaks are observed in all the samples; an asymmetric vibration peak at 978 cm^{-1} referring to α-nitrogen linkage (N–C) and asymmetric stretching at 1158 cm^{-1} corresponding to (CO–O–C) that can be the branching points on the main backbone of ASC. For S3 and S4, a significant peak is observed at 1060 cm^{-1}

associated with C–O–C stretching vibration and the highest intensity of C=O is observed in S4.

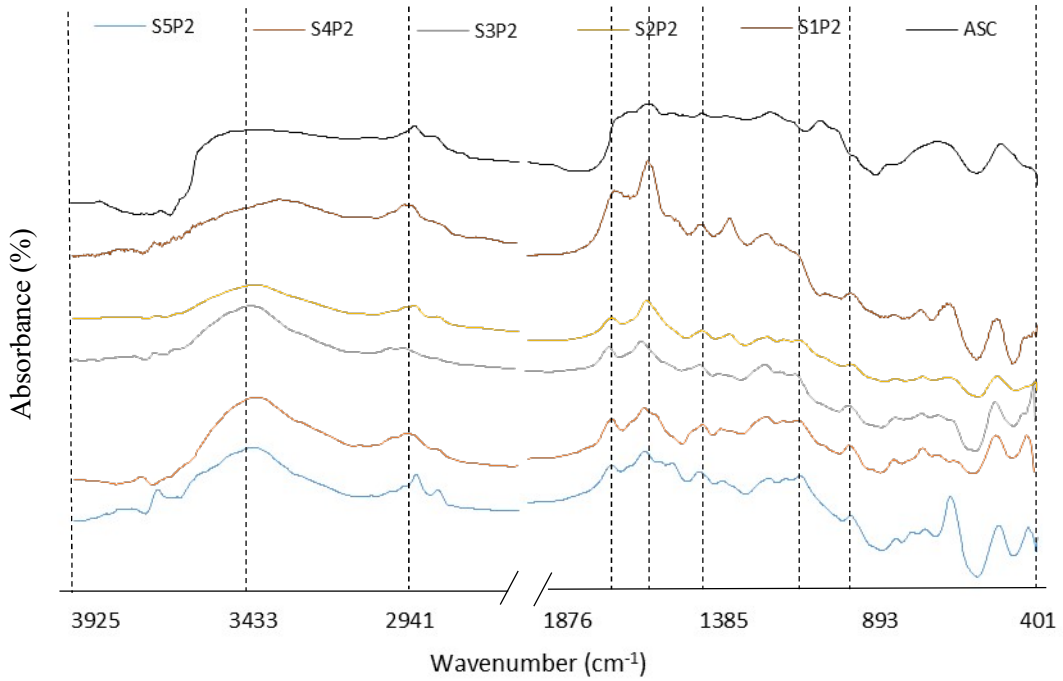

Figure 6-2 FTIR absorbance vs. frequency for Acid soluble collagen (ASC) and electrospun fibre samples with varied branching density of ASC–g–poly(MMA–co–EA).

Thermogravimetric analysis (TGA) was carried out using a thermogravimetric analyser (Mettler TC 10A/TC 15 Instrument) over the range of 35–600°C on samples (5 mg) at a heating rate of 10 °C min−1. This analysis was to further investigate the fibre compositions. TGA curves of the fibre samples of collagen graft copolymers were compared to the ASC fibres, as shown in Figure 6-3.

The highest thermal stability was observed in the fibre sample of S3 at 380 ºC while the other samples lost the same mass (about 24 %) at 307, 324, 346 and 360 ºC for ASC, S5, S1 and (S2 and S4), respectively. The mass residues at 550 ºC were also significantly different; 5.75 %, 7.35 %, 9.32 % and about 17% for ASC, (S3 and S2), S1 and (S5 and S4), respectively. This variation may be due to the carbonization of poly(MMA–co–EA) that occurs in temperatures above 450 ºC while decomposition of the ASC segment is achieved in temperatures below 450 ºC [332, 333]. This suggests that the analysis of TGA is accompanied with the carbonization of long side chains of methylene. Hence, higher mass residues can confirm the presence of long grafted chains onto the ASC backbone with the following descending order: S5, S4, S1, S2, S3, and ASC.

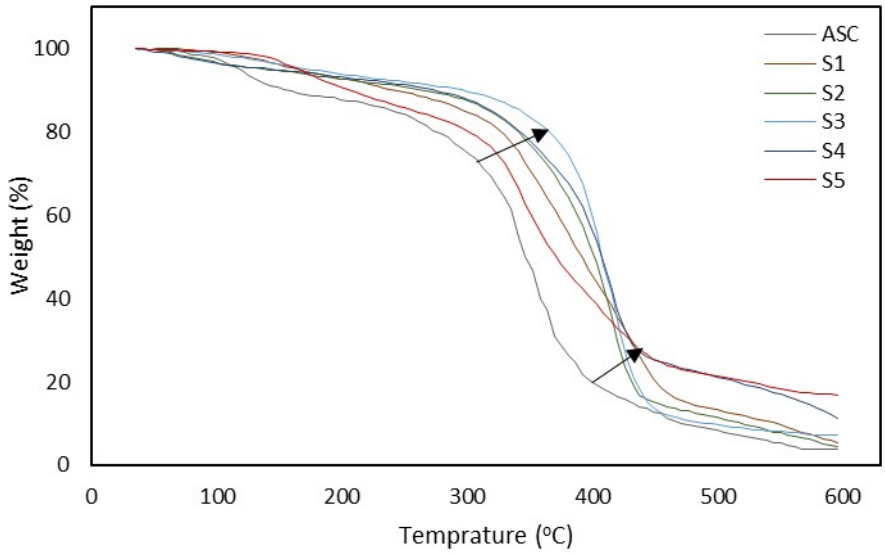

Figure 6-3 TGA analysis of the ASC and electrospun fibres from collagen graft copolymers, S1… S5, at a heating rate of 10 °C min^{-1}.

Furthermore, to compare signals of the end groups before and after electrospinning, the processed and unprocessed collagen graft copolymers were dissolved in deuterated acetic acid. High-resolution ^{1}H–NMR spectra of the fibre samples and bulk collagen graft copolymers were recorded on a Buker AVI–400 spectrometer, Figure 6-4. This was to analyse the chemical functionality of end-group variations before and after electrospinning.

This analysis was performed to study the end group signal changes that may be caused by processing factors. We assume that the shifted signals in the ^{1}H NMR spectra can represent chemical structure alterations caused by the denaturation of ASC during the process. Therefore, the lesser change in end group signals after the process compared with what recorded for the unprocessed copolymer, can characterize more stability and processability of collagen graft copolymer as a key factor in the processing of biopolymers.

In the ^{1}H NMR spectra, all samples of the bulk copolymers represent approximately the same main resonances in varied intensities that can be attributed to protons of methyl (0.9–1 ppm), methylene (1.3–1.5 ppm), amine (—NH_2, 1.35 ppm), R–N–C–R and R–CO–C–R (2–3 ppm, branching points), RO–CH_3 (3.64 PPM, side chains) and amide (R–CO–NHR, 7.5–8.5 ppm) as shown in Figure 6-4A.

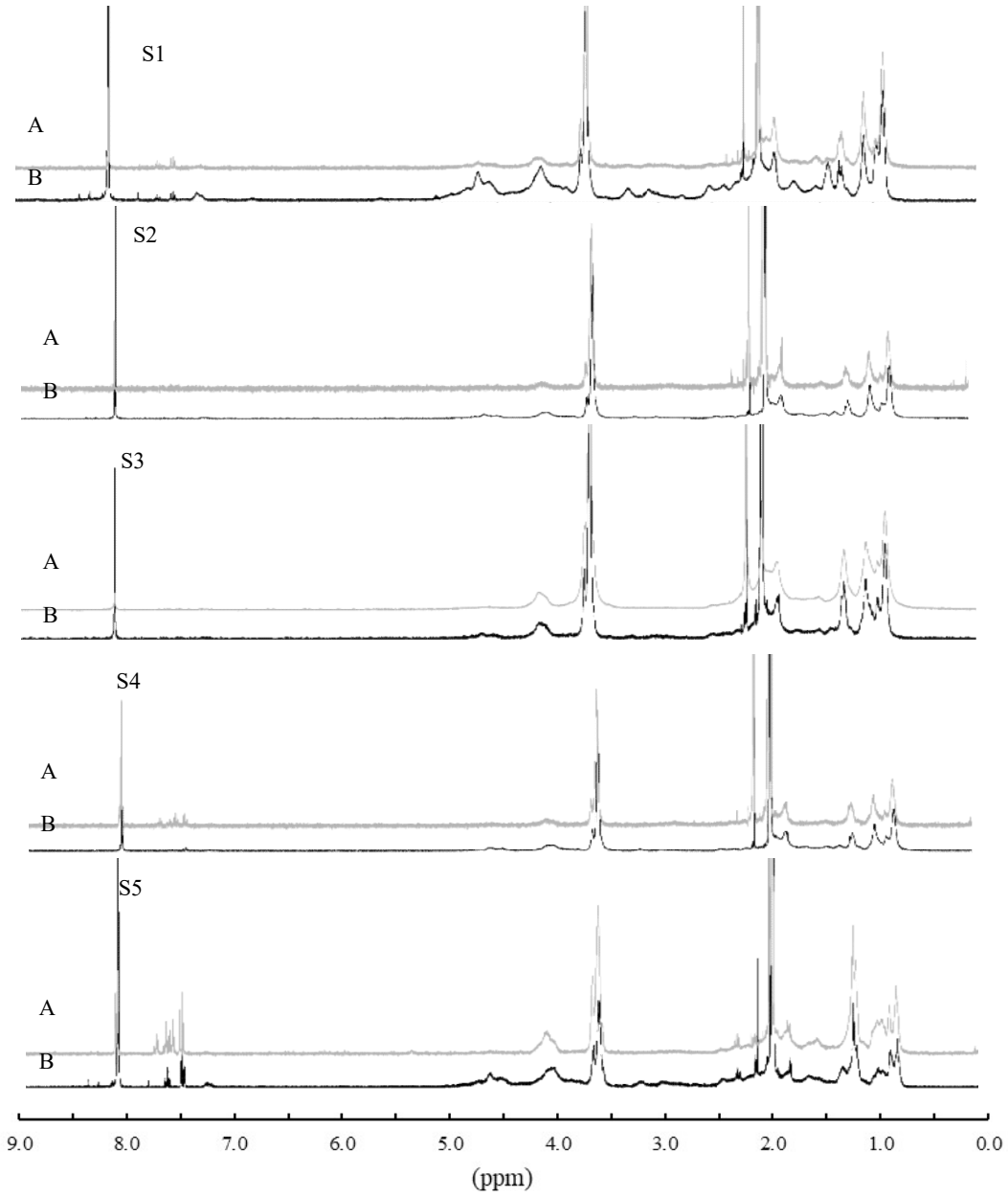

Figure 6-4 ^{1}H NMR Spectra of the bulk collagen graft copolymers (A) and the electrospun fibres of collagen graft copolymers (B).

By contrast, the changes in signals of the end groups of the fibre samples are simply visible in Figure 6-4B where S1 and S5 have undergone more structural change, observed within the region of 1.35–5 ppm, shifting to a higher electronegativity (deshielding). Furthermore, a significant increase in the integral value of the amide signals from 7–9 ppm occurred, more specifically in S1, S2 and S5 after electrospinning that can be due to the amidation caused by the electrospinning conditions, even though no clear sign of the presence of water was observed as a result of this reaction. However, S3 and S4 underwent no significant structural change whereas S3, having the

highly short branch densities, is the least affected collagen graft copolymer by electrospinning.

The structure of the fibre samples was also characterized by X–ray diffraction (XRD) using a Bruker D8 Advance powder diffractometer, shown in Figure 6-5. The broad peak for ASC at around 2θ = 21.5º is attributed to the overlapped diffraction from the collagen's crystal planes of (020) and (110), while the more intense peak at 2θ = 14.02° and also a weak peak at 29.68º are observed in the poly(MMA–co–EA)'s crystal planes of (110) and (200).

In the XRD spectra of graft copolymers, it can be observed that the diffraction intensity of the peak at around 21.5° is obviously shifted to a lower angle, indicating that the crystallinity of the ASC decreases after grafting modification. Furthermore, poly(MMA–co–EA) in S4 and S5 represent long enough chains that form a distinctive overlapped broad crystalline region at around 2θ = 13°.

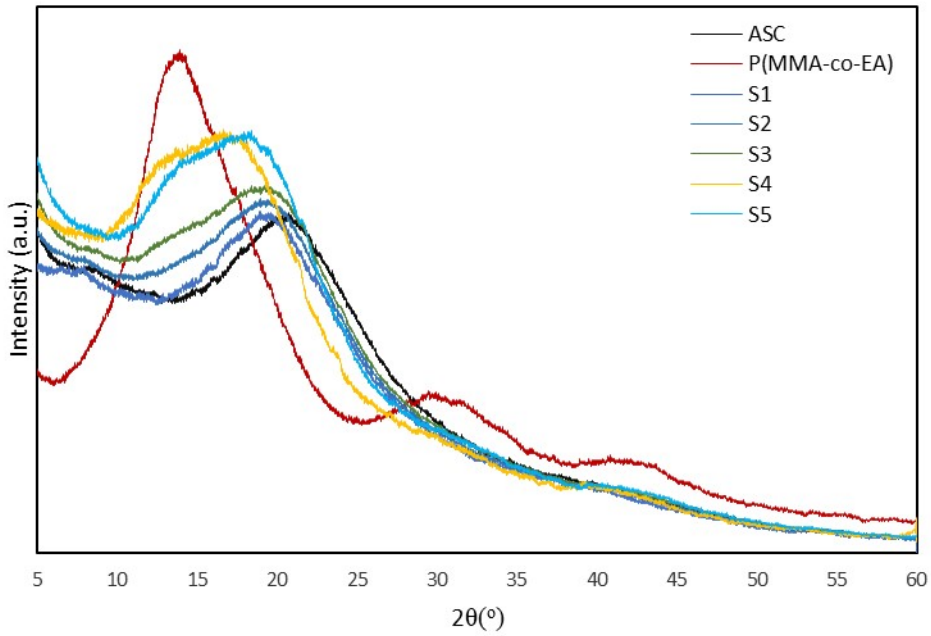

Figure 6-5 X-ray Diffraction (XRD) spectra of the electrospun fibres of collagen graft copolymers, ASC, and Poly (MMA–co–EA).

Thermal analysis of the achieved fibres was performed by Differential Scanning Calorimetry (DSC, Mettler DSC 12E). Temperature ranges up to 250°C with a heating rate of 10 °C min^{-1} in nitrogen atmosphere were run. Sensitivity curve analysis was carried out on samples (10 mg) to evaluate changes in their thermal behaviour.

As shown in Figure 6-6, the DSC curve for non-processed ASC demonstrates endothermic peaks at 85 °C, 160 °C and 220 °C related to melting temperature (T_m) of

ASC and branches, and denaturation process (T_d), respectively. In fibre samples, T_m drops to between 59 and 80 °C. This reduction in melting region may be due to several factors e.g. undergoing slight denaturing of the backbone in the polymerisation and subsequent electrospinning processes in which the average molecular weight may be lowered. Also, as the thermal behaviour is size dependent, this reduction can be explained by the size of the fibre samples in contrast with ASC, in the shape of a bulk mass.

The enthalpy of denaturation (ΔH_d), on the other hand, is not clearly observed in the fibre samples. This may be due to hidden peaks by transferring the samples into T_g of Poly methyl methacrylate in the branches. These results indicate that ASC is thermally altered by the presence of side branched poly(MMA–co–EA), as verified by the shifting of the melting peak towards lower temperatures with no considerable changes in the enthalpy of denaturation, compared to non-processed ASC.

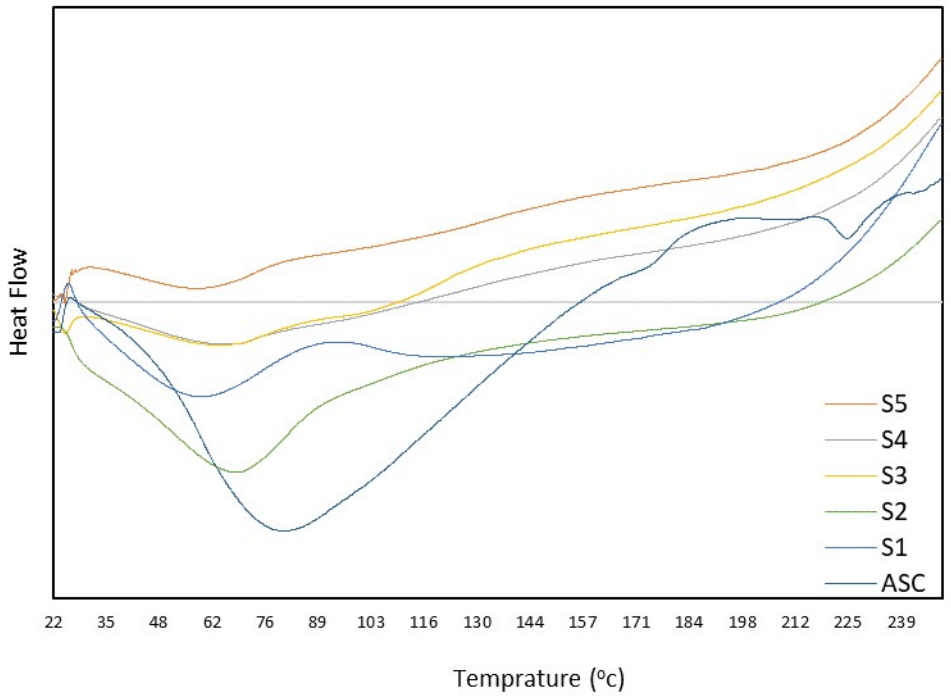

Figure 6-6 DSC thermograms of ASC and the electrospun fibres from collagen graft copolymers, S1...S5, using Aluminium pans at a heating rate of 10 °C min^{-1}.

However, if we compare our results with those of Yang et al [204] in which they reported the melting point of 45 °C for pure collagen electrospun fibres, it can be realized that irrespective of the benefits of a tailored branching density, ASC modification by graft polymerisation can improve the thermal stability of the electrospun fibres possessing a higher T_m of 59 to 71 °C.

Our aim is also to study the amphiphilic behaviour in unstable humidity conditions. Thus, to better understand the functionality of the electrospun fibres in high humidity and non-stable temperatures, water absorption (hydration degree) of the samples was studied as a function of time and temperature by considering the water contact angle (Water CAs), and the correlation between temperature, time and mass transfer.

The water contact angles for different fibre samples were measured by a contact angle analyser (One–Attension v. 2.3, Boilin Scientific, n=5). Figure 6-7a shows the water contact angles for nonwoven fibrous mats of S1 to S5. To investigate the degradation and water absorption capacity of the electrospun collagen fibres, a series of comparisons was performed between the unprocessed bulky graft collagen copolymers and processed fibres.

The water CA analysis indicates high surface wettability of the fibre samples. The water CAs decreased from 80.33º to 56.21º in the first 10 seconds. The higher value for S1 is due to more hydrophilic end groups that can instantly form hydrogen bonding with the water droplet, by contrast to other fibre samples with higher branching densities that seem to penetrate into the fibre samples as shown by a decrease in values of water CAs. After 10 minutes; as shown in Figure 6-7b, the water CA of S1 still possesses a higher value of water CA.

Heat and mass transfer mechanisms were studied by weighing the fibre samples (n=5) before and after immersion in distilled water. Excess water was removed from the samples by gently blotting with filter paper prior to each weighing.

The results of water CAs are in good agreement with the water absorption measured after 12 hours, Figure 6-7c; where the initial weight of bulk polymer S1 achieved a 43.64% growth in mass and fibre sample of S1 had a weight increase of 24.03%. Also, a non-equivalent mass transfer was observed in fibre mass loss where the fibre samples were dried at room temperature; this substantial deviation was not observed in other samples. Hence, it can be suggested that increasing in branching density can significantly enhance molecular packing, not only preserving the collagen chains to be affected by the destructive conditions of electrospinning, but also to mass loss of the electrospun fibres in high humidity situations.

As shown in Figure 6-7d, the water absorption capacity of fibre samples was studied as a function of temperature where the fibre samples were soaked in water and were heated up to 100 ºC for 9 hours before cooling to room temperature (20 ºC) for 11 hours. This measurement was performed to consider the impact of increased chain mobility on the absorption capacity of fibres as a consequence of increasing temperature on amphiphilic

behaviour of the samples with flexible chains. It was observed that heating can accelerate the absorption behaviour of the fibre samples in contrast with what is achieved at lower temperatures below the melting region, as specified in DSC, Figure 6-6.

It can be clearly observed that fibre samples of S1, S2, and S5 show a significant weight loss by increasing temperature above their melting point and follow the same behaviour in their cooling phase afterwards, while the rest of the samples demonstrate higher absorption behaviour. Even though all samples lost their fibrous morphology after this test, S4 continues to absorb even in the cooling stage.

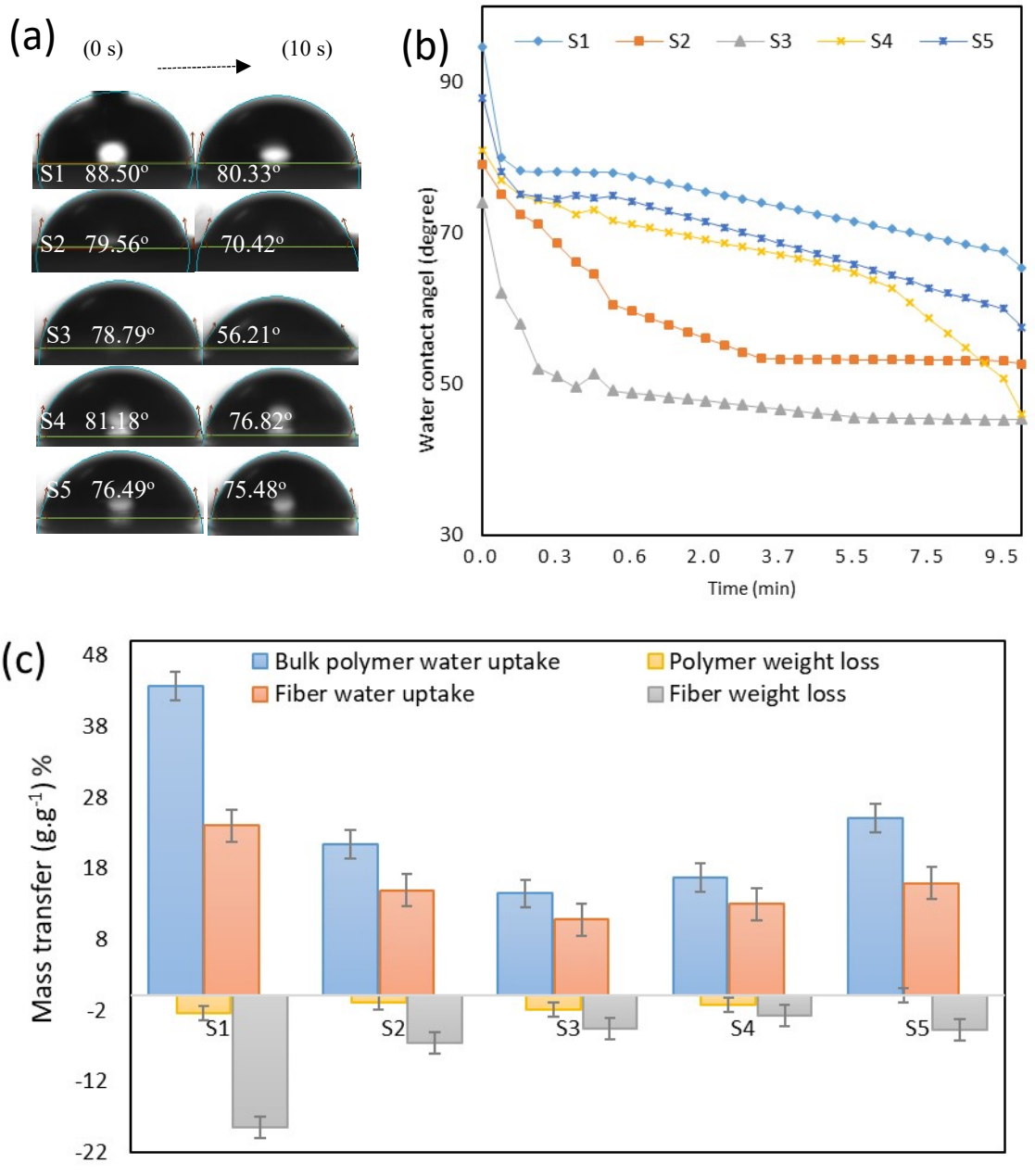

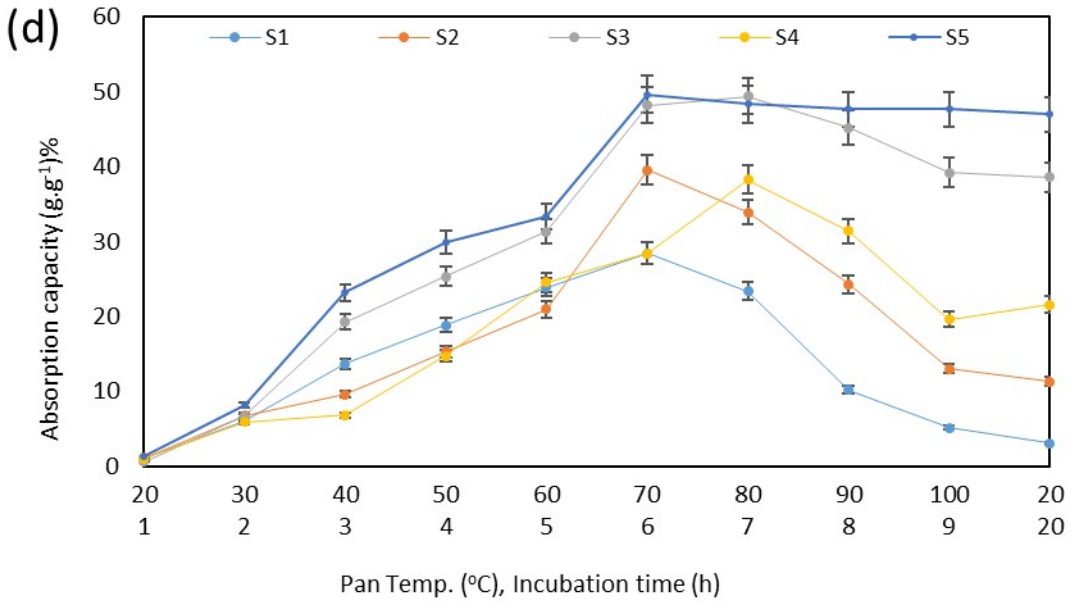

Figure 6-7 Water contact angle vs. time (a and b): a) 10 seconds, b) 10 minutes. c) Mass transfer in wet and dry phase inversion after a period of 12 hours at room temperature. d) The correlation between heat and mass transfer in aqueous medium.

These observations are in agreement with increased chain flexibility, as a result of increased temperature in the orientated chains up to the melting region of each fibre sample. By contrast, above the melting region, when the side chains achieve their T_g. This heat transfer to the side chains can significantly preserve the main backbone chain of ASC. This can be clearly observed in the water absorption capacity of S3, S4 after the cooling stage, in which their mass loss is not significant.

Chapter 7 Reinforced Collagen–g–poly(methyl methacrylate–co–Ethyl Acrylate)/ Nylon 66 core–shell fibres from custom-built electrostatics and supplementary bonding, using coaxial electrospinning

Collagen chains with excellent biocompatibility, which cannot be applied freely due to their inherent drawbacks such as poor mechanical properties and high degradability, when they are switched to random coil conformation [29, 53, 89, 94, 204]. Thus far, we focused on reducing their hydrophilic behaviour and enhancing the thermal properties of collagen graft copolymers by graft polymerisation and attempted to control the deteriorative effects of the electrospinning condition whilst benefiting from its controllable grown branches in length and number on the surface of main back bone of collagen chains [24, 51]. We realised that in fibre formation from collagen-based copolymers with the branched structure, it is essential to be spun under specific conditions of viscosity to prevent Rayleigh instability of high entanglements. We realised that this issue is successfully addressed by the electrospinning method [330, 334, 335], when the branched copolymers can be spun in low concentrations.

When it comes to mechanical reinforcement of collagen-based materials, blending with (semi-)synthetics is recommended mainly in traditional fibre formation methodologies [336, 337]. Even though, this method is not as simple as it seems; phase segregations and viscosity changes are simple examples of incompatible (co)polymeric fluids. This issue is due to different e.g. electrical and structural properties that can significantly limit the application [338] of collagen-based materials in fibrous assemblies [95].

Interestingly, we realised that with coaxial electrospinning, fluids with a wide variety of properties can be tuned to create core–shell nanostructures [67] simply with pure solvents [240, 339]. However, the performance of this technique for large scale fibre formation and fibre collection is still in its infancy.

In this chapter, we investigate a new approach to form hierarchical, robust fibrous electrospun collagen-based materials which have potential to conjugate with a variety of nanostructure materials from minerals to medicines. This is a novel method for spinning hydrophilic collagen-based polymers whilst improving their mechanical properties.

This was achieved by optimising the performance of the participating materials and supplementary bonding. The ASC–g–poly(MMA–co–EA (CME) was co-electrospun wherein Nylon 66 was used as a core fluid. End uses can consequently benefit from in-

situ fibre formation of the natural segment of collagen in the shell and the mechanical strength of the core as a composite in the shape of a fibre to fabric, as shown in Figure 1.

Different polymeric content in the core and shell materials can demonstrate varied properties by means of a tunable intensity of the electric field. The mechanical, chemical, thermal and swelling behaviours of the core–shell composite fibre structure were established. This work can be considered to provide an alternative to fibrous assemblies to exploit the advantages of chain flexibility in hydrophilic copolymers that reinforced with electrically and structurally incompatible polymers.

7.1 Experimental section

7.1.1 Synthesis of ASC–g–poly(MMA–co–EA)

The procedure of the copolymer synthesis has been reported in detail in chapter 4. MMA–co–EA ($109.83*10^{-4}$ M, 0.5% EA Content) was used as the monomer. A graft polymerisation procedure (See Figure 4.3) was used for the synthesis of ASC–g–poly(MMA–co–EA) (CME) with a branched molecular structure when Acid soluble collagen (11g) was used as a starting raw material. The resulted copolymer (CME) was dried in a vacuum oven at room temperature until a constant weight was achieved.

7.1.2 Preparation of spinning solutions and coaxial electrospinning

FA was used as the solvent for solutions of both the core and the shell fluids. D&C Red 28 (Rdye, Acid Red 92, Clariant, Switzerland) and Sanolin Tartrazine X90 (Ydye, Acid Yellow 23) were utilized as tinted indicators to distinguish the core and shell components, respectively. These colorants, with no overlay in their colour specta, were used to follow the electrospinning procedure. The core solution consisted of Nylon 66 (N66, 262.35 g mol^{-1}, Sigma Aldrich) and Rdye in FA under stirring for 4 h at 70 ^{o}C. The shell solution made up of CME and Ydye was dissolved in FA for 8 h at room temperature. The solutions were loaded into a 10–mL and a 5–ml syringe for the core and shell components, respectively. Detailed sample descriptions, including electrospinning parameters, are shown in Table 7-1.

A positively charged coaxial needle (gauge 20 & 26) was used as the spinneret. The coaxial electrospinning set up that was used in this work is shown in Figure 3-2b. A rotating drum with nails was applied as the collector with a fixed rotation speed (423 rpm) for all experiments.

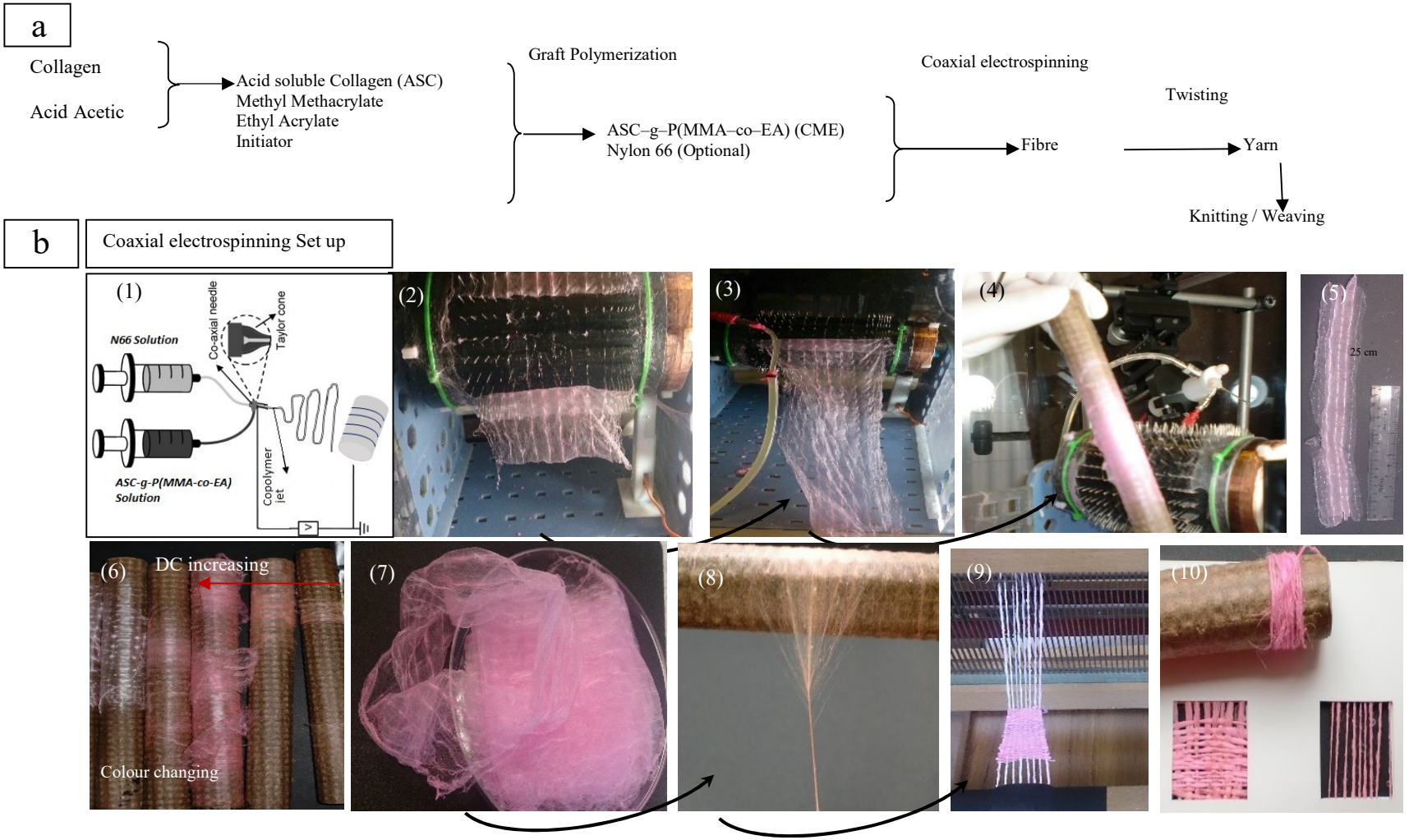

Figure 7-1 (a) Process chart of CME/N66 yarn and potentially fabric production. (b) Coaxial electrospinning process and yarn twisting. (1) Coaxial electrospinning using rotating drum as collector. (2-5) Manually CME/N66 filaments were taken up around the nail drum (6) the colour changing from pinkish yellow to yellowish pink by increasing the applied voltage that indicates the varied fibre in component. (7-10) The fibres were twisted into a yarn with clockwise twisting (S-twists) that is mechanically strong to be knitted /woven.

Table 7-1 Process Parameters

Solution [a]	Distance (cm)	Voltage (kV)	Flowrate (ml/h)	T (^{O}C)	RH (%)	Observation
CME, 10 wt/v %+ Ydye 0.1 wt % in FA	12	5–11	0.5	22 ± 2	35 ± 5	A nonwoven mat is formed, in yellow color, on the drum in 5 minutes, no solution dropping observed
	12	12–20	1.5	22 ± 2	35 ± 5	
N66,18 wt/v % + Rdye 0.1 wt % in FA	12	5–12	0.5–1	22 ± 2	35 ± 5	Dropping, no tailor cone angle, no electrospun fibre is observed
	12	14–20	0.5–1	22 ± 2	35 ± 5	2d nano mat in the shade of light pink is achieved all over the drum in 20 minutes

Core solution [b]	Sheath solution	Distance (cm)	Voltage (kV)	Flowrate (ml/h)		T (^{o}C)	RH (%)	Comments (Coaxial CME/N6)
				core	Shell			
N6, 25 wt/v % + Rdye 0.1 wt% in FA	CME, 10 wt/v %+ Ydye 0.1 wt % in FA	12	9.5–10	1	0.5	22 ± 2	35 ± 5	Occasional droplets of N6 observed
		12	17–17.5	1	0.5	22 ± 2	35 ± 5	Chaotic CME polymer jet whipping in the air while a thin layer of 2d nonwoven mat forming on drum
		12	12–12.5	1	0.5	22 ± 2	35 ± 5	No droplets observed

a) The process parameters when they were electrospun separately

b) The coaxial electrospinning process parameters

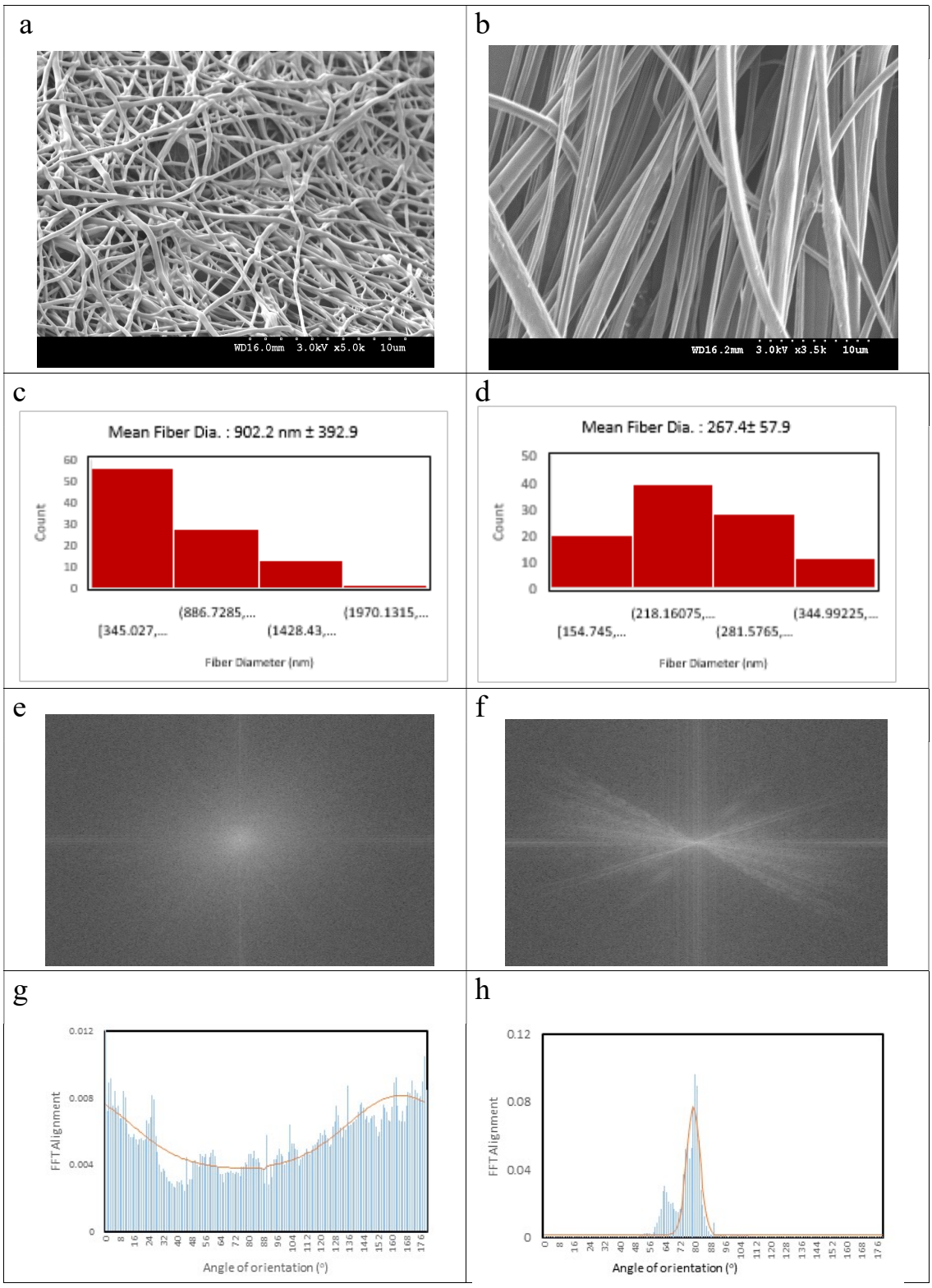

Figure 7-2 Investigation of morphology and alignment of the electrospun Nylon 66 nanofibres (a, c, e, g) and ASC–g–P(MMA–co–EA) nanofibres (b, d, f, h). (a, b) SEM images of the Nylon 66 and ASC–g–P(MMA–co–EA) nanofibres collected by a rotating drum with constant rotary speed of 423 rpm, using a typical electrospinning setup and (c, d) fibre diameter frequency plots; (e, f) ImageJ Raw output of the 2-D FFT alignment analysis of electrospun fibres corresponding to SEM images in (a, b); (g, h) the directionality histogram reporting 2D-FFT alignment based on peak shape and the relative principle axis of orientation for the fibres.

7.2 Results

7.2.1 Factors to control CME/N66 fibre formation

To study the fibre morphology of any of the components in the core and shell individually, a typical single needle as spinneret was applied to spin the materials. The mean fibre diameter and the uniformity of the fibres (standard deviation value) were estimated statistically by using ImageJ software from SEM micrographs.

As shown in Figure 7-2a–d, fibre morphologies are quite uniform with no bead formation. To determine the relative degree of fibre alignment, FFT analysis on the SEM images was performed using ImageJ on representative images, Figure 7-2e–h. FFT analysis creates a pixel intensity image based on the frequency and direction of the fibres. The reverse FFT data were plotted over 180° from the radial summation of pixel intensity from the FFT analysis.

A randomly oriented fibre sample displays a radially diffuse image in FFT analysis, whereas a highly aligned fibre sample shows a high-intensity line normal to the fibre orientation. The FFT images were then analysed in directionality profile, wherein the radial intensity was summed and plotted with regard to the angle of orientation.

As shown in Figures 7-2e and g, the fibres produced from N66 are least aligned. The fibres formed from CME, applying the same process parameters, had a narrow peak, with a small area under the curve. Larger fibre diameter and higher orientation are observed in the nanofibres from CME, indicating greater chain entanglements.

Table 7-1 reveals the controlled process parameters and observations in two sections of the typical electrospinning and the coaxial electrospinning to understand the component response when both solutions were supplied simultaneously to the coaxial needle.

In the case of coaxial electrospinning, it is observed that by applying less than 10 kV voltage, yellowish fibres were formed on the collector, whilst pink droplets were dropping form the core capillary.

Afterwards, by increasing the applied voltage, the pink solution of polar polymer (N66) was electrostatically initiated to orient towards the collector when associated dipole polarization occurred. Hence, the colour of the fibres altered from pinkish yellow to a yellowish pink by increasing the intensity of the electrical field. This response to the variable intensity of the electric field can be considered as an observable variation in the core–shell fibre composition. For voltages above 20 kV, a pinkish 2D nonwoven mat was gradually fabricated over the collector. Thus, to understand the effect of the intensity of the electric field on the electrospun fibre composition by coaxial

electrospinning, three samples were studied that were obtained at the following distinctive voltages: 8 kV (SN1), 12 kV (SN2) and 16 kV (SN3); then the properties of the core–shell structure of nanofibres were investigated.

Figure 7-3 shows the SEM micrographs and the associated fibre diameter scattering of the electrospun fibres at the studied voltages. It can be seen that the average fibre diameter significantly increases when increasing the electric field, from 1876 nm to 5951 nm approximately. The studied samples show a narrow peak and are mostly similar to CME nanofibres in orientation.

CIE00 colour difference was used as evidence of hue difference for the samples (ΔH) as shown in Table 7-2. Due to the size dependency of brightness of the samples, the differences in this value were eliminated during the calculation [176, 177].

Table 7-2 CIE DE 2000 hue difference between the references and samples

Sample	ΔH_1[a)]	ΔH_2[b)]
SN1	30.521	17.281
SN2	33.655	17.272
SN3	38.802	12.912
N66	124.108	0
CME	0	124.108

a) The LAB coordinates of CME were used as the reference colour
b) The LAB coordinates of Nylon 66 were used as the reference colour

It can be seen from the ΔH values that the hue differences for ΔH_2 are significantly lesser than those for ΔH_1. This can be addressed by considering the mechanism of the core–shell fibre formation in the following section.

7.2.2 Yarn modulus and tenacity

The mechanical properties of twisted yarns from electrospun nanofibres and core–shell nanofibres from coaxial electrospinning were studied. The gauge length was set at 50 mm for all specimens and a rate of extension of 10 mm/min under standard atmospheric conditions for testing. Figure 7-4 shows the tensile stress/strain relationship of the twisted fibre yarn tested by the Instron tensile testing apparatus following the yarn tensile testing standard (BS–EN–ISO 2062:2009). The fibre yarn samples were prepared with the same linear density using ASTM D5344– 99(2017).

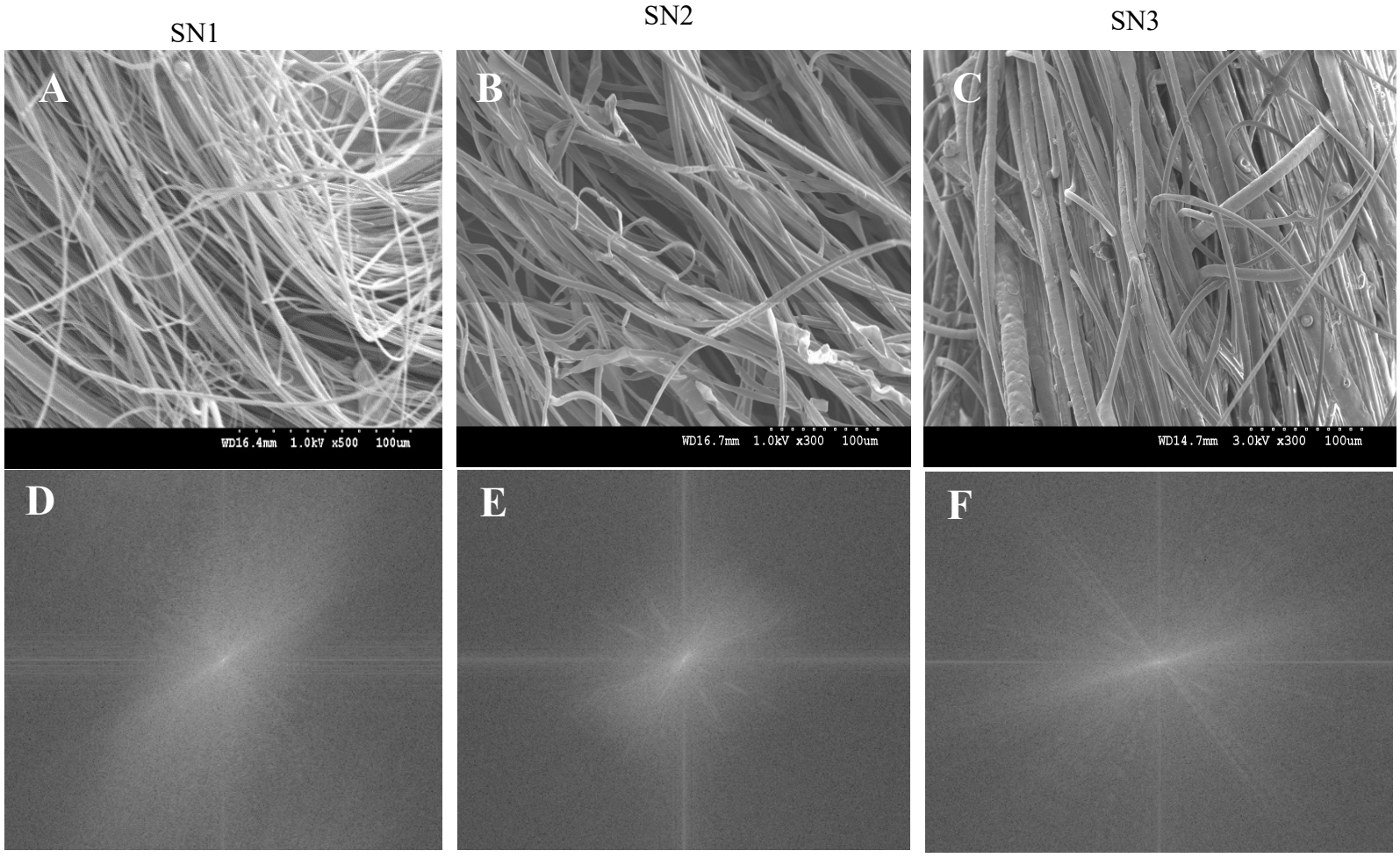
SN1
SN2
SN3
A
B
C
WD16.4mm 1.0kV x500 100um
WD16.7mm 1.0kV x300 100um
WD14.7mm 3.0kV x300 100um
D
E
F

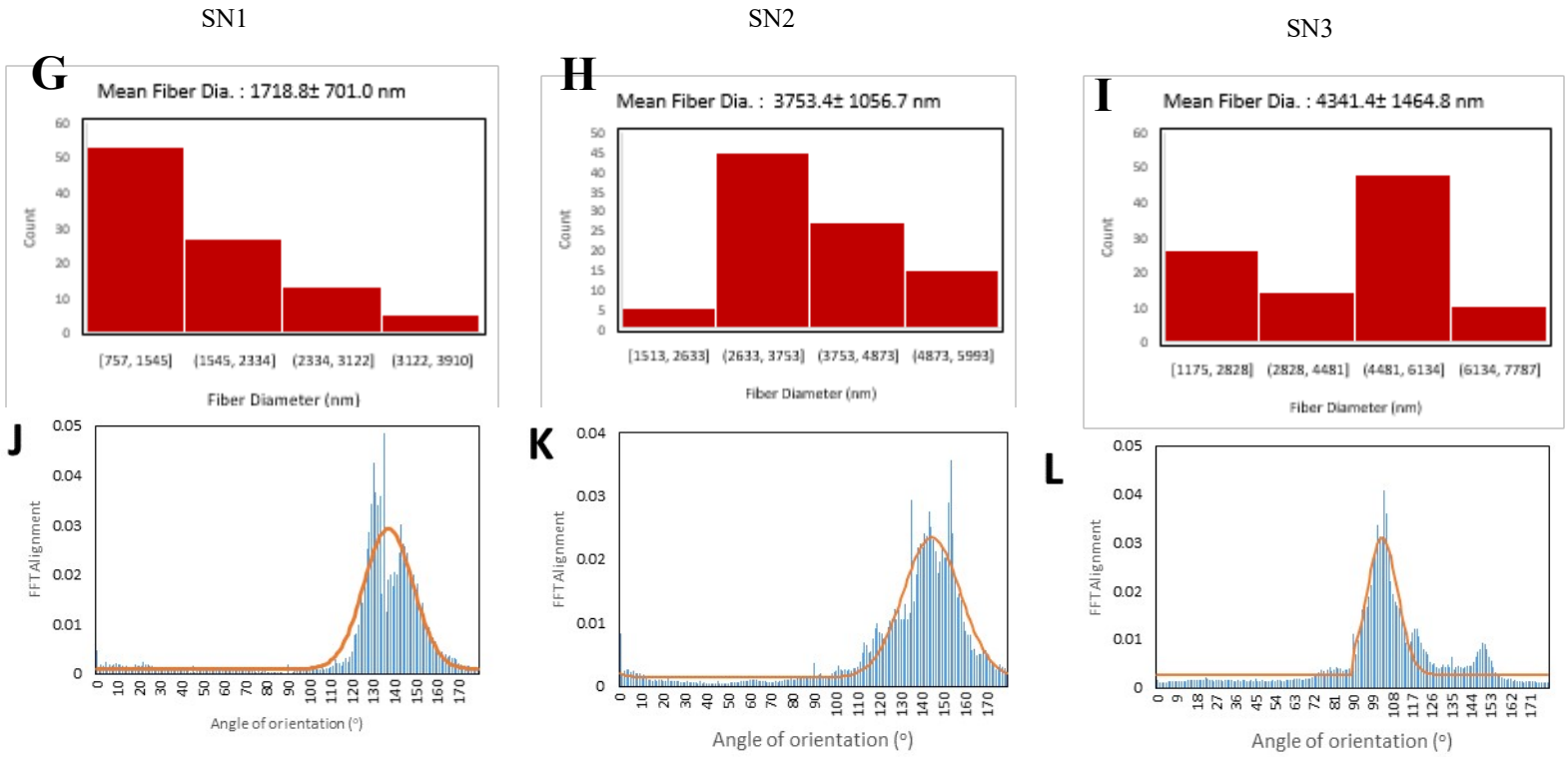

Figure 7-3 The effect of applied voltage on the mean fibre diameter and the uniformity of the core-shell fibres (standard deviation value) and the alignment of the core-shell nanofibres of coaxial electrospinning from ASC–g–P(MMA–co–EA) and Nylon 66: SN1, 8 kV (A, D, G, J); b) SN2, 12kV (B, E, H, K); SN3, 16 kV (C, F, I, L). (A- C) SEM images of ASC–g–P(MMA–co–EA)/ Nylon 66 the core-shell nanofibres collected by a rotating drum with constant rotary speed of 423 rpm. (D- F) ImageJ Raw output of the 2-D FFT alignment analysis of core-shell nanofibres corresponding to SEM images in (A- C); (G- I) fibre diameter frequency plots; (J -L) directionality histogram plots reporting 2D-FFT alignment based on peak shape and the relative principle axis of orientation for the core-shell nanofibres.

For each sample, five specimens were prepared. Each specimen was held between the jaws of the Instron Tensile Tester applying load until breaking, wherein their two ends were fixed using a paper frame, Figure 3-4. The samples were then compared with nanofibres from the core and shell components that were electrospun individually; electrospun nanofibres of CME and N66 were studied as reference.

Modulus and tenacity were calculated for each specimen by the software; by dividing the load (N) to give yarn linear density (Tex). The mean and standard deviation values were calculated for each group of specimens (n=5) referring to initial modulus and tenacity of the samples Table 7-3, and stiffness and strength of the samples, respectively. Modulus represents their resistance to deformation. This measurement was performed at the ratio of tenacity to strain, wherein the tenacity was calculated based on the breaking force divided by the initial linear density of the samples, representing the mass stress at break.

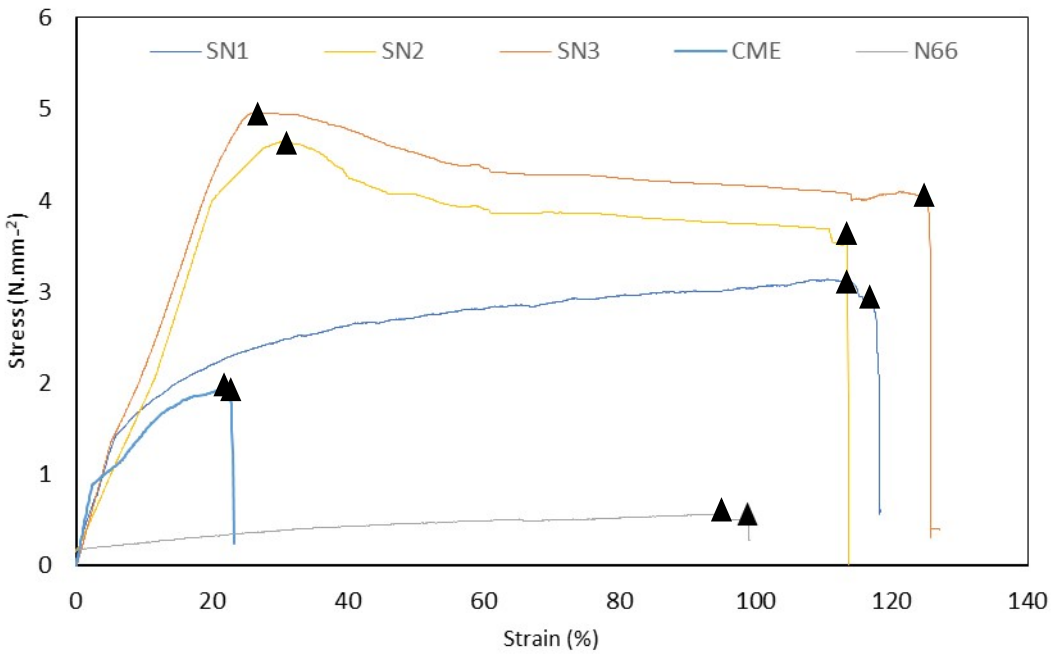

Figure 7-4 A typical stress strain curve recorded from tensile test of fibre yarns; Tensile strength point and Breaking point are displayed with black marks on the curves.

According to Table 7-3, a significant enhancement is observed in the studied samples in contrast to those nanofibres obtained from the core (N66) and the shell (CME) individually. Necking occurred beyond the yielding point in SN2 and SN3. Thereafter, elongation progressed to reach breaking extension, this behaviour was not observed in SN1. SN1 is brittle in terms of lower breaking stress at a lower elongation by contrast with SN2 and SN3 that are fabricated in a higher intensity of electric field.

7.2.3 Thermal behaviour of Coaxial Composite Nanofibres

Thermal analysis of fibres was performed using DSC, Mettler DSC 12E. Runs with temperature ranges from 23 °C up to 300 °C, and vice versa for cooling scans, with a heating/cooling rate of 10 °C min^{-1} in the nitrogen atmosphere were performed. Before evaluating changes during the cooling scans, the samples were held for 3 minute at 300 ℃ to erase the history of thermal behaviour of the samples (7 mg). Endotherms are represented with upward curves in the scans. A heat of fusion of 255.8 $J.g^{-1}$ (ΔHm^o) was presumed for 100 % crystalline N66 in the crystallinity measurements. The degree of crystallinity (%) of the samples was obtained from [340]:

$$C(\%) = \frac{[\Delta Hm - \Delta Hc]}{\Delta Hm^o} * 100$$

where (ΔH m- ΔH c) is the measured heat of fusion.

The results of heat flow versus temperature for CME, N66 and the studied samples, are shown in Figure 7-5a. The samples were analysed from 23 °C to above the melting temperature (T_m) of N66 (300 °C) at a rate of 10 °C min^{-1}. The melting curves are shown with the same scaling but are displaced in the same graph for clarity, Figure 7-5a.

The DSC curve of CME demonstrates an endothermic peak (downward) at 57.2 °C and 152 °C associated with T_m of the ASC segment and T_m of poly methyl methacrylate (PMMA), respectively.

As the denaturation process temperature (T_d) of ASC was expected in the melting region of PMMA, the second endothermic peak contributes to T_d of the ASC segment as affected by Tm of PMMA. The glass transition temperature (T_g) and T_m for N66 are commonly reported at 57 °C and 265 ºC. Due to the size-dependent T_g and T_m of the electrospun N66 fibres, a significant decrease in these temperatures is observed.

Due to the varied thermal performance of the CME + N66 coaxial composite, the impact of CME on the well-known thermal behaviour of N66 was analysed. According to Figure 7-5a and Table 7-4, the nanofibres of N66 demonstrate T_g at 55 °C and two peaks of 256.6 °C and 259.8 ºC in the melting region. Interestingly, an endothermic peak of CME is observed at 57.4 °C for SN1 while this peak is not observed for SN2 and SN3. Above 250 °C, multiple melting peaks are detected in all the CME/N66 samples.

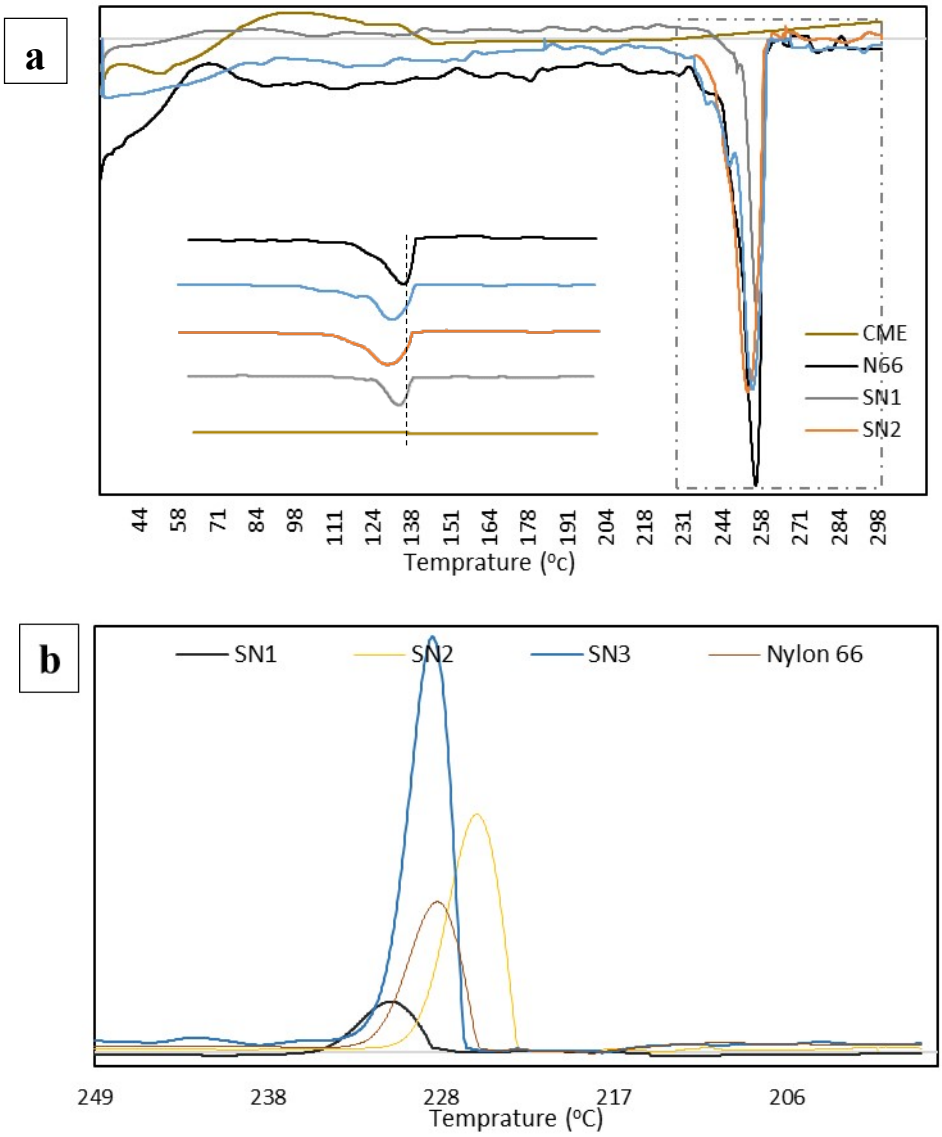

Figure 7-5 a) Heat flow vs. temperature for nanofibres, in DSC heating phase with rate of 10 °C min^{-1} in aluminium pan. To clarify, curves associated with the melting region of Nylon 66 are demonstrated vertically in the same graph. b) Dev. Heat flow vs. temperature of nanofibres, during DSC cooling phase from the melt with the rate of 10 °C min^{-1}.

Table 7-3 Mechanical properties of the samples

Samples	Breaking Stress ($N.mm^{-2}$) [a)]	Breaking Strain ($mm.mm^{-1}$) [a]	Tensile Stress ($N.mm^{-2}$) [b]	Tensile Strain (mm.mm) [c]	Tenacity ($cN.Tex^{-1}$) [b]	Modules ($cN.Tex^{-1}$) [b]
SN1	2.75 ± 0.29	1.17 ± 0.12	3.14 ± 0.13	1.14 ± 0.29	5.53 ± 0.29	21.33 ± 1.92
SN2	3.54 ± 0.71	1.13 ± 0.21	4.52 ± 0.27	0.30 ± 1.40	1.57 ± 1.40	110.52 ± 3.14
SN3	4.01 ± 0.36	1.25 ± 0.11	4.86 ± 0.33	0.29 ± 0.16	15.29 ± 0.16	104.75 ± 6.02
CME	1.77 ± 0.17	0.22 ± 0.02	1.93 ± 0.10	0.21 ± 0.03	25.30 ± 0.03	25.58 ± 2.41

a) ($p = 0.001$)
b) ($p < 0.01$)
c) ($p < 0.003$)

The minor melting peak (T_{m1}) is attributed to the melting of the original chain arrangement (crystals) of N66 in the fibres. The higher melting peaks (Tm_2) are caused by the melting of crystals that are either re-crystallized or reorganized in heating after melting of the original chain arrangement. T_{m1} and T_{m2} for all samples are shifted to a lower temperature, as shown in Table 7-4.

Another explanation for the interaction of CME/N66 may be the heightening of N66 crystals in contrast with those observed for N66 fibres (6.99%). This value was obtained from the area of the crystallization exothermic event during cooling. The crystallinity (C %) of N66 in the samples is shown in the last column of Table 7-4. While C% decreases in SN1, an increase is observed in SN2 and SN3. The DSC results of CME/N66 fibres for cooling phase are shown in Figure 7-5b. The crystallization temperature of CME/N66 fibres slightly decreases, with the exception of SN1.

Crystallinity

Table 7-4 Melting and crystallization temperatures of the samples

Samples	T_{m1} (°C)	T_{m2} (°C)	T_c (°C)	Crystallinity %
N66	256.61	259.81	228.63	6.99
SN1	250.66	258.14	231.11	5.78
SN2	256.41	257.22	226.84	10.91
SN3	257.02	257.96	229.71	19.06
CME	57.25	152.01	—	—

7.2.4 Surface wettability, water absorption and degradation properties of the electrospun fibres

The water contact angles of different fibre samples were measured using OneAttention v. 2.3, Boilin Scientific (n=5). As mentioned in chapter 3, degrees of hydration (water absorption) were studied by weighing the fibre samples before and after immersion in distilled water for 12 hours. Excess water was removed from the samples by gently blotting with filter paper prior to each weighing. The degradation valuations were achieved as defined by Zhu et al [285]. The measurements were performed on five replicated samples, they were immersed in 20 ml of 154 mM phosphate buffered saline (PBS, pH 4), containing 0.02% sodium azide as a bacteriostatic agent. The mixture was

maintained in a controlled temperature of 37 ºC. At predetermined time intervals, the reduced buffer was added back with fresh PBS for continuing incubation.

Figure 7-6a shows the water contact angles (Water CAs) of CME/N66 nonwoven fibrous mats. The water CAs decrease in all samples, from 54.62º to 69.18º, in the first 10 seconds, while that of the CME and N66 fibres shows the values of 65.80º and 76.07º respectively. The water CA analysis of CME/N66 indicates high surface wettability.

However, the water CA of N66 shows a significant decrease after 10 minutes that is not comparable with that for CME and CME/N66 fibre samples, Figure 7-6b. This is due to the high polarity of the N66 which causes the water droplet to penetrate through the fibre porous structure, while the samples inherited their surface behaviour from CME. These results are in good agreement with the water absorption measured after 12 hours, where the initial weight of CME achieves 44.20 % growth and the samples show a value between the water absorptions of N66 and CME, Figure 7-6c.

As shown in Figure 7-6c, t(0) indicates the water uptake of samples in the first moment when they are soaked in water, which is calculated as a percentage, depending on added weight, and t(12) based on the added weight after 12 hours into t(0) divided by the whole weight at t(0). The final water absorption was considered by adding the percentage of t(0) and t(12). Water absorption capacity of the studied fibres did not exceed 15 $g.g^{-1}$% with significantly reduced water penetration according to the contact angle studies. From the incubation in PBS for 5 weeks (Figure 7-6d), it is found that all core–shell samples presented a postponed starting point of degradation. Interestingly, from mass residual percentage observations, a significant decrease to 95% was found for CME during the second and third week, the ASC degradation started after about 4 weeks in CME/N66 core–shell composite nanofibres.

7.3 Discussion

Details of the synthesis of the graft copolymers have been reported in chapter 4 [51] in which the side branched hydrophilic collagen graft copolymer (CME), significantly influences the initial viscosity in the studied feed ratios of the comonomer. It demonstrated a meaningful reduction for the conductivity value, where the side chain copolymer with dielectric properties covalently bonds onto the collagen. In the current research, CME was used as mentioned in the experimental section to evaluate the handling of the fibre formation through (coaxial) electrospinning.

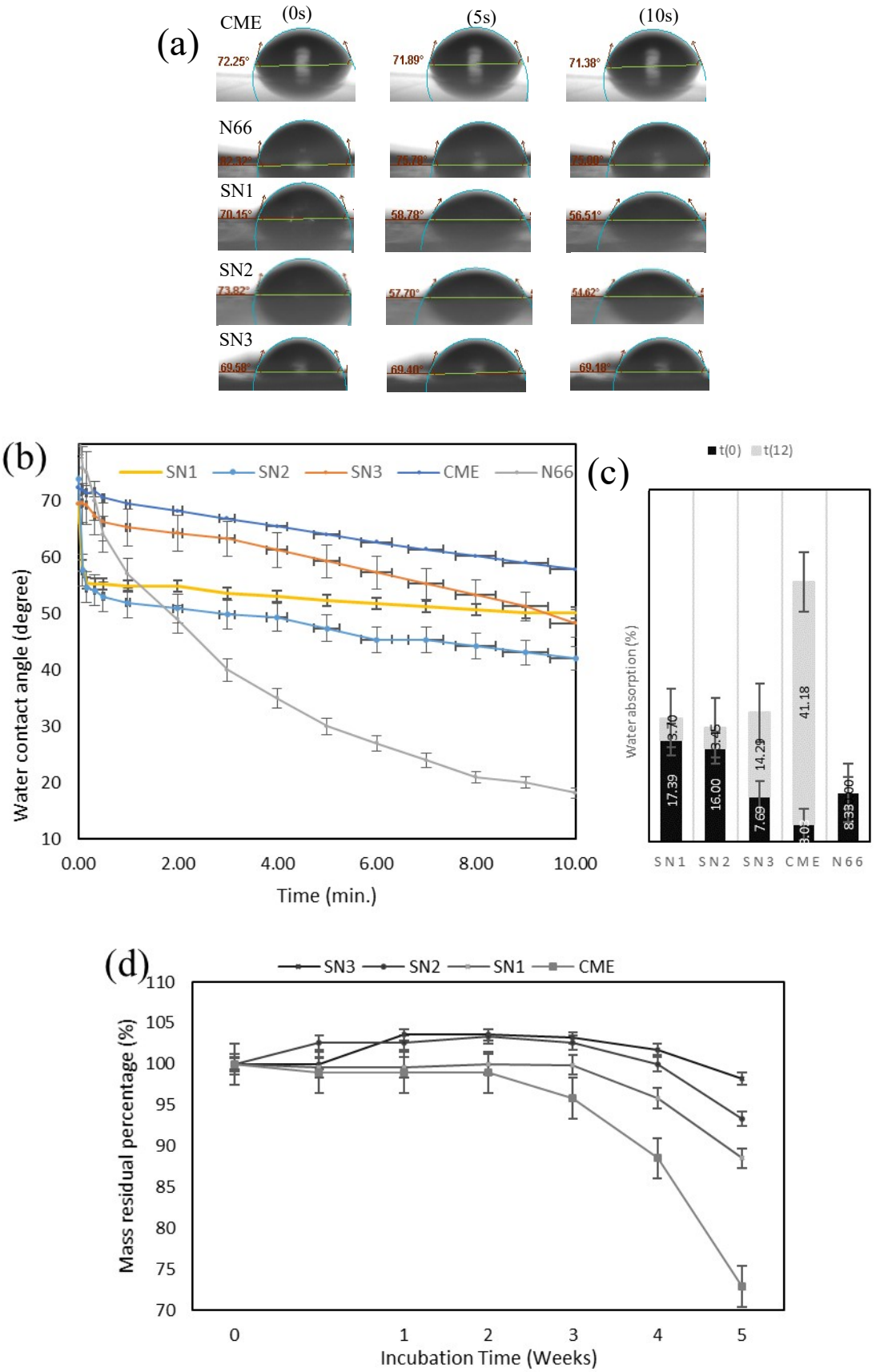

Figure 7-6 The water contact angle vs. time: a) 10 seconds, b) 10 minutes; c) Water absorption of the samples as a percentage, d) Mass residual percentage vs. incubation time (week)

7.3.1 Assembly mechanism of core–shell fibres

In this part of the work, we hypothesize:

(i) the coaxial electrospinning provides the possibility to process both components in the core and shell simultaneously, in which they are unlikely to spin by conventional spinning methods such as melt spinning and wet spinning, or through blending systems;

(ii) the polarization of the polymers in core and shell with a varied capacity of built-in dipoles is dependent on the intensity of the applied electric field, i.e. the fluids in core and shell can move and orientate freely when they are placed in an electrical field. However, it is possible to have a region in the intensity of the electric field that allows both components to form a single fibre by coaxial electrospinning;

(iii) consequently, varied fibre compositions can be fabricated when increasing the intensity of the electric field within that region.

It is noted that N66 possesses a greater dielectric constant in contrast to poly(MMA–co–EA) that is settled as the side chain of ASC. Furthermore, ASC is a polyelectrolyte [67, 341], but the dielectric properties of poly(MMA–co–EA) in the side chain of ASC are more likely to be overcome vigorously due to electrostatic induction and polarization [51]. Then, a higher polarization orientation can occur with a larger factor of the dielectric constant under the influence of the electric field [150, 342-344].

Hence, we used the same solvent for all components in the core and the shell to eliminate the influence of the medium. Additionally, other solution and process parameters were constantly controlled, to study the influence of the intensity of the electric field on tuning the fibre properties for all achieved fibre compositions.

To understand the behaviour of these two incompatible polymers in terms of structure and electrical properties, we used dyes with no overlay in colour which allow us to distinguish the fabricated fibres by changing colour. To understand varied dielectric polarization of the core and the shell components, a negatively charged rod was placed close to the edge of the fibres obtained from each component, CME and N66, individually. It was observed that the negatively charged rod repelled the non-woven mat from CME and attracted the edge of the N66 nanofibres.

As shown in Table 7-1, there is a limited region in the strengthening electrical field that allow both components, the core and the shell, to make a single fibre while stretching towards the collector. Hence, it can be explained that by increasing the voltage, a significantly varied orientation in the core and shell components happens when they are exposed to the electric field. And, due to the different polarization extent of materials in

the core and shell, a specific region of strengthening electrical field can initiate built-in dipoles of both components to fabricate a single fibre that will lead the whole spun fibres towards the minimum of dipole energy in a partially ordered shape of deposition.
In other words, by increasing the voltage, one particular moment in time is achieved when a certain electrostatic force is reached; N66 in core (red) is to accompany the shell component (CME, yellow) which is already initiated in a low electric field intensity, Table 7-1. The shell polymer is influenced by the impulsion of the dipoles oriented by N66 due to the greater polarization orientation into the strengthened electric field.
By further increasing the intensity of the electric field, increasing orientation of N66 can be achieved, as shown by the stronger colour of N66, Figure 7-1(6). It is also possible that the branched copolymer of CME provides sufficient entanglement to form the continuous fibres which can act as a preventive scaffold for stretching N66 in the core.
This phenomenon enables aligned fibres in the axis of drum rotation in voltages from 8–16 kV. This explanation is in good agreement with the increase in the mean fibre diameter when increasing the applied voltage from 8 to 16 kV which is observed in SN1 to SN3 samples, Figure 7-3. This is also apparent in the hue differences when the LAB coordinates of N66 are used as the reference colour, Table 7-2.

7.3.2 FTIR study and Thermal Analysis of the electrospun fibres

To study the interaction between N66 and CME chains, FTIR and DSC were applied. The chemical structure of the electrospun fibres without dyes was considered using FT–IR at room temperature. To prepare the discs, the fibres (1 wt %) were prepared in KBr.
The main characteristic features of the processed samples are observed in the spectra, Figure 7-7. ASC has several characteristic absorption bands identified as amide A (3425 cm^{-1}), amide B (2857–2953 cm^{-1}), amide I (1615–1711 cm^{-1}) and amide II 1446 cm^{-1} in the infrared region of the spectrum [53]. Characteristic bands of poly(MMA–co–EA) are carbonyl (C=O) stretching vibration at 1720 cm^{-1}, CH stretching vibration at (2900–2970 cm^{-1}) and 2865 cm^{-1}, C–O–C stretching at 1060 cm^{-1}, and C–O–C stretching at 1260 cm^{-1}.
The amide I adsorption that originates largely from the C=O stretching vibration, is specifically sensitive to the secondary structure of the polypeptides [304]. For the amide B, the amide II region is affected by poly(MMA–co–EA) absorptions, the amide A band and amide I were used as the reference peaks to confirm the presence of Collagen in CME. This was helpful to study the interaction between CME and N66 in fibres.

For CME fibres, the Amide I peak at 1625 cm^{-1} is assigned to the shift from 1655 to 1625 cm^{-1} that can be caused by β–sheet conformation in contrast with the random–coil backbone conformation (1655 cm^{-1}) [340, 345]. For CME/N66 fibres cast from KBR, apparent peaks are observed at 1628, 1612, 1618 cm^{-1} (SN3, SN2, SN1 respectively), indicating that β–sheet secondary structures (i.e. parallel chains, chain orientation) are formed in either CME or CME/N66 fibres.

Furthermore, due to the N–H stretching vibration, the amide A does not depend on the conformation but is very sensitive to the strength of the hydrogen bond. When the Amide A of CME is observed at 3421 cm^{-1}, it is shifted to higher wavelengths of about 3415, 3383, 3361 in all the samples (SN1– SN3), respectively. However, the amide A peak of N66 improves from 3302 cm^{-1} to 3320, 3305, 3307 in all samples from SN1 to SN3, respectively.

In the CME/N66 fibres, the Amide II peak of N66 (1542 cm^{-1}) is still at the new absorption bands at 1551, 1551,1563 cm^{-1} (SN3, SN2 and SN1, respectively), causing a new vibration of C=O stretching in the CME/N66 fibres which cannot be distinguished simply in CME due to interaction between the ASC chain and poly(MMA–co–EA). These band shifts can be related to the interaction between the N66 and CME backbone chains. This can be explained by some hydrogen bonds that may be shaped between CME and N66 chains. The presence of new hydrogen bonds between CME and N66

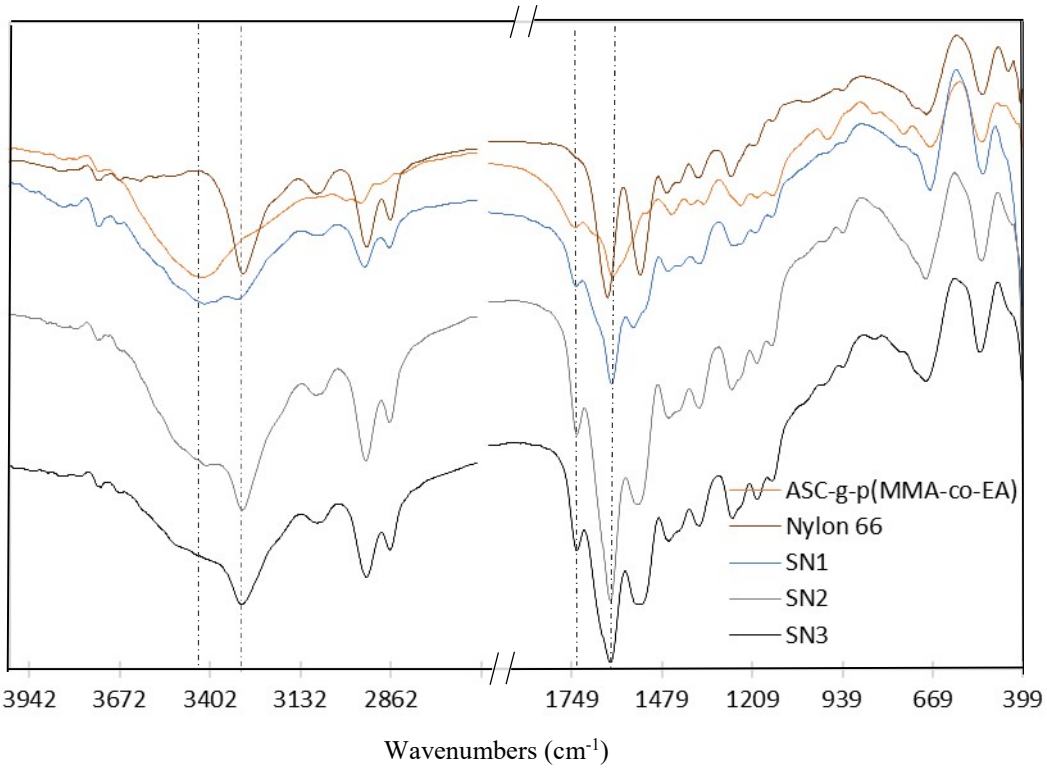

Figure 7-7 FTIR Transmittance vs. frequency for the samples

will affect the vibrations of the C=O bonds and can be seen as a change in Amide A, I and II regions. Since the CME chain is affected by the interaction of ASC and poly(MMA–co–EA), it is difficult to discuss the interaction between CME and N66 in the Amide II absorbance bands. The same situation arises with the Amide III region, as observed in all samples at 1366 cm^{-1}.

Typically, it is believed that a strong interaction between the components of a material can alter the thermal stability of the whole system [340]. The altered thermal performance of the CME/N66 coaxial fibres is important due to two main reasons. The core–shell structure of the fibres is beneficial for the performance of the CME segment in heat transfer efficiency compared with the nanofibres from pure ASC–g–poly(MMA–co–EA).

This unique tunable core–shell structure of coaxial nanofibres showed improved thermal stability when compared to the electrospun nanofibres from any individual component. The DSC curves in the cooling phase indicate that the maximum crystallinity percentage of coaxial nanofibres is much higher than that for pure electrospun N66 nanofibres. The crystallinity percentage of SN3 nanofibres is about three times greater than that for pure N66 nanofibres. This can be due to a firmly interconnected network, e.g. hydrogen bonding that is formed during electrospinning between CME and N66.

This investigation continued with a study of the mechanical effects of the tunable core–shell composite structure of coaxial nanofibres using a mechanical load/extension test with statistical characterization. This enabled a measurable comparison between the core–shell components individually and the core–shell fibres of coaxial electrospinning, as shown in a representative tensile stress–strain curve, Figure 7-4.

According to Table 7-3, the tensile characteristics of the electrospun nanofibres from any individual component are far lower than those for the core–shell structure of coaxial electrospinning with the exception of Young's modulus of CME, which show a higher stiffness than SN1.

It is often reported that a reduction in fibre diameter can significantly enhance the mechanical properties of electrospun fibres in typical electrospinning [67, 346, 347], and also several studies have shown that nanofibres with high alignment exhibit remarkable advantages in terms of their mechanical properties [137, 147-149].

An increase in fibre diameter and also partial fibre alignment were found in the studied samples of the CME/N66 composite coaxial fibres, along with the reinforcement of their mechanical performance. The reinforced mechanical performance of the CME/N66

composite coaxial nanofibres benefits from the branched structure of the CME segments due to increased stress transfer efficiency.

By comparing the mechanical performance and the morphologies of the individual components of the nanofibres, we can say that the morphology cannot be the only reason for this enhancement. But it is rather the synergy of a variety of factors that affect the composite nanofibre from a mechanical point of view. Among them, the dipole-dipole interactions of components in the CME/N66 core–shell composite fibres, e.g. hydrogen bonding, are highlighted as a key factor for stress transfer.

Chain entanglement within the fibres can rely on intermolecular interactions. Additionally, the intrinsic stiffness of the branched CME and a possible rod-like orientation of N66 within the nanofibre structure can increase the mechanical performance of the core–shell composite fibres. Therefore, due to strong intermolecular interactions, the fibre samples not only achieve chain orientation but also a significant enhancement in mechanical properties is observed.

Chapter 8 High performance of covalently grafting onto collagen in the presence of Graphene oxide

The use of fillers for the enhancement of polymer properties such as chemical, thermal, mechanical, and optical properties has been well documented [274]. Among them, nanofillers, due to their large surface–to–volume ratio over conventional fillers, have used as a smart candidate as fillers [20, 268]. This large specific interfacial area allows them theoretically to have higher interactions with the polymer matrix [20, 150].

Nanofillers can be categorized by their dimensions. The newest class of 2–dimensional carbon based nano–sheets is graphene and its derivatives, which have found some applications, to promote the polymer matrix [267, 270, 347]. However, due to undesirable interactions in the polymer matrix, their processability is still problematic [268, 274].

The nanofiller dispersion in the polymer matrix is an important aspect of processing wherein the nanofillers are likely to agglomerate [274]. Several advantages that graphene can impart on the host (co)polymer include improved mechanical properties, such as modulus and tensile strength, as well as dimensional stability and increased heat resistance [269]. Among them, a mechanical reinforcement can be the most beneficial approach in bio-based materials that typically suffer from poor mechanical strength and stability in high humidity [150, 268-270]. The extent of enhancement is directly related to the exfoliation of graphene and its dispersion thereafter.

As discussed earlier, the purified collagen through helix to coil conversion, cannot be processed on its own due to drawbacks such as its super-hydrophilicity and poor mechanical properties, but due to its excellent properties [134, 348], it has been processed with a series of compatible materials to enhance their properties [69, 349]. To reduce the super-hydrophilicity of purified collagen chains, a variety of monomers can be branched over the surface of collagen chain, as discussed in chapter 4. Thereby, the modified collagen can benefit from the newly achieved structure while receiving some of the physiochemical properties of branches, such as thermal and mechanical [256, 350-353]. Several attempts have been devoted to optimising the synthesis parameters for increasing the grafting performance (grafting yield) of this methodology [322, 354]. Among them, the increased monomer feed ratio plays a key role in grafting performance, as used for chapter 4 [5, 217, 219, 221, 225, 280, 355, 356]. To the best

of our knowledge, the effect of fillers such as graphene-based nanofillers on the performance of in-situ polymerisation onto collagen has yet reported.

Graphene oxide (GO) is a widely employed form of modified graphene [266, 269, 270]. GO has a layered structure with numerous oxygen functionalities (epoxide, hydroxyl, carboxyl and etc.) on the basic planes and edges [266, 275, 276] and Collagen as a polyelectrolyte can be identified by the amine and carboxyl groups. Thereafter, covalent bonds, Vander Waals forces such as hydrogen bonding, electrostatic interaction or π–π stacking between collagen chains, macromonomers and GO is expected to elevate the grafting efficiency and stability of the nanocomposites.

Therefore, the novelty of this work is to create a collagen-based nanocomposite using GO to enhance its performance, in terms of quality and quantity, by interactions of covalent and non-covalent conjugations between the nanofiller and host polymers. This work is important because:

i) water is used as the medium of polymerisation in which GO is highly dispersed;
ii) it increases the efficiency and yield of the polymerisation when GO is grafted to the collagen chain, as the host polymer, and to the introduced monomers;
iii) it facilitates the process of the obtained nanocomposite by the eliminating of challenges in relation to the GO dispersion and GO re-agglomeration while processing;
iv) GO as a reinforcing agent with highly active functional groups can simply improve the functionality of the collagen-based nanocomposites by controlling the mechanical properties and degradation rate of collagen.

The processability of the collagen-based nanocomposite was investigated using a casting and electrospinning methodology to mimic the structure of collagen fibrils as in native tissue. The nano-layered composite structure was achieved by casting methodology which can potentially be attractive to other applications such as nanomechanical systems, and hydrophilic transparent and paper-like collagen-based nanocomposites.

Therefore, in this part of the study, a set of six samples was synthesised by in-situ polymerisation onto acid soluble collagen (ASC) and were further examined to consider the influence of GO loadings on nanocomposite performance in terms of mechanical strength and degradation ratio.

8.1 Experimental section

8.1.1 Synthesis of GO–ASC–g–poly(MMA–co–EA)

GO was synthesised from natural Graphite flake (3.0 g, 99%, Alfa Aesar), using the modified Hummers' method, purified and dried by following the same procedure [268, 348] as in for the modified method; a 9:1 mixture of concentrated Sulphuric acid (H_2SO_4, 95–98%, Alfa Aesar)/ Phosforic acid (H_3PO_4, 85%, Alfa Aesar) (360:40 mL), was added to a mixture of graphite flakes and Potassium permanganate (18.0 g, $KMnO_4$, 99%, Alfa Aesar) producing a minor exotherm reaction to about 40 °C. The mixture was then heated to 50 °C and stirred for 12 h, before cooling to room temperature by pouring onto ice cubes (400 mL) mixed with Hydrogen Peroxide (3 mL, H_2O_2, 35%, Alfa Aesar). This mixture was filtered through a PTFE membrane (0.2µm pore size, life Sciences Super ®–200).

The remaining solid material was then washed in turn with 200 mL of water, 200 mL of Hydrochloric Acid (HCl, 36%, Alfa Aesar) and 200 mL of ethanol (Alfa Aesar); each wash was filtered through a polyester membrane. The remained material was coagulated with 200 mL of ether (Alfa Aesar) and filtered again. The solid remaining on the filter was dried in a vacuum oven at room temperature. The final product of Graphene oxide achieved a mass of 5.32 g at the end.

Thereafter, the GO–ASC–g–poly(MMA–co–EA) nanocomposite was synthesised by an in-situ polymerisation technique applying benzoyl peroxide as an initiator, a GO aqueous suspension, an ASC solution and comonomer with desired ratios at 80 ºC for 30 min [51]. In a typical preparation, GO powder was dispersed in distilled water and stirred for 1h using a magnetic stirrer followed by 15–min sonication to achieve a fully exfoliated GO suspension (13 mg ml^{-1}), and then diluted 5 times in distilled water.

The ASC solution was prepared using collagen in diluted AA in distilled water to reach pH 3± 0.5. The mixture was incubated for 5 h at 45 °C in a 250–ml three necked round bottom flask with a stirrer bar. This step was stopped when the temperature of 80 °C suddenly achieved, seen ASC in water as a homogenous solution.

Then, N_2 gas was applied through the solution while stirring. The GO suspension was added to the ASC (150 ml, 36 mg ml^{-1}) solution three portions within 15 min. After 1 h, the dissolved BPO in 2 ml Acetone as the initiator was added gently to the reaction vessel within 10 min.

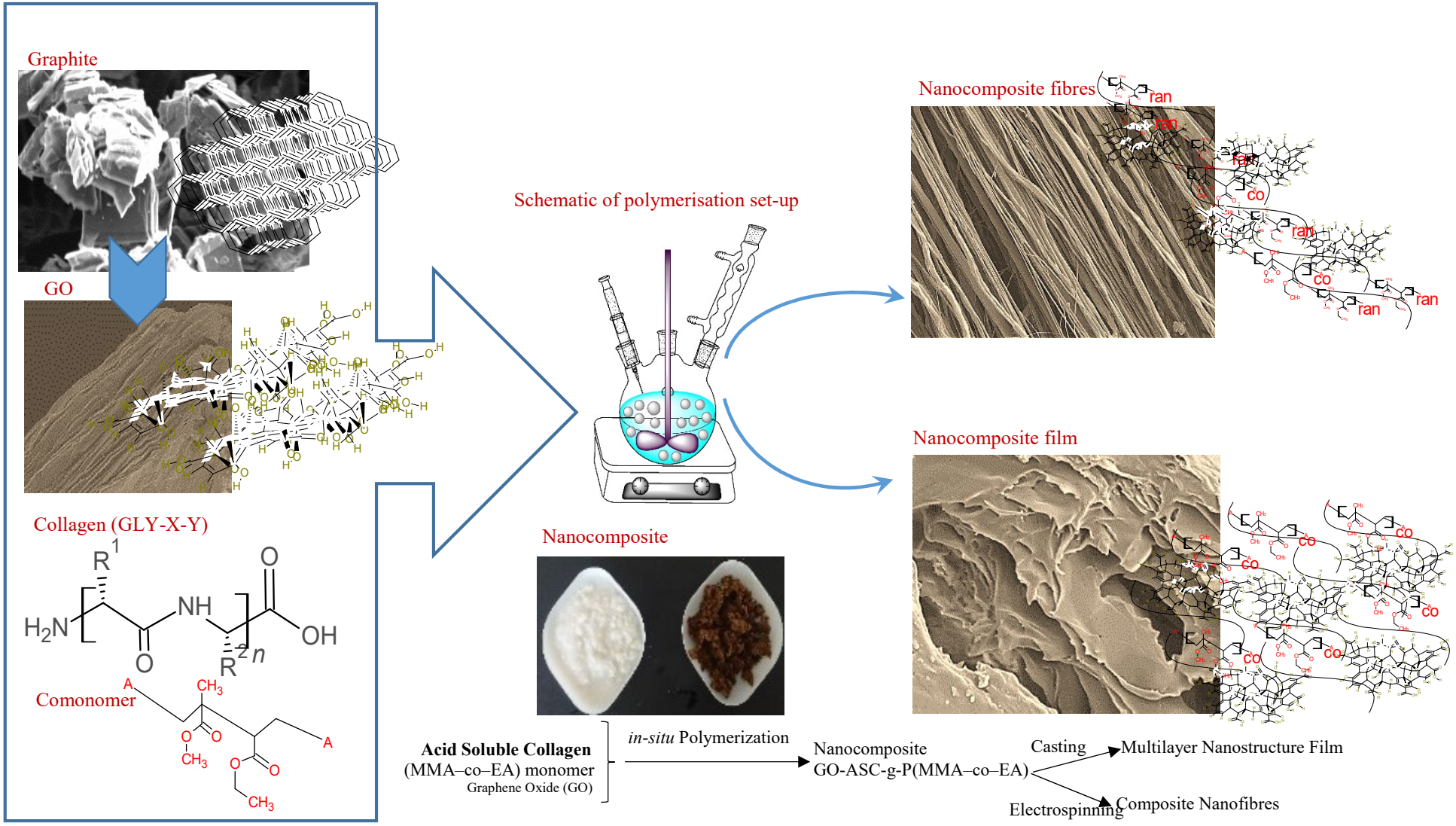

Figure 8-1 The scheme of main interactions: Nanocomposite of GO-ASC-g-P(MMA–co–EA) was synthesised in the presence of Acid soluble collagen, monomers and Graphene oxide and Graphene oxide (GO)

The mixture of distilled MMA and EA in the rates mentioned in Table 8-1, were then introduced via a syringe over 30 min. The temperature and reaction time were fixed at 80 °C and 60 min after adding the initiator and the monomers. The stirrer speed was fixed at 2400 rpm during the reaction. Precipitation of the graft copolymer occurred after 10 min of reaction time. The reaction mixture was then added to an excess amount of cool methanol for complete precipitation. As with any free radical copolymerisation reaction, the formation of the attendant polymer of poly(MMA–co–EA) always forms along with that of the desired nanocomposite (GO–ASC–g–poly(MMA–co–EA) owing to reactivity ratio effects or the segregation of macromonomers from main and side chains with the presence of GO.

An extraction step was needed to remove ungrafted ASC and GO, unreacted MMA–co–EA macromonomers and poly(MMA–co–EA) from the desired copolymer product. A simple isolation method of selective solvent extraction, based upon the difference in solubility, was employed. Therefore, the resulting product was extracted by repeated washing with boiling water followed by acetone at room temperature, to remove by-products using a sintered glass filter under reduced pressure. All samples were dried in a vacuum oven at room temperature until a constant weight was achieved.

The grafting parameters, i.e. grafting-percentage (GP, %), and grafting-efficiency (GE, %) were used to characterize the identified copolymer. GP shows an increase in weight of original ASC subjected to grafting with comonomers. Grafting efficiency (GE) indicates the fraction of comonomer grafted onto ASC among the amount of MMA–co–EA converted to graft copolymer plus poly(MMA–co–EA).

Due to the negligible mass of GO compared with the mass of the host polymer and the monomers, the weight of GO was discounted from the calculations that were introduced in chapter 3, section 3.1. The samples were labelled as S1–8, S1–16, S2–8, S2–16; ASC–g–poly(MMA–co–EA) without GO content were then used as reference samples and were named as S1–0 and S2–0.

8.1.2 Preparation of films and nanofibres

A 10 % (w/v) solution of each sample was prepared using a mixture of Acetic Acid and Acetone (4:1) was used as a selective solvent. Films were obtained from 10 ml of the solutions, on the bottom of Petri dishes (6 cm in diameter) after solvent evaporation at room temperature. Then, each film sample was labelled as F1–8, F1–16, F2–8, and F2–16; the films of ASC–g–poly(MMA–co–EA) without GO content were used as reference samples and named F1–0 and F2–0.

For fibre formation, A Spraybase electrospinning apparatus was used with a high voltage power supply, a syringe pump, a syringe and tubing, a 20–gauge needle and a grounded rotating collector with surface length of 25 cm and diameter of 9 cm at a speed of about 1.7 m/s. The processing set up has been shown in chapter 3, Figure 3-1 and Figure 3-2a.

Each solution was fed through a Teflon tube, to the needle that was placed in a syringe pump. All the above-mentioned samples were electrospun into nanofibres by using the following electrospinning conditions: applied voltage (10 kV), needle to collector distance (TDS, 12 cm), and solution flow rate (0.5 ml/min, room temperature and relative humidity (RH, 30–35%). Electrospun nanofibres were labelled according to GO content as follows; M1–8, M1–16, M2–8, M2–16.

Table 8-1 Effect of GO content on grafting parameters

Sample	Comonomer cont. in feed (mmol)	EA cont. (%)	Initiator (mmol)	GO (13 mg ml^{-1}) content (ml)	GP (%)	GE (%)	Nitrogen content (%)
S1	54.91	0.5	4.51	0	16.09	30.67	6.16
				8.00	68.7	97.63	6.32
				16.00	94.47	97.42	6.21
S2	109.85	5.00	9.10	0	46.48	36.74	5.86
				8.00	101.66	94.02	6.09
				16.00	108.93	87.90	6.13

8.2 Results and discussion

In this part of the work, the modified Hummers' method for the preparation of GO was applied; increasing the amount of KMnO4 and performing the reaction in a 9:1 mixture of H_2SO_4/H_3PO_4 in which it is believed that the efficiency of the oxidation process can be improved. This improved method offers a higher amount of hydrophilic oxidized graphene-based material in contrast with the common Hummers' method ($KMnO_4$, H_2SO_4, and $NaNO_3$). This modified method was utilised due to achieving GO with more oxidized end groups. In addition, this method does not produce any toxic gas and the reaction temperature can also be easily controlled [259, 260, 266, 346, 357, 358].

Hence, the method allows GO being developed by the oxidative exfoliation of graphite flakes as the first step; the TEM image of few layers of GO was shown in Figure 8-1. Then, an ASC–GO complex was then successfully achieved. According to literature, GO provides a good synergetic effect when mixed with collagen and its derivations due to having high concentration of oxygen functionalities [267, 276]. For instance, a GO–

collagen-based hydrogel was recently synthesised by melt-coupling reactions of an aqueous GO suspension and a gelatin–water solution at 95 ^{o}C. They claimed that amines can be conjugated onto GO wherein reducing them into RGO [276]. This reaction can be considered by two main routes; the amidation reaction of carboxylic acid groups on the GO edges and the ring-opening amination of epoxy on the GO surface [267, 276].

Using thermal treatment, both reactions are likely to occur for the amino groups of ASC. Furthermore, hydrogen bonding between amine and hydroxyl on GO was reported several times in the literature [264, 269, 270, 273, 274, 276]. Although the exact mechanisms of attachment and the detail of chemical reactions are not clear due to the complexity of the GO structure, the main interactions between ASC and GO during the synthesis and processing can be as noticed above.

In the next step, the synthesis including grafting MMA–co–EA onto ASC–GO conjugated complex by in-situ polymerisation was stablished. Even though there are few concerning with the effect of introducing monomers to poly amines/proteins in the presence of nanofillers, it is reported that with respect CNT–PA6 composites as a poly amide-based material [115, 359, 360], the polymer chains bond to the surface of nanofillers; they suggest that molecules of initiator or monomer attach to the surface to act as initial points for chain initiation and propagation [354, 361].

Therefore, due to the physiochemical interactions between ASC and GO, ASC is expected to be coupled on GO, while poly(MMA–co–EA) chains are grown and covalently bonded onto the ASC backbone via free radical polymerisation at a temperature below the denaturation process temperature of ASC which is expected to be between 90 – 100 ^{o}C.

This hypothesis was followed to preserve a higher fraction of ASC as raw material to be converted to the desired product of in-situ polymerisation; ‘’collagen graft composite’’. These proposed main interactions are illustrated in the process scheme, Figure 8-1. As shown in Table 8-1, a significant increase was achieved in Grafting Performance (GP) by increasing the GO content; this confirms a notable increase in the weight of ASC subjected to grafting with GO and poly(MMA–co–EA). A significant increase was achieved in Grafting Efficiency (GE) which indicates that a higher fraction of MMA–co–EA that converts to the collagen graft composite.

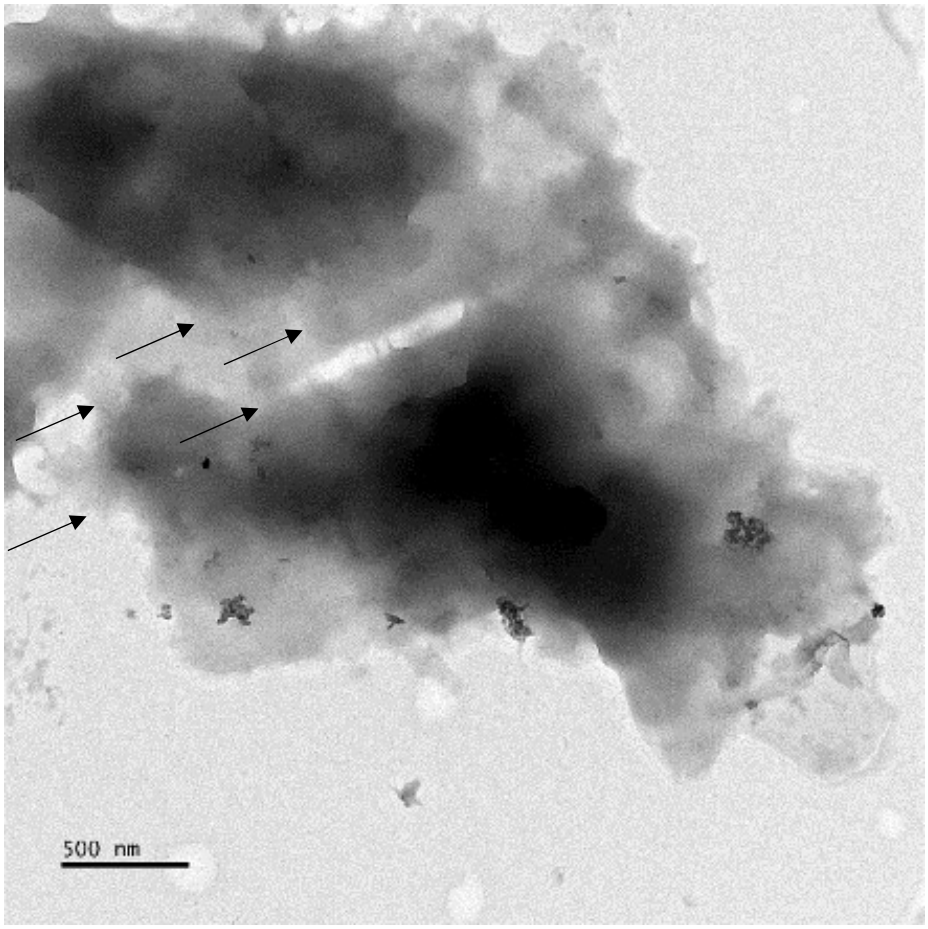

Figure 8-2 TEM image of few-layers Graphene Oxide that (black arrows) stacked on top of one another. The scale bar shown at the bottom of image is 500 nm.

These enhancements are obviously due to the presence of GO that provides ability for reactants to bond to the variety of functional groups on the surface and the edges of GO. Therefore, the tailored nanocomposite is structurally modified to a branched collagen-based macromolecule conjugated with GO, despite a high probability for macromonomers to be grafted onto GO individually as well. This covalently bonding of comonomer on the GO surface is unavoidable, even though it can be considered as an advantage for the composite to benefit from the interfacial repulsions preventing the reagglomerating of GO in the solvent while processing. In other words, the presence of ASC–poly(MMA–co–EA) on the surface of GO suggests the availability of strong interfacial bonding between the copolymers and GO; which should promote the stability of the GO dispersion within the organic solvents.

Finally, GO grafted onto the collagen graft nanocomposite could not be dispersed in water while extraction stage, proving the idea of good interfacial attachments during polymerisation, since GO can be easily dispersed in water due to having oxygen groups

increasing its hydrophilicity [262, 270, 276, 362, 363]. However, as mentioned above, our work is due to benefitting from a higher proportion of participating ASC in the reaction.

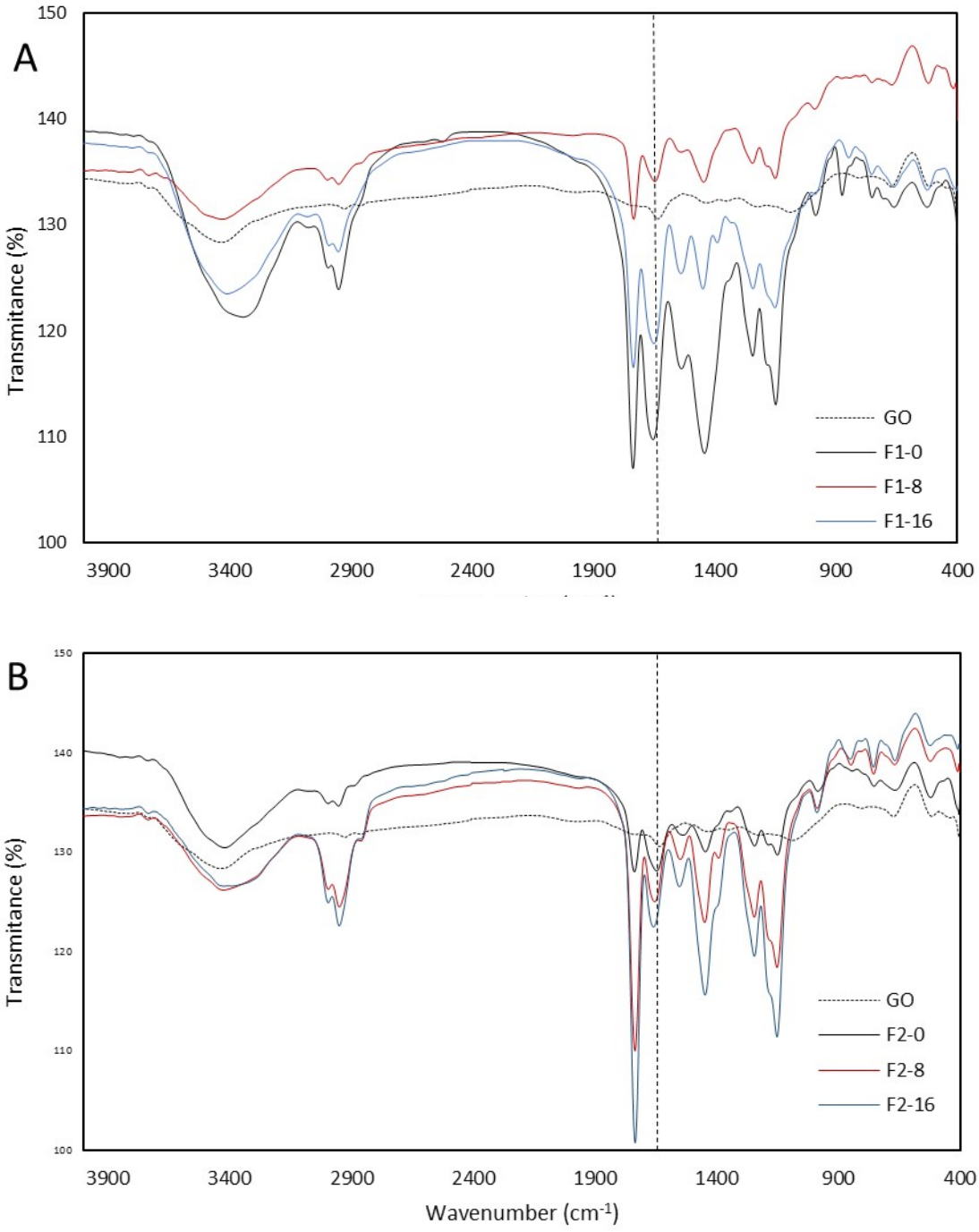

Figure 8-3 FTIR Transmittance vs. frequency for ASC–g–P(MMA–co–EA) with/without GO content; to clarify, curves associated with comonomer feed ratios were demonstrated as following: a) composite films of lower comonomer feed ratio and b) composite films of higher comonomer feed ratio.

The effect of Graphene Oxide on physiochemical properties of collagen grafted nanocomposite

Referring to Figure 8-3, the structure of the nanocomposite films was evaluated by Fourier Transform Infrared Spectroscopy (FT–IR, Thermo Nicolet Avatar 370 DTGS) at room temperature. This was to investigate the structure of ASC–g–poly(MMA–co–EA) in the presence of GO. For more clarity of the variation of the FTIR peaks, these spectra were shown in two graphs.

The FTIR spectrum of GO reveals the presence of different oxygen functionalities: carbonyl groups (C=O, 1735 cm^{-1}, 1640 cm^{-1}), (broad stretching vibration C=C in rings, 1550 –1710 cm^{-1}), alkoxy groups (C–O, 1050 cm^{-1}, 1352 cm^{-1}), epoxy groups (C–O–C, 1225 cm^{-1}), (C–OH stretching bond at 3539 cm^{-1}) and also C–H stretching symmetric bands at 2852–2906 cm^{-1} [358, 364, 365]. F1–0 and F2–0 were characterized for comparison wherein synthesised without GO, and their main characteristic groups are identified in Figure 8-3a and b, respectively. In the case of F1–0, the absorption bands at 2991–2948, 1733,1536–1644 ,1441,1148,1242, 978 and 3100–3500 cm^{-1} are attributed to the stretching vibration of Alkynes (CH, CH2 and CH_3), strong stretching vibration (C=O), asymmetric vibration NH2 (amide I & II), CH_3 and CH_2 bending deformation, stretching vibration of the C–O bond in the CO–O–C moiety, asymmetric vibration peak (N–C), stretching vibrations (C–N), and amide A broad stretching vibration (N–H/OH), espectively. In the case of the FTIR spectrum of F2–0, the profile is almost the same as F1–0 in different intensities without showing any other peaks.

Upon in-situ polymerisation in the present of GO and poly(MMA–co–EA), the oxygen functionalities in the corresponding FTIR peaks of GO are affected by ASC–g–poly(MMA–co– EA) absorptions. The amide I vibration and amide II bending vibration and CH_3 and CH_2 bending deformation from ASC–g–poly(MMA–co–EA) dominate in the studied nanocomposites with GO content, overshadowing the C=C vibrations from GO.

However, from the peak at 1050 cm^{-1}, referring to Alkoxy group of GO, that cannot be observed in the nanocomposites, it can be predicted that the oxygen functionalities were weakened during the reaction. Furthermore, the FTIR peak of the C=O at 1730 cm^{-1} was elevated with increase in the GO content due to higher contribution of C=O groups from poly(MMA–co–EA) in the structure of collagen graft nanocomposite.

The feature of the Amide I and II was slightly shifted to a higher frequency due to hydrogen bonding between GO and ASC–g–poly(MMA–co–EA) in samples with

higher P(MMA–co–EA) content (F2–8 and F2–16) wherein a new peak of CH_3 deformation bending vibration was observed approximately at 1387 cm^{-1}. The reduced oxygen functionalities of GO and the similarities of the main features of ASC–g–poly(MMA–co–EA) indicate the dominance of polymer segment in the studied nanocomposites and the presence of newly formed bonds between GO and ASC–g–poly(MMA–co–EA).

To identify the GO content, UV–Vis spectroscopic studies were performed, Figure 8-4. UV–VIS spectra were recorded by Perkin Elmer Lambda 35. It is inferred that the presence of GO content is identified by the optical absorption of GO, dominated by the π–π stacking at the more intense peak of 230 nm [357, 362]. The π–π stacking peak on film samples with GO content was recorded, representing a slightly blue shift compared with GO at 212, 213, 216, and 220 nm for F2–16, F2–8, F1–8, and F1–16, respectively. This can be due to linking units of GO such as C–O and C=O, and C=C bonds that altered during in-situ polymerisation. However, a red shift was observed within the film samples by increasing the GO content. This can be attributed to a higher intensity of C=C and oxygen-containing bands in samples with higher GO content.

The effect of GO content with different loadings on the thermal behaviour of the collagen graft nanocomposite is shown in Figure 8-5. Thermal analysis of the films was performed by Differential Scanning Calorimetry (DSC, Mettler DSC 12E). Temperature ranges from 23°C up to 280°C and vice versa for cooling scans with a heating/cooling rate of 10 °C min^{-1} in a nitrogen atmosphere was performed. A 3–minute time remaining at 300°C was applied to erase the history of the thermal behaviour of samples (7 mg) for evaluating changes during the cooling scans. Endotherms were represented with upward curves in the scans.

It is known that ASC shows two endothermic events in thermal analysis referring to melting temperature (T_m) and denaturation process temperature (T_d) [72, 366, 367]. The first endothermic peak referring to T_m occurs at a temperature between 35–50 ºC depending on the structural hierarchy of peptide chains. The second event (Td) arises at a range between 80–110 ºC. In ASC–g–poly(MMA–co–EA), a clear melting peak of ASC was observed at 61.64 ºC (F1–0) while this peak couldn't be clearly observed by increasing the poly(MMA–co–EA) segment (F2–0). This can be due to heat transfer carried out by a higher density of poly(MMA–co–EA) as the side chains on ASC. On the other hand, a wide endothermic region was observed in F2–0 that can be counted as a complex peak for T_m and T_d of ASC at 86.64 ºC.

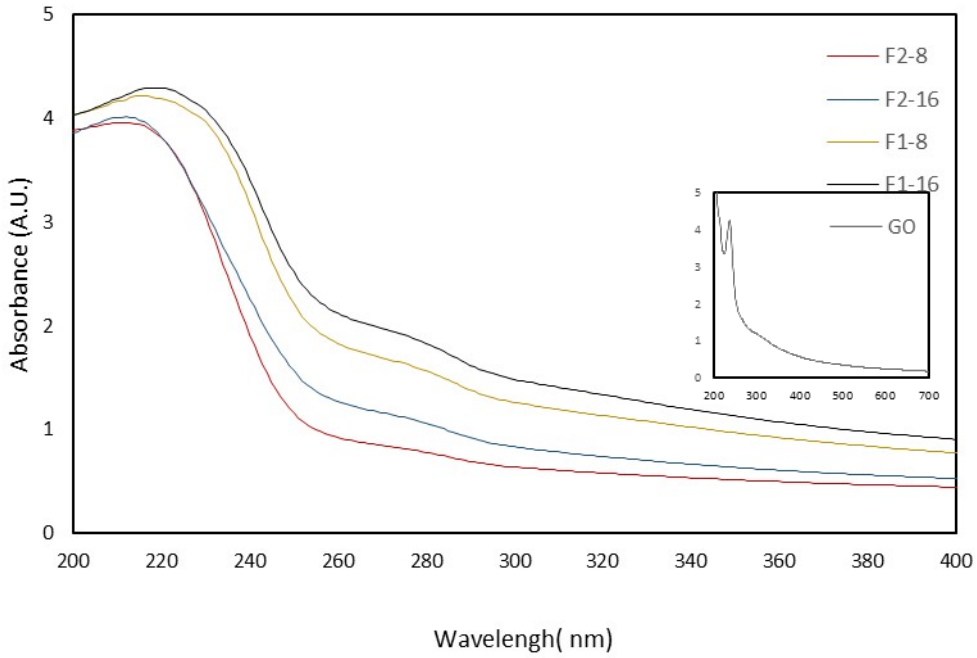

Figure 8-4 The UV/vis spectra of composite films from ASC–g–P(MMA–co–EA) with GO content show a redshift, suggesting π–π stacking of the components with increasing the GO content.

In this case, although Tm of ASC was postponed to a higher temperature by increased density of the side chains, the enthalpy changes of this thermal transition (ΔH) is approximately the same value of F1–0, 1703 $J.g^{-1}$ and 1523 $J.g^{-1}$, respectively. Also, an obvious melting region at about 160±0.5 ºC was recorded referring to the melting temperature of side chains for both F1–0 and F2–0 without GO content. For the samples of GO–ASC–g–poly(MMA–co–EA), the above-mentioned complex peaks were observed at mean value of 87.31±7.34 ºC; wherein the highest temperature (99.28 ºC) is associated to F1–8 possessing a less side branch density (From nitrogen content, Table 8-1) and also less GO content, and the lowest temperature (74.27 ºC) is for F2–8 due to a higher branch density and less GO content. Therefore, increasing the GO content has insignificant effect on Tm and Td of ASC.

However, unlike the samples without GO, the endothermic transition correlated to side branch melting in the presence of GO were recorded in a lower diversity (standard deviation) at a mean value of 150±5.66 ºC. Interestingly, all samples with GO content were found to have a decrease in melting temperature of the side chains. This can be due to a reduced average length of side chains when comonomers grafted onto ASC chain as a consequence of enhanced grafting performance and efficiency, coupled with the increased Nitrogen content in collagen graft nanocomposites, Table 8-1.

Additionally, ΔH was decreased significantly in endothermic transition events by Go content. In general, the thermal stability of collagen graft nanocomposites can be enhanced with the present of GO in which the increasing temperature induces exothermic transitions due to reformed carbon–oxygen bonds on the surface and edges of GO.

Furthermore, an irreversible exothermic event is also observed at 233.13 ^{o}C and 221.17 ^{o}C during the heating phase of samples with GO content due to higher GO content (F1–16 and F2–16) (Figure 8-5) that is attributed to the reduction (defunctionalisation) of GO. This feature is not observed in DSC profiles recorded in the cooling phase (not shown).

Defunctionalisation which is ascribed to decomposition of the labile oxygen functionalities such as –OH, –COOH, –C=O; can be referred to the density of free functionalities on the surface and edges of GO that probably have not been bonded during polymerisation and the process.

In the case of F1–8 and F2–8 with less GO content, it is more likely that the formation of covalent bonds within the polymeric matrix renders the oxygen functionalities and this can mark F1–8 and F2–8 less amendable and more stable samples by increasing temperature as compared to other samples.

The thermal stability of the samples was further measured using Thermo–gravimetric

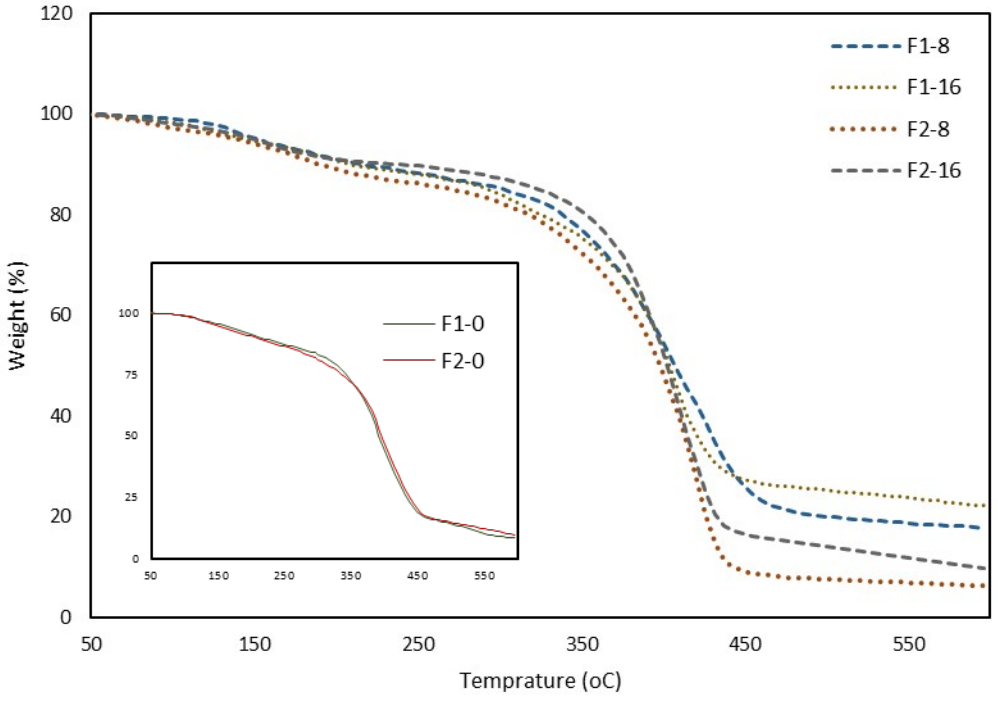

Figure 8-5 TGA graph of weight change as a function of temperature for composite films from ASC–g–P(MMA–co–EA) with GO content.

analysis (TGA). TGA was carried out by using the Mettler TC 10A/TC 15 Instrument, as mentioned in chapter 3. The film samples were heated from 35 ºC to 600 ºC at 10 ºC/min monitoring the sample weight variance; the results are shown in Figure 8-6.

A mass loss of about 10% was recorded by 200 ºC which can be due to the loss of acidic functional groups in either ASC or GO. While the mass loss was then carried out with the same rate till 30% at 350 ºC in samples without GO content, a higher thermal stability was observed from the higher residual mass of 80%, 76%, 74%, and 71% by 350 ºC in F2–16, F1–8, F1–16, and F2–8.

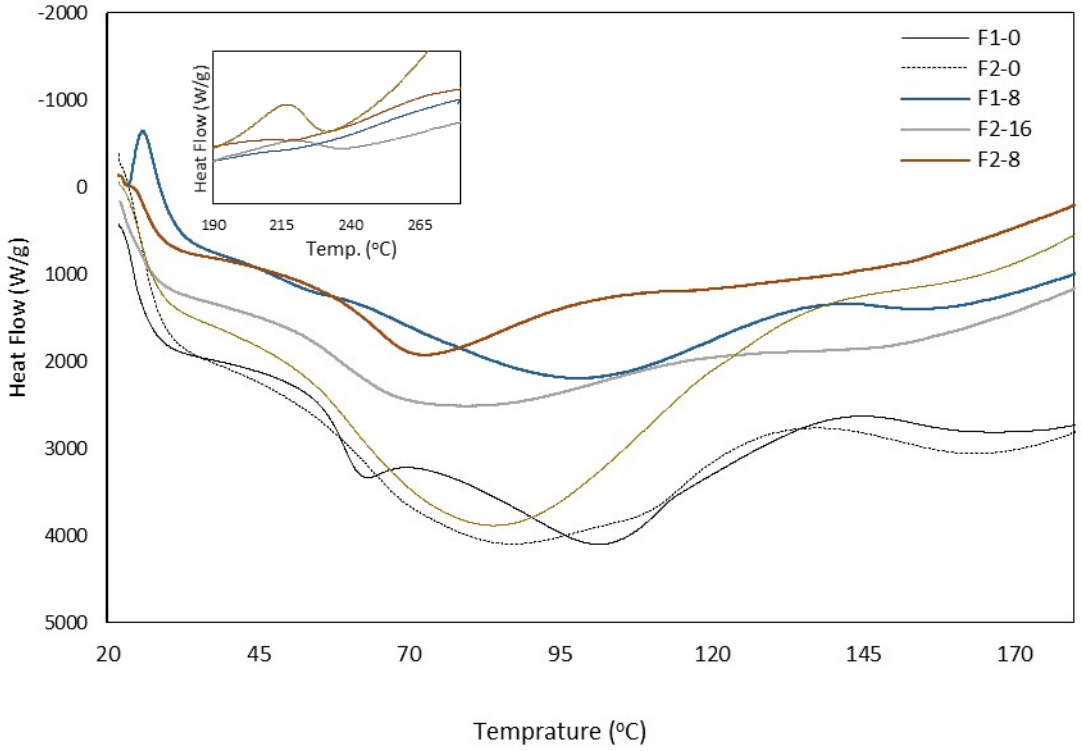

Figure 8-6 Heat flow vs. temperature of composite films from ASC–g–P(MMA–co–EA) with/without GO content, in DSC heating phase with the rate of 10°C min^{-1} in an aluminium pan. To clarify, curves associated with the decomposition transition of GO content were demonstrated in the same graph happening within the temperature ranges between 190-280 ºC) in samples with high GO content.

And then the samples immediately encountered a significant decrease in weight at temperature ranges from 350 ºC to 443 ºC for F1–16, F2–16, and F2–8. This rapid mass reduction occurred for F1–8 in a wider range of temperatures between 350 ºC to 460 ºC. Additionally, F1–16 exhibited a higher residual mass of 23% at 550 ºC in contrast to other samples with GO content; 19%, 11% and 7% for F1–8, F2–16, and F2–8 respectively. These results suggest that GO content and branching densities are both

responsible for the thermal stability of the nanocomposite since a more stability was observed in higher GO content and branching densities (F2–16).

To investigate further, the morphology of the film samples was analysed via Scanning Electron Microscope (SEM) (Figure 8-7). The films were coated with a gold thin film before SEM imaging to ensure higher conductivity. SEM images of samples without GO content clearly show a porous structure (Figure 8-7 a and b) which is caused by the amphiphilic nature of ASC–g–poly(MMA–co–EA), forming a foam-like porous structure. However, a smooth surface representing a layered inner structure was observed in all SEM images of samples with GO content.

This is due to the presence of GO layers in nanoscale providing higher possibilities for both polar and nonpolar segments of GO–ASC–g–poly(MMA–co–EA) to conjugate during the morphological transformation from fluid to film. Additionally, from the SEM images of the samples with GO content, no clear GO agglomeration was observed, confirming high exfoliation and uniform dispersion during in-situ polymerisation followed by spatially multilayer film formation.

The nanocomposite films on a blue substrate have been shown in Figure 8-7(2). It can be observed that films depending on the Go content, representing a transparent to opaque appearance along with a shade of brown colour from light to dark, while no uniformity can clearly be observed on the surface of the films without GO content. Again, the observations confirm the complexity of the structure and the mechanisms of attachments that causes this highly structured arrangements as the solvents evaporates away.

Furthermore, appropriate mechanical responses play a key role for any matrix-filler to be considered for a range of applications. Mechanical characterization was studied on strip-shaped films, 50*10 mm and thickness of around 25µ determined by a micrometre. Stress–strain curves were recorded on relaxed samples over night (temperature: 22 ºC, RH= 62%), using an INSTRON Testing Machine (3345 series) with a load cell of 500 N capacity under standard atmospheric conditions for testing the films; the crosshead speed was set at 5 $mm.min^{-1}$.

(1)

(a)

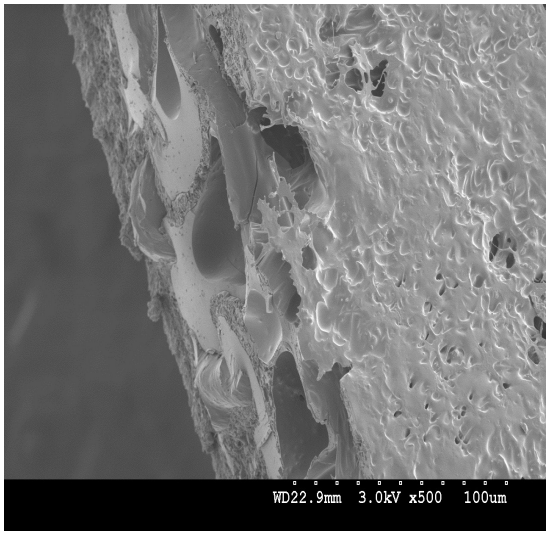
WD22.9mm 3.0kV x500 100um

(b)

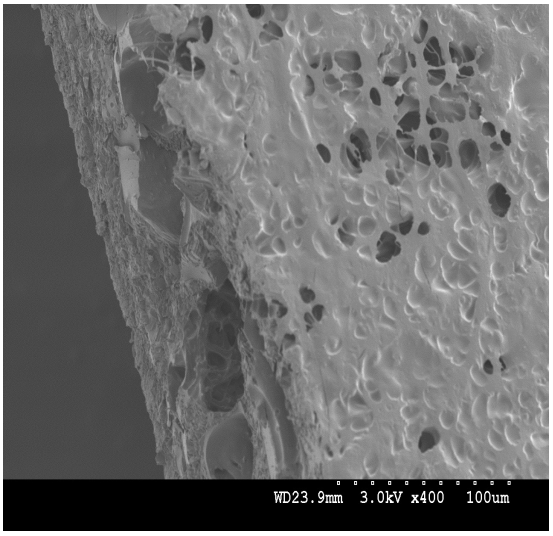
WD23.9mm 3.0kV x400 100um

(c)

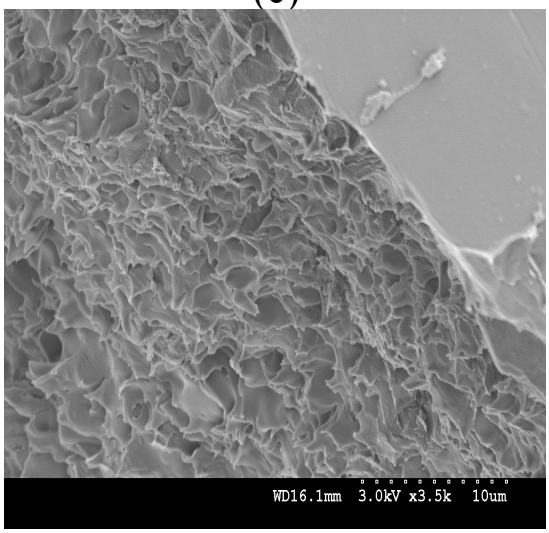
WD16.1mm 3.0kV x3.5k 10um

(d)

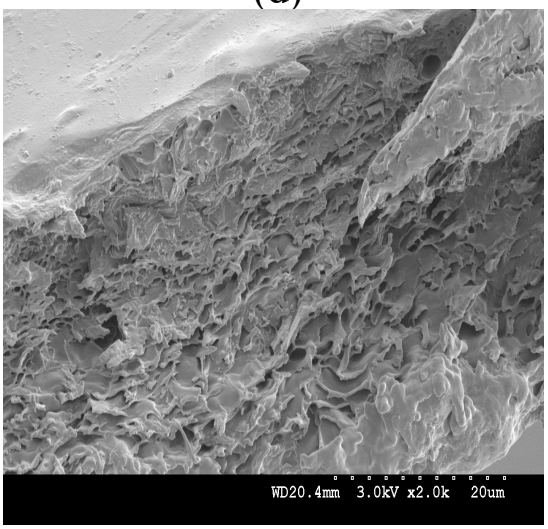
WD20.4mm 3.0kV x2.0k 20um

(e)

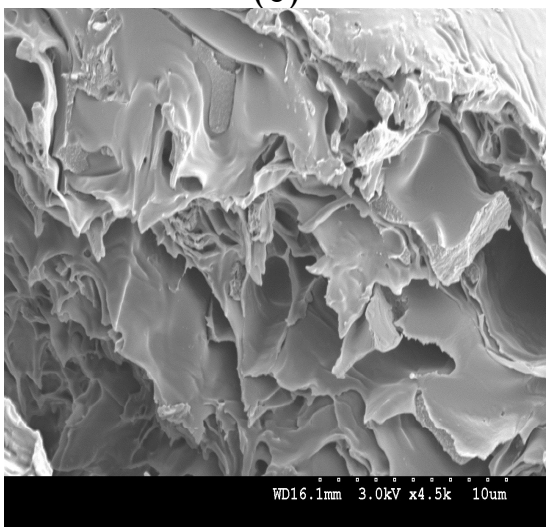
WD16.1mm 3.0kV x4.5k 10um

(f)

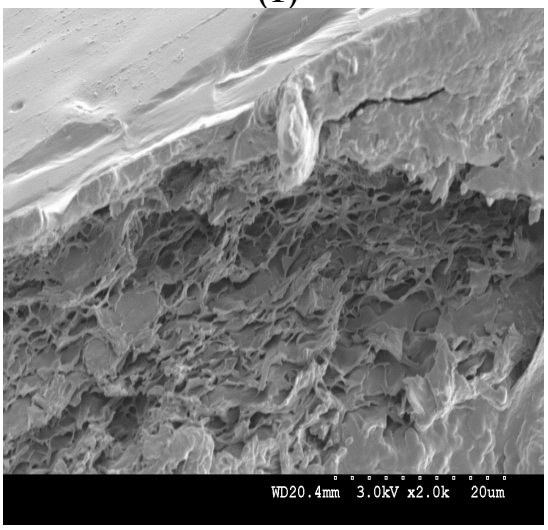
WD20.4mm 3.0kV x2.0k 20um

(2)

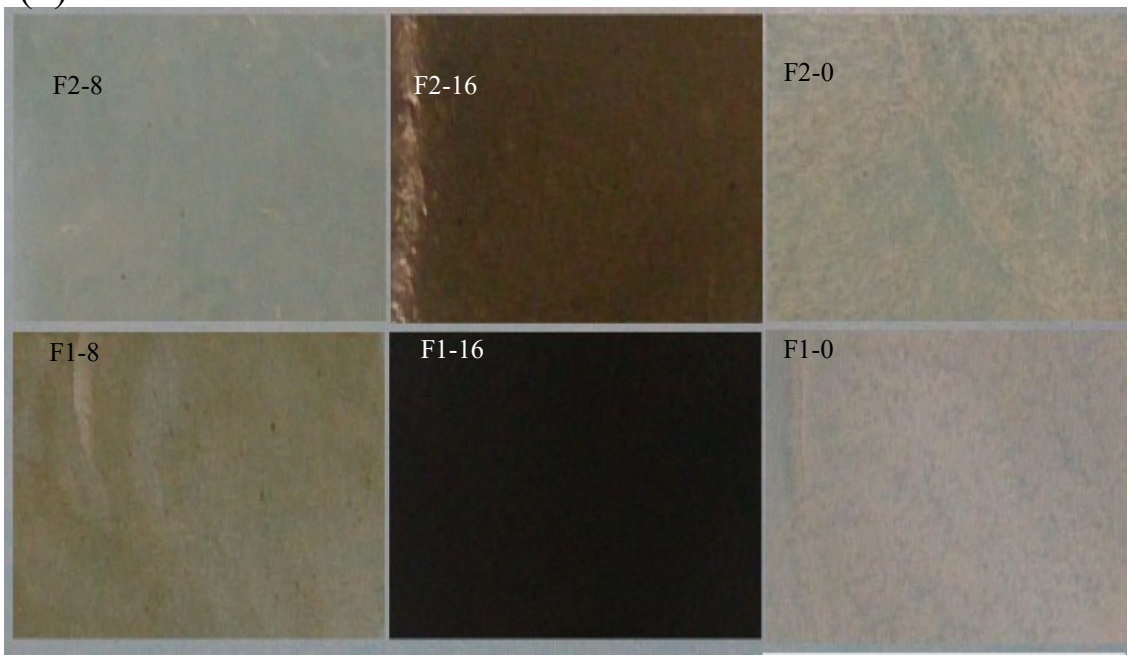

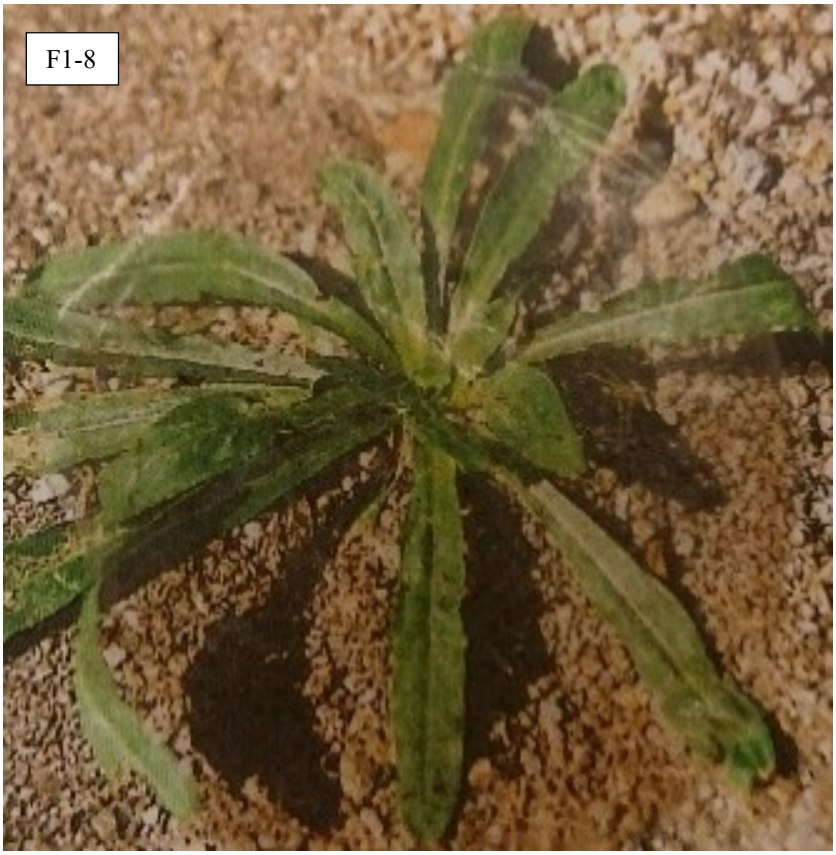

Figure 8-7 (1) Investigation of cross–sectional morphology of porous composite films of ASC–g–poly(MMA–co–EA) without GO content: a) F1–0, b) F2–0; the multilayer nanostructure of ASC–g–poly(MMA–co–EA) with GO content: c) F1–8, d) F1–16. e) F2–8 and f) F2–16, (2) the nanocomposite films on a blue substrate and a round sample of F1–8 on a photo representing the transparency of the thin films in low GO content.

The Young's modulus (E), tenacity, stress and strain at break of the strips were statistically determined in which 5 specimens were evaluated for each sample. The results were calculated as the average values and standard deviation. Each specimen was held between the jaws of the Instron Tensile Tester applying load until breaking. The samples without GO content were studied as reference to investigate the effect of GO loadings on GO–ASC–g–poly(MMA–co–EA).

Modulus and tenacity were calculated for each specimen; by dividing the load (N) to the area (mm2). And the mean and standard deviation of the mechanical properties were calculated for each group of specimens (n=5), Table 8-2. Modulus and tenacity refer to stiffness and strength of the samples. This measurement was performed at the ratio of tenacity to strain, wherein the tenacity was calculated based on the breaking force divided by the initial mass of the samples, representing the mass stress at break. Representative stress–strain curves of GO–ASC–g–poly(MMA–co–EA) are shown in Figure 8-8. All samples exhibited elastoplastic behaviour. The mean values of their Young's modulus (E), the tenacity, the tensile stress (δ), the tensile strain (ε), and the deformation at break of every samples are reported in Table 8-2.

Table 8-2 Mechanical properties of samples

Samples	Tensile Stress ($N.mm^{-2}$)	Tensile Strain ($mm.mm^{-1}$)	Tenacity ($N.mm^{-2}$)	Breaking Stress ($N.mm^{-2}$)	Breaking Strain ($mm.mm^{-1}$)	Modules ($cN.mm^{-2}$)
F1–8	6.42 ± 0.96	0.20 ± 0.15	15.11 ± 2.57	6.00 ± 0.90	0.31 ± 0.05	84.52 ± 13.13
F1–16	1.02 ± 0.20	0.19 ± 0.04	2.72 ± 0.54	0.86 ± 0.17	0.26 ± 0.06	14.66 ± 2.93
F2–8	7.00 ± 1.40	0.17 ± 0.09	16.66 ± 1.87	6.99 ± 0.70	0.17 ± 0.16	107.85 ± 9.79
F2–16	4.11 ± 0.49	0.17 ± 0.02	9.95 ± 1.31	3.66 ± 0.44	0.19 ± 0.04	61.41 ± 7.73
F1–0	0.99 ± 0.09	0.18 ± 0.08	2.63 ± 0.24	0.71 ± 0.06	0.19 ± 0.02	14.31 ± 1.29
F2–0	1.23 ± 0.07	0.25 ± 0.05	3.28 ± 0.20	1.13 ± 0.07	0.26 ± 0.03	13.37 ± 0.80

According to Figure 8-8 and Table 8-2, the variation of the mechanical properties as a function of composition clearly shows a significant advantage of the samples with GO content as compared to those samples without GO content. The results indicate that GO as a reinforcing agent significantly affect the mechanical properties of the films for two reasons; one by the GO content wherein higher chain entanglement can be achieved with branched density along with inter and intramolecular interaction of the components and the other by the multilayer morphology of the films in the nano-scale in which the

nano-layers and intermolecular conjugations are conflicting with deformation mechanism.

Additionally, from the higher strain at break in F1–8 and F1–16, it seems that larger elongation can arise in samples with less branching density (higher nitrogen content), while the branching density can provide higher chain entanglements in the elastic phase (F2–8 and F2–16). More specifically, the enhancement in tensile strength was observed for F1–8 and F2–8 with less GO content, whereas the greater GO content did not cause further improvement of mechanical properties confirming the challenges that should be considered over the GO loadings onto composite components as a cause of inhomogeneity, as mentioned in thermal studies reducing the molecular dynamics.

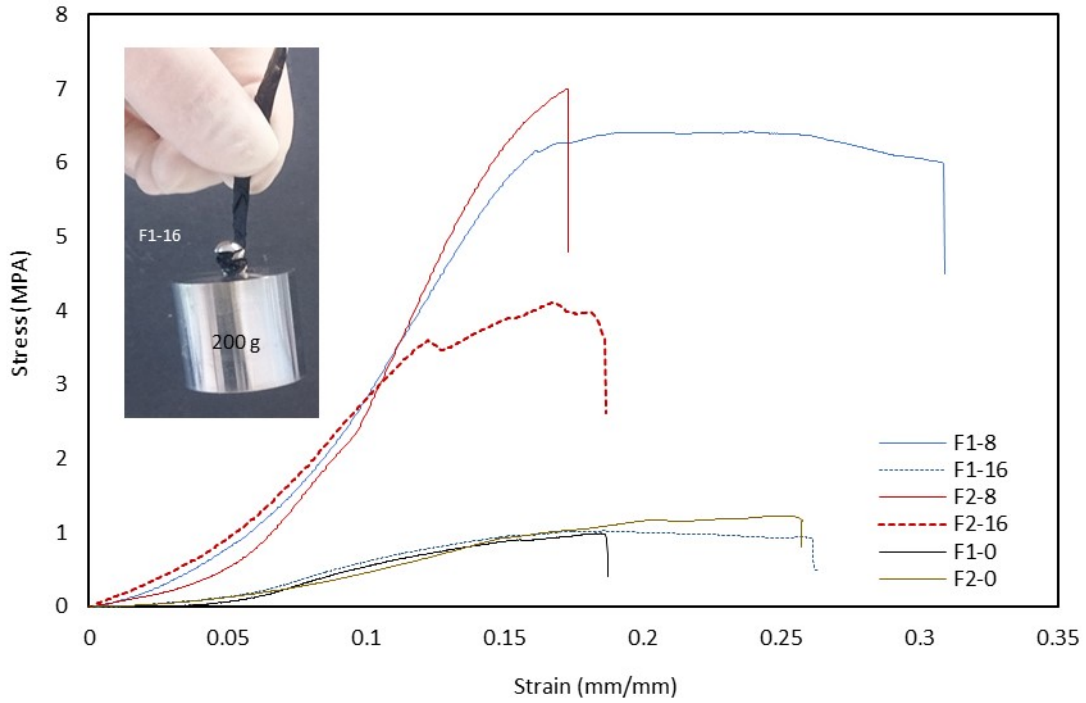

Figure 8-8 A representative stress–strain curve recorded from tensile test of composite films from ASC–g–poly(MMA–co–EA) with/without GO content.

To better understand the influence of the presence of GO on ASC–g–poly(MMA–co–EA), surface wettability, water absorption and degradation properties of the samples were studied. The measurements were performed on five replicated samples. The results of contact angle measurements are shown in Figure 8-9a.

The average contact angles (CA) of the samples in the first 10 seconds are about the same value (CA< 80^{O}) representing the high hydrophilicity of the film surface, even though after 10 minutes varied surface wettability was observed, Figure 8-9a. More specifically, the

samples with GO content and lower hydrophobic segment (F1–8 and F1–16) showed higher surface wettability after 10 minutes, whilst F2–8 and F2–16 possessing higher hydrophobic segment, showed lower surface wettability. This result shows that the hydrophobic segment of the composite can have a higher influence on surface wettability as an inhibitor by contrast to GO loadings. Additionally, water absorption (hydration ratio) of the samples (about 50 mg) was studied by immersing in 20 ml PBS (pH 7.4) at room temperature for 12 hours and then dried in a vacuum oven until a constant weight was achieved. The hydration ratio of the nanocomposites was calculated according to the equation that has been mentioned in chapter 3, section 3.3.1. As shown in Figure 8-9b, the mass transfer rate reduced initially in samples with increased hydrophobic segment of poly(MMA–co–EA) in the nanocomposites, whilst increasing the GO content influences the degree of water absorption after 12 hours. Due to the collagen denaturation during the processing, a mass loss is expected to be dissolved during one set of soaking in water. Interestingly, in the samples with GO content, a smaller mass loss was observed with increasing GO loadings. However, an insignificant fraction of mass loss was observed in all the samples with the exemption of F1–16 with the lower hydrophobic segment and higher GO content. This can be due to additional bonds that can happen between the GO and ASC segment of nanocomposite during solubilisation and/or solidification. This result indicates that the presence of GO can act as an inhibitor to ASC denatured by the effect of solvents during the processing.

Further investigation into water absorption capacity of the samples was undertaken as shown in Figure 8-9c, the water uptake of the samples was measured as a function of temperature. Hence, the samples were heated up to 100 ºC and then cooled overnight. From room temperature to 60 ºC, the samples showed almost a slow water uptake rate of 10–30%. In temperatures between 60 ºC to 100 ºC, the water uptake ratio was increased between 10–50 %, with the exemption of F2–0 which was far away from any other samples. In the range of 10–50%, the highest water uptake was for F1–8 and the lowest ratio was observed in F1–16. These two samples with lower hydrophobic segment have almost the same water uptake at 50 ºC, whilst F1–8 showed upward water uptake ratio and F1–16 reacted in an opposite direction in temperature above 50 ºC. shrinkage was observed for F2–8 and F2–18 in temperatures above 80 ºC followed by an increased water uptake after cooling. This response is due to interfering the glass transition temperature of the hydrophobic segment that causing more chain flexibility to agglomerate by the increasing temperature and probably released the hydrophilic segment to absorb water during the cooling phase.

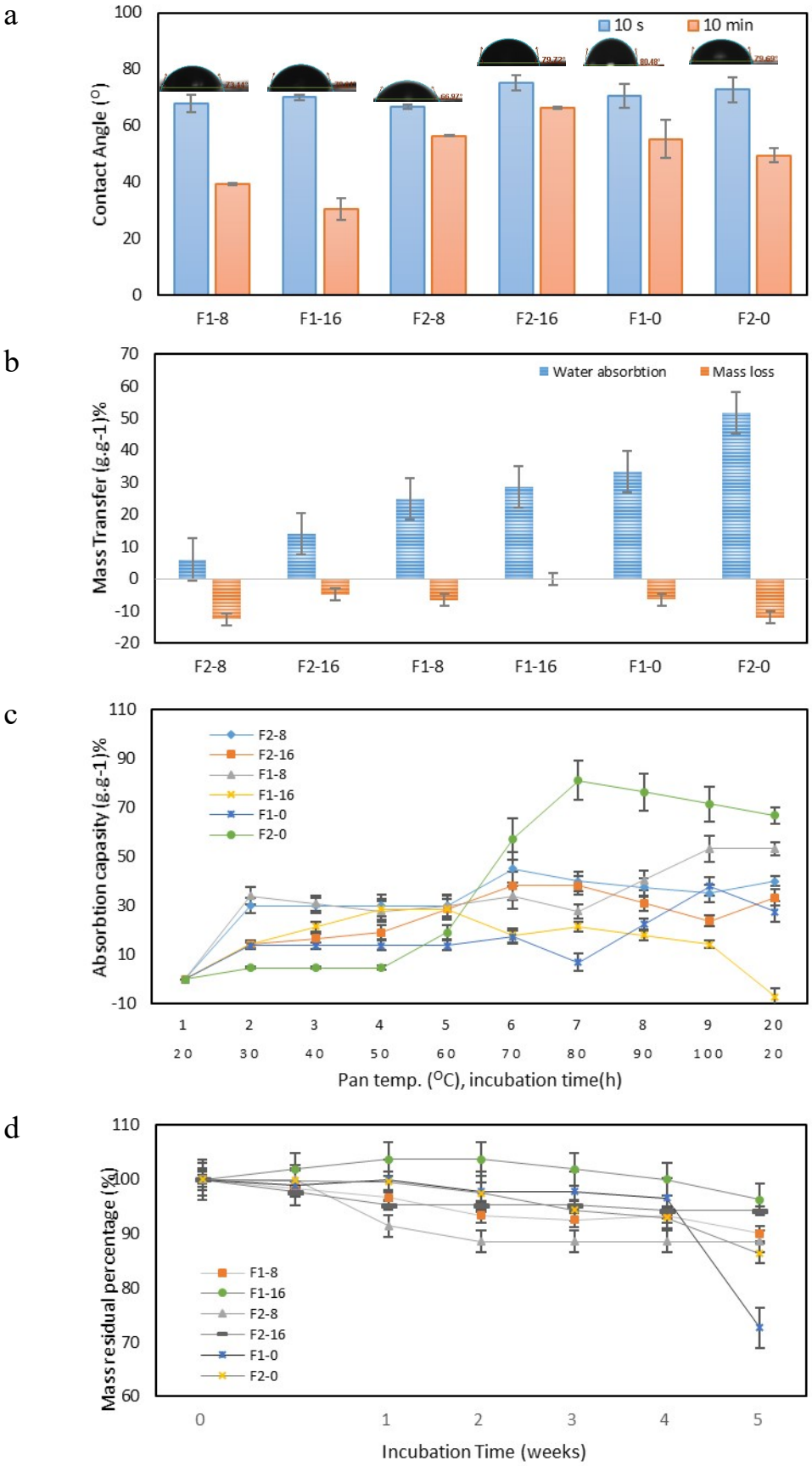

Figure 8-9 a) The water contact angle vs. time after 10 seconds and 10 minutes; b) water absorption (hydration degree) and mass loss after incubation time of 12 hours at room temperature; c) Water absorption capacity of the samples as a function of temperature in percentage; d) Mass residual percentage vs. incubation time (week).

The degradation was calculated by dividing the lost weight of the samples with their original weight. The degradation evaluations were achieved as a function of time as defined by Zhu et al [283]. The measurements were performed on five replicated samples, they were immersed in 100 ml of 154 mM phosphate buffered saline (PBS, pH 4), containing 0.02% sodium azide as a bacteriostatic agent. The mixture was maintained in a controlled temperature of 37 _C. At predetermined time intervals, the reduced buffer was added back with fresh PBS for continuing incubation. As shown in Figure 8-9d, apart from the sample behaviour during the incubation time, the samples with GO content showed almost a small gradient of mass loss in contrast to the samples without GO content that experienced a significant degradation within the fifth week. Interestingly, F1–16 with high GO content and low density of grafted copolymer showed the highest resistance to mass loss (degradation) and F2–16 displayed the second stability. This is in agreement with the mechanical studies revealing the effect of decrease load bearing capabilities due to a reduction in molecular dynamics which here resulted in the efficiency of collagen chain packing within the nanocomposite to be more stable in degradation process.

These results show that within a steady temperature, e.g. room temperature, the increasing in the GO content can significantly reduce the water uptake and deter the degradation rate of ASC–g–poly(MMA–co–EA) in contrast with increasing the monomer feed ratios. This can be due to existence of supplementary bindings such as hydrogen bonding between GO and collagen graft copolymer that can be stronger than those between water molecules and the collagen graft copolymers [95]. During all measurements in contact with water, the samples retained their original form, and no migration of GO into the water was observed.

Even though it is less problematic to process amorphous polymeric nanocomposites in molds to a variety of shapes and dimensions for creating complex 2D/3D objects [255, 265, 368], formation of the fibres can cause new challenges referring to amorphous macromolecular polymeric systems when it comes to Raleigh instability of the branched structure of ASC–g–poly(MMA–co–EA) and the 2D geometry of graphene nano-sheets in which the dimensions of GO nano-sheets are comparable to fibre diameters. We used electrospinning that allows the chain alignment of composite fibres in low solution concentrations as discussed in chapters 5 and 6. This was due to reducing the deteriorative impact of branched structure of ASC–g–poly(MMA–co–EA) on the uniformity of fibres. Hence, to study the effect of the GO content in fibre formation, a set of four solutions of GO–ASC–g–poly(MMA–co–EA) were successfully electrospun. Electrospinning conditions used to fabricate the fibres (environmental and experimental parameters) were optimised to obtain fibres along the axes of a rotating drum. Figure 8-10 reveals the fibre morphologies representing mean and

standard deviation of the fibre diameters; the standard deviations were to identify the uniformity of the diameter of nanofibres. The mean fibre diameter and the uniformity of the fibres were determined statistically by using ImageJ software from SEM micrographs through the measurement of about 150 fibres and the results were given as the average diameter ± standard deviation.

Even though the presence of GO in the composite fibres does not seem to affect the morphology of fibre alignment; the uniformity of the nanofibres was affected by both GO and branch density, since the reduction in fibre diameter (751.52 nm) and also increase in smoothness and uniformity (290.86 nm) was observed in F1–8 possessing lower GO content and branch density.

Generally speaking, the decrease in the electrospun fibre diameter with GO content has been reported in various polymeric systems and attributed to the increased conductivity of the electrospinning solution with increasing the GO content, resulting in small fibre diameters [282, 358, 369]. The increased conductivity has been also claimed by some other research groups as the GO is functionalized by amino groups [267, 276, 370]. However, GO nano-sheets can appear as an electrical insulator, due to the disorder of their sp2 bonding networks as a product of strong acid/base treatment [259, 364]. Therefore, our results on fibre morphology are likely attributable to more complex combination of causes and effects; e.g. the presence of GO with comparable size to the fibre diameter when comes along with branched structure of ASC–g–poly(MMA–co–EA) that can strongly influence the density of built-in dipoles and viscosity of the solutions and eventually vary their response to the external electric field.

Finally, we studied the electrospun fibres with GO content via Transmission Electron Microscopy (TEM). This was to provide in–depth understanding of the GO arrangements within the structure of the fibres. Figure 8-11 reveals the TEM image of GO which is to identify the GO within the fibres. It can be seen that a distinguished appearance can be observed on the surface of the nanofibres bearing more GO content (M1–16, and M2–16) as compared with nanofibres with less GO content (M1–8 and M2–8). Even though this notable GO decoration on the fibre surface can be beneficial for applications requiring highly active functional groups of GO on the surface of the fibres, addition of GO content can simply increase the average fibre diameter and decrease its uniformity, which is also in agreement with SEM studies. Therefore, increasing the GO content even though can significantly increase the performance of in situ polymerisation as a modification method for purified collagen, but the effect of GO addition on physical properties and morphology of Collagen

graft nanocomposite can be like a parabola in which its vertex must be realised to obtain the optimum physical properties.

(a) Mean Fibre diameter: 751.52 ± 290.86 nm

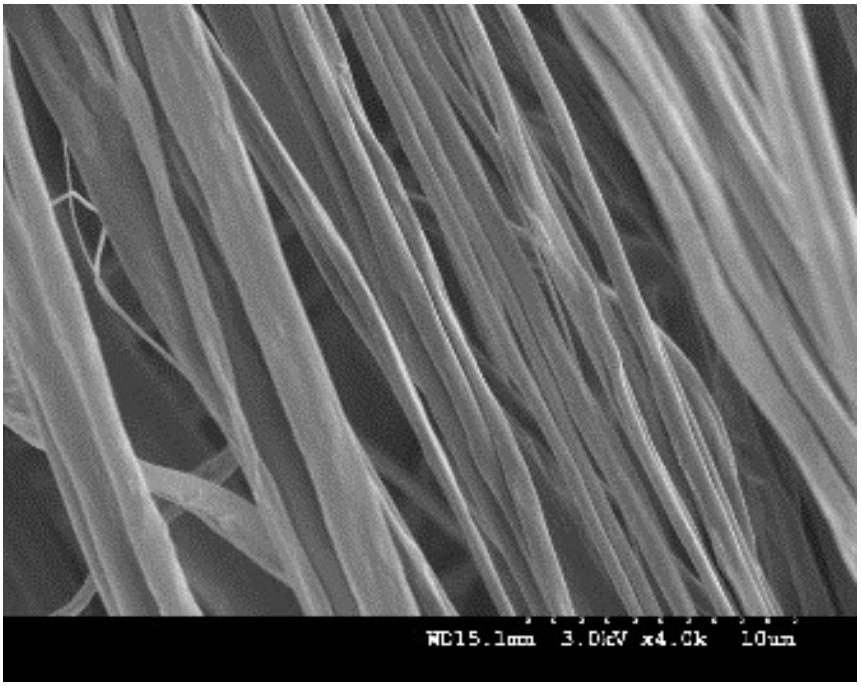

(b) Mean Fibre diameter: 846.91 ± 589.07 nm

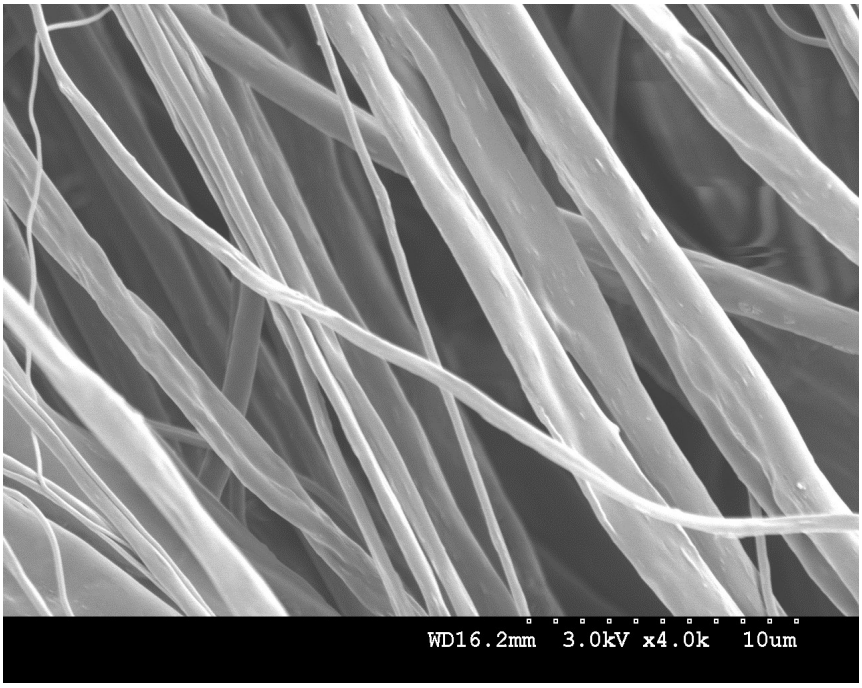

(c) Mean Fibre diameter: 899.26 ± 430.06 nm

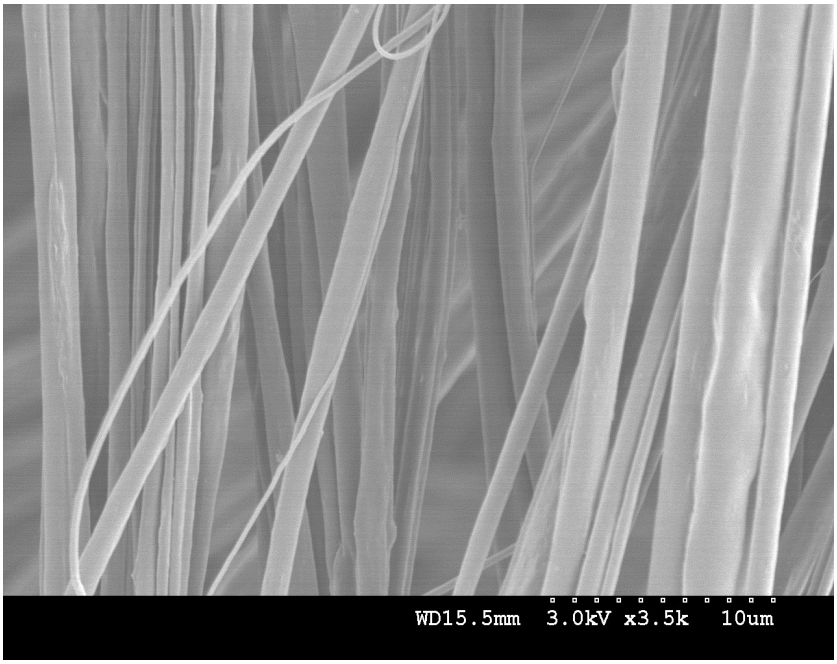

(d) Mean Fibre diameter: 1179.45 ± 466.32 nm

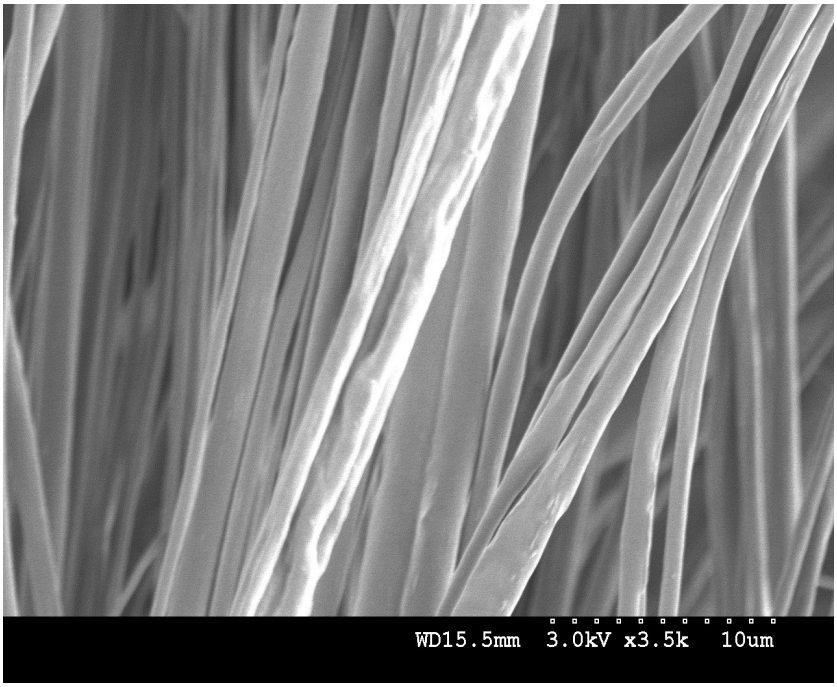

Figure 8-10 The effect of the GO content on the mean fibre diameter and the uniformity (standard deviation value) of the electrospun fibre from the ASC-GO-g-P(MMA–co–EA nanocomposite: SEM images of a) M1-8, b)M1-16, c)M2-8 and d) M2-16.

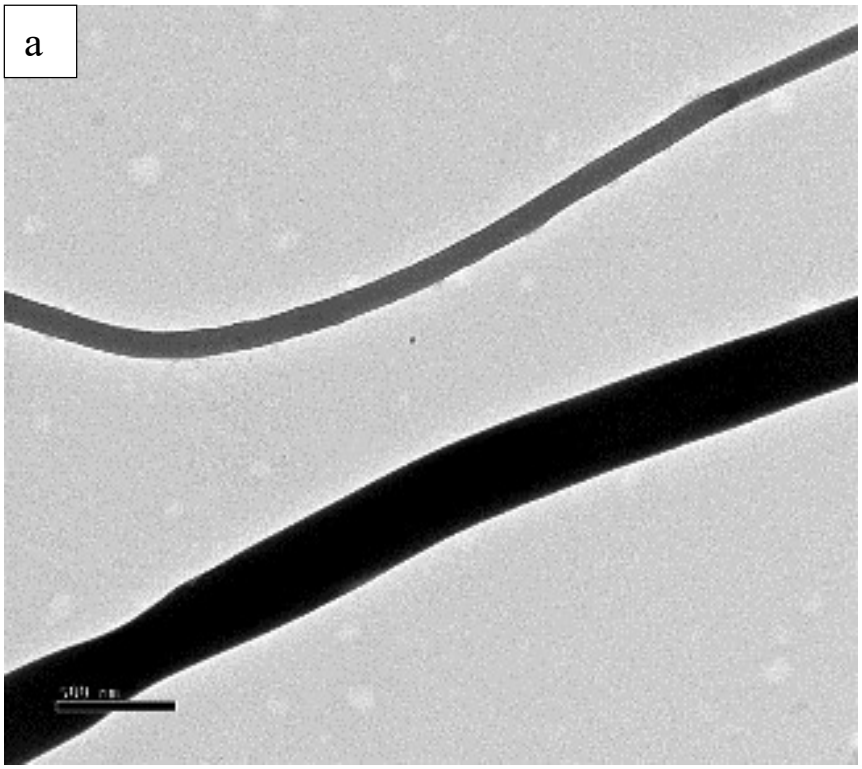
a

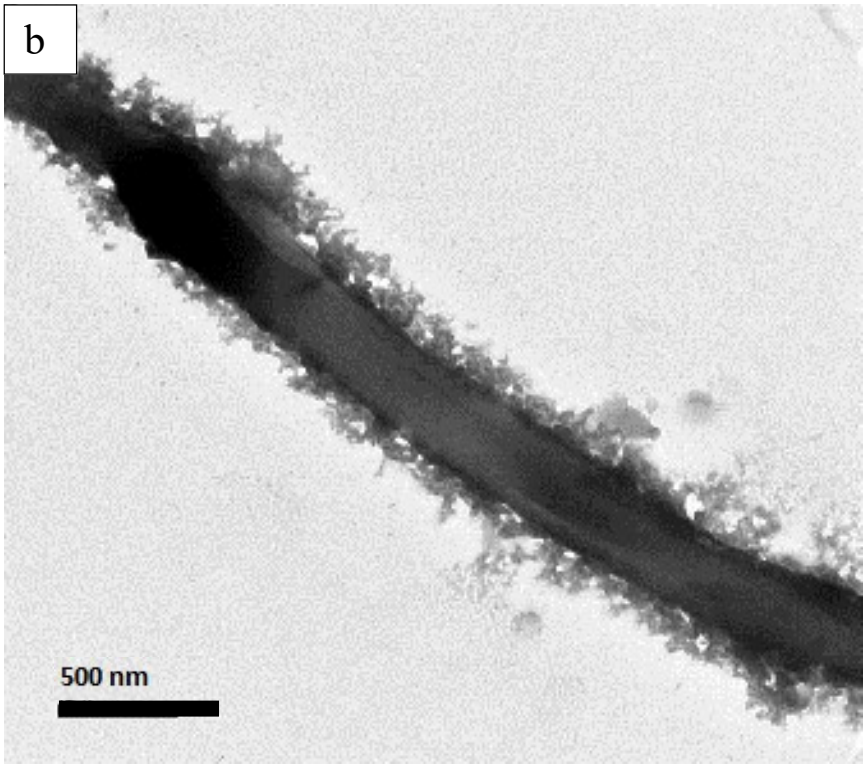
b
500 nm

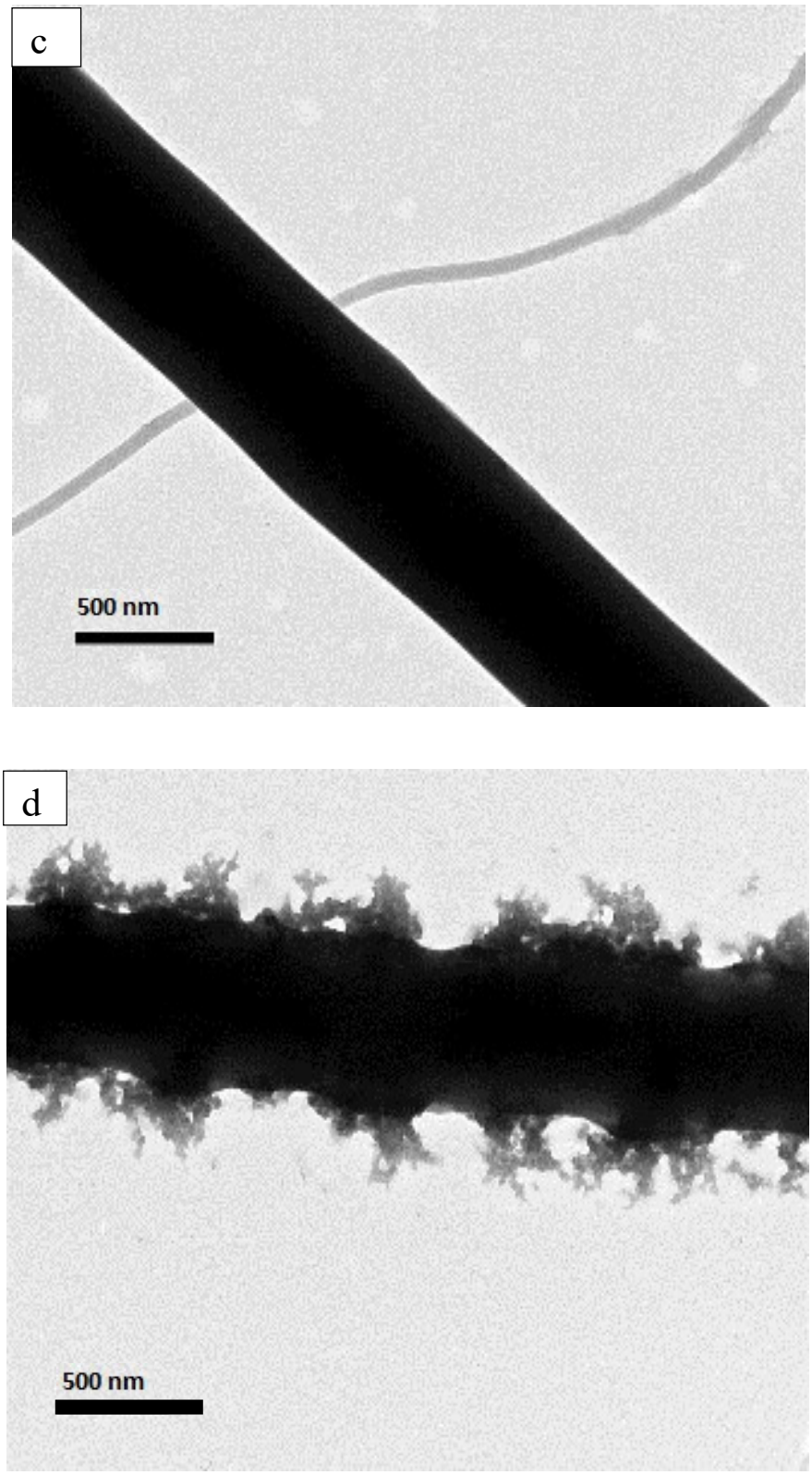

Figure 8-11 The arrangement of GO in the electrospun fibre from the ASC-GO-g-P(MMA–co–EA nanocomposite: TEM images of a) M1-8, b) M1-16, c) M2-8 and d) M2-16; the scale bar shown on the bottom bar is 500 nm.

Chapter 9 Conclusions and Future work

9.1 Conclusions

One of the most important and essential aspects in biomaterial choice is high availability and processability for a variety of end uses. Collagen is one of the most abundant biopolymers in the family of biomimetic materials. Collagen fibrils are fully constructed from the biochemical details of the amino acid sequence and nanoscale chain arrangements within the hierarchical structure leading to combined mechanical properties such as strength and elasticity, where the lowest hierarchical level consists of triple helical collagen molecules. The purification methods isolate the collagen chains by uncoiling and releasing them from their hierarchical structure. Hence, uncoiled collagen chain, acid soluble collagen (ASC), is the product of the purification and isolation process that is being used as pure collagen. Even though collagen chains lose the properties, such as high mechanical strength and stability in moisture, from their hierarchical structure built up by covalent and none covalent bonding, they provide the properties from the amino acid sequence that are highly biocompatible and non-cytotoxic. However, despite the excellent properties of collagen chains, it cannot be used widely due to its instability and super hydrophilicity; most research on collagen, is focused on methods for reducing its hydrophilic behaviour controlling its biodegradation. These methods are being performed as post-treatment on processed collagen-based materials, such as films and fibrous assemblies.

The demand for diverse usage of collagen fibres is because it can mimic its native structure in living tissues in a shape of the collagen network and the aligned fibrils that is similar in all species. This can be achieved by electrospinning which can lead to a variety of fibre formations for many more end uses that are not currently available.

However, it has been reported that during electrospinning, collagen chains are significantly degraded by process conditions leading to losing some of their properties, such as rheological, due to fast denaturation of the hydrolysing chain of collagen in the presence of high H^+ concentration in a spinning solution; free hydrogen ions are produced by a strong acidic solvent, a higher amount of hydrogen ions is attracted onto the surface of collagen, which increases the electrostatic repulsion force between the collagen chains leading to denaturation of collagen depending on electrostatic repulsion resulting from the positive charge build-up within the electrospinning solution.

Collagen has been modified in this research by graft polymerisation for reducing its super-hydrophilicity and to control its biodegradation. This methodology can be applied to collagen and its derivations before any process as a pre-treatment. In this approach, different vinyl group monomers with varied physiochemical properties can be branched over collagen chains.

The achieved branched copolymer represents enhanced properties such as rheological, thermal, and electrical. However, this methodology may present new challenges; collagen graft copolymers with a branched structure require to be spun under specific conditions to prevent Rayleigh instability. This issue has been addressed in this research by the electrospinning method when the branched copolymers are spun in low concentrations.

When it comes to mechanical reinforcement of collagen-based materials, blending with (semi-)synthetics is mainly recommended in fibre formation methodologies. Even though, this method is not as simple as it seems; phase segregations and viscosity changes are frequent examples of problems posed by incompatible (co)polymeric fluids. These problems are due to different electrical and structural properties that significantly limit the further development of collagen-based materials for fibrous assemblies with diverse properties. To promote the mechanical properties of the collagen graft copolymers, irrespective to their compatibility, they can be simultaneously spun with a variety of polymers via coaxial electrospinning. This method has been established in this research and have shown opportunities for working fluids with a wide variety of properties to be tuned for creating core–shell composite nanostructures with superior properties.

This research has successfully achieved collagen graft copolymers and revealed its novelty investigating their processability by electrospinning (i) on their own, (ii) with incompatible polymers, and (iii) while they have been functionalised with nanofillers as additives/reinforcements; hence, it has established methodologies for producing collagen-based fibrous assemblies for a variety of end-uses. The perspectives of this research are based on our belief that electrospun fibres will continue to innovative adding new functionalities to conventional materials as highlighted in this work.

The consequence of this work is that natural-based polymers can be modified to achieve multifunctional properties, not restricted to biomedical, but expand to technical and high-performance applications requiring hydrophilic biopolymers such as smart filtrations and protecting clothes. During our investigations in this work, the effect of branching onto collagen and intermolecular interactions on the formation of electrospun

fibres of collagen graft copolymer/nanocomposite has been the centre of focus of this research and the following conclusions were specifically achieved.

9.1.1 Collagen graft copolymers: Isolation, synthesis, and properties

This study has shown that poly(MMA–co–EA) can be grafted onto collagen chains (ASC) in aqua medium. The surface of pure ASC was modified using a free radical copolymerisation method. The density of branching was investigated by increasing monomer feed ratios in relation to grafting parameters and molecular weight of side branches. While some discussion was devoted to the synthesis of collagen graft copolymers, the influence of branching were further investigated in relation to viscosity, conductivity and thermal behaviour at different branching densities. The shear rate dependence of the viscosity of highly branched copolymers was studied and their related Newtonian behaviour was identified. The viscosity of the diluted solutions was significantly affected by increasing the comonomer feed ratio in which high viscosity was observed in samples with the highest grafting percentage. The conductivity value of the solutions showed a considerable decrease due to low dielectric behaviour of poly(MMA–co–EA) in side chains. While increasing the grafting density was the main reason for decreasing the conductivity of the samples, increasing the number of branching points showed an insignificant change in the conductivity of the resulted copolymers. The thermal stability of all samples was influenced by grafting polymerisation, as verified by the shifting of the melting peak towards higher temperatures, with no considerable changes on the enthalpy of denaturation and the glass transition temperature of the studied samples.

9.1.2 Systematical optimisation of the electrospinning solution as a function of viscosity

During our experiments we found that solution viscosity can be the most important factor in fibre formation of collagen graft copolymers, since the varied branch densities on ASCs can significantly influence the initial viscosity of solutions to be electrospun. This is due to varied chain entanglements and intermolecular interactions that affect the viscosity such as molecular interactions of the copolymers and solvent, which directly influence factors forming the viscosity.

To find a single answer for the viscosity of the studied electrospinning solutions, calculations have been based on a one-factor response surface methodology evaluating dilute to semi-dilute solutions of collagen graft copolymers. To isolate the effect of other electrospinning parameters, we considered them as controlled factors and the

viscosity was optimised by a set of predetermined goals to achieve a lowest viscosity of the highest spinnable solution. This was due to two main reasons: To prevent Rayleigh instability of the polymer jet by increasing the hydrodynamic volume of the solutions that may be caused by highly chain entanglements at high concentrations and also to study the effect of the chain length and the density of the branched chains on fibre morphology when the delicate structure of the collagen chain is likely to be affected by the electrospinning conditions.

Even though our calculations and predictions were based on our observations on overall morphology of the electrospun fibres, the study led to the identification of a critical optimised solution that can be used for the graft copolymers with varied branching densities. Hence, the optimised solution allowed us to examine the reproducibility of the model using the same viscosity for the samples. We expected that while the same molecular interactions are present between the factors that represented by viscosity of graft copolymers, the degree of the intermolecular interactions will be varied in functionality and structural properties which was further considered in our study as given in next chapters.

9.1.3 Electrospinning of collagen graft copolymers at optimised viscosity

In this study, we investigated the dependency of entanglement concentration on branch densities having the same viscosity; in which the mean fibre diameters of the considered samples remained broadly constant. The increased density of the branches onto ASC is not the sole factor determining the functionality of electrospun graft copolymer. The influence of branching on fibre formation through electrospinning as a challenging processing method in relation to the delicate structure of acid soluble collagen is a critical factor that was further studied. Surface characterizations were then performed on the bulk and electrospun collagen graft copolymers to study the effect of processing parameters on physiochemical properties.

Increasing the number of branching onto ASC chains significantly decreased the deteriorative impact of the electrospinning conditions. It has also increased the stability of the electrospun fibres under high humidity conditions. The short chain branched ASC–g–poly(MMA–co–EA) can effectively influence the thermal stability of electrospun collagen fibres while the long chain branched ASC–g–poly(MMA–co–EA) can provide a higher chain entanglement density that enhances fibre uniformity.

The consequence of this part of the work is that a tailored side branching as a pre-treatment can add unique properties and allow fibre formation from ASC that would

otherwise be degraded during processing. This has a significant impact for new end-uses of collagen within a stable fibrous structure free from any further treatment.

9.1.4 Coaxial electrospinning of collagen graft copolymer/Nylon 66

Due to diverse applications of hydrophilic fibrous assemblies and their ever-increasing demand for multi-functional properties, we investigated a new approach, using incompatible polymers, for the formation of a composite fibre with enhanced chemical and mechanical properties.

Collagen–g–poly (methyl methacrylate–co–Ethyl Acrylate) (CME) was electrospun simultaneously with Nylon 66 by coaxial electrospinning as a composite that are otherwise unlikely to be spun through conventional spinning methods or blending systems. The capacity of built-in dipoles of the components in the core (Nylon 66 (N66)) and the shell (CME) with varied electrical properties is dependent on the intensity of the external electric field. The effect of chain orientation and intermolecular interactions between the polymer chains were investigated by thermal and mechanical properties, hydration degree and degradability.

The mechanical properties of electrospun composite fibres were significantly improved; theses electrospun fibres were oriented by sufficient chain entanglements of branched polymer chain of CME, internally filled with linear polymer of N66 and secondary by the mechanical force of rotating drum collector which collects and partially stretches the spun fibres. Varied fibre compositions were achieved by increasing the applied voltage. The fibre samples received tunable properties from the core and the shell components; the studied samples displayed different thermal behaviour as well as surface wettability, water absorption and degradation rate, due to varied material compositions. It was found that an increase in fibre diameter and also partial fibre alignment in the studied samples of the core–shell fibres along with reinforcement of their mechanical strength varied from 3.14 to 4.86 N/mm2. The reinforced mechanical performance of the CME/N66 composite coaxial nanofibres is benefitted from the branched structure of the CME segments due to increasing stress transfer efficiency. By comparing the mechanical performance and the morphologies of the individual components of nanofibres, we can say that the high chain orientation cannot be the only reason for this enhancement, but it is rather the synergy of a variety of factors that affect the composite nanofibre from the mechanical point of view. Among them, the dipole-dipole interactions of components of the core-shell composite fibres, e.g. hydrogen bonding, is highlighted as a key factor for stress transfer in chain entanglements within the fibres

that can rely on strong intermolecular interactions. Additionally, the intrinsic stiffness of the branched CME and a possible rod-like orientation of N66 within the nanofibre structure can increase the mechanical performance of the core-shell composite fibres. Therefore, due to the strong intermolecular interactions, the fibre samples not only achieved chain orientation but also a significant enhancement was observed in mechanical properties.

The value of this part of the work may be summarised as:

- This is a novel attempt for hydrophilic CME by improving their mechanical properties coupling with optional incompatibles by using coaxial electrospinning.
- Different physiochemical properties can be achieved by in-situ fibre formation from electrical and structural incompatibles influenced by the intensity of the external electric field.
- End uses can consequently take the advantage of in-situ fibre formation of the natural segment of collagen in the shell and mechanical strength of the core as a composite in shape of a fibre or a fabric.

9.1.5 Functionalisation of collagen graft copolymers with Graphene Oxide

Grafting polymerisation can be applied to modify the surface of acid soluble collagen before electrospinning. However for tailored applications in which the productivity is considered within enhanced grafting parameters such as grafting efficiency and performance, the nanofillers can represent interesting properties. The development of nanofillers are relatively at their early stage.

A collagen graft nanocomposite (ASC–g–Poly(methyl methacrylate–co–Ethyl Acrylate) was synthesised in the presence of graphene oxide (GO). The reaction of a free radical polymerisation onto ASC with and without presence of GO were considerd to investigate the grafting performance and grafting efficiency. The main objective of this part of the work was to enhance the grafting parameters which led to increasing the amount of conversion so that this modification method can make collagen graft copolymers economically viable. The presence of GO acted as a coupling reagent to bond ASC and homopolymerised poly (MMA–co–EA) within ASC–g–poly(MMA–co–EA) copolymer. This suggested that GO as a geometrically two dimensional (2D) nanofillers increase the accessible surface area for easier attachment of the initiated ASC chains. Hence the presence of GO provided an accelerated polymerisation reaction with highly improved grafting performance and efficiency. This technique was also

useful in making GO nanocomposites which is covalently entangled with polymer chains preventing GO reagglomerating during the process.

Hetero-phase polymerisation in aqueous media was applied, as an environmentally friendly technique that was highly compatible for swelling the collagen chains as well as GO to be easily dispersed within the medium. This was conducted from two polymerisation systems with varied comonomer feed ratios, in which two distinguished GO loadings were used.

Since the final properties of nanocomposites are dependent on the processing methods and processing conditions. The processability of the achieved nanocomposites were then evaluated through casting and electrospinning processing methods. The nanocomposite films showed a unique morphology; multilayer nanostructure of the grafted GO monolayers that deposited simultaneously one on top of another. A multi-layered composite structure of the nanocomposite films is an attractive candidate for novel applications in nano-mechanical systems and paper-like collagen-based composites. The morphology of the electrospun fibres was affected by the addition of GO loadings in which the increase in fibre diameter was observed wherein the surface of the nanofibres was decorated by the GO nano-layers. The active end group of GO on the surface of the fibres, can render these collagen-based electrospun fibres capable of uses which require high polar functional groups on the surface of fibres. The coupling interaction of the GO content also reduced the degree of swelling of the nanocomposites and decelerated the degradation rate of the collagen segment of the nanocomposite as a function of temperature.

To modify collagen, this part of the study highlights the importance of introducing functional groups of GO and substitution of GO loadings as an active nanostructure filler to be replaced with high monomer feed ratios, and hence improving the physiochemical properties of collagen in the same way. This approach is suggested for end uses requiring enhancement of the physical properties and to significantly provide stable collagen-based materials with less degradation.

9.2 Suggested future work

Nowadays, electrospun fibres are designed and fabricated out of newly developed polymers, mostly composites of different materials which with their synergies produce various desirable chemical, physical, biological, and weathering effects. Successful Fabrication of these fibres demands interdisciplinary understandings to achieve high added value products such as SMART textiles. In this

work, we introduced new approaches to fabricate collagen-based fibres and extended its use in new multifunctional applications. By achieving this work, other areas can benefit by extending its outputs as discussed below.

9.2.1 Formation of collagen-based fibres automatically taken off and collected as spinning

In electrospinning, fibre spinning and web formation are more likely to be integrated into one process, yielding a nonwoven mat of electrospun fibres to partially oriented yarn because of the varied moving velocity of polymer jets affected by the intensity of the electrical field, the gap between spinneret and collector, mechanical force of rotating drum etc. There is no further drawing as the fibres are collected as a mat on a rotating drum during conversions into nonwoven fabrics. Hence, the size of the electrospun fabrics is mostly restricted to the surface of collectors.

We realised in our theoretical and experimental studies that an opposite electrostatic force can act as a take-off element when fibre formation is achieved this depending on the electromotive force and electrical potential difference between the tip of the spinneret and a neutral collector. The influence of the presence of a secondary external electrical field in opposite charge not only can facilitate the scaling up the continuous fibre formation when the process set–up is normally time consuming to be adjusted for each experiment but can also provide a balance between chain orientation and post fibre drawing to fabricate high-quality nanofibres.

This can be achieved by a similar technology to electrophotography (toner printing) using the same theory to convert the charged toner particles onto a tailored substrate. In fact, an electrophotographic printing method consists of six processes comprising of charging, exposure, developing, transfer, fusing, and cleaning. Interestingly, the principals of these two technologies are closely similar from the beginning to the end. It is suggested that transferring the fibres can apply the same principal as the toner spherical particles in the diameter of less than 10 microns are transferred, particularly when continuous fibre formation is desired in large scale.

9.2.2 Formation of reinforced collagen-based core–shell fibres with other (semi-crystalline) biodegradable polymers applying the methodology of this work

Based on the importance of sustainability and the significance of renewable bio-based materials, cellulose materials as well-known polysaccharides are achieving a significant attention. Cellulose comprises with amorphous and crystalline regions which can highly order rod-like cellulose nanocrystals (CNCs) that obtained via an acid hydrolysis.

Apart from the optical properties of CNCs, they represent high mechanical properties, biocompatibility, thermal stability, and are widely available. CNCs as a reinforcing agent can be used as an alternative to Nylon 66, as discussed in chapter 7. For this approach, collagen graft copolymer as the shell/carrier for CNCs, can line up the nanocrystals in the core. The fabricated fibres can then benefit from chain entanglements of the branched structure of the collagen graft copolymers and CNCs as a biodegradable reinforcement.

Apart from the unique properties of CNCs, the study of inter and intramolecular interactions of structurally and electrically varied biopolymers using coaxial electrospinning may improve fibre functionality such as mechanical properties, and improve the processability of problematic biopolymers, by following the methodology we applied in this study.

9.2.3 Formation of collagen-based nanofibres from more vulnerable sources with a low molecular weights

This work can be also suggested for collagen chains with a low molecular weight that are more likely to be degraded during electrospinning. The fibre formation via electrospinning, requires the presence of chain entanglements in solution as a critical factor, limiting the spinnability of low molecular weight polymers.

In fact, this work expands the use of polymer chains that can be converted into graft copolymers in order to enhance the processability of the ultra-low polymer chains into copolymers, as discussed in chapter 4. This develops a system of producing high-quality nanofibres in a controlled situation when the purity of the nanofibres is not the first priority.

9.2.4 Electrospun collagen-based composites with interactive functionalities

A large number of electrospun fibrous biosensors have been developed over the last decade, using a variety of approaches to integrate polymers to inorganic/organic nanofillers (e.g., conducting NMs; ZnO, TiO_2, Mn_2O_3–Ag, Carbon–Cu, Carbon–Ni) [274, 373-376]and post-treatment processes to produce robust bio-sensing platforms with analytical performances and enhanced functionalities. These approaches mostly aim at improving the biocompatibility of the surface and introducing functional groups from NMs, using physical or wet chemical processes and employing post modification processes e.g. crosslinking. The design and assembly of fibrous biosensors is a growing topic of research and is still at an early stage.

Since fibrous biosensors mostly rely on electrochemical transduction, preserving the biosensor functionality is one of the most important challenges associated with the formation of nanocomposite fibrous bio-sensing limited by complicated post treatments and physical and chemical characteristics of both bio-receptors and nanofibres as carriers of nanofillers with active end group, and their interfacial interactions.

As discussed in chapter 8, the in-situ fibre formation from bio-nanocomposites with the presence of carbon, metal oxide or polymer electrospun nanofibres integrating bio-receptors and conductive nanomaterials (e.g., carbon nanotubes, metal nanoparticles) can be one of the major advantages since they are free from the need of post treatments by applying in-situ polymerisation; biocompatible polymers possessing dielectric properties are therefore as new features in biosensor technology.

9.2.5 Formation of collagen-based nanofibres from smart dyes

Since newly developed devices for spectrophotometric analysis of colour changing are widely being used in medical sciences, this is suggested that the use of thermo/ electro/ photochromic dyes, photo-luminescent/ fluorescent markers, and encapsulated pigments are used to design collagen-based smart medical fibrous assembles that can be off the record both as sensors and protective textiles to response to stimuli at a right time and also to provide additional advanced functionalities.

9.2.6 Analysis the antimicrobial performance of collagen-based nanofibres

Investigating the antimicrobial properties of fibres from both collagen graft copolymers and collagen graft nanocomposite is very important. This evaluation should be performed by comparing the alteration of antimicrobial behaviour between cationic polyelectrolyte nanofibres from pure collagen and amphiphilic nature of graft copolymer/nanocomposites. It must be stated that the functionalization of fibres, binding of graphene to the surface of nanofibres has already been studied by different research groups. But again, post treatment is required to stable the components. The results encounter the challenges referring to non-appropriate exfoliation, non-uniform dispersion and reagglomeration of nanofillers.

To achieve a robust antimicrobial property, in-situ polymerisation approach may be used with the presence GO–Ag nanofillers. This approach can bond the oxygen functional groups of graphene Ag+ ions and the primary amine functional groups of collagen chains via a chemical reaction as discussed in chapter 8. The new feature of one-pot approach for production of cost-effective, scalable collagen graft nanocomposites will reveal the advantages of high specific surface area nano

composite fibres to hinder microbial proliferation for medical and protective clothing applications.

9.2.7 Modelling the behaviour of Polycations and Polyanions (Polyelectrolytes) to form 3D shapes out of bi-component electrospun fibres

Electrospun fibres are normally accumulated layer by layer on top of each other to form a 2D nonwoven mats with cross conjugations representing isotropic behaviour. Polyelectrolyte nanofibres, mostly Poly cations; have been investigated by a number of research groups to study the reduction in fibre diameters encountering the positively charged spinnerets [124, 125, 213, 270, 341, 377]. We also dealt with the dielectric properties in the formation of core–shell fibres with high chain orientation in chapter 7.

In our theoretical study, we realised that polyelectrolytes with varied chargeability can facilitate the fabrication of a varied intensity of build-in dipoles between the polymer jets from two distinguished solution components. More in depth study can be applied in future work which can be from a mathematical model from experimental and analytical measurements, to fabricate fibres with no cross conjugations (attached bundles).

This is to benefit the varied chargeability of polymer chains encountering an electrical field in order to form nanofibres with spatial arrangements /orientations.

And the resulted fibres are more likely to achieve anisotropic behaviour demonstrating a higher mechanical strength. In fact, study of the effect of anisotropy in electrospun fibres is suggested to evaluate the possible enhancement in mechanical properties by adjusting the secondary electrostatic charge formed by varied chargeability of the solutions.

References

1. Agarwal, S., A. Greiner, and J.H. Wendorff, *Polymer nanophase by use of electrospinning.* Chemie Ingenieur Technik, 2008. **80**(11): p. 1671-1676.
2. Brown, T.A., et al., *Improved collagen extraction by modified longin method.* Radiocarbon, 1988. **30**(2): p. 171-177.
3. Panek, R., et al., *Slice-selective single scan proton COSY with dynamic nuclear polarisation.* Physical chemistry chemical physics : PCCP, 2010. **12**(22): p. 5771.
4. Yildirim, M.S., et al., *Adsorption of human salivary mucin MG1 onto glow-discharge plasma treated acrylic resin surfaces.* Journal of Oral Rehabilitation, 2006. **33**(10): p. 775-783.
5. Tan, S.H., et al., *Systematic parameter study for ultra-fine fiber fabrication via electrospinning process.* Polymer, 2005. **46**(16): p. 6128-6134.
6. Averous, L. and E. Pollet, *Biorenewable nanocomposites.* M R S Bulletin, 2011. **36**(9): p. 703-710.
7. Hasegawa, T., *Quantitative Infrared Spectroscopy for Understanding of a Condensed Matter by Takeshi Hasegawa*. 2017: Tokyo : Springer Japan : Imprint: Springer.
8. Ojeda, J.J. and M. Dittrich, *Fourier transform infrared spectroscopy for molecular analysis of microbial cells*, in *Microbial Systems Biology*. 2012, Springer. p. 187-211.
9. Meyers, M.A., et al., *Biological materials: Structure and mechanical properties.* Progress in Materials Science, 2008. **53**(1): p. 1-206.
10. Mescher, A.L. and L.C.U.a. Junqueira, *Junqueira's Basic Histology: Text and Atlas*. 14 ed. 2013, New York: McGraw-Hill Education
11. *Monomers, Polymers, and Plastics-Chapter 14*. 2011: Elsevier Inc. 499-537.
12. Pethrick, R.A., *Polymer structure characterization : from nano to macro organization in small molecules and polymers / by Richard A. Pethrick*. 2nd ed. ed, ed. C. Royal Society of. 2014, Cambridge: Cambridge: Royal Society of Chemistry.
13. *Advanced synthetic polymer biomaterials derived from organic sources-3*. 2014: Elsevier Ltd. 71-99.
14. Zong, X.H., et al., *Structure and process relationship of electrospun bioabsorbable nanofiber membranes.* Polymer, 2002. **43**(16): p. 4403-4412.
15. Pillay, V., et al., *A Review of Polymeric Refabrication Techniques to Modify Polymer Properties for Biomedical and Drug Delivery Applications.* Aaps Pharmscitech, 2013. **14**(2): p. 692-711.
16. Plesa, I., et al., *Properties of Polymer Composites Used in High-Voltage Applications.* Polymers, 2016. **8**(5).

17. Kumbar, S., C. Laurencin, and M. Deng, *Natural and synthetic biomedical polymers / edited by Sangamesh Kumbar, Cato Laurencin, Meng Deng*. First edition. ed. 2014, Amsterdam ; Boston: Amsterdam ; Boston : Elsevier Science.
18. Sitter, H., *Small Organic Molecules on Surfaces Fundamentals and Applications*. Springer Series in Materials Science, ed. C. Ambrosch-Draxl, M. Ramsey, and SpringerLink. 2013: Berlin, Heidelberg : Springer Berlin Heidelberg : Imprint: Springer.
19. Barbari, T.A., *Polymer science and technology. By J. R. Fried, Prentice Hall PTR, Englewood Cliffs, NJ, 1995, 509 pp., $70.00*. 1997: New York. p. 283-285.
20. Bazrafshan, Z. and G.K. Stylios, *A novel approach to enhance the spinnability of collagen fibers by graft polymerisation.* Materials Science and Engineering: C, 2019. **94**: p. 108-116.
21. Bhattacharya, A. and B.N. Misra, *Grafting: a versatile means to modify polymers - Techniques, factors and applications.* Progress in Polymer Science, 2004. **29**(8): p. 767-814.
22. Johnson, R.P., J.V. John, and I. Kim, *Recent developments in polymer-block-polypeptide and protein-polymer bioconjugate hybrid materials.* European Polymer Journal, 2013. **49**(10): p. 2925-2948.
23. Müller, W.E.G., *Biomedical Inorganic Polymers Bioactivity and Applications of Natural and Synthetic Polymeric Inorganic Molecules*. Progress in Molecular and Subcellular Biology, ed. X. Wang, H.C. Schröder, and SpringerLink. 2014: Berlin, Heidelberg : Springer Berlin Heidelberg : Imprint: Springer.
24. Mohanty, A.K., M. Misra, and G. Hinrichsen, *Biofibres, biodegradable polymers and biocomposites: An overview.* Macromolecular Materials and Engineering, 2000. **276**(3-4): p. 1-24.
25. Fang, P., et al., *Synthesis and Properties of a Ternary Polyacrylate Copolymer Resin for the Absorption of Oil Spills.* Journal of Applied Polymer Science, 2014. **131**(8): p. 9.
26. Li, M.Y., et al., *Electrospun protein fibers as matrices for tissue engineering.* Biomaterials, 2005. **26**(30): p. 5999-6008.
27. Dash, M., et al., *Chitosan—A versatile semi-synthetic polymer in biomedical applications.* Progress in polymer science, 2011. **36**(8): p. 981-1014.
28. Kumar, N., P. Kaur, and S. Bhatia, *Advances in bio-nanocomposite materials for food packaging: a review*. 2017, Emerald Group Publishing Limited: Bradford. p. 591-606.
29. Chiellini, E., et al., *Environmentally degradable bio-based polymeric blends and composites.* Macromol. Biosci., 2004. **4**(3): p. 218-231.
30. Freed, L.E., et al., *Biodegradable polymer scaffolds for tissue engineering.* Bio-Technology, 1994. **12**(7): p. 689-693.
31. *Studying molecular-scale protein–surface interactions in biomaterials-6*. 2013: Elsevier Ltd. 182-223.

32. Waksman, G., *Proteomics and Protein-Protein Interactions Biology, Chemistry, Bioinformatics, and Drug Design*. Protein Reviews, ed. G. Waksman, SpringerLink, and Link. 2006, Boston, MA: Boston, MA : Springer US.
33. Halley, P., *Starch Polymers From Genetic Engineering to Green Applications*. Starch Polymers, ed. L.R. Averous. 2014, Burlington: Burlington : Elsevier Science.
34. Ferry, L., A. Crespy, and V. Vialettes, *Processability of Cottonseed Proteins into Biodegradable Materials.* Biomacromolecules, 2001. **2**(4): p. 1104-1109.
35. Luo, C.J. and M. Edirisinghe, *Core-Liquid-Induced Transition from Coaxial Electrospray to Electrospinning of Low-Viscosity Poly(lactide-co-glycolide) Sheath Solution.* Macromolecules, 2014. **47**(22): p. 7930-7938.
36. Morro, A., et al., *New blends of ethylene-butyl acrylate copolymers with thermoplastic starch. Characterization and bacterial biodegradation.* Carbohydrate Polymers, 2016. **149**: p. 68-76.
37. Tian, M., et al., *Separated-structured all-organic dielectric elastomer with large actuation strain under ultra-low voltage and high mechanical strength.* Journal of Materials Chemistry A, 2015. **3**(4): p. 1483-1491.
38. Sisson, K., et al., *Evaluation of Cross-Linking Methods for Electrospun Gelatin on Cell Growth and Viability.* Biomacromolecules, 2009. **10**(7): p. 1675-1680.
39. Xiang, J.X., et al., *The effect of riboflavin/UVA cross-linking on anti-degeneration and promoting angiogenic capability of decellularized liver matrix.* Journal of Biomedical Materials Research Part A, 2017. **105**(10): p. 2662-2669.
40. Ebnesajjad, S., *Handbook of Biopolymers and Biodegradable Plastics Properties, Processing and Applications*. Handbook of Biopolymers and Biodegradable Plastics, ed. S. Ebnesajjad. 2012, Burlington: Burlington : Elsevier Science.
41. Pal, K., A.T. Paulson, and D. Rousseau, *Biopolymers in Controlled-Release Delivery Systems-14*. 2013: Elsevier Inc. 329-363.
42. Bhuiyan, D., et al., *Novel synthesis and characterization of a collagen-based biopolymer initiated by hydroxyapatite nanoparticles.* Acta Biomaterialia, 2015. **15**: p. 181-190.
43. Pal, S., et al., *A mechanistic model on the role of "radially-running" collagen fibers on dissection properties of human ascending thoracic aorta.* Journal of Biomechanics, 2014. **47**(5): p. 981-8.
44. Sáez, P., E. Peña, and M. Martínez, *A Structural Approach Including the Behavior of Collagen Cross-Links to Model Patient-Specific Human Carotid Arteries.* The Journal of the Biomedical Engineering Society, 2014. **42**(6): p. 1158-1169.

45. Thavarajah, R., et al., *Chemical and physical basics of routine formaldehyde fixation.* Journal of Oral and Maxillofacial Pathology : JOMFP, 2012. **16**(3): p. 400-405.
46. Sommer, I. and P.M. Kunz, *Improving the water resistance of biodegradable collagen films.* Journal of Applied Polymer Science, 2012. **125**(S2): p. E27-E41.
47. Bazrafshan, Z. and G. Stylios, *High Performance of Covalently Grafting onto Collagen in The Presence of Graphene Oxide.* Nanomaterials, 2018. **8**(9): p. 703.
48. Bazrafshan, Z. and G.K. Stylios, *One-pot approach synthesizing and characterization of random copolymerisation of ethyl acrylate-co-methyl methacrylate with broad range of glass transition temperature onto collagen.* Polymer Engineering & Science, 2018. **58**(8): p. 1261-1267.
49. Mariod, A.A. and H.F. Adam, *Review: Gelatin, source, extraction and industrial applications.* Acta Scientiarum Polonorum, Technologia Alimentaria, 2013. **12**(2): p. 135-147.
50. Li, Z.R., et al., *Isolation and characterization of acid soluble collagens and pepsin soluble collagens from the skin and bone of Spanish mackerel (Scomberomorous niphonius).* Food Hydrocolloids, 2013. **31**(1): p. 103-113.
51. Bai, J., *Advanced Fibre-Reinforced Polymer (FRP) Composites for Structural Applications*. Woodhead Publishing Series in Civil and Structural Engineering, ed. J. Bai. 2013, Burlington: Burlington : Elsevier Science.
52. Hussein, N., *Enhancement of the mechanical performance of semi-crystalline polyamides by tailoring the intermolecular interaction in the amorphous phase*. 2013, INSA de Lyon.
53. Friedrich, K., *Polymer Composites From Nano-to-macro-scale*. Polymer Composites : From Nano- to Macro-Scale, ed. S. Fakirov, et al. 2005, Boston, MA: Boston, MA : Springer US.
54. Roff, *Fibres, films, plastics and rubbers: a handbook of common polymers / Roff, W.J. compiler*. 1971: Butterworth.
55. Kadolph, S.J., *Textiles*. 10th. ed. 2007, Hemel Hempstead: Hemel Hempstead : Prentice-Hall International.
56. Mouritz, A.P., *Fire Properties of Polymer Composite Materials*. Solid Mechanics & Its Applications S., v. 143, ed. A.G. Gibson, SpringerLink, and Link. 2007, Dordrecht: Dordrecht : Springer Netherlands.
57. Poveda, R.L., *Carbon nanofiber reinforced polymer composites / Ronald L. Poveda, Nikhil Gupta*. 1st ed. 2016. ed, ed. N. Gupta. 2016: Cham, Switzerland : Springer.
58. Gajjar, C.R., *Resorbable Fiber-Forming Polymers for Biotextile Applications*. SpringerBriefs in Materials, ed. M.W. King and P. SpringerLink Content. 2014, Dordrecht: Dordrecht : Springer.

59. Zhang, D., *Advances in Filament Yarn Spinning of Textiles and Polymers*. Woodhead Publishing Series in Textiles, ed. D. Zhang. 2014, Burlington: Burlington : Elsevier Science.
60. Teramoto, Y., *Functional thermoplastic materials from derivatives of cellulose and related structural polysaccharides.* Molecules, 2015. **20**(4): p. 5487-5527.
61. Li, Z., *One-Dimensional nanostructures Electrospinning Technique and Unique Nanofibers*. SpringerBriefs in Materials, ed. C. Wang and P. SpringerLink Content. 2013: Berlin, Heidelberg : Springer Berlin Heidelberg : Imprint: Springer.
62. Huang, Z.-M., et al., *A review on polymer nanofibers by electrospinning and their applications in nanocomposites.* Composites Science and Technology, 2003. **63**(15): p. 2223-2253.
63. Teo, W.E. and S. Ramakrishna, *Areview on electrospinning design and nanofibre assemblies*. 2006. p. R89-R106.
64. Bhardwaj, N. and S.C. Kundu, *Electrospinning: A fascinating fiber fabrication technique.* Biotechnology Advances, 2010. **28**(3): p. 325-347.
65. Mirjalili, M. and S. Zohoori, *Review for application of electrospinning and electrospun nanofibers technology in textile industry.* Journal of Nanostructure in Chemistry, 2016. **6**(3): p. 207-213.
66. Barnes, C.P., et al., *Nanofiber technology: Designing the next generation of tissue engineering scaffolds.* Advanced Drug Delivery Reviews, 2007. **59**(14): p. 1413-1433.
67. Tuin, S.A., B. Pourdeyhimi, and E.G. Loboa, *Interconnected, microporous hollow fibers for tissue engineering: Commercially relevant, industry standard scale-up manufacturing*. 2014. p. 3311-3323.
68. Yu, D.G., et al., *Electrospinning of Concentrated Polymer Solutions.* Macromolecules, 2010. **43**(24): p. 10743-10746.
69. Amariei, G., et al., *Dendrimer-functionalized electrospun nanofibres as dual-action water treatment membranes.* Science of the Total Environment, 2017. **601-602**: p. 732-740.
70. Cao, J., et al., *Novel stellate poly(vinylidene fluoride)/polyethersulfone microsphere-nanofiber electrospun membrane with special wettability for oil/water separation.* Materials Letters, 2017. **207**: p. 190-194.
71. Aytac, Z., et al., *Antibacterial electrospun zein nanofibrous web encapsulating thymol/cyclodextrin-inclusion complex for food packaging.* Food Chemistry, 2017. **233**: p. 117-124.
72. Zhang, X., X. Yang, and G.G. Chase, *Filtration performance of electrospun acrylonitrile-butadiene elastic fiber mats in solid aerosol filtration.* Separation and Purification Technology, 2017. **186**: p. 96-105.

73. Coverdale, B.D.M., et al., *Use of lecithin to control fiber morphology in electrospun poly (-caprolactone) scaffolds for improved tissue engineering applications.* Journal of Biomedical Materials Research Part A, 2017. **105**(10): p. 2865-2874.
74. Naseri-Nosar, M., M. Salehi, and S. Hojjati-Emami, *Cellulose acetate/poly lactic acid coaxial wet-electrospun scaffold containing citalopram-loaded gelatin nanocarriers for neural tissue engineering applications.* International Journal of Biological Macromolecules, 2017. **103**: p. 701-708.
75. Tavassoli-Kafrani, E., S.A.H. Goli, and M. Fathi, *Fabrication and characterization of electrospun gelatin nanofibers crosslinked with oxidized phenolic compounds.* International Journal of Biological Macromolecules, 2017. **103**: p. 1062-1068.
76. Esmaeili, A. and M. Haseli, *Optimization, synthesis, and characterization of coaxial electrospun sodium carboxymethyl cellulose-graft-methyl acrylate/poly(ethylene oxide) nanofibers for potential drug-delivery applications.* Carbohydrate Polymers, 2017. **173**: p. 645-653.
77. Sarioglu, O.F., et al., *Bacteria immobilized electrospun polycaprolactone and polylactic acid fibrous webs for remediation of textile dyes in water.* Chemosphere, 2017. **184**: p. 393-399.
78. He, F.-A., et al., *Tough and porous piezoelectric P(VDF-TrFE)/organosilicate composite membrane.* High Performance Polymers, 2017. **29**(2): p. 133-140.
79. Deniz, D.Y., M.V. Kahraman, and S.E. Kuruca, *UV-reactive electrospinning of keratin/4-vinyl benzene boronic acid-hydroxyapatite/poly(vinyl alcohol) composite nanofibers.* Polymer Composites, 2017. **38**(7): p. 1371-1377.
80. Simonič, M., et al., *Alternative cleaning of compost leachate using biopolymer chitosan.* Fibers and Polymers, 2017. **18**(3): p. 445-452.
81. Ju, J., et al., *Designing waterproof breathable material with moisture unidirectional transport characteristics based on a TPU/TBAC tree-like and TPU nanofiber double-layer membrane fabricated by electrospinning.* RSC Adv., 2017. **7**(51): p. 32155-32163.
82. Yan, X., et al., *Colorful Hydrophobic Poly(Vinyl Butyral)/Cationic Dye Fibrous Membranes via a Colored Solution Electrospinning Process.* Nanoscale Research Letters, 2016. **11**(1): p. <xocs:firstpage xmlns:xocs=""/>.
83. Amini, G., et al., *Fabrication of Polyurethane and Nylon 66 Hybrid Electrospun Nanofiber Layer for Waterproof Clothing Applications.* Advances in Polymer Technology, 2016. **35**(4): p. 419-427.
84. Pezzoli, D., et al., *Biomimetic coating of cross-linked gelatin to improve mechanical and biological properties of electrospun PET: A promising approach for small caliber vascular graft applications.*

Journal of Biomedical Materials Research Part A, 2017. **105**(9): p. 2405-2415.
85. Castellano, D., et al., *A comparison of electrospun polymers reveals poly(3-hydroxybutyrate) fiber as a superior scaffold for cardiac repair.* Stem Cells and Development, 2014. **23**(13): p. 1479-1490.
86. Poormasjedi-Meibod, M.S., et al., *Development of a nanofibrous wound dressing with an antifibrogenic properties in vitro and in vivo model.* Journal of Biomedical Materials Research Part A, 2016. **104**(9): p. 2334-2344.
87. Hofman, K., et al., *Effects of the molecular format of collagen on characteristics of electrospun fibres.* Journal of Materials Science, 2012. **47**(3): p. 1148-1155.
88. Law, J.X., et al., *Electrospun Collagen Nanofibers and Their Applications in Skin Tissue Engineering.* Tissue Engineering and Regenerative Medicine, 2017. **14**(6): p. 699-718.
89. Sahoo, S., et al., *Growth factor delivery through electrospun nanofibers in scaffolds for tissue engineering applications.* Journal of Biomedical Materials Research Part A, 2010. **93A**(4): p. 1539-1550.
90. Pierschbacher, M.D. and E. Ruoslahti, *Cell attachment activity of fibronectin can be duplicated by small synthetic fragments of the molecule.* Nature, 1984. **309**(5963): p. 30-33.
91. Zeugolis, D.I., et al., *Electro-spinning of pure collagen nano-fibres - Just an expensive way to make gelatin?* Biomaterials, 2008. **29**(15): p. 2293-2305.
92. Bazrafshan, Z. and G.K. Stylios, *Custom-built electrostatics and supplementary bonding in the design of reinforced Collagen-g-P(methyl methacrylate-co-ethyl acrylate)/ nylon 66 core-shell fibers.* Journal of the Mechanical Behavior of Biomedical Materials, 2018. **87**: p. 19-29.
93. Sinha, V.R. and A. Trehan, *Biodegradable microspheres for protein delivery.* Journal of Controlled Release, 2003. **90**(3): p. 261-280.
94. Lee, C.H., A. Singla, and Y. Lee, *Biomedical applications of collagen.* International Journal of Pharmaceutics, 2001. **221**(1-2): p. 1-22.
95. Craig, A.S. and D.A. Parry, *Collagen Fibrils During Development and Maturation and their Contribution to the Mechanical Attributes of Connective Tissue*, in *Collagen*. 2018, CRC Press. p. 1-23.
96. How, T., R. Guidoin, and S. Young, *Engineering design of vascular prostheses.* Proceedings of the Institution of Mechanical Engineers, Part H: Journal of Engineering in Medicine, 1992. **206**(2): p. 61-71.
97. Shields, K.J., et al., *Mechanical properties and cellular proliferation of electrospun collagen type II.* Tissue Engineering, 2004. **10**(9-10): p. 1510-1517.

98. Matthews, J.A., et al., *Electrospinning of collagen nanofibers.* Biomacromolecules, 2002. **3**(2): p. 232-238.
99. Lynn, A.K., I.V. Yannas, and W. Bonfield, *Antigenicity and immunogenicity of collagen.* Journal of Biomedical Materials Research Part B-Applied Biomaterials, 2004. **71B**(2): p. 343-354.
100. Curtin, C.M., I.M. Castano, and F.J. O'Brien, *Scaffold-Based microRNA Therapies in Regenerative Medicine and Cancer.* Advanced Healthcare Materials, 2018. **7**(1).
101. Abdal-Hay, A., et al., *Electrospun biphasic tubular scaffold with enhanced mechanical properties for vascular tissue engineering.* Materials Science & Engineering C-Materials for Biological Applications, 2018. **82**: p. 10-18.
102. Strobel, H.A., et al., *Fabrication and characterization of electrospun polycaprolactone and gelatin composite cuffs for tissue engineered blood vessels.* Journal of Biomedical Materials Research Part B-Applied Biomaterials, 2018. **106**(2): p. 817-826.
103. Wang, M., A. Hsieh, and G. Rutledge, *Electrospinning of poly (MMA-co-MAA) copolymers and their layered silicate nanocomposites for improved thermal properties.* Polymer, 2005. **46**(10): p. 3407-3418.
104. Abbah, S.A., et al., *Harnessing Hierarchical Nano- and Micro-Fabrication Technologies for Musculoskeletal Tissue Engineering.* Advanced Healthcare Materials, 2015. **4**(16): p. 2488-2499.
105. Agarwal, S., A. Greiner, and J.H. Wendorff, *Polymer nanophase by use of electrospinning.* Chemie Ingenieur Technik, 2008. **80**(11): p. 1671-1676.
106. Kai, D., et al., *Sustainable and antioxidant lignin–polyester copolymers and nanofibers for potential healthcare applications.* ACS Sustainable Chemistry & Engineering, 2017. **5**(7): p. 6016-6025.
107. Shin, Y., et al., *Experimental characterization of electrospinning: the electrically forced jet and instabilities.* Polymer, 2001. **42**(25): p. 09955-09967.
108. Demir, M.M., et al., *Electrospinning of polyurethane fibers.* Polymer, 2002. **43**(11): p. 3303-3309.
109. Ki, C.S., et al., *Characterization of gelatin nanofiber prepared from gelatin-formic acid solution.* Polymer, 2005. **46**(14): p. 5094-5102.
110. Geng, X.Y., O.H. Kwon, and J.H. Jang, *Electrospinning of chitosan dissolved in concentrated acetic acid solution.* Biomaterials, 2005. **26**(27): p. 5427-5432.
111. Buchko, C.J., et al., *Processing and microstructural characterization of porous biocompatible protein polymer thin films.* Polymer, 1999. **40**(26): p. 7397-7407.

112. Zhao, C., et al., *Synthesis and characterization of multi-walled carbon nanotubes reinforced polyamide 6 via in situ polymerisation.* 2005. **46**(14): p. 5125-5132.
113. Zhang, Y.Z., et al., *Characterization of the surface biocompatibility of the electrospun PCL-collagen nanofibers using fibroblasts.* Biomacromolecules, 2005. **6**(5): p. 2583-2589.
114. Sill, T.J. and H.A. von Recum, *Electro spinning: Applications in drug delivery and tissue engineering.* Biomaterials, 2008. **29**(13): p. 1989-2006.
115. Zhang, C.X., et al., *Study on morphology of electrospun poly(vinyl alcohol) mats.* European Polymer Journal, 2005. **41**(3): p. 423-432.
116. Zhang, D.M. and J. Chang, *Electrospinning of Three-Dimensional Nanofibrous Tubes with Controllable Architectures.* Nano Letters, 2008. **8**(10): p. 3283-3287.
117. Nayak, R., et al., *Effect of viscosity and electrical conductivity on the morphology and fiber diameter in melt electrospinning of polypropylene.* Textile Research Journal, 2013. **83**(6): p. 606-617.
118. Sun, Z.C., et al., *The effect of solvent dielectric properties on the collection of oriented electrospun fibers.* Journal of Applied Polymer Science, 2012. **125**(4): p. 2585-2594.
119. Okutan, N., P. Terzi, and F. Altay, *Affecting parameters on electrospinning process and characterization of electrospun gelatin nanofibers.* Food Hydrocolloids, 2014. **39**: p. 19-26.
120. Zhao, Z.Z., et al., *Preparation and properties of electrospun poly(vinylidene fluoride) membranes.* Journal of Applied Polymer Science, 2005. **97**(2): p. 466-474.
121. Son, W.K., et al., *The effects of solution properties and polyelectrolyte on electrospinning of ultrafine poly(ethylene oxide) fibers.* Polymer, 2004. **45**(9): p. 2959-2966.
122. Haider, S., et al., *Preparation of the Chitosan Containing Nanofibers by Electrospinning Chitosan-Gelatin Complexes.* Polymer Engineering and Science, 2010. **50**(9): p. 1887-1893.
123. Kim, B., et al., *Poly(acrylic acid) nanofibers by electrospinning.* Materials Letters, 2005. **59**(7): p. 829-832.
124. Gupta, P., et al., *Electrospinning of linear homopolymers of poly (methyl methacrylate): exploring relationships between fiber formation, viscosity, molecular weight and concentration in a good solvent.* Polymer, 2005. **46**(13): p. 4799-4810.
125. Gong, G.M. and J.T. Wu, *Novel Polyimide Materials Produced by Electrospinning*. High Performance Polymers - Polyimides Based - from Chemistry to Applications, ed. M.J.M. Abadie. 2012. 127-144.
126. Bak, S.Y., et al., *Effect of humidity and benign solvent composition on electrospinning of collagen nanofibrous sheets.* Materials Letters, 2016. **181**: p. 136-139.

127. Li, M.M. and Y.Z. Long, *Fabrication of self-assembled three-dimensional fibrous stackings by electrospinning.* Nano-Scale and Amourphous Materials, 2011. **688**: p. 95-101.
128. Li, D. and Y.N. Xia, *Electrospinning of nanofibers: Reinventing the wheel?* Advanced Materials, 2004. **16**(14): p. 1151-1170.
129. Reneker, D.H. and I. Chun, *Nanometre diameter fibres of polymer, produced by electrospinning.* Nanotechnology, 1996. **7**(3): p. 216-223.
130. Haghi, A.K. and M. Akbari, *Trends in electrospinning of natural nanofibers.* Physica Status Solidi a-Applications and Materials Science, 2007. **204**(6): p. 1830-1834.
131. Huang, Z.M., et al., *A review on polymer nanofibers by electrospinning and their applications in nanocomposites.* Composites Science and Technology, 2003. **63**(15): p. 2223-2253.
132. Baji, A., et al., *Electrospinning of polymer nanofibers: Effects on oriented morphology, structures and tensile properties.* Composites Science and Technology, 2010. **70**(5): p. 703-718.
133. Dalton, P.D., D. Klee, and M. Moller, *Electrospinning with dual collection rings.* Polymer, 2005. **46**(3): p. 611-614.
134. De Pra, M.A.A., et al., *Effect of collector design on the morphological properties of polycaprolactone electrospun fibers.* Materials Letters, 2017. **193**: p. 154-157.
135. Seidlits, S.K., J.Y. Lee, and C.E. Schmidt, *Nanostructured scaffolds for neural applications.* Nanomedicine, 2008. **3**(2): p. 183-199.
136. Subbiah, T., et al., *Electrospinning of nanofibers.* Journal of Applied Polymer Science, 2005. **96**(2): p. 557-569.
137. Wang, Y.Z., et al., *Electrospinning of Polymer Nanofibers with Ordered Patterns and Architectures.* Journal of Nanoscience and Nanotechnology, 2010. **10**(3): p. 1699-1706.
138. Wendorff, J.H., S. Agarwal, and A. Greiner, *Versatile Nanofiber Structures by Electrospinning.* Nachrichten Aus Der Chemie, 2011. **59**(7-8): p. 714-718.
139. Yarin, A.L., W. Kataphinan, and D.H. Reneker, *Branching in electrospinning of nanofibers.* Journal of Applied Physics, 2005. **98**(6): p. 12.
140. Li, Z. and C. Wang, *Effects of working parameters on electrospinning*, in *One-dimensional nanostructures*. 2013, Springer. p. 15-28.
141. Eda, G. and S. Shivkumar, *Bead-to-fiber transition in electrospun polystyrene.* Journal of Applied Polymer Science, 2007. **106**(1): p. 475-487.
142. Bazbouz, M.B. and G.K. Stylios, *Alignment and optimization of nylon 6 nanofibers by electrospinning.* Journal of Applied Polymer Science, 2008. **107**(5): p. 3023-3032.

143. Bazbouz, M.B. and G.K. Stylios, *Novel mechanism for spinning continuous twisted composite nanofiber yarns.* European Polymer Journal, 2008. **44**(1): p. 1-12.
144. Chen, F., et al., *Biocompatibility, Alignment Degree and Mechanical Properties of an Electrospun Chitosan–P(LLA-CL) Fibrous Scaffold.* Journal of Biomaterials Science, Polymer Edition, 2009. **20**(14): p. 2117-2128.
145. Kharaziha, M., M.H. Fathi, and H. Edris, *Development of novel aligned nanofibrous composite membranes for guided bone regeneration.* Journal of the Mechanical Behavior of Biomedical Materials, 2013. **24**: p. 9-20.
146. Yan, J., et al., *Effect of fiber alignment in electrospun scaffolds on keratocytes and corneal epithelial cells behavior.* Journal of Biomedical Materials Research Part A, 2012. **100A**(2): p. 527-535.
147. Yousefi, N., et al., *Highly Aligned Graphene/Polymer Nanocomposites with Excellent Dielectric Properties for High-Performance Electromagnetic Interference Shielding.* Advanced Materials, 2014. **26**(31): p. 5480-5487.
148. Sun, Z., et al., *The effect of solvent dielectric properties on the collection of oriented electrospun fibers.* Journal of Applied Polymer Science, 2012. **125**(4): p. 2585-2594.
149. Reneker, D.H. and A.L. Yarin, *Electrospinning jets and polymer nanofibers.* Polymer, 2008. **49**(10): p. 2387-2425.
150. Long, Y.Z., et al., *Recent advances in synthesis, physical properties and applications of conducting polymer nanotubes and nanofibers.* Progress in Polymer Science, 2011. **36**(10): p. 1415-1442.
151. Reneker, D.H., et al., *Bending instability of electrically charged liquid jets of polymer solutions in electrospinning.* Journal of Applied physics, 2000. **87**(9): p. 4531-4547.
152. Yarin, A.L., S. Koombhongse, and D.H. Reneker, *Bending instability in electrospinning of nanofibers.* Journal of applied physics, 2001. **89**(5): p. 3018-3026.
153. Pham, Q.P., U. Sharma, and A.G. Mikos, *Electrospinning of polymeric nanofibers for tissue engineering applications: a review.* Tissue engineering, 2006. **12**(5): p. 1197-1211.
154. McCann, J.T., M. Marquez, and Y.N. Xia, *Melt coaxial electrospinning: A versatile method for the encapsulation of solid materials and fabrication of phase change nanofibers.* Nano Letters, 2006. **6**(12): p. 2868-2872.
155. Han, T., A.L. Yarin, and D.H. Reneker, *Viscoelastic electrospun jets: Initial stresses and elongational rheometry.* Polymer, 2008. **49**(6): p. 1651-1658.
156. Thompson, C., et al., *Effects of parameters on nanofiber diameter determined from electrospinning model.* Polymer, 2007. **48**(23): p. 6913-6922.

157. Burger, C., B.S. Hsiao, and B. Chu, *Nanofibrous materials and their applications.* Annu. Rev. Mater. Res., 2006. **36**: p. 333-368.
158. McKee, M.G., et al., *Electrospinning of linear and highly branched segmented poly (urethane urea) s.* Polymer, 2005. **46**(7): p. 2011-2015.
159. Pant, H.R., et al., *Effect of polymer molecular weight on the fiber morphology of electrospun mats.* Journal of colloid and interface science, 2011. **364**(1): p. 107-111.
160. Sawicka, K.M. and P. Gouma, *Electrospun composite nanofibers for functional applications.* Journal of Nanoparticle Research, 2006. **8**(6): p. 769-781.
161. Khajavi, R. and M. Abbasipour, *Electrospinning as a versatile method for fabricating coreshell, hollow and porous nanofibers.* Scientia Iranica, 2012. **19**(6): p. 2029-2034.
162. Chang, S.W. and M.J. Buehler, *Molecular biomechanics of collagen molecules.* Materials Today, 2014. **17**(2): p. 70-76.
163. Collier, T.A., et al., *Effect on the mechanical properties of type I collagen of intra-molecular lysine-arginine derived advanced glycation end-product cross-linking.* Journal of Biomechanics, 2018. **67**: p. 55-61.
164. Theocharis, D.A., et al., *Hyaluronan and chondroitin sulfate proteoglycans in the supramolecular organization of the mammalian vitreous body.* Connective Tissue Research, 2008. **49**(3-4): p. 124-128.
165. Zhou, Z., M. Minary-Jolandan, and D. Qian, *A simulation study on the significant nanomechanical heterogeneous properties of collagen.* Biomechanics and Modeling in Mechanobiology, 2015. **14**(3): p. 445-457.
166. Gray, S.D., et al., *Biomechanical and histologic observations of vocal fold fibrous proteins.* Annals of Otology Rhinology and Laryngology, 2000. **109**(1): p. 77-85.
167. Shen, J.N., et al., *Purification and concentration of collagen by charged ultrafiltration membrane of hydrophilic polyacrylonitrile blend.* Separation and Purification Technology, 2009. **66**(2): p. 257-262.
168. Nam, K., T. Kimura, and A. Kishida, *Physical and biological properties of collagen-phospholipid polymer hybrid gels.* Biomaterials, 2007. **28**(20): p. 3153-3162.
169. Babu, P.R., et al., *Hydrogels based on gelatin poly(hydroxyethyl methacrylate) and poly(butyl acrylate) graft copolymer impregnated with fibrin.* Journal of Applied Polymer Science, 1997. **65**(3): p. 555-560.
170. Gao, J.P., et al., *Preparation of gelatin - N-vinylpyrrolidone graft copolymer.* Journal of Applied Polymer Science, 1998. **68**(9): p. 1485-1492.

171. Gu, L., S. Zhu, and A.N. Hrymak, *Modeling molecular weight distribution of comb-branched graft copolymers.* Journal of Polymer Science Part B-Polymer Physics, 1998. **36**(4): p. 705-714.
172. Feairhel.Sh, et al., *Graft polymerisation of vinyl monomers onto chromium-tanned collagen.* Abstracts of Papers of the American Chemical Society, 1972. **164**(AUG-S): p. 35-&.
173. Bazrafshan, Z., M. Ataeefard, and F. Nourmohammadian, *Physicochemical colourants effects on polymeric composites printing toner.* Pigment & Resin Technology, 2014. **43**(5): p. 245-250.
174. Bazrafshan, Z., M. Ataeefard, and F. Nourmohammadian, *Modeling the effect of pigments and processing parameters in polymeric composite for printing ink application using the response surface methodology.* Progress in Organic Coatings, 2015. **82**: p. 68-73.
175. Harwood, H.J., *Copolymerisation at high conversion when the concentration of one monomer does not change.* Journal of Polymer Science Part a-Polymer Chemistry, 2000. **38**(7): p. 1118-1128.
176. Lai, P., et al., *Overview of the preparation of organic polymeric nanoparticles for drug delivery based on gelatine, chitosan, poly(D,L-lactide-co-glycolic acid) and polyalkylcyanoacrylate.* Colloids and Surfaces B-Biointerfaces, 2014. **118**: p. 154-163.
177. Muyonga, J.H., C.G.B. Cole, and K.G. Duodu, *Characterisation of acid soluble collagen from skins of young and adult Nile perch (Lates niloticus).* Food Chemistry, 2004. **85**(1): p. 81-89.
178. Friess, W., *Collagen - biomaterial for drug delivery.* European Journal of Pharmaceutics and Biopharmaceutics, 1998. **45**(2): p. 113-136.
179. Sell, S.A., et al., *Electrospinning of collagen/biopolymers for regenerative medicine and cardiovascular tissue engineering.* Advanced Drug Delivery Reviews, 2009. **61**(12): p. 1007-1019.
180. Cheng, W., et al., *The content and ratio of type I and III collagen in skin differ with age and injury.* African Journal of Biotechnology, 2011. **10**(13): p. 2524-2529.
181. Gautieri, A., et al., *Hierarchical structure and nanomechanics of collagen microfibrils from the atomistic scale up.* Nano letters, 2011. **11**(2): p. 757.
182. Carter, P. and N. Bhattarai, *Bioscaffolds: Fabrication and Performance*. Engineered Biomimicry, ed. A. Lakhtakia and R.J. MartinPalma. 2013. 161-188.
183. Zhao, S., et al., *A hierarchical, stretchable and stiff fibrous biotemplate engineered using stagger-electrospinning for augmentation of rotator cuff tendon-healing.* Journal of Materials Chemistry B, 2015. **3**(6): p. 990-1000.
184. Gautieri, A., et al., *Viscoelastic properties of model segments of collagen molecules.* Matrix Biology, 2012. **31**(2): p. 141-149.

185. Gautieri, A., et al., *Modeling and measuring visco-elastic properties: From collagen molecules to collagen fibrils.* International Journal of Non-Linear Mechanics, 2013. **56**: p. 25-33.
186. Yamada, M. and K. Ohshima, *Method of manufacturing cellulose/gelatin composite viscose rayon filament*. 2012, Google Patents.
187. Oliveira, L.C.A., et al., *Solid waste from leather industry as adsorbent of organic dyes in aqueous-medium.* Journal of Hazardous Materials, 2007. **141**(1): p. 344-347.
188. Pucci, F. and M. Rooman, *Physical and molecular bases of protein thermal stability and cold adaptation.* Current Opinion in Structural Biology, 2017. **42**(C): p. 117-128.
189. Yang, H.Q., et al., *Rational Design to Improve Protein Thermostability: Recent Advances and Prospects.* Chembioeng Reviews, 2015. **2**(2): p. 87-94.
190. Hirano, S., et al., *Wet spun chitosan-collagen fibers, their chemical N-modifications, and blood compatibility.* Biomaterials, 2000. **21**(10): p. 997-1003.
191. Tonndorf, R., et al., *Wet spinning and riboflavin crosslin king of collagen type I/III filaments.* Biomedical Materials, 2019. **14**(1).
192. Stoessel, P.R., et al., *Fibers Mechanically Similar to Sheep Wool Obtained by Wet Spinning of Gelatin and Optional Plasticizers.* Macromolecular Materials and Engineering, 2015. **300**(2): p. 234-241.
193. Fukae, R. and T. Midorikawa, *Preparation of Gelatin Fiber by Gel Spinning and Its Mechanical Properties.* Journal of Applied Polymer Science, 2008. **110**(6): p. 4011-4015.
194. Yang, L., et al., *Mechanical properties of single electrospun collagen type I fibers.* Biomaterials, 2008. **29**(8): p. 955-962.
195. Zhan, J.C., et al., *In vitro evaluation of electrospun gelatin-glutaraldehyde nanofibers.* Frontiers of Materials Science, 2016. **10**(1): p. 90-100.
196. Huang, G.P., et al., *An investigation of common crosslinking agents on the stability of electrospun collagen scaffolds.* Journal of Biomedical Materials Research Part A, 2015. **103**(2): p. 762-771.
197. Panzavolta, S., et al., *Electrospun gelatin nanofibers: Optimization of genipin cross-linking to preserve fiber morphology after exposure to water.* Acta Biomaterialia, 2011. **7**(4): p. 1702-1709.
198. Su, G.W., et al., *Effect of xylose on the molecular and particle size distribution of peanut hydrolysate in Maillard reaction system.* Journal of the Science of Food and Agriculture, 2011. **91**(13): p. 2457-2462.
199. Ahmad, Z., et al., *Effect of 1-ethyl -3-(3-dimethylaminopropyl) carbodiimide and N-hydroxysuccinimide concentrations on the mechanical and biological characteristics of cross-linked collagen*

fibres for tendon repair. Regenerative Biomaterials, 2015. **2**(2): p. 77-85.
200. Krishnamoorthy, G., et al., *Experimental and theoretical studies on Gallic acid assisted EDC/NHS initiated crosslinked collagen scaffolds.* Materials Science & Engineering C-Materials for Biological Applications, 2014. **43**: p. 164-171.
201. Cheng, S., et al., *Cross-linking and film-forming properties of transglutaminase-modified collagen fibers tailored by denaturation temperature.* Food Chemistry, 2019. **271**: p. 527-535.
202. Inoue, N., et al., *A novel collagen hydrogel cross-linked by gamma-ray irradiation in acidic pH conditions.* Journal of Biomaterials Science-Polymer Edition, 2006. **17**(8): p. 837-858.
203. Hsu, S.H., H.J. Tseng, and M.S. Wu, *Comparative in vitro evaluation of two different preparations of small diameter polyurethane vascular grafts.* Artificial Organs, 2000. **24**(2): p. 119-128.
204. Tu, R., et al., *Fixation of bioprosthetic tissues with monofunctional and multifunctional polyepoxy compounds.* Journal of Biomedical Materials Research, 1994. **28**(6): p. 677-684.
205. Guo, H., et al., *Kinetic study of modification of collegen peptide with allyl glycidyl ether.* Progress in Reaction Kinetics and Mechanism, 2011. **36**(1): p. 83-93.
206. Nagura, M., et al., *Structures and physical properties of cross-linked gelatin fibers.* Polymer Journal, 2002. **34**(10): p. 761-766.
207. Stoessel, P.R., et al., *Porous, Water-Resistant Multifilament Yarn Spun from Gelatin.* Biomacromolecules, 2015. **16**(7): p. 1997-2005.
208. Sionkowska, A., et al., *Molecular interactions in collagen and chitosan blends.* Biomaterials, 2004. **25**(5): p. 795-801.
209. Chen, Z.G., et al., *Electrospun collagen-chitosan nanofiber: A biomimetic extracellular matrix for endothelial cell and smooth muscle cell.* Acta Biomaterialia, 2010. **6**(2): p. 372-382.
210. Wang, X., et al., *Regenerated collagen fibers with grooved surface texture: Physicochemical characterization and cytocompatibility.* Materials Science & Engineering C-Materials for Biological Applications, 2016. **58**: p. 750-756.
211. Deng, A.P., et al., *Electrospinning of in situ crosslinked recombinant human collagen peptide/chitosan nanofibers for wound healing.* Biomaterials Science, 2018. **6**(8): p. 2197-2208.
212. He, Y.Z., et al., *An Antimicrobial Peptide-Loaded Gelatin/Chitosan Nanofibrous Membrane Fabricated by Sequential Layer-by-Layer Electrospinning and Electrospraying Techniques.* Nanomaterials, 2018. **8**(5): p. 13.
213. Bazrafshan, Z. and K.S. George, *One-Step Fabrication of Three-Dimensional Fibrous Collagen-Based Macrostructure with High*

Water Uptake Capability by Coaxial Electrospinning. Nanomaterials, 2018. **8**(10): p. 803.
214. Weiler, J.M. and R.J. Linhardt, *Comparison of the activity of polyanions and polycations on the classical and alternative pathways of complement.* Immunopharmacology, 1989. **17**(2): p. 65-72.
215. Krissinel, E. and K. Henrick, *Inference of macromolecular assemblies from crystalline state.* Journal of Molecular Biology, 2007. **372**(3): p. 774-797.
216. Liu, Y., et al., *Gelatin-g-Poly(methyl methacrylate)/Silver Nanoparticle Hybrid Films and the Evaluation of Their Antibacterial Activity.* Journal of Applied Polymer Science, 2010. **116**(5): p. 2617-2625.
217. Parthiban, A., et al., *Triblock copolymers composed of soft and semi-crystalline segments-synthesis and characterization of poly (n-butyl acrylate)-block-(epsilon-caprolactone)-block-(L-lactide).* Polymer Chemistry, 2010. **1**(3): p. 333-338.
218. Jou, C.H., et al., *Biofunctional properties of polyester fibers grafted with chitosan and collagen.* Polymers for Advanced Technologies, 2007. **18**(3): p. 235-239.
219. Yuan, S.J., et al., *Surface modification of polycaprolactone substrates using collagen-conjugated poly(methacrylic acid) brushes for the regulation of cell proliferation and endothelialisation.* Journal of Materials Chemistry, 2012. **22**(26): p. 13039-13049.
220. Shan, Y.M., et al., *NHS-mediated QDs-peptide/protein conjugation and its application for cell labeling.* Talanta, 2008. **75**(4): p. 1008-1014.
221. Gentile, P., et al., *Biosynthetic PCL-graft-Collagen Bulk Material for Tissue Engineering Applications.* Materials, 2017. **10**(7): p. 17.
222. Panzavolta, S., et al., *Structural reinforcement and failure analysis in composite nanofibers of graphene oxide and gelatin.* Carbon, 2014. **78**: p. 566-577.
223. Kang, S., et al., *Covalent conjugation of mechanically stiff graphene oxide flakes to three-dimensional collagen scaffolds for osteogenic differentiation of human mesenchymal stem cells.* Carbon, 2015. **83**: p. 162-172.
224. Amsaveni, M., et al., *Green Synthesis and Characterization of Hybrid Collagen-Cellulose-Albumin Biofibers from Skin Waste.* Applied Biochemistry and Biotechnology, 2013. **171**(6): p. 1500-1512.
225. Goldin, A., et al., *Advanced glycation end products - Sparking the development of diabetic vascular injury.* Circulation, 2006. **114**(6): p. 597-605.

226. Nagahama, H., et al., *Preparation of biodegradable chitin/gelatin membranes with GlcNAc for tissue engineering applications.* Carbohydrate Polymers, 2008. **73**(3): p. 456-463.
227. Nakajima, K., et al., *Soft textural and emulsifiable gelatin formed by conjugating with fatty-acylated saccharide.* Bioscience Biotechnology and Biochemistry, 2008. **72**(2): p. 295-302.
228. Englert, C., et al., *Bonding of articular cartilage using a combination of biochemical degradation and surface cross-linking.* Arthritis Research & Therapy, 2007. **9**(3).
229. Weadock, K.S., et al., *Physical cross-linking of collagen-fibers - comparison of ultraviolet-irradiation and dehydrothermal treatment.* Journal of Biomedical Materials Research, 1995. **29**(11): p. 1373-1379.
230. Chen, Z.G., et al., *Intermolecular interactions in electrospun collagen-chitosan complex nanofibers.* Carbohydrate Polymers, 2008. **72**(3): p. 410-418.
231. Li, C.Y., F. Xue, and E.Y. Ding, *Preparation of polyacrylamide grafted collagen extracted from leather wastes and their application in kaolin flocculation.* Journal of Applied Polymer Science, 2015. **132**(13): p. 11.
232. Chen, J.P. and C.H. Su, *Surface modification of electrospun PLLA nanofibers by plasma treatment and cationized gelatin immobilization for cartilage tissue engineering.* Acta Biomaterialia, 2011. **7**(1): p. 234-243.
233. Li, Z.C., et al., *Graft-copolymerisation of butyl acrylate onto gelatin in the presence of ceric ion.* Journal of Macromolecular Science-Chemistry, 1988. **A25**(12): p. 1487-1513.
234. Fu, Z.F., W.P. Tao, and Y. Shi, *Synthesis of densely grafted comblike copolymers.* Journal of Polymer Science Part a-Polymer Chemistry, 2008. **46**(1): p. 362-372.
235. Keles, H. and M. Sacak, *Graft copolymerisation of methyl methacrylate onto gelatin using KMnO4-H2SO4 redox system.* Journal of Applied Polymer Science, 2003. **89**(10): p. 2836-2844.
236. Ye, P., et al., *Nanofibrous poly(acrylonitrile-co-maleic acid) membranes functionalized with gelatin and chitosan for lipase immobilization.* Biomaterials, 2006. **27**(22): p. 4169-4176.
237. Kaur, I., et al., *Graft-copolymerisation of acrylonitrile and methacrylonitrile onto gelatin by mutual irradiation method.* Journal of Applied Polymer Science, 1994. **54**(8): p. 1131-1139.
238. Kaur, I., et al., *Radiochemical grafting of methacrylonitrile and its binary mixture with methyl acrylate onto gelatin.* Polymer International, 1998. **46**(4): p. 275-279.
239. Keles, H., et al., *Graft copolymerisation of methyl methacrylate upon gelatin initiated by benzoyl peroxide in aqueous medium.* Journal of Applied Polymer Science, 1999. **74**(6): p. 1547-1556.

240. Curcio, M., et al., *Grafted thermo-responsive gelatin microspheres as delivery systems in triggered drug release.* European Journal of Pharmaceutics and Biopharmaceutics, 2010. **76**(1): p. 48-55.
241. Binsi, P.K., et al., *Rheological and functional properties of gelatin from the skin of Bigeye snapper (Priacanthus hamrur) fish: Influence of gelatin on the gel-forming ability of fish mince.* Food Hydrocolloids, 2009. **23**(1): p. 132-145.
242. Chaochai, T., et al., *Preparation and Properties of Gelatin Fibers Fabricated by Dry Spinning.* Fibers, 2016. **4**(1): p. 11.
243. Thitirat, C., et al., *Preparation and Properties of Gelatin Fibers Fabricated by Dry Spinning.* Fibers, 2016. **4**(1): p. 2.
244. Fukae, R., A. Maekawa, and S. Sangen, *Gel-spinning and drawing of gelatin.* Polymer, 2005. **46**(25): p. 11193-11194.
245. Meyer, M., H. Baltzer, and K. Schwikal, *Collagen fibres by thermoplastic and wet spinning.* Materials Science & Engineering C-Materials for Biological Applications, 2010. **30**(8): p. 1266-1271.
246. Tronci, G., et al., *Wet-spinnability and crosslinked fibre properties of two collagen polypeptides with varied molecular weight.* International Journal of Biological Macromolecules, 2015. **81**: p. 112-120.
247. Yang, C.Y., et al., *Fabrication of Porous Gelatin Microfibers Using an Aqueous Wet Spinning Process.* Artificial Cells Blood Substitutes and Biotechnology, 2009. **37**(4): p. 173-176.
248. Liivak, O., et al., *A microfabricated wet-spinning apparatus to spin fibers of silk proteins. Structure-property correlations.* Macromolecules, 1998. **31**(9): p. 2947-2951.
249. STOESSEL, P.R., R.N. Grass, and W.J. Stark, *Improved spinning process and novel gelatin fibers*. 2014, Google Patents.
250. Um, I.C., et al., *Wet spinning of silk polymer: I. Effect of coagulation conditions on the morphological feature of filament.* International Journal of Biological Macromolecules, 2004. **34**(1): p. 89-105.
251. Lu, Y., et al., *Coaxial electrospun fibers: applications in drug delivery and tissue engineering.* Wiley Interdisciplinary Reviews-Nanomedicine and Nanobiotechnology, 2016. **8**(5): p. 654-677.
252. Su, Y., et al., *Controlled release of bone morphogenetic protein 2 and dexamethasone loaded in core-shell PLLACL-collagen fibers for use in bone tissue engineering.* Acta Biomaterialia, 2012. **8**(2): p. 763-771.
253. Wang, Q., et al., *Electrospun hypromellose-based hydrophilic composites for rapid dissolution of poorly water-soluble drug.* Carbohydrate Polymers, 2017. **174**: p. 617-625.
254. Gulfam, M., et al., *Highly Porous Core-Shell Polymeric Fiber Network.* Langmuir, 2011. **27**(17): p. 10993-10999.
255. Huang, Z.M., Y.Z. Zhang, and S. Ramakrishna, *Double-layered composite nanofibers and their mechanical performance.* Journal of

Polymer Science Part B-Polymer Physics, 2005. **43**(20): p. 2852-2861.
256. Yu, J.H., S.V. Fridrikh, and G.C. Rutledge, *Production of submicrometer diameter fibers by two-fluid electrospinning.* Advanced Materials, 2004. **16**(17): p. 1562-+.
257. Shenoy, S.L., et al., *Role of chain entanglements on fiber formation during electrospinning of polymer solutions: good solvent, non-specific polymer–polymer interaction limit.* Polymer, 2005. **46**(10): p. 3372-3384.
258. Zhang, Y.Z., et al., *Preparation of core-shell structured PCL-r-gelatin Bi-component nanofibers by coaxial electrospinning.* Chemistry of Materials, 2004. **16**(18): p. 3406-3409.
259. Saville, D.A., *Electrohydrodynamics: The Taylor-Melcher Leaky Dielectric Model.* Annual Review of Fluid Mechanics, 1997. **29**(1): p. 27-64.
260. Hohman, M.M., et al., *Electrospinning and electrically forced jets. I. Stability theory.* Physics of Fluids, 2001. **13**(8): p. 2201-2220.
261. Hohman, M.M., et al., *Electrospinning and electrically forced jets. II. Applications.* Physics of Fluids, 2001. **13**(8): p. 2221-2236.
262. Schnitzer, O. and E. Yariv, *The Taylor–Melcher leaky dielectric model as a macroscale electrokinetic description.* 2015. **773**: p. 1-33.
263. Kidoaki, S., I.K. Kwon, and T. Matsuda, *Mesoscopic spatial designs of nano- and microfiber meshes for tissue-engineering matrix and scaffold based on newly devised multilayering and mixing electrospinning techniques.* Biomaterials, 2005. **26**(1): p. 37-46.
264. Choi, S.M., et al., *Bioactive fish collagen/polycaprolactone composite nanofibrous scaffolds fabricated by electrospinning for 3D cell culture.* Journal of biotechnology, 2015. **205**: p. 47-58.
265. Zeugolis, D.I., et al., *Collagen solubility testing, a quality assurance step for reproducible electro-spun nano-fibre fabrication. A technical note.* Journal of Biomaterials Science-Polymer Edition, 2008. **19**(10): p. 1307-1317.
266. Liu, T., et al., *Photochemical crosslinked electrospun collagen nanofibers: Synthesis, characterization and neural stem cell interactions.* Journal of Biomedical Materials Research Part A, 2010. **95A**(1): p. 276-282.
267. Qi, P.W., et al., *A new collagen solution with high concentration and collagen native structure perfectly preserved.* Rsc Advances, 2015. **5**(106): p. 87180-87186.
268. Elamparithi, A., A.M. Punnoose, and S. Kuruvilla, *Electrospun type 1 collagen matrices preserving native ultrastructure using benign binary solvent for cardiac tissue engineering.* Artificial Cells Nanomedicine and Biotechnology, 2016. **44**(5): p. 1318-1325.

269. Nagarajan, S., et al., *Design of Boron Nitride/Gelatin Electrospun Nanofibers for Bone Tissue Engineering.* Acs Applied Materials & Interfaces, 2017. **9**(39): p. 33695-33706.
270. Bhattacharya, M., *Polymer Nanocomposites-A Comparison between Carbon Nanotubes, Graphene, and Clay as Nanofillers.* Materials, 2016. **9**(4).
271. Sadeghi, M. and H. Hosseinzadeh, *Synthesis and properties of collagen-g-poly(sodium acrylate-co-2-hydroxyethylacrylate) superabsorbent hydrogels.* Brazilian Journal of Chemical Engineering, 2013. **30**(2): p. 379-389.
272. Buttafoco, L., et al., *Electrospinning of collagen and elastin for tissue engineering applications.* Biomaterials, 2006. **27**(5): p. 724-734.
273. Pal, S., et al., *A mechanistic model on the role of "radially-running" collagen fibers on dissection properties of human ascending thoracic aorta.* Journal of Biomechanics, 2014. **47**(5): p. 981-8.
274. Huang, X., et al., *Graphene-Based Materials: Synthesis, Characterization, Properties, and Applications.* Small, 2011. **7**(14): p. 1876-1902.
275. Singh, V., et al., *Graphene based materials: Past, present and future.* Progress in Materials Science, 2011. **56**(8): p. 1178-1271.
276. Stankovich, S., et al., *Graphene-based composite materials.* Nature, 2006. **442**(7100): p. 282-286.
277. Wang, R.J., et al., *In Situ Polymerisation Approach to Poly(epsilon-caprolactone)-Graphene Oxide Composites.* Designed Monomers and Polymers, 2012. **15**(3): p. 303-310.
278. Bian, S.S., S. Jayaram, and E.A. Cherney, *Electrospinning as a New Method of Preparing Nanofilled Silicone Rubber Composites.* Ieee Transactions on Dielectrics and Electrical Insulation, 2012. **19**(3): p. 777-785.
279. Ji, X.Q., et al., *Review of functionalization, structure and properties of graphene/polymer composite fibers.* Composites Part a-Applied Science and Manufacturing, 2016. **87**: p. 29-45.
280. Marcano, D.C., et al., *Improved Synthesis of Graphene Oxide.* Acs Nano, 2010. **4**(8): p. 4806-4814.
281. Mohammadi, A., et al., *High performance of covalently grafted poly(o-methoxyaniline) nanocomposite in the presence of amine-functionalized graphene oxide sheets (POMA/f-GO) for supercapacitor applications.* Journal of Materials Science-Materials in Electronics, 2017. **28**(8): p. 5776-5787.
282. Cai, N., et al., *Enhancing mechanical properties of polyelectrolyte complex nanofibers with graphene oxide nanofillers pretreated by polycation.* Composites Science and Technology, 2016. **135**: p. 128-136.

283. Jalaja, K., et al., *Graphene oxide decorated electrospun gelatin nanofibers: Fabrication, properties and applications.* Materials Science & Engineering C-Materials for Biological Applications, 2016. **64**: p. 11-19.
284. Piao, Y.Z. and B.Q. Chen, *Synthesis and mechanical properties of double cross-linked gelatin-graphene oxide hydrogels.* International Journal of Biological Macromolecules, 2017. **101**: p. 791-798.
285. Chaiyakun, S., et al., *Preparation and characterization of graphene oxide nanosheets.* 2012. **32**: p. 759-764.
286. Gan, X.R. and H.M. Zhao, *A Review: Nanomaterials Applied in Graphene-Based Electrochemical Biosensors.* Sensors and Materials, 2015. **27**(2): p. 191-215.
287. Kanayama, I., et al., *Comparative study of bioactivity of collagen scaffolds coated with graphene oxide and reduced graphene oxide.* International Journal of Nanomedicine, 2014. **9**: p. 3363-3373.
288. Tan, Y.Q., Y.H. Song, and Q. Zheng, *Hydrogen bonding-driven rheological modulation of chemically reduced graphene oxide/poly(vinyl alcohol) suspensions and its application in electrospinning.* Nanoscale, 2012. **4**(22): p. 6997-7005.
289. Piao, Y.Z. and B.Q. Chen, *One-pot synthesis and characterization of reduced graphene oxide-gelatin nanocomposite hydrogels.* Rsc Advances, 2016. **6**(8): p. 6171-6181.
290. Shih, Y.R.V., et al., *Growth of mesenchymal stem cells on electrospun type I collagen nanofibers.* Stem Cells, 2006. **24**(11): p. 2391-2397.
291. Stoessel, P.R., et al., *Spinning Angora Rabbit Wool-Like Porous Fibers from a Non-Equilibrated Gelatin/Water/2-Propanol Mixture.* Advanced Functional Materials, 2014. **24**(13): p. 1831-1839.
292. Gürdağ, G. and S. Sarmad, *Cellulose graft copolymers: synthesis, properties, and applications*, in *Polysaccharide based graft copolymers*. 2013, Springer. p. 15-57.
293. Gao, J.P., Z.C. Li, and M.Z. Huang, *Graft-copolymerisation of n-vinylpyrrolidone onto gelatin.* Journal of Applied Polymer Science, 1995. **55**(9): p. 1291-1299.
294. Gul-E-Noor, F., et al., *Grafting of 2-Ethylhexyl Acrylate with Urea on to Gelatin Film by Gamma Radiation.* Journal of Macromolecular Science Part a-Pure and Applied Chemistry, 2009. **46**(6): p. 615-624.
295. Bai, Y., et al., *Micro-mesoporous graphitic carbon nanofiber membranes.* Carbon, 2018. **132**: p. 746-748.
296. Zhu, Y.Q., et al., *A highly flexible paclitaxel-loaded poly(epsilon-caprolactone) electrospun fibrous-membrane-covered stent for benign cardia stricture.* Acta Biomaterialia, 2013. **9**(9): p. 8328-8336.
297. lorinczy, d. and D. Lörinczy, *The Nature of Biological Systems as Revealed by Thermal Methods edited by Dénes Lörinczy*, ed. D.

Lörinczy, SpringerLink, and Link. 2005, Dordrecht: Dordrecht : Springer Netherlands.
298. Wunderlich, B., *Thermal Analysis of Polymeric Materials by Bernhard Wunderlich*, ed. SpringerLink and Link. 2005, Berlin, Heidelberg: Berlin, Heidelberg : Springer Berlin Heidelberg.
299. Šesták, J., *Thermal analysis of Micro, Nano- and Non-Crystalline Materials Transformation, Crystallization, Kinetics and Thermodynamics / edited by Jaroslav Šesták, Peter Šimon*, ed. J. Šesták and P. Šimon. 2013: Dordrecht : Springer Netherlands : Imprint: Springer.
300. Wen, J., et al., *Applications of differential scanning calorimetry for thermal stability analysis of proteins: Qualification of DSC.* Journal of Pharmaceutical Sciences, 2012. **101**(3): p. 955-964.
301. France, W.G. and W. Derby Laws, *Differential Thermal Analysis of Proteins.* Analytical Chemistry, 1949. **21**(9): p. 1058-1059.
302. Pucci, F. and M. Rooman, *Improved insights into protein thermal stability: from the molecular to the structurome scale.* Philosophical Transactions of the Royal Society a-Mathematical Physical and Engineering Sciences, 2016. **374**(2080): p. 12.
303. Egerton, R.F., *Physical Principles of Electron Microscopy An Introduction to TEM, SEM, and AEM / by R.F. Egerton*. 2nd ed. 2016. ed. 2016: Cham : Springer International Publishing : Imprint: Springer.
304. Egerton, R.F., *The Scanning Electron Microscope*, in *Physical Principles of Electron Microscopy: An Introduction to TEM, SEM, and AEM*. 2016, Springer International Publishing: Cham. p. 121-147.
305. Van Oss, C.J., R.J. Good, and M.K. Chaudhury, *Additive and nonadditive surface tension components and the interpretation of contact angles.* Langmuir, 1988. **4**(4): p. 884-891.
306. Gomez-Guillen, M.C., et al., *Functional and bioactive properties of collagen and gelatin from alternative sources: A review.* Food Hydrocolloids, 2011. **25**(8): p. 1813-1827.
307. Chi, C.F., et al., *Antioxidant and Functional Properties of Collagen Hydrolysates from Spanish Mackerel Skin as Influenced by Average Molecular Weight.* Molecules, 2014. **19**(8): p. 11211-11230.
308. Jeevithan, E., et al., *Type II Collagen and Gelatin from Silvertip Shark (Carcharhinus albimarginatus) Cartilage: Isolation, Purification, Physicochemical and Antioxidant Properties.* Marine Drugs, 2014. **12**(7): p. 3852-3873.
309. Zhang, Z.B., et al., *A Promising Combo Gene Delivery System Developed from (3-Aminopropyl)triethoxysilane-Modified Iron Oxide Nanoparticles and Cationic Polymers.* Journal of Nanoparticle Research, 2013. **15**(5).

310. Kuwajima, T., H. Yoshida, and K. Hayashi, *Graft-polymerisation of methyl-methacrylate onto gelatin.* Journal of Applied Polymer Science, 1976. **20**(4): p. 967-974.
311. Brock, F., et al., *Reliability of nitrogen content (% N) and carbon: nitrogen atomic ratios (C: N) as indicators of collagen preservation suitable for radiocarbon dating.* Radiocarbon, 2012. **54**(3-4): p. 879-886.
312. Bella, J., *Collagen structure: new tricks from a very old dog.* Biochemical Journal, 2016. **473**: p. 1001-1025.
313. Muyonga, J.H., C.G.B. Cole, and K.G. Duodu, *Fourier transform infrared (FTIR) spectroscopic study of acid soluble collagen and gelatin from skins and bones of young and adult Nile perch (Lates niloticus).* Food Chemistry, 2004. **86**(3): p. 325-332.
314. Camacho, N.P., et al., *FTIR microscopic imaging of collagen and proteoglycan in bovine cartilage.* Biopolymers, 2001. **62**(1): p. 1-8.
315. Pielesz, A., *Temperature-dependent FTIR spectra of collagen and protective effect of partially hydrolysed fucoidan.* Spectrochimica Acta Part a-Molecular and Biomolecular Spectroscopy, 2014. **118**: p. 287-293.
316. Long, T.E., et al., *POLY 1-Advances in the design of branched topologies: A tutorial of emerging strategies.* Abstracts of Papers of the American Chemical Society, 2008. **235**.
317. Berry, G.C., L.M. Hobbs, and V.C. Long, *Solution and bulk properties of branched polyvinyl acetates .3. intrinsic viscosity and light scattering measurements.* Polymer, 1964. **5**(1): p. 31-50.
318. Rosu, R.F., R.A. Shanks, and S.N. Bhattacharya, *Dynamic rheology of branched poly(ethylene terephthalate).* Polymer International, 2000. **49**(2): p. 203-208.
319. Lusignan, C.P., et al., *Viscoelasticity of randomly branched polymers in the vulcanization class.* Physical Review E, 1999. **60**(5): p. 5657-5669.
320. Kezwon, A., et al., *Effect of surfactants on surface activity and rheological properties of type I collagen at air/water interface.* Colloids and Surfaces B-Biointerfaces, 2016. **148**: p. 238-248.
321. Avila, H.A., et al., *Dielectric Behavior of Epoxy/BaTiO3 Composites Using Nanostructured Ceramic Fibers Obtained by Electrospinning.* Acs Applied Materials & Interfaces, 2013. **5**(3): p. 505-510.
322. Van Krevelen, D.W. and K. Te Nijenhuis, *Properties of polymers: their correlation with chemical structure; their numerical estimation and prediction from additive group contributions*. 2009: Elsevier.
323. Dobraszczyk, B.J. and M. Morgenstern, *Rheology and the breadmaking process.* Journal of Cereal Science, 2003. **38**(3): p. 229-245.
324. Halperin, A., M. Tirrell, and T.P. Lodge, *Tethered chains in polymer microstructures.* Advances in Polymer Science, 1992. **100**: p. 31-71.

325. Kaith, B.S., R. Jindal, and M. Maiti, *Induction of Chemical and Moisture Resistance in Saccharum spontaneum L Fiber Through Graft Copolymerisation with Methyl Methacrylate and Study of Morphological Changes.* Journal of Applied Polymer Science, 2009. **113**(3): p. 1781-1791.
326. Sun, Z.H. and F.S. Chen, *Homogeneous grafting copolymerisation of methylmethacrylate onto cellulose using ammonium persulfate.* Cellulose Chemistry and Technology, 2014. **48**(3-4): p. 217-223.
327. Bockova, J., et al., *Collagen-grafted ultra-high molecular weight polyethylene for biomedical applications.* Chemical Papers, 2008. **62**(6): p. 580-588.
328. Vazquez, B., M. Gurruchaga, and I. Goni, *Hydrogels based on graft-copolymerisation of hema bma mixtures onto soluble gelatin - swelling behavior.* Polymer, 1995. **36**(11): p. 2311-2314.
329. Zheng, J.P., et al., *Swelling behavior of gelatin-g-methyl methacrylate copolymers.* Journal of Materials Science, 2005. **40**(15): p. 4029-4033.
330. Zheng, J.P., et al., *Swelling behavior of gelatin-g-poly(butyl acrylate) copolymers.* Journal of Applied Polymer Science, 2005. **97**(3): p. 1033-1037.
331. Liu, J., et al., *Effects of chemical composition and post-spinning stretching process on the morphological, structural, and thermo-chemical properties of electrospun polyacrylonitrile copolymer precursor nanofibers.* Polymer, 2015. **61**: p. 20-28.
332. Heydarkhan-Hagvall, S., et al., *Three-dimensional electrospun ECM-based hybrid scaffolds for cardiovascular tissue engineering.* Biomaterials, 2008. **29**(19): p. 2907-2914.
333. Cross, V.L., et al., *Dense type I collagen matrices that support cellular remodeling and microfabrication for studies of tumor angiogenesis and vasculogenesis in vitro.* Biomaterials, 2010. **31**(33): p. 8596-8607.
334. Zeugolis, D.I., R.G. Paul, and G. Attenburrow, *Extruded Collagen Fibres for Tissue-Engineering Applications: Influence of Collagen Concentration and NaCl Amount.* Journal of Biomaterials Science-Polymer Edition, 2009. **20**(2): p. 219-234.
335. Fujisawa, S. and Y. Kadoma, *Tri-n-Butylborane/WaterComplex-Mediated Copolymerisation of Methyl Methacrylate with Proteinaceous Materials and Proteins: A Review.* Polymers, 2010. **2**(4): p. 575-595.
336. Solouk, A., et al., *Biomimetic modified clinical-grade POSS-PCU nanocomposite polymer for bypass graft applications: A preliminary assessment of endothelial cell adhesion and haemocompatibility.* Materials Science & Engineering C-Materials for Biological Applications, 2015. **46**: p. 400-408.

337. Hoshino, M., et al., *Inhaled corticosteroids decrease subepithelial collagen deposition by modulation of the balance between matrix metalloproteinase-9 and tissue inhibitor of metalloproteinase-1 expression in asthma.* Journal of Allergy and Clinical Immunology, 1999. **104**(2): p. 356-363.
338. Zhou, Q.H., et al., *Implication of stable jet length in electrospinning for collecting well-aligned ultrafine PLLA fibers.* Polymer, 2013. **54**(25): p. 6867-6876.
339. Yan, Y., *2 - Developments in fibers for technical nonwovens*. 2016: Elsevier Ltd. 19-96.
340. Olsson, R.T., et al., *Extraction of Microfibrils from Bacterial Cellulose Networks for Electrospinning of Anisotropic Biohybrid Fiber Yarns.* Macromolecules, 2010. **43**(9): p. 4201-4209.
341. McKee, M.G., et al., *Correlations of solution rheology with electrospun fiber formation of linear and branched polyesters.* Macromolecules, 2004. **37**(5): p. 1760-1767.
342. Zheng, X.F., et al., *Preparation and characterization of temperature-memory nanoparticles of MIP-CS-g-PMMA.* Rsc Advances, 2016. **6**(112): p. 110722-110732.
343. Singh, V., et al., *Poly(methylmethacrylate) grafted chitosan: An efficient adsorbent for anionic azo dyes.* Journal of Hazardous Materials, 2009. **161**(2-3): p. 955-966.
344. Udhayakumar, S., et al., *L-Arginine intercedes bio-crosslinking of a collagen-chitosan 3D-hybrid scaffold for tissue engineering and regeneration: in silico, in vitro, and in vivo studies.* Rsc Advances, 2017. **7**(40): p. 25070-25088.
345. Wood-Adams, P.M., et al., *Effect of molecular structure on the linear viscoelastic behavior of polyethylene.* Macromolecules, 2000. **33**(20): p. 7489-7499.
346. Song, H.Y., S.J. Park, and K. Hyun, *Characterization of Dilution Effect of Semidilute Polymer Solution on Intrinsic Nonlinearity Q(0) via FT Rheology.* Macromolecules, 2017. **50**(16): p. 6238-6254.
347. Satyanarayana, K.G., G.G.C. Arizaga, and F. Wypych, *Biodegradable composites based on lignocellulosic fibers-An overview.* Progress in Polymer Science, 2009. **34**(9): p. 982-1021.
348. Mercader, C., et al., *Kinetics of fiber solidification.* Proceedings of the National Academy of Sciences of the United States of America, 2010. **107**(43): p. 18331-18335.
349. Yu, D.G., et al., *High-quality Janus nanofibers prepared using three-fluid electrospinning.* Chemical Communications, 2017. **53**(33): p. 4542-4545.
350. Chen, H., X. Hu, and P. Cebe, *Thermal properties and phase transitions in blends of Nylon-6 with silk fibroin.* Journal of Thermal Analysis and Calorimetry, 2008. **93**(1): p. 201-206.

351. Wang, Z.L., et al., *Effect of Thermal Annealing on Mechanical Properties of Polyelectrolyte Complex Nanofiber Membranes.* Fibers and Polymers, 2014. **15**(7): p. 1406-1413.
352. Rao, Y., et al., *Novel polymer-ceramic nanocomposite based on high dielectric constant epoxy formula for embedded capacitor application.* Journal of Applied Polymer Science, 2002. **83**(5): p. 1084-1090.
353. Kuo, C.C., C.T. Wang, and W.C. Chen, *Highly-Aligned Electrospun Luminescent Nanofibers Prepared from Polyfluorene/PMMA Blends: Fabrication, Morphology, Photophysical Properties and Sensory Applications.* Macromolecular Materials and Engineering, 2008. **293**(12): p. 999-1008.
354. Lee, C.H., et al., *Directed assembly of gold nanorods using aligned electrospun polymer nanofibers for highly efficient SERS substrates.* Nanotechnology, 2011. **22**(27).
355. Aluigi, A., et al., *Structure and properties of keratin/PEO blend nanofibres.* European Polymer Journal, 2008. **44**(8): p. 2465-2475.
356. Kwon, I.K., S. Kidoaki, and T. Matsuda, *Electrospun nano- to microfiber fabrics made of biodegradable copolyesters: structural characteristics, mechanical properties and cell adhesion potential.* Biomaterials, 2005. **26**(18): p. 3929-3939.
357. Huang, Z.M., et al., *Electrospinning and mechanical characterization of gelatin nanofibers.* Polymer, 2004. **45**(15): p. 5361-5368.
358. Marcano, D.C., et al., *Correction to Improved Synthesis of Graphene Oxide.* ACS nano, 2018. **12**(2): p. 2078.
359. Wu, W.J., C.Y. Wan, and Y. Zhang, *Graphene oxide as a covalent-crosslinking agent for EVM-g-PA6 thermoplastic elastomeric nanocomposites.* Rsc Advances, 2015. **5**(49): p. 39042-39051.
360. Yoshimoto, H., et al., *A biodegradable nanofiber scaffold by electrospinning and its potential for bone tissue engineering.* Biomaterials, 2003. **24**(12): p. 2077-2082.
361. Liang, D., B.S. Hsiao, and B. Chu, *Functional electrospun nanofibrous scaffolds for biomedical applications.* Advanced Drug Delivery Reviews, 2007. **59**(14): p. 1392-1412.
362. Tronci, G., et al., *An entropy-elastic gelatin-based hydrogel system.* Journal of Materials Chemistry, 2010. **20**(40): p. 8875-8884.
363. Kojima, K., et al., *Grafting of methyl-methacrylate onto collagen initiated by tributylborane.* Journal of Applied Polymer Science, 1983. **28**(1): p. 87-95.
364. Harada, O., K. Kadota, and T. Yamamoto, *Initiator-free photo-graft polymerisations of various vinyl monomers onto solubilized collagen films and characterization of grafted films.* Kobunshi Ronbunshu, 1999. **56**(5): p. 307-313.

365. Chang, W.J., et al., *Type I collagen grafting on titanium surfaces using low-temperature glow discharge.* Dental Materials Journal, 2008. **27**(3): p. 340-346.
366. Zhao, B. and W.J. Brittain, *Polymer brushes: surface-immobilized macromolecules.* Progress in Polymer Science, 2000. **25**(5): p. 677-710.
367. Roy, P. and A. Kumar, *Graft-copolymerisation of gelatin with poly(methyl methacrylate) in aqueous-medium.* Polymer Engineering and Science, 1991. **31**(14): p. 1001-1008.
368. Stejskal, J., D. Strakova, and P. Kratochvil, *Grafting of gelatin during polymerisation of methyl-methacrylate in aqueous-medium.* Journal of Applied Polymer Science, 1988. **36**(1): p. 215-227.
369. Singhbabu, Y.N., et al., *Capsule-embedded reduced graphene oxide: synthesis, mechanism and electrical properties.* Journal of Materials Chemistry C, 2013. **1**(5): p. 958-966.
370. Papkov, D., et al., *Improved Graphitic Structure of Continuous Carbon Nanofibers via Graphene Oxide Templating.* Advanced Functional Materials, 2013. **23**(46): p. 5763-5770.
371. Qu, L., et al., *Soluble nylon-functionalized carbon nanotubes from anionic ring-opening polymerisation from nanotube surface.* 2005. **38**(24): p. 10328-10331.
372. Saeed, K. and S.Y.J.J.o.a.p.s. Park, *Preparation of multiwalled carbon nanotube/nylon-6 nanocomposites by in situ polymerisation.* 2007. **106**(6): p. 3729-3735.
373. Minko, S., *Grafting on solid surfaces:"Grafting to" and "grafting from" methods*, in *Polymer surfaces and interfaces*. 2008, Springer. p. 215-234.
374. Hu, C.F., et al., *One-step preparation of nitrogen-doped graphene quantum dots from oxidized debris of graphene oxide.* Journal of Materials Chemistry B, 2013. **1**(1): p. 39-42.
375. O'Neill, A., D. Bakirtzis, and D. Dixon, *Polyamide 6/Graphene composites: The effect of in situ polymerisation on the structure and properties of graphene oxide and reduced graphene oxide.* European Polymer Journal, 2014. **59**: p. 353-362.
376. Mattevi, C., et al., *Evolution of Electrical, Chemical, and Structural Properties of Transparent and Conducting Chemically Derived Graphene Thin Films.* Advanced Functional Materials, 2009. **19**(16): p. 2577-2583.
377. Seresht, R.J., et al., *Synthesis and characterization of thermally-reduced graphene.* 2012.
378. Khanna, N.D., et al., *Effect of Biodegradation on Thermal and Crystalline Behavior of Polypropylene-Gelatin Based Copolymers.* Journal of Applied Polymer Science, 2010. **118**(3): p. 1476-1488.

379. Tornberg, E., *Effects of heat on meat proteins - Implications on structure and quality of meat products.* Meat Science, 2005. **70**(3): p. 493-508.
380. Wang, X., et al., *3D printing of polymer matrix composites: A review and prospective.* Composites Part B-Engineering, 2017. **110**: p. 442-458.
381. Nan, D., J. Liu, and W. Ma, *Electrospun phenolic resin-based carbon ultrafine fibers with abundant ultra-small micropores for CO2 adsorption.* Chemical Engineering Journal, 2015. **276**: p. 44-50.
382. Liu, K.P., et al., *Green and facile synthesis of highly biocompatible graphene nanosheets and its application for cellular imaging and drug delivery.* Journal of Materials Chemistry, 2011. **21**(32): p. 12034-12040.
383. Lee, S.H., J.H. Sung, and T.H. Park, *Nanomaterial-Based Biosensor as an Emerging Tool for Biomedical Applications.* Annals of Biomedical Engineering, 2012. **40**(6): p. 1384-1397.
384. Yin, T.J. and W. Qin, *Applications of nanomaterials in potentiometric sensors.* Trac-Trends in Analytical Chemistry, 2013. **51**: p. 79-86.
385. Guo, S.J. and S.J. Dong, *Biomolecule-nanoparticle hybrids for electrochemical biosensors.* Trac-Trends in Analytical Chemistry, 2009. **28**(1): p. 96-109.
386. Guo, C.X. and C.M. Li, *Direct electron transfer of glucose oxidase and biosensing of glucose on hollow sphere-nanostructured conducting polymer/metal oxide composite.* Physical Chemistry Chemical Physics, 2010. **12**(38): p. 12153-12159.
387. Ji, X.Y., et al., *Integration of Artificial Photosynthesis System for Enhanced Electronic Energy-Transfer Efficacy: A Case Study for Solar-Energy Driven Bioconversion of Carbon Dioxide to Methanol.* Small, 2016. **12**(34): p. 4753-4762.